TARGETING DRUG RESISTANCE IN CHRONIC MYELOID LEUKEMIA

A Dissertation Presented

By

LEYUAN MA

Submitted to the Faculty of the
University of Massachusetts Graduate School of Biomedical Sciences, Worcester
in partial fulfillment of the requirements for the degree of

DOCTOR OF PHILOSOPHY

Nov 08, 2016

INTERDISCIPLINARY GRADUATE PROGRAM

TARGETING DRUG RESISTANCE IN CHRONIC MYELOID LEUKEMIA

A Dissertation Presented
By

LEYUAN MA

This work was undertaken in the Graduate School of Biomedical Sciences

Interdisciplinary Graduate Program

Under the mentorship of

_____
Michael R. Green, M.D, Ph.D., Thesis Advisor

The signatures of the Dissertation Defense Committee signify completion and approval as to style and content of the Dissertation

_____
Daniel N. Bolon, Ph.D., Member of Committee

_____
Glen D. Raffel, M.D, Ph.D., Member of Committee

_____
Scot A. Wolfe, Ph.D., Member of Committee

_____
Timothy Graubert, M.D., External Member of Committee

The signature of the Chair of the Committee signifies that the written dissertation meets the requirements of the Dissertation Committee

_____
Michelle A. Kelliher, Ph.D., Chair of Committee

The signature of the Dean of the Graduate School of Biomedical Sciences signifies that the student has met all graduation requirements of the School

_____
Anthony Carruthers, Ph.D.,
Dean of the Graduate School of Biomedical Sciences

Nov 08, 2016

DEDICATION

This thesis dissertation is dedicated to my parents, my uncle and aunt, and all my friends in China and the United States, who have always stand by me, supported me and motivated me along the way to realize my dream. Without you, I'll never make it this far.

ACKNOWLEDGEMENTS

My deepest gratitude goes to those who dedicatedly helped and contributed to this work. First and foremost, I would like to thank my PhD advisor, Michael R. Green for his great mentorship. He is very open-mined and bright, and offered me a lot of opportunities to explore innovative areas, such as pioneering single cell RNA-sequencing. His great sense of scientific research guided me through the mist to find my own way. Also, his great sense of humor reminded me of important things to be learned beyond science. Previous Green lab member, Zhi Sheng, currently an assistant professor at Virginia Tech, also offered his friendship and great mentorship, trained me and guided me into the field of Leukemia research.

I would also like to thank my Thesis Research Advisory Committee for their advices, and people from Green lab for their insightful critiques during lab meeting and everyday discussion. Robert Bai, a HHMI medical student, has also dedicatedly contributed his one-year training time helping me with the genome-wide RNAi screen project. I would also like to thank our lab manager, Amy Virbasius, for her great work making superior viruses, and Sara Deibler for her great dedication to all the editing work. Julie Zhu and her bioinformatic team contributed to all the statistical and large dataset analysis. Thanks to those seminal discussions and advice from Dan Bolon and Scot A. Wolfe, it is their help

that makes me eventually capable of developing a new CRISPR-Cas9 mediated saturated mutagenesis platform.

Finally, we have obtained valuable clinical samples for this work from our collaborators, including Brain Druker's lab from OHSU Knight Cancer Institute, Hanna Jean Koury from Winship Cancer Institute of Emory University, Lloyd Hutchinson and Jan Cerny from UMass Medical School.

ABSTRACT

Inhibiting BCR-ABL kinase activity with tyrosine kinase inhibitors (TKIs) has been the frontline therapy for CML. Resistance to TKIs frequently occurs, but the mechanisms remain elusive.

First, to uncover survival pathways involved in TKI resistance in CML, I conducted a genome-wide RNAi screen in human CML cells to identify genes governing cellular sensitivity to the first generation TKI called IM (*Gleevec*). I identified genes converging on and activating the MEK/ERK pathway through transcriptional up-regulation of *PRKCH*. Combining IM with a MEK inhibitor synergistically kills TKI-resistant CML cells and CML stem cells.

Next, I performed single cell RNA-seq to compare expression profiles of CML stem cells and hematopoietic stem cells isolated from the same patient. Among the genes that are preferentially expressed in CML stem cells is *PIM2*, which encodes a pro-survival serine-threonine kinase that phosphorylates and inhibits the pro-apoptotic protein BAD. Inhibiting PIM2 function sensitizes CML stem cells to IM-induced apoptosis and prevents disease relapse in a CML mouse model.

Last, I devised a CRISPR-Cas9 based strategy to perform insertional mutagenesis at a defined genomic location in murine hematopoietic Ba/F3 cells. As proof of principle, we showed its capability to perform unbiased, saturated point mutagenesis in a 9 amino acid region of BCR-ABL encompassing the so-called “gatekeeper” residue, an important determinant of TKI binding. We found

that the ranking order of mutations from the screen correlated well with their prevalence in IM-resistant CML patients.

Overall, my findings reveal novel resistance mechanisms in CML and provide alternative therapeutic strategies.

TABLE OF CONTENTS

LIST OF TABLES

LIST OF FIGURES

LIST OF SYMBOLS, ABBREVIATIONS OR NOMENCLATURES

5-FU	5-fluorouracil
ALL	Acute lymphoblastic leukemia
Alox5	Arachidonate 5-lipoxygenase
AML	Acute Myeloid Leukemia
Bcl-2	B-cell lymphoma 2
BCL6	B cell lymphoma 6
BMT	Bone marrow transplantation
CAR-T	Chimeric antigen receptor T cells
CFU	Colony forming unit
CHIP	Chromatin Immunoprecipitation
CLP	Common lymphoid progenitor
CML	Chronic Myeloid Leukemia
CMLSC	Chronic Myeloid Leukemia Stem Cell
CMP	Common myeloid progenitor
CRISPR	Clustered regularly interspaced short palindromic repeat
CSC	Cancer stem cell
DSB	Double strand break
EMPIRIC	Exceedingly Meticulous and Parallel Investigation of Randomized Individual Codons
FACS	Fluorescence-activated cell sorting
FISH	Fluorescence in situ hybridization
Flt3	Fms-related tyrosine kinase 3
FOXO	Forkhead box O
GAP	GTPase-Activating Protein
GEF	Guanine nucleotide exchange factor
GMP	Granulocyte-macrophage progenitor
GSK3β	Glycogen synthase kinase 3β
HDR	Homology Directed Repair

HIF1α	Hypoxic inducible factor 1 alpha
HSC	Hematopoietic stem cells
IFNα	interferon-alpha
IL-3	Interleukin-3
IL-6	Interleukin-6
IM	Imatinib
IMSG	Imatinib-sensitizing gene
Indels	mini-insertion or deletion
JAK	Janus kinase
LNA	Locked Nucleic Acids
LSC	Leukemia stem cell
LSK	Lin-Sca1+cKit+
LTC-IC	Long-term culture-initiating cells
LTR	Long terminal repeat
M-MLV	Moloney Murine Leukemia Virus
MAPK	Mitogen-activated protein kinases
MDR1	Multi-drug resistance 1
MMTV	Mouse Mammary Tumor Virus
MPD	Myeloproliferative disease
MPSV	Myeloproliferative sarcoma virus
MSCV	Murine Stem Cell Virus
MT	Metallothionein
NHEJ	Non-Homologour End Joining
NSG	NOD/SCID/interleukin 2 receptor gamma(null) [IL2γ-/-]
Ph	Philadelphia Chromosome
PI3K	Phosphoinositide 3-kinases
RNA-seq	RNA-sequencing
RNAi	RNA interference
SCF	Stem cell factor

SCL	Stem cell leukemia
sgRNA	short guide RNA
shRNA	short-hairpin RNA
siRNA	small interfering RNA
STAT	Signal transducers and activator of transcription
TALEN	Transcription activator-like effector nucleases
TGFα	Transforming growth factor alpha
TKI	Tyrosine kinase inhibitor
TRC	The RNAi Consortium
TSO	Template switching oligo
tTA	Tetracycline transactivator
ZFN	Zinc-finger nucleases

PREFACE

This dissertation is the original work from Leyuan Ma, under guidance from Dr. Michael R. Green. The publication status and detailed contribution is described below.

Data in Chapter II has been published as "**Ma L**, Shan Y, Bai R, Xue L, Eide CA, Ou J, Zhu LJ, Hutchinson L, Cerny J, Khoury HJ, Sheng Z, Druker BJ, Li S, Green MR. A Therapeutically Targetable Mechanism of BCR-ABL-Independent IM Resistance in Chronic Myeloid Leukemia. ***Sci Transl Med.,*** 6, 252ra121 (2014)". The experiments in this chapter are designed by L.M., Z.S., S.L., and M.R.G, L.M. performed most of the experiments with Y.S. assisting with the CML mouse models and FACS analysis, R.B. assisting with immunoblotting and qRT-PCR, and L.X. assisting with oral gavage experiments. C.A.E., L.H., J.C., B.J.D., and H.J.K. provided CML patient samples. J.O. and L.J.Z. performed statistical analyses. L.M., C.A.E., B.J.D., H.J.K., S.L., and M.R.G. interpreted the data. L.M. and M.R.G. wrote the manuscript.

Data in chapter III is submitted as "**Ma L**, Pak M, Ou J, Yu J, Yi S, Zhu LJ, Hutchinson L, Li S, Green MR. Single-cell RNA-seq reveals a targetable IM-resistance pathway in leukemic stem cells." The experiments in this chapter are designed by L.M., S.L., and M.R.G. L.M. performed most of the experiments, with M.P., and Y.S. assisting with the CML mouse models. J.O., J.Y., and L.J.Z.

performed single cell RNA-seq and statistical analyses. L.H. provided CML patient samples. L.M., M.P., L.J.Z.,S.L., and M.R.G. interpreted the data. L.M. and M.R.G. wrote the manuscript.

Data in chapter VI is being prepared for submission as "**Ma L**, Boucher J, Paulsen J, Matuszewski S, Jensen JD, Schiffer C, Green MR, Bolon D. CRISPR-Cas9 mediated saturated mutagenesis screen in BCR-ABL predicts clinical TKI resistant mutations." The experiments in this chapter are designed by L.M., B.J., M.R.G., and B.D. L.M. generated the reporter cell lines, developed the CRISPR-Cas9 screen system and performed all the cell culture experiments. B.J. and B.D. generated the BCR-ABL mutant library, performed deep-sequencing and most of data analysis. P.J and S.C performed MD simulation BCR-ABL mutations, M.S. and J.D.J performed MCMC analysis. L.M., B.J., and B.D., wrote the manuscript.

CHAPTER I: INTRODUCTION

1.1 Chronic Myeloid Leukemia (CML)

A Brief History of CML

The first description of leukemia dates back to 1840s, David Craigie and his college John Hughes Bennett saw a few cases of patients experiencing fever, splenomegaly and leukocytosis, and subsequent death between 1841 and 1845(Goldman, 2010). These characteristics suggest the possibility of first case of chronic myeloid leukemia (CML). Later in 1872, Ernst Neumann recognized the origination of leukemia from bone marrow(Goldman, 2010).

The specific association of cytogenetic defect and leukemia was first established in 1960 when Nowell and Hungerford described a consistent abnormal minute chromosome in the blood of seven patients with chronic granulocytic leukemia(Nowell PC, 1960). Later, the finding of this minute chromosome was confirmed by others and became known as “Philadelphia chromosome” (Ph chromosome). With the improvement of chromosome banding techniques, Rowley further demonstrated in 1973 that the Ph chromosome comprised truncated version of chromosome 9 and 22 that originate from a reciprocal chromosomal translocation event, designated t(9;22)(Rowley, 1973).

A seminal study from Groffen and colleagues in 1984 reported the presence of a “breakpoint cluster region” in 17 different CML patients, and this region constitutes a part of the BCR gene(Groffen et al., 1984). Meanwhile, Witte and

colleagues showed that c-Abl, encoded by ABL gene, was associated with abnormal kinase activity of in K562 CML cells, establishing a possible casual link between BCR and ABL(Konopka et al., 1984; Lozzio and Lozzio, 1975). Between 1984 and 1985, studies led by Eli Canaani from Weizmann Institute confirmed the presence of a BCR-ABL fusion transcript in cells from CML patients, revealing the major molecular abnormality in CML(Canaani et al., 1984; Shtivelman et al., 1985). In 1990, the casual relationship of BCR-ABL and CML was further established by Daley *et al*(Daley et al., 1990) and Kelliher *et al* (Kelliher et al., 1990), who demonstrated that retroviral transduction of BCR-ABL gene into murine stem cells could induce CML-like leukemia in mice, resembling the chronic phase of CML in patients.

CML Pathology and Epidemiology

CML is a myeloproliferative disease (MPD), characterized by unregulated growth of immature granulocytes in peripheral blood and bone marrows(Faderl et al., 1999). One obvious symptom of CML is the elevated white blood cell count, with majority of cell being mature neutrophils, myelocytes, basophils and eosinophils, usually with few blasts(Faderl et al., 1999). While around 40% of CML patients are asymptomatic at diagnosis of the disease, other patients demonstrate splenomegaly(Redaelli et al., 2004; Sawyers, 1999). Uncontrolled granulocyte accumulation in the peripheral blood, and infiltration of lung and liver will finally lead to patient death(Daley et al., 1990).

The annual incidence of CML is about one to two cases per 100,000 people with a median onset age at 53 years(Redaelli et al., 2004). CML is typically present in chronic, accelerated and blast crisis phases(Faderl et al., 1999). Chronic phase CML usually has a long latency, which are typically 4-5 years, and majority of the cells in peripheral blood are neutrophils. Impairment of ATR signaling by BCR-ABL promotes genomic instability and the accumulation of additional genetic lesions(Dierov et al., 2004). Additionally, BCR-ABL suppressed expression of a myeloid-specific transcription factor CEBPα by increasing stability of its translational regulator HNRNPE2, leading to differentiation arrest of CML cells(Melo and Barnes, 2007). These events lead to accumulation of immature blast cells in peripheral blood and CML progression. When some CML patients may go through a transient accelerated phase, which last for 6-9 months, other patients may directly enter blast crisis phase with more than 20% of blood cells being CML blasts(Schiffer et al., 2003). Without therapy, blast crisis CML patients may only survive for 3-6 months(Faderl et al., 1999).

Conventional Therapy for CML

In early 20th century, CML patients were predominantly treated with radiotherapy, which usually is directed to the spleen (Goldman, 2010). In 1960s, chemotherapies using busulfan and hydroxyurea often replaced radiotherapy as an alternative, but none of them were able to eradicate Ph+ cells(Goldman, 2010). In early 1980s, interferon-α (IFNα) was introduced to treat CML patients in chronic phase. Unlikely busulfan and hydroxyurea, IFNα was capable of

achieving complete and durable Ph- hematopoiesis in a minority group of patients, and even can be discontinued without disease relapse in rare cases(Talpaz et al., 1986). A meta-analysis of seven randomized trials involving 1,554 patients showed that IFNα treatment leads to ~57% of 5-year survival rate compared to 42% using chemotherapy(1997). Therefore, IFNα has been considered the major option for newly diagnosed CML patients.

Up to now, the only proven cure for CML could be allogeneic bone marrow transplantation (BMT). A case was reported in 1979 using total body irradiation followed by transfusion of bone marrow cells from human leukocyte antigen(HLA) identical siblings(Fefer et al., 1979). In this case, patient remained Ph- in his marrows at follow-up interval of 22-31 months, therefore becoming the first case of CML that can be cured by bone marrow transplantation(Fefer et al., 1979). The 5 year overall survival rate of CML patients receiving allogeneic BMT are 60% to 80%, while the leukemia-free survival rate are 55% to 70%(Goldman, 2010). Majority of survivors show no evidence of leukemia or Ph chromosome, but certain patients do relapse within the first 3 years of transplant(Gaziev et al., 2002).

1.2 Molecular and Cellular basis of CML

Ph Chromosome and BCR-ABL oncogene

Since its first description by Nowell and Hungerford in 1960, Ph Chromosome has been shown to be present in >95% of CML patients, strongly suggesting the

causal relationship with CML. In addition, Ph chromosome was also found in ~20% of acute lymphoblastic leukemia (ALL)(Kurzrock et al., 2003). Ph chromosome produces a constitutively active oncogenic tyrosine kinase, BCR–ABL, by fusing Abelson kinase gene (ABL or ABL1) with the breakpoint cluster region gene (BCR)(Kurzrock et al., 1987).

ABL gene is located on the long arm of chromosome 9 and encodes a 145kb protein product, c-Abl, which acts as a non-receptor tyrosine kinase(Rosenberg and Witte, 1988). c-Abl protein can shuttle between nucleus, where it binds to DNA and regulates cell cycle and genotoxicity, and cytoplasm, where it is involved in cytoskeleton remodeling and substrate phosphorylation(Van Etten, 1999; Wang, 1998; Wetzler et al., 1993). Normal c-Abl function is tightly regulated, replacement with N-terminal BCR leads to high and constitutive c-Abl kinase activity in the cytoplasm, leading to oncogenic transformation (Pendergast et al., 1991; Pluk et al., 2002; Van Etten, 1999).

BCR gene is located on the long arm of chromosome 22, and produces two major isoforms, 130kd and 160kd, respectively(Dhut et al., 1988; Stam et al., 1987). Similar to c-Abl, Bcr protein also resides in both the cytoplasmic and nuclear compartments(Dhut et al., 1988; Laurent et al., 2000; Wetzler et al., 1993). When ABL gene breaks at the identical location, BCR gene has several breakpoint region (m-bcr, M-bcr, μ-bcr)(Kurzrock et al., 2003). The first exon of BCR possesses several highly conserved Src-Homology-2 (SH2) binding

domain, which is important for assembling signal transduction complexes(Sadowski et al., 1986). This exon exists in all BCR-ABL fusion proteins and is thought to play a pivotal role in oncogenesis(Kurzrock et al., 2003).

The classic fusion event in CML is *b2a2* or *b3a2*, which fuses exon2 (*b2*) or exon3 (*b3*) of BCR to exon 2 (*a2*) of ABL, leading to an oncoprotein of 210 kd molecular weight, dubbed p210 BCR-ABL(Melo, 1996). Depending on the junction, BCR-ABL has two other isoforms, p190 and p230. Among them, p210 isoform is predominantly found in CML, and p230 was also present in a small percentage of CML. p190 is the major isoform found in BCR-ABL+ Acute Lymphoblastic Leukemia(Melo, 1996), and it was thought to have higher tyrosine kinase activity and therefore more transforming capability than p210 and p230(Li et al., 1999).

In contrast to c-Abl and Bcr protein, BCR-ABL protein was found exclusively in the cytoplasm(Kurzrock et al., 2003). The fusion event brings together the functional domains of Bcr and Abl, therefore making a variety of cytoplasmic signaling proteins accessible to phosphorylation and activation by Abl. BCR-ABL could either directly activate these pathways by interacting with the key signaling molecule or by indirectly increased cytokine or growth factor secretion, therefore establishing an autocrine feedback loop.

Oncogenic BCR-ABL signaling pathways

The growth and differentiation of hematopoietic cells is maintained by various cytokine-stimulated signaling pathway. However, oncogene BCR-ABL bypasses the requirement of these extracellular stimuli and drives cytokine-independent cell growth and proliferation while inhibiting apoptosis, leading to subsequent cell transformation and CML development (Ren, 2005). The key signaling pathways activated by BCR-ABL include, but not limited to, RAF/MEK/ERK, JAK/STAT, and PI3K/AKT pathway(Steelman et al., 2004) as described below.

The RAF/MEK/ERK pathway is also known as mitogen-activated protein kinase (MAPK) pathway, and can be stimulated by mitogen, cytokines and growth factors(Steelman et al., 2004). MAPK pathway mediates signal transduction from cell surface to the nucleus(McCubrey et al., 2007). One well-studied example is RAS mediated MAPK activation(Yan et al., 1998). Ras is a small GTP-binding protein. Once growth factor receptor encounters its ligand and becomes phosphorylated on tyrosine residues. A docking protein Grb2 will then be recruited by directly binding to the phosphotyrosine through its SH2 domain while forming a complex with a guanine nucleotide exchange factor (GEF), SOS, through its SH3 domain. RAS can be activated by SOS, which promotes exchanging of GDP to GTP, but inactivated by GTPase-Activating Protein (GAP), which catalyzes the removal of phosphate from GTP. The GTP-bound active conformation of RAS recruits RAF protein to the membrane through the Ras binding domain present in RAF. Subsequent phosphorylation events at several serine/threonine sites lead to RAF activation(Fabian et al., 1993). Then RAF

protein phosphorylates and activates of primary downstream target MEK, which further phosphorylates and activates ERK. Activated ERK transmits signal into nucleus by phosphorylating and activating downstream targets, such as the 40S ribosomal protein S6 kinase, c-Myc, and Elk1, to regulate protein translation and gene expression required for cell cycle entry and mitosis.

BCR-ABL transformed cells have constitutively RAF/MEK/ERK pathway activation(Steelman et al., 2004). It was shown that BCR-ABL autophosphorylates itself at Y177 position, which serves as docking site for Grb2(Million and Van Etten, 2000). BCR-ABL further recruits scaffolding Gab2 adaptor protein via Grb2/Gab2 complex as a signal amplifier to mediate downstream pathway activation, including RAF/MEK/ERK pathway(Lock et al., 2000; Sattler et al., 2002). Y177F mutation abolishes this interaction and dramatically impairs myeloid leukemogenesis. Gab2 knockout in mice blocks PI3K/AKT and RAF/MEK/ERK pathway activation and BCR-ABL transformation(Sattler et al., 2002). In addition, BCR-ABL could stimulate RAF/MEK/ERK pathway by directly regulating RAF1(Skorski et al., 1995).

JAK/STAT pathway mediates sensing of extracellular stimuli, including cytokines, and transmitting the signal into nucleus by directly modulating transcription of gene involved in proliferation, differentiation and immunity(Leonard, 2001; Rawlings et al., 2004). JAK/STAT pathway consists of three components: cell surface receptor, Janus kinase(JAK), and STAT proteins(Steelman et al., 2004).

Ligand binding induces receptor homodimerization or heterodimerization, and this receptor aggregation facilitates transphosphorylation and subsequent activation of associated JAKs(Rawlings et al., 2004). Once activated, JAKs could phosphorylate additional tyrosine residues on the receptor, leading to recruitment and subsequent phosphorylation of SH2 domain-containing STAT proteins. Phosphorylation of STATs induces their dimerization through SH2 domain interaction, which promotes their movements into nucleus, DNA binding and transcription activation ability.

Constitutive STATs activation has also been shown in CML cells and BCR-ABL+ ALL cells(Danial and Rothman, 2000). In cells containing p210 BCR-ABL, the major activated STAT protein is STAT1 and STAT5, while only p190 was reported to have the ability to activate STAT6(Ilaria and Van Etten, 1996). Unlike v-Abl, which mediates STAT5 activation via direct associating with JAK kinase at its c-terminal domain, there is no evidence showing physical interaction of BCR-ABL with STATs. It was demonstrated that kinase inactive JAK2 fails to block STAT5 activity in BCR-ABL transformed Ba/F3 cells(Ilaria and Van Etten, 1996). SRC family kinases (e.g., Hck, and Lyn) can activate STAT5 independent of JAK2 during IL-3 signaling(Silva, 2004). Because SRC family kinases are often stimulated by BCR-ABL in CML cells, this leads to the characterization of Hck as an intermediate in BCR-ABL-dependent activation of STAT5 via its binding to BCR-ABL SH2 and SH3 domain(Klejman et al., 2002).

PI3K/AKT pathway was first discovered during the characterization of insulin signaling in early 1980s, and it has been shown to play a pivotal role in regulating cell growth, proliferation, and apoptosis(Hemmings and Restuccia, 2012; Vanhaesebroeck et al., 2012). PI3Ks (Phosphatidylinositol-3 kinases) constitute a lipid kinase family that can phosphorylate the 3'-OH group of inositol ring in inositol phospholipids(Steelman et al., 2004). As an example, activated insulin receptor could directly stimulate bound class I PI3K via its regulatory subunit to catalyze the conversion of phosphatidylinositol (3,4)-bisphosphate (PIP2) lipids to phosphatidylinositol (3,4,5)-trisphosphate (PIP3) in seconds. Then, protein kinase B (PKB, also known as AKT) binds to PIP3 at the plasma membrane via its pleckstrin-homology (PH) domain, leading to the conformation change and allowing 3-phosphoinositide-dependent protein kinase 1 (PDPK1) to access and phosphorylate the activation loop at T308 site. This phosphorylation event is thought to stabilize the activation loop and result in partial activation of PKB/AKT. Full activation of PKB/AKT requires a second phosphorylation event at S473 site in its hydrophobic C-terminal region by PDPK2(Feng et al., 2004; Sarbassov et al., 2005). Fully activated PKB/AKT regulates a number of cellular functions, including metabolism, survival, proliferation and protein synthesis, by phosphorylating both cytoplasmic and nuclear substrates(Hemmings and Restuccia, 2012). Notably, one of such phosphorylation event leads to inhibition of pro-apoptotic FOXO family proteins(Guertin et al., 2006).

PI3K/AKT pathway activation contributes to another signaling downstream of

BCR-ABL to promote cell transformation(Steelman et al., 2004). Activation of PI3K/AKT pathway by BCR-ABL depends on the binding of BCR-ABL SH2 domain to the p85 regulatory subunit(Steelman et al., 2004). Cells expressing BCR-ABL Y177F mutant exhibited marked reduction of tyrosine phosphorylation in Gab2, and reduced association of PI3K with Gab2 and BCR-ABL(Sattler et al., 2002). In addition, it was shown that elevated ROS level by BCR-ABL in TonB.210 cells also contributes to activation of PI3K/AKT pathway by activating AKT, GSK3β, as well as its downstream targets such as β-catenin, and Mcl-1(Naughton et al., 2009). A negative regulator of PI3K/AKT pathway, PP2A, is also inhibited by BCR-ABL mediated SET protein expression, which is a potent physiological inhibitor of PP2A(Neviani et al., 2005).

Cancer stem cells in CML

Like normal stem cells, which can self-new and fuel the growth of normal proliferative tissues such as bone marrow, skin and intestinal epithelium, cancer stem cells are also thought to be capable of self-renewal and serve as the unlimited source of rapidly proliferating bulk cancer cells(Huntly and Gilliland, 2005; Reya et al., 2001; Visvader and Lindeman, 2008). The concept of cancer stem cells was first introduced by the study in Acute Myeloid Leukemia (AML) (Bonnet and Dick, 1997), Bonnet and Dick transplanted the leukemic counterpart of normal HSCs, CD34+CD38- population, from AML samples into NOD/SCID mice and found that they possess the ability of leukemia initiation and differentiation into leukemic blast. The capability of transferring AML into

secondary recipients by serial transplantation confirmed the self-renewal nature of CD34+CD38- cell population(Bonnet and Dick, 1997). It is thought that cancer stem cells are phenotypically the same as normal stem cells(Tang, 2012). Cancer stem cells were thereafter reported in many solid tumors, including breast cancer(Al-Hajj et al., 2003), pancreatic cancer(Li et al., 2007), brain tumor(Singh et al., 2003), and lung cancer(Kim et al., 2005).

Despite compelling evidence of the presence of cancer stem cells, there remain some controversies, particularly on their definition and origination. Many tumors are derived from a single transformed cell which acquired the ability to proliferation and form tumor in vivo(Bjerkvig et al., 2005). Such cancer initiating cells have often been designated as cancer stem cells. One misconception is that cancer stem cell must have arisen from a normal stem cells(Jordan, 2009). Although this argument is true in some cases, it does not generally apply to all cancer types. For example in acute myeloid leukemia, committed progenitor transformed by MLL-AF9 acquired self-renewal ability and became cancer stem cells(Krivtsov et al., 2006). Like normal stem cells, any given cancer cell will qualify as cancer stem cell if it could self-renew, differentiate and reconstitute the original heterogeneous cancer population. That said, functional assays to characterize *in vivo* self-renewal capacity will serve as the ultimate criteria to define a cancer stem cell population(Lathia, 2013).

Although certain cell surface markers have been demonstrated to be associated

with enhanced cancer stem cell property, such as CD44/CD24(Al-Hajj et al., 2003) for breast cancer stem cells, CD133 for glioblastoma stem cells(Singh et al., 2004), it is important not attaching the label of cancer stem cells solely based on these phenotypic traits. Recent observation of cancer cell plasticity and cell phenotype switching also argues that cancer stem cells may not be a fixed state, but rather a transitional or adaptive state depending on environmental factors(Lathia, 2013). For example, in breast cancer, $CD44^{low}/CD24^{high}$ non-stem cancer cells could be converted to $CD44^{high}/CD24^{low}$ cancer stem cells in response to IL-6 mediated activation of inflammatory feedback loop(Iliopoulos et al., 2011).

Regardless of these controversies, CML stem cells have been demonstrated to originate from early multipotent progenitor or stem cells(Savona and Talpaz, 2008). Using CML mouse model, several groups have confirmed that only the BCR-ABL transduced Lin-Sca1+Kit+ (LSK) population, which are enriched for stem cells, are capable of full engraftment and reestablishment of functional hematopoiesis, and being serially transplanted, but not the more differentiated common myeloid progenitor (CMP), granulocyte-macrophage progenitors (GMP) or common lymphoid progenitor (CLP) (Hu et al., 2006; Huntly et al., 2004; Reynaud et al., 2011). Therefore, in chronic phase CML patient, BCR-ABL+ HSCs are the source of self-renewal capacity and provides proliferative and survival advantages.

1.3 Animal models in Chronic Myeloid Leukemia

Multiple animal models have been developed to recapitulate the clinical phenotypes of CML and study CML leukemogenesis(Ilaria, 2004; Sontakke et al., 2016). Among them, three models are widely used: retroviral transduction and bone marrow transplantation model(Daley et al., 1990; Kelliher et al., 1990; Li et al., 1999), BCR-ABL transgenic model(Honda et al., 1995; Huettner et al., 2000), and patient sample xenograft NSG mice model(Eisterer et al., 2005).

Retroviral transduction mouse model

In 1990, a retroviral transduction model was first reported to induce CML in mice(Daley et al., 1990). The retrovirus contains p210 isoform of BCR-ABL and was controlled by LTR promoter of myeloproliferative sarcoma virus(MPSV). Bone marrow cells from young BALB/c mice were harvested, infected with high titer virus, and transplanted into lethally irradiated syngeneic recipient mice. Some recipient mice developed a CML-like myeloproliferative disease with an average 9-week latency, and displayed typical clinical CML features, such as massive splenomegaly, increased peripheral white blood cell counts (15,000~500,000 cells/mm3), and extensive infiltration of the bone marrow, liver, spleen with granulocytes, and loss of normal splenic architecture. However, there were also some mice developing acute lymphoblastic leukemia or mixed lineage tumor with longer latency. The retroviral transduction strategy was further improved later by replacing MPSV LTR with MSCV LTR to ensure high level of

BCR-ABL expression in hematopoietic stem/progenitor cells(Hawley et al., 1994), leading to a nearly 100% of CML disease induction (Li et al., 1999; Pear et al., 1998).

Because of the technical convenience of this model, it has been widely used for studying genes involved in CML leukemogenesis and testing novel therapeutic strategies.

BCR-ABL transgenic mouse model

Although resembling most of the clinical characteristics of CML, the well established retroviral based model has short latency, usually 2-3 weeks, before the mice develop lethal phenotype, such as pulmonary hemorrhage, which is a disadvantage in evaluating genes involved in leukemia progression.

Since 1990s, several BCR-ABL transgenic mouse models have also been developed using different regulatory elements to modulate BCR-ABL expression, including mouse “housekeeping gene” metallothionine-1(MT) gene promoter driving p210 BCR-ABL expression(Honda et al., 1995). However, this BCR-ABL transgenic model develops T cell leukemia rather than a CML-like MPD. To understand if BCR-ABL is required for both induction and maintenance of leukemia, Tenen group engineered a double transgenic mice line by crossing a tetracycline transactivator (tTA) repressive promoter controlled p210 BCR-ABL transgenic line with another line bearing mouse mammary tumor virus (MMTV) – tTA transactivator(Huettner et al., 2000). After withdrawal of tetracycline, 100% of

the double transgenic progenies start expressing BCR-ABL and develop lymphoid leukemia. Lineage analysis of the leukemic cells from peripheral blood, bone marrow, or lymph node using flow cytometry, however, showed that majority of cells were positive for B cell surface antigen, such as B220, while no detection of T cell marker or myeloid markers, indicating its useful application to study BCR-ABL+ ALL(Huettner et al., 2000). All the above evidence suggests that the leukemic phenotype induced by BCR-ABL largely depends on the cell type expression of BCR-ABL. And a highly controlled expression of BCR-ABL in hematopoietic stem cells is required to establish a CML-like model given that CML is a stem cell based disease. After a series of effort, an enhancer region identified in the 3' region of Stem Cell Leukemia (SCL) gene was found to restrict heterologous LacZ expression in hematopoietic stem and progenitor cells and megakaryocytes, and were therefore employed to generate a new *SCL*tTA/BCR-ABL transgenic mouse model(Koschmieder et al., 2005). In this model, BCR-ABL induction by withdrawal of tetracycline led to neutrophilia, splenomegaly and myeloid infiltration in different organs, and more importantly expansion of myeloid progenitor and hematopoietic stem cells, recapitulating many clinical features of human CML.

Patient sample xenograft NSG mouse model

Engrafting human CML patient cells into humanized mice may provide a more clinical and physiological relevant model to study CML disease and evaluate therapeutic strategies. Several initial trials in NOD/SCID mice using CML cells

from chronic phase patients failed to obtain efficient leukemic engraftment even with co-injection of recombinant cytokines(Lewis et al., 1998; Sirard et al., 1996). Recently, a new nonobese diabetic/severe combined immunodeficient mouse line was generated by incorporating a complete null mutation of the common cytokine receptor gamma chain (NOD/SCID/interleukin 2 receptor gamma(null) [IL2γ-/-]), known as NSG mice(Ishikawa et al., 2005) . These mice are able to efficiently support human blood HSC engraftment and multilineage differentiation(Ishikawa et al., 2005; Shultz et al., 2005). In contrast to NOD/SCID mice, which requires up to 7-10x10^6 CML CD34+ cells for engraftment, 1-2x10^6 CD34+ cells are sufficient to establish engraftment and reconstitute hematopoiesis in NSG mice for at least 16 weeks.

Modeling blast crisis CML

In addition to the above strategies modeling chronic phase CML, several mouse models of blast crisis CML have been reported. Daley *et al* generated the first BC CML model by transplanting primary CML cells to secondary recipients in *BALB/c* mice(Daley et al., 1991). Albeit with low efficiency, they were able to observe retrovirally transduced primary CML cells progress from chronic into acute leukemia in a small number of recipients, with elevated level of immature blast cells from either lymphoid or myeloid lineage(Daley et al., 1991). Progression of CML into blast crisis stage is often accompanied by of secondary mutations that have synergistic effect with BCR-ABL(Melo and Barnes, 2007). Effort has also been made by combining BCR-ABL expression with a defined second hit, such

as *p53*(Honda et al., 2000; Skorski et al., 1996), *Dok1/Dok2* null mutation(Yasuda et al., 2004) or *NUP98-HOXA9* overexpression(Dash et al., 2002), driving rapid expansion of immature blast cells.

Although the above mouse models displays many features resembling CML, they failed to recapitulate the entire disease development course in human subject. Most recently, Giotopoulos *et al* introduced a sleeping beauty transposon, *GrOnc*, into the chronic phase BCR-ABL transgenic mouse model(Giotopoulos et al., 2015). Induction of transposition leads to CML progression from an initial chronic phase stage to a blast crisis stage, with ~85% mice developing Blast crisis phase-like phenotype, ~10% mice demonstrating accelerated phase-like phenotype, and only ~5% remaining in chronic phase phenotype(Giotopoulos et al., 2015). Notably, the *GrOnc* transposon, in combination with BCR-ABL, promote myeloid but not lymphoid leukemogenesis, recapitulating many clinical and laboratory aspects of human CML blast crisis.

1.4 Targeted Therapy in CML

Development of Tyrosine Kinase inhibitors (TKIs)

Given that over 95% of CML patients contain the Ph chromosome and express the BCR-ABL oncoprotein, it is noted that CML might respond to inhibition of BCR-ABL kinase activity(Druker, 2002).

In the early 1990s, Brian Druker collaborated with Novartis expecting to identify

such a tyrosine kinase inhibitor that can be orally administrated, and they found that a 2-phenylaminopyrimindin derivative, CGP57-148B, now widely known as imatinib (IM), with a brand name Gleevec, capable of potently inhibiting BCR-ABL and killing CML cells while leaving normal cells unaffected(Deininger et al., 2005; Druker et al., 1996).

IM inhibits BCR-ABL kinase activity by occupying the ATP-binding pocket through forming hydrogen bonds and blocking its access to ATP, thereby locking it at inactive confirmation and precluding subsequent substrate phosphorylation and activation of downstream signaling pathways(Schindler et al., 2000).

Although IM shows great efficacy in controlling CML progression in chronic phase patients, it is less effective in patients with advanced disease, or even ineffective in blast crisis patients(Sawyers et al., 2002). Collectively, these unresponsive events were considered to be IM resistance(Shah, 2005). In certain cases, patients don’t respond to IM at all, which is called primary resistance(Quintas-Cardama et al., 2009) and is largely due to unknown genetic alterations that shift the dependence away from BCR-ABL for survival. IM is also vulnerable to MDR1, p-Glycoprotein, mediated drug efflux(Illmer et al., 2004). In other cases, which are regarded as secondary resistance(Quintas-Cardama et al., 2009), patients may respond to IM at first but lose established response overtime. These cases often involve BCR-ABL mutations that block IM binding.

To overcome IM resistance, second generation inhibitors, represented by

Nilotinib and Dasatinib, and third generation inhibitor, represented by Ponatinib, were developed to recognize and inhibit a variety of BCR-ABL mutants.

Unlike IM, which is discovered through drug screening, Nilotinib was developed with rational drug design based on the structure of ABL-IM complex to overcome resistance related to BCR-ABL mutations(Kantarjian et al., 2006). Nilotinib binds to the inactive confirmation of ABL kinase domain through lipophilic and weak van der wall interactions and blocks its catalytic activity(Manley et al., 2005), and is not dependent on OCT1 or P-glycoprotein for influx and efflux(White et al., 2006). Nilotinib is 10-30 fold more potent than IM in inhibiting BCR-ABL activity and proliferation of BCR-ABL+ cells, and is effectively against 32/33 BCR-ABL mutations at physiologically relevant concentration(Kantarjian et al., 2007). Notably, a limited number of P-loop associated mutations, such as E255K and Y253H, causes resistance to Nilotinib, but can be suppressed by increased drug concentration(Jabbour et al., 2009). However, the loss of effectiveness against T315I mutation might be a consequence of the steric hindrance between the isoleucine-methyl group of BCR-ABL and 2-methylphenyl phenyl group of Nilotinib(Manley et al., 2005).

In contrast to most TKIs, which bind to the inactive confirmation of BCR-ABL, Dasatinib exclusively targets the active confirmation of ABL kinase, but with less stringent conformation requirement and reduced selectivity(Eck and Manley, 2009). It is noteworthy that this binding characteristic makes Dasatinib ~325-fold

more potent against wildtype BCR-ABL than IM and effectively against majority of BCR-ABL mutations except for T315I(Olivieri and Manzione, 2007). Dasatinib is also a highly potent inhibitor of SRC family kinases including FRG, FYN, HCK, LCK, LYN, and YES, and has activity against additional tyrosine kinases, such as KIT and PDGFR(Schittenhelm et al., 2006). This lack of selectivity is likely related to the similarity between the active conformation of BCR-ABL and SRC family kinases, therefore making Dasatinib a multi-target inhibitor of ABL and SRC kinases(Schittenhelm et al., 2006).

Ponatinib is derived from AP23464, one of Ariad's dual ABL/SRC inhibitor, and is the first TKI demonstrating effectiveness against T315I mutation(Cortes et al., 2012). Ponatinib possesses a linear structure, which possibly helps it avoid steric clashes with hydrophobic gatekeeper residues and making it a potent inhibitor of most of know BCR-ABL mutations, particularly T315I(O'Hare et al., 2009).

1.5 Drug resistance in CML

BCR-ABL dependent TKI resistance

Therapeutic efficacy of IM is often compromised by BCR-ABL mutations, and BCR-ABL gene amplification(Gorre et al., 2001). Clinically, at least 50% of IM resistant patients have detectable BCR-ABL mutations depending on the study(Lange et al., 2005). Up to now, there have been over 100 mutations found to be relevant to TKI resistance, most of these mutations are located at BCR-ABL kinase domain(Laboratory, 2007; Soverini et al., 2011) (Figure 1.1). Since these

mutant cells are still depending on BCR-ABL for survival, it is called BCR-ABL dependent TKI resistance(Bhamidipati et al., 2013).

Newly diagnosed CML or Ph+ ALL patients were usually prescribed with IM as first line therapy, and only switched to second generation inhibitor, Nilotinib or Dasatinib, when disease become refractory to IM due to resistant mutations(Weisberg et al., 2007). Although many of these mutations could be overcome by second generation inhibitors, sequential treatment does not always guarantee long-term disease remission. Patients often relapse due to acquired mutations at other amino acid positions, which blocks new TKIs again(Cortes et al., 2007). One of such mutations is the notorious gatekeeper mutation, T315I, which does not respond to either drug(Weisberg et al., 2007).

However, mutation from Threonine to Isoleucine at 315 AA position is not the only way causing resistance to Nilotinib or Dasatinib as revealed by several studies. And substitution of 315 position to Methionine even leads to resistance to Ponatinib, which was designed to inhibit T315I mutation(Zabriskie et al., 2014). In addition to such mutations at single amino acid position, which is likely due to selection of polyclonal mutations or sequential mutations(Zabriskie et al., 2014), acquired mutations at the second or third amino acid sites in the same BCR-ABL protein molecule, dubbed “compound mutations”, is another major cause of acquired resistance and disease relapse(Shah et al., 2007; Zabriskie et al., 2014).

BCR-ABL independent TKI resistance

The causes of TKI resistance in primary resistance cases are more diverse and complicated. Donato et al, established an IM resistant K562 cell line(K562R) by treating an IM sensitive K562 cell line with increasing dose of IM, and found that overexpression of an SRC family kinase, Lyn, being the main driver of resistance(Donato et al., 2003). This is further supported by the fact that K562R cells respond well to Dasatinib, which inhibits both BCR-ABL and SRC family kinases(Wu et al., 2008). Our recent work to identify genes involved in IM resistance using a genome-wide shRNA library revealed dozens of IM-sensitizing genes(Ma et al., 2014). Knocking down many of them using shRNA leads to IM resistance which is at least partially due to transcriptional upregulation of a PKC family member, PRKCH. Overexpression of PRKCH sustains the activity of MEK/ERK pathway upon IM treatment by directly phosphorylating and activating upstream CRAF. PRKCH/MAPK pathway was found to be a common resistance pathway in many BCR-ABL independent IM resistant cases.

It is thought that BCR-ABL inhibition is the trigger of cell death due to quick loss of pro-survival signals while gaining pro-apoptotic signals(Sharma et al., 2006). However, cell signaling is always responding in a network fashion, and compensatory pathways may be transiently activated to slow down or circumvent cell death program(Logue and Morrison, 2012), there by causing TKI resistance.

One of such examples is BCL6, which is an oncogene suppressed by JAK/STAT pathway. Upon TKI treatment, JAK/STAT pathway losses the activation signal from BCR-ABL, and releases the brake on BCL6, which then acts as an anti-apoptotic protein(Duy et al., 2011).

TKI Insensitivity and Mechanisms of CML stem cells

One attractive postulate of cancer therapy would be targeting these aberrant stem cells in order to prevent eradicate cancer. Although non-stem cancer cells are sensitive to variety of chemical or irradiation therapy, cancer stem cells are generally difficult to remove primarily due to its quiescent nature(Moore and Lyle, 2011; Saito et al., 2010).

IM, the first FDA approved tyrosine kinase inhibitor, inhibits BCR-ABL kinase activity and leads to CML cell death(An et al., 2010b), and has been the front-line therapy for chronic phase CML patients. Despite its great efficacy in suppressing CML progression, it can barely lead to a cure. Accumulating evidence reveals that CML stem cells remain alive even with effective inhibition of BCR-ABL activity by TKIs(Graham et al., 2002; Hamilton et al., 2012; Jiang et al., 2007), indicating that BCR-ABL itself is not an essential survival factor of CML stem cells in contrast to more differentiated CML cells. And CML often relapses after IM discontinuation and the relapse does not involve BCR-ABL mutation(Ross et al., 2013; Yhim et al., 2012), suggesting persistence of these residual CML stem cells.

Holyoke and colleagues first noted that IM treatment fails to kill all Lin-CD34+ cells isolated from peripheral blood of chronic phase CML patient(Graham et al., 2002). They observed that IM was able to kill all proliferating cells but a significant portion of cells, particularly the non-dividing CD34+ cells, were unaffected although confirmed to be leukemic. Additionally, CD34+ cells derived from bone marrow cells of CML patients under long-term IM therapy also demonstrate the presence of BCR-ABL transcripts (Bhatia et al., 2003). After further separation of CD34+ cells into progenitor (CD34+CD38+) and stem cell(CD34+CD38-) population, Jiang and colleagues demonstrated that CD34+CD38- population showed significantly less sensitivity to IM treatment in the presence or absence of growth factors(Jiang et al., 2007). Druker and colleagues also showed that IM treatment is capable of inhibiting tyrosine phosphorylation using intracellular phospho-staining. CRKL and STAT5 phosphorylation in FACS-isolated CD34+CD38- cells is also efficiently inhibited using immunohistochemistry(Corbin et al., 2011). However, cell viability is not significantly affected in the presence or absence of growth factors(Corbin et al., 2011).

Similar to what is observed in human CML stem cells, TKI also showed minimal effect on Leukemic Stem Cells (LSCs) from CML mouse model(Hamilton et al., 2012; Ma et al., 2014). Oral administration of IM in CML mice significantly reduced the accumulation of leukemic cells in peripheral blood and prolongs

animal survival, however, it does not reduce the percentage or number of BCR-ABL+ Lin-Sca1+Kit+ cells, and did not induce significant level of apoptosis in LSK cells either(Ma et al., 2014). Both *in vitro* and *in vivo* studies reported that second generation inhibitor, Dasatinib, is moderately effective in inducing apoptosis and suppressing LSCs expansion in CML mice, but remain incapable of eradicating LSCs(Hamilton et al., 2012). Most importantly, the side population (GFP+CD34-c-Kit+Hoe-) from bone marrow cells of TKI-treated CML mice could still be serially transplanted to recipient mice(Hu et al., 2006). And IM, even the second generation inhibitor Dasatinb, treated mice eventually succumbed to CML. Collectively, all these studies suggest that the residual CML stem cells are not addicted to BCR-ABL for their survival.

Up to now, many studies have revealed critical pathways for maintenance of CML stem cells. For example, Wnt/β-catenin pathway has been shown to be required for the self-renewal and differentiation of normal HSC and also leukemic stem cells(Zhao et al., 2007). Microarray analysis of gene expression in mouse HSCs, CML stem cells(Lin-Sca1+Kit+GFP+) treated with placebo or IM revealed Alox5 as a LSC specific maintenance gene(Chen et al., 2009). PRKCH mediated MAPK activation also contributes to IM insensitivity of CML stem cells(Ma et al., 2014). Most recently, the gene expression and proteomic network analysis of CML stem cells demonstrates the deregulation of p53 and c-Myc signaling network(Abraham et al., 2016). Maintenance of p53 stability and inhibition of c-Myc expression using small molecules markedly increased CML stem cell death,

and engraftment in NSG mice. Other signaling pathways related to IM resistance of CML stem cells includes hedgehog(Zhao et al., 2009), TGF-FOXO(Naka et al., 2010), BCL6(Hurtz et al., 2011), and HIF1α(Wang et al., 2011).

1.6 Current technologies to study drug resistance in CML and CML stem cells.

Genome-wide RNA interference screen

RNA interference (RNAi) is a mechanism by which expression of a specific gene is post-transcriptionally inhibited. RNAi is mediated by a double-stranded RNA, which recognizes and induces sequence-specific degradation of the corresponding mRNA, resulting in silencing or “knocking down” the gene. The development of RNAi as a genetic tool initially held great promise for analyzing loss-of-function phenotypes in mammalian cells using high-throughput, unbiased, function-based genetic screens. However, it was not until the development of RNAi expression libraries about 10 years ago(Berns et al., 2004; Kittler et al., 2004; MacKeigan et al., 2005; Paddison et al., 2004) that such large-scale screens became feasible. Using these and other RNAi libraries, many studies have uncovered previously unappreciated genes and mechanisms involved in diverse biological processes in mammalian cells, particularly in the context of cancer, such as unknown tumor suppressor genes (Gobeil et al., 2008; Zender et

al., 2008), synthetic lethal interactions (Luo et al., 2009), and potential drug targets (Ngo et al., 2006; Zuber et al., 2011).

Today, a wide variety of RNAi libraries are commercially available. These libraries typically use a lentiviral vector to express a chimeric short hairpin RNA (shRNA), which is subsequently processed into a small interfering RNA (siRNA) to induce target mRNA degradation (Moffat et al., 2006; Paddison et al., 2002). Lentiviral-based libraries have high titers and broad trophism, making them suitable for use in a variety of mammalian cell types. Each shRNA in the library contains an easily sequenced barcode, which enable unambiguous identification of the shRNA. The genome-wide screen described in this protocol uses the human lentiviral shRNA library from The RNAi Consortium (TRC), which has ~85,000 shRNA constructs with 3-5 shRNAs per gene, targeting ~22,000 human genes (Moffat et al., 2006; Root et al., 2006). To facilitate screening such a large number of shRNAs, we have divided the library into “pools”, with ~5000 shRNAs per pool for a total of 22 pools.

BCR-ABL mutation-independent resistance to TKIs frequently occurs in CML (Donato et al., 2004; Khorashad et al., 2006; Quintas-Cardama et al., 2009). Identifying TKI resistance-related genes helps increase our knowledge of how resistance occurs and may lead to the development of better therapeutic strategies for CML. As an example, in chapter II, we employed a genome-wide

screening strategy in a human CML cell line to identify genes involved in resistance to the first generation TKI, IM (Ma et al., 2014).

Single cell RNA-sequencing

Global gene expression analysis has been widely used to profile cell differentiation, therapeutic and disease related gene expression changes(Golub et al., 1999; Gu et al., 2004). Microarray and RNA-sequencing (RNA-seq) is two major ways of achieving this purpose(Schena et al., 1995; Wang et al., 2009). Traditionally, in order to obtain reliable and reproducible data, microarray requires microgram level of total RNA as input material, while RNA-seq requires substantially less but still significant initial amount for depletion of ribosome RNA. In contrast to microarray, which are covered by pre-designed probes for a known number of genes, RNA-seq is more powerful in identifying splicing variants, isoforms and new genes. Additionally, mRNA-seq provides a larger dynamic range than microarray, therefore, more likely to capture subtle gene expression difference(Fu et al., 2009; Marioni et al., 2008).

However, total RNA used for global gene expression analysis is typically extracted from bulk cell population comprising phenotypically similar but likely functionally distinct cells. The development of ultra-low input RNA-seq technology allows for transcriptome analysis at single cell level to address many new and longstanding questions, such as revealing functional heterogeneity within a phenotypically homogeneous population, refining lineage relationships

defined previously by cell surface marker system, and identifying rare cell types, etc(Patel et al., 2014; Tang et al., 2010; Zeisel et al., 2015).

The first integrated study of single cell analysis dates back to 2002, when Klein and colleagues used microarray readout to study single micrometastic cells(Klein et al., 2002). In 2009, Surani and colleagues reported the first single cell RNA-seq analysis using oocytes and blastomeres which are relatively easy to manipulate compare to more differentiated cells because of relative abundance of mRNA molecules(Tang et al., 2009).

Up to now, multiple single cell mRNA-seq protocols have been developed for all cell types, such as smart-seq(Ramskold et al., 2012), CEL-seq(Hashimshony et al., 2012), STRT(Islam et al., 2011), Drop-seq/Indrop(Klein et al., 2015; Macosko et al., 2015), each having its own pros and cons. Smart-seq protocol was selected for the current thesis study and described in more detail below. Smart-seq was first developed by Sandberg lab and published in 2012. What makes it stand out is its capability of generating more full-length cDNA. By further optimizing the conditions and essential reagents, an updated protocol, Smart-seq2, was released with improved yield and length of cDNA libraries for individual cells(Picelli et al., 2013). In this improved protocol, single cells were collected and lysed in a relatively mild hypotonic lysis buffer, which does not interfere with RT reaction. Full-length cDNA synthesis and amplification was achieved through a template-switching reaction which relies on a Moloney

Murine Leukemia Virus (M-MLV) based reverse transcriptase and a Locked Nucleic Acids (LNA)-containing template switching oligo(Krivtsov et al.). M-MLV typically adds 2-5 non-templated cytosine to the cDNA 3'end(Schmidt and Mueller, 1999). Similar to the original TSO containing three riboguanosines, Smart-seq2 TSO carries two riboguanosines and one modified guanosine at last position to produce a LNA but with enhanced thermostability and binding strength. Once template switching and synthesis of full-length first-strand cDNA is done, an artificial sequence introduced at both end of the cDNA will serve as binding site of ISPCR primer for subsequent PCR pre-amplification. cDNA is amplified using a limited number of cycles, usually 18 cycles for a single mammalian cell or as many as needed to get enough material for following reactions. Given that only low nanogram level of cDNA could be obtained from a typical single cell, conventional biorupter or mechanic-based physical shearing and barcoding methods is not a practical option. In this ultralow input scenario, a TN5 transposase-based tagementation and barcoding strategy was employed to construct cDNA library for deep-sequencing(Gertz et al., 2012). Briefly, TN5 transposase was preassembled with two double-stranded oligonucleotides carrying illumina adapter sequences. Incubation of TN5 transposases with cDNAs from each cell will result in unbiased fragmentation and insertion of adapter with unique barcodes at a single step. After PCR enrichment and purification, a library spanning 200-1kb but centralized at ~500bp could be obtained.

Illumina dual-index strategy provides an option of high-multiplexing by using index1 (i5) and index2 (i7) for the enrichment PCR then pooling 96~384 cDNA libraries together on a single lane for deep-sequencing. The new generation of illumina table-top sequencer, Nextseq, offers a fast and economical way of sequencing hundreds of cells on a single lane and a high yield of up to 500 million total reads, usually with >70% alignment efficiency.

Conventional study using genetically unrelated individuals shows extensive gene expression variation(Cheung et al., 2003). Variability of drug response among patients has long been known to be attributed to such individual variances(Roden and George, 2002). Profiling gene expression in paired normal and disease samples from the same patient would be helpful to circumvent such genetic variability, patient-specific and common drug targets could be identified through intra-sample and inter-sample comparison. However, this strategy has often been hampered by the inability to completely separate normal and disease cells due to factors, such as phenotypic similarity(Carter et al., 2010).

In this case, single cell RNA-seq offers a unique advantage to clearly separate disease cells from normal cells based on definitive molecular markers of individual cells. As an example, in chapter III, we use CML as a model, and report clear separation of normal hematopoietic stem cells (HSCs) from CML stem cells (CMLSCs) based on a unique molecular marker in CML, the fusion oncogene BCR-ABL, and performed gene expression profiling in both population

using single cell RNA-seq.

High-throughput and Saturated point mutagenesis

Genetic mutation is one of the major evolution forces shaping the fitness a particular gene or even the whole organism(Kacser and Beeby, 1984; Mitchell-Olds et al., 2007). While most mutations are neutral, and are passed onto the progenies by random genetic drift, certain mutations could be deleterious, and be depleted during evolution(Charlesworth et al., 1993; Kimura, 1979). However, upon environmental changes or the presence of selection pressure, such as addition of antibiotics or kinase inhibitors, some of the non-advantageous mutations may be adapted to the new condition, therefore enriched and preserved(Eyre-Walker and Keightley, 2007; Nielsen, 2005). Conventionally, random mutagenesis was performed using UV exposure in bacteria or carcinogen exposure in mammalian cells, but this mutagenesis is far from saturation(Sarasin, 2003; Witkin, 1976). It is usually more controllable over a small genomic region or a particular gene than a whole genome. Error-prone PCR(Fujii et al., 2004) or DNA-repair deficient bacteria(Greener et al., 1997) were often employed to reach a high level coverage of mutagenesis for such study. Despite extensive coverage, none of these methods were able to offer a fully controlled condition and equal representation of each mutation for systematic evaluation of the contribution of each mutation to the cell fitness or a particular phenotype.

To overcome these drawbacks, research group led by Dr. Bolon at UMass Medical School developed a method which they refer to as EMPIRIC(exceedingly methodical and parallel investigation of randomized individual codons) for systematic generation of all possible point mutations in regions of an important gene and quantification of the fitness effect of each mutants(Hietpas et al., 2011).

In this method, a 10 amino acid(AA) region is randomized to all possible codons(Hietpas et al., 2012). Two complementary 40-base long oligonucleotides were synthesized with 30 bases for a 10aa region flanked by a 3-base cohesive end for annealing into expression vector. Each double-stranded oligo bears a degenerate codon(i.e., NNN) at desired position on both strands. The library size for a single randomized codon is 64, and 640 for the 10AA region. Typically, 10 fold or greater coverage is required for confident assessment of all mutants in the library. To increase the throughput and recovery rate, hundreds of mutations in a single bulk competition experiment were analyzed at once by deep-sequencing to accurately measure the relative abundance of each mutation(Hietpas et al., 2012).

However, several drawbacks remain unsolved with the saturated mutagenesis strategy in mammalian cells because of the inherent characteristics of retroviral delivery method, particularly, inconsistent gene expression resulted from random integration(Day et al., 2000).

CRISPR-Cas9 mediated genome editing for improved mutagenesis

Programmable endonucleases, such as zinc-finger nucleases (ZFNs), transcription activator-like effector nucleases (TALENs) or clustered regularly interspaced short palindromic repeat (CRISPR)-Cas9 based RNA-guided DNA endonucleases, offer a practical and accurate way of genome editing(Gaj et al., 2013). Among them, the CRISPR-Cas9 system could easily target any genomic region of interest by customizing the short guide-RNA(sgRNA) sequence.

The CRISPR-Cas9 system was first discovered and derived from bacteria, *Streptococcus pyogenes(Hsu et al., 2014; Jinek et al., 2012),* as a bacteria defense system for eliminating of exogenous DNA. Guide-RNA associated Cas9 nuclease locates the target DNA sequence by searching for a PAM (NGG) element followed by formation of a heteroduplex between the guide and the complementary DNA sequence (Jinek et al., 2012). Once activated, a Cas9-induced double strand break(DSB) is usually introduced between the 3rd and 4th nucleotide position 5' of the PAM sequence(Tsai et al., 2015). While in most cases, such DSB will be fixed by non-homologous end-joining(NHEJ) pathway, resulting in mini-insertion or deletion(indels) which could disrupt normal gene function by causing frame-shift and formation of pre-mature stop codon(Rothkamm et al., 2003). In the presence of a DNA template with suitable homology arms flanking the target region, a subset of DSB can be fixed by utilizing this exogenous donor DNA as a repair template via the homology directed repair (HDR) pathway(Liang et al., 1998). This process results in tailor-

made sequence alterations at the target locus that are dictated by the contents of the repair template (Cong et al., 2013; Sander and Joung, 2014).

When the DSB is fixed by HDR pathway, only a single donor plasmid will be used as template due to the requirement of paired homology arms. This fact raises the possibility of introducing a library of pre-defined templates into a single genomic location in a cell population, with each cell fixed by only one template. Recently, Findlay et al successfully performed a saturated mutagenesis at a specific genomic locus, the first 6 bases of BRCA1 exon, using a random hexamer library by leveraging the CRISPR-Cas9 system and associated HDR mechanism(Findlay et al., 2014). This CRISPR-Cas9 based saturated mutagenesis strategy was conducted in a completely endogenous condition, therefore providing the most physiologically relevant information for mutation induced phenotypic variation. However, the short length of their donor library, only randomizing a hexamer region, poses a big limit on its application.

As an example, in chapter VI, we describe the development of an improved and more flexible CRISPR-Cas9 HDR-based strategy for a large-scale saturation mutagenesis screen in Ba/F3 cells, its application to analyze fitness landscape and TKI resistance of BCR-ABL mutations, and its capability to reveal clinically relevant and meaningful mutations with minimal false positive rates.

1.7 Focus of this dissertation

This dissertation focuses on drug resistance in CML. Three major aspects of drug resistance are studied: 1, RNA inference screen was performed to study BCR-ABL independent drug resistance mechanism and exploit new therapeutic strategies. 2, Single cell RNA-seq was conducted to profile gene expression heterogeneity in primary CML stem cell population and reveal common therapeutic targets to eradicate CML stem cells. 3, An improved saturated point mutagenesis strategy was devised using CRISPR-Cas9 to more precisely evaluate contribution of each amino acid substitution to BCR-ABL function and fitness with or without drug selection pressure.

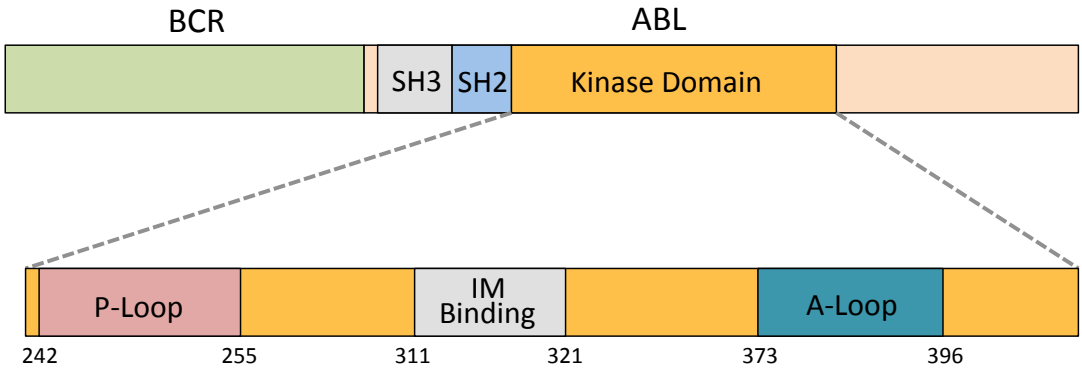

M236E	E275K	F311L/I/V	L324Q	V379I	A397P
M237I	D276G	**T315I**/N	M343T	F382L	S417Y
M244V	T277A/N	**F317L**	A344V	G383D	I418V
K247R	E279K	Y320C	S348L	L387F/M	S438C
L248V	E281A		A350V	M388L	Q447R
G250E/A/F	K285N		**M351T**/L	**H396R**/P	E450G/Q/K
Q252H	V289A/I		**E355G**/D		E453G/K/A/V
Y253H/F	E292V		K357R		E459K/Q
E255K/V	L298V		**F359V**/C/I		M472I
	V299L		L364I		F486S

Figure 1.1. Schematic illustration of functional domains in BCR-ABL and location of clinically identified mutations associated with IM resistance. Mutations with 2-10% frequency are highlighted in **bold**, while those with >10% frequency are in **red**. P-loop: phosphate binding loop; IM binding: imatinib binding region; and A-loop: activation loop. Data were collated from (Hughes et al., 2006; Jones et al., 2009; Soverini et al., 2011)

CHAPTER II: A THERAPEUTICALLY TARGETABLE MECHANISM OF BCR-ABL-INDEPENDENT IMATINIB RESISTANCE IN CHRONIC MYELOID LEUKEMIA

ABSTRACT

Resistance to the BCR-ABL inhibitor imatinib mesylate (IM) poses a major problem for the treatment of chronic myeloid leukemia (CML). IM resistance often results from a secondary mutation in BCR-ABL that interferes with drug binding. However, in many instances there is no mutation in BCR-ABL, and the basis of such BCR-ABL-independent IM resistance remains to be elucidated. To gain insight into BCR-ABL-independent IM resistance mechanisms, we performed a large-scale RNA interference (RNAi) screen and identified IM-sensitizing genes (IMSGs) whose knockdown renders BCR-ABL+ cells IM-resistant. In these IMSG knockdown cells, RAF/MEK/ERK signaling is sustained after IM treatment due to upregulation of *PRKCH*, which encodes the protein kinase C (PKC) family member PKCη, an activator of CRAF. *PRKCH* is also upregulated in samples from CML patients with BCR-ABL-independent IM resistance. Combined treatment with IM and trametinib, an FDA-approved MEK inhibitor, synergistically kills BCR-ABL+ IMSG knockdown cells and prolongs survival in mouse models of BCR-ABL-independent IM-resistant CML. Finally, we showed that CML stem cells contain high levels of *PRKCH* and this contributes to their intrinsic IM resistance. Combined treatment with IM and trametinib synergistically kills CML stem cells with negligible effect on normal hematopoietic stem cells. Collectively,

our results identify a therapeutically targetable mechanism of BCR-ABL-independent IM resistance in CML and CML stem cells.

INTRODUCTION

Chronic myeloid leukemia **(**CML) is a hematopoietic malignancy characterized by an increase and unregulated growth of predominantly myeloid cells in the bone marrow, and their accumulation in the blood (Faderl et al., 1999). A hallmark of CML is the Philadelphia chromosome, resulting from a reciprocal translocation between the long arms of chromosomes 9 and 22 (Deininger et al., 2000; Kurzrock et al., 2003). This chromosomal translocation leads to expression of BCR-ABL, an oncogenic fusion protein with a constitutively activated ABL tyrosine kinase. BCR-ABL can transform myeloid progenitor cells and drives the development of 95% of CML cases. BCR-ABL promotes leukemogenesis by activating downstream signaling proteins that increase cell survival and proliferation (Colicelli, 2010). These pathways include, but are not limited to, the RAS/mitogen-activated protein kinase (RAF/MEK/ERK), phosphatidylinositol 3-kinase/AKT (PI3K/AKT), and JAK/STAT signaling cascades (Steelman et al., 2004).

The first-line treatment for CML is imatinib mesylate (IM), which binds to the ABL kinase domain and inhibits phosphorylation of substrates (An et al., 2010a). Although IM dramatically improves patient survival when used to treat early-stage disease, the drug is not curative. Resistance to IM can develop, especially in advanced-stage disease, leading to disease relapse and progression (von Bubnoff et al., 2003). Resistance to IM can result from multiple mechanisms that can be broadly classified as either BCR-ABL-dependent or

BCR-ABL-independent (Quintas-Cardama et al., 2009). BCR-ABL-dependent resistance is most commonly due to the acquisition of point mutations in the ABL kinase domain that interfere with IM binding and subsequent kinase inhibition (Jabbour et al., 2006; Shah et al., 2002; Weisberg et al., 2007). However, in 50% or more of IM-resistant CML patients there is no mutation in BCR-ABL (Donato et al., 2004; Khorashad et al., 2006), and the basis of such BCR-ABL-independent IM resistance is not understood.

CML, like several other malignancies, is propagated by a small population of stem cells, elimination of which is likely required to achieve long-term remission and cure (Dean et al., 2005; Graham et al., 2002). An important limitation of IM treatment is that although IM inhibits BCR-ABL activity in CML stem cells, these cells do not depend on BCR-ABL activity for survival and are thus not eliminated (Corbin et al., 2011; Hamilton et al., 2012). These findings imply that CML stem cells use survival signals other than BCR-ABL to maintain viability in the presence of IM. Understanding the mechanism by which CML stem cells are intrinsically resistant to IM is essential for devising strategies to eradicate residual leukemia. To gain insight into how IM resistance can occur in the absence of BCR-ABL mutations, we performed an RNA interference (RNAi) screen to identify genes that regulate IM responsiveness. Our results reveal a survival pathway that promotes BCR-ABL-independent IM resistance and also contributes to the IM resistance of CML stem cells.

RESULTS

A large-scale shRNA screen identifies IM-sensitizing genes

To identify IM-sensitizing genes (IMSGs), IM-sensitive human CML K562 cells (Andersson et al., 1979) were stably transduced with pools of a genome-wide human short hairpin (shRNA) library (Silva et al., 2005) followed by IM treatment (Figure 2.1 a). Surviving cells from all pools were combined, and shRNAs corresponding to 89 genes were identified by sequence analysis. Validation experiments with individual shRNAs corresponding to those isolated from the primary screen, as well as second, unrelated shRNAs targeting the same genes, confirmed that knockdown of 25 genes conferred >2-fold increased K562 cell survival in the presence of IM relative to a control non-silencing (NS) shRNA (Figure 2.1 b and Figure 2.2 and Figure 2. 3 a). The extent of IM resistance after IMSG knockdown was roughly similar to that of the well-studied experimentally-derived IM-resistant cell line K562R and an IM-resistant patient-derived cell line, SUPB15 (Figure 2.3 b). Quantitative real-time RT-PCR (qRT-PCR) confirmed in all cases that expression of the target gene was decreased in the corresponding K562 knockdown (KD) cell line (Figure 2.3 c-d).

To confirm that our results are generalizable, we analyzed the validated candidates in KYO-1 cells, another IM-sensitive human CML cell line (Ohkubo et al., 1985). Figure 2.1 c shows that 21 of the 25 shRNA candidates validated in KYO-1 cells. Finally, we tested whether knockdown of the validated candidates

would also confer IM resistance in BCR-ABL+ mouse primary bone marrow cells. Toward this end, we induced CML-like disease in C57BL/6 mice with a BCR-ABL-expressing retrovirus (Daley et al., 1990; Li et al., 1999). Primary bone marrow cells were harvested, infected with a mouse candidate IMSG shRNA, and tested for their ability to form colonies in methylcellulose containing IM. We found that knockdown of 19 candidate IMSGs (Figure 2.4 a) rendered BCR-ABL+ primary bone marrow cells IM-resistant (Figure 2.1 d). Equivalent results were obtained with a second, unrelated shRNA for each IMSG (Figure 2.4. b and c).

To quantify IM resistance, we determined the IC50 for imatinib ($IC50^{IM}$) of IMSG KD K562 cells. Knockdown of 11 IMSGs increased the $IC50^{IM}$ greater than 5-fold (Figure 2.1 e and Figure 2.5), and we therefore focused on these IMSGs in our subsequent experiments. Notably, the $IC50^{IM}$s of these 11 IMSG KD K562 cell lines are similar to those of IM-resistant cell lines derived from CML patients (Quentmeier et al., 2011). These 11 IMSGs are involved in diverse biological processes including transcriptional regulation, signal transduction, protein metabolism and DNA/RNA metabolism (Table 2.1).

Next, we tested whether knockdown of IMSGs would cause resistance to the second-generation tyrosine kinase inhibitor, dasatinib (Shah et al., 2004). As a control, we analyzed in parallel K562R cells, which are resistant to IM but sensitive to dasatinib due to over-expression of the Src family kinase (SFK) LYN

(Donato et al., 2003). All of the IMSG shRNAs that conferred IM resistance also caused resistance to dasatinib (Figure 2.1 f).

Knockdown of IMSGs in BCR-ABL+ cells results in sustained RAF/MEK/ERK signaling after IM treatment

We next performed a series of experiments to identify the regulatory pathway(s) through which IMSGs promote IM sensitivity. IMSG KD K562 cell lines were cultured in the presence or absence of IM followed by immunoblotting for characteristic markers of relevant cell signaling pathways. The results in Figure 2.6 indicate that knockdown of IMSGs had no effect on total BCR-ABL. Moreover, in all IMSG KD K562 cell lines, IM inhibited BCR-ABL protein kinase activity, as evidenced by decreased BCR-ABL autophosphorylation and decreased phosphorylation of the BCR-ABL substrate CRKL (ten Hoeve et al., 1994). We also monitored the effect of IMSG knockdown on SFK activity, whose elevation, as mentioned above, is responsible for IM resistance in K562R cells. None of the IMSG KD K562 cell lines had elevated SFK activity or expression, consistent with their resistance to dasatinib.

We next analyzed the effect of IMSG knockdown on known downstream signaling pathways of BCR-ABL. All IMSG KD K562 cell lines had normal amounts of phosphorylated STAT5 and AKT, indicating that JAK/STAT and PI3K/AKT signaling pathways were not affected by IMSG knockdown. In

contrast, most of the IMSG KD K562 cell lines had increased RAF/MEK/ERK kinase pathway activity, as evidenced by elevated phosphorylation of ERK1/2. As expected, after IM treatment of control K562 cells, there was a substantial decrease in phosphorylated ERK1/2. However, all of the IMSG KD K562 cell lines had, to varying extents, sustained phosphorylation of ERK1/2 after IM treatment. Thus, in IMSG KD K562 cell lines, there is an alternative pathway that activates RAF/MEK/ERK signaling after inhibition of BCR-ABL.

Previous studies have reported that the protein kinase C (PKC) pathway can stimulate RAF/MEK/ERK signaling (Takahashi et al., 1999; Ueda et al., 1996; Uht et al., 2007). We therefore analyzed PKC pathway activity in IMSG KD K562 cells by monitoring phosphorylation of a universal PKC substrate, MARCKS (Aderem, 1992). Phosphorylation of MARCKS was elevated in all IMSG KD K562 cell lines, indicating increased PKC activity.

PRKCH is upregulated in BCR-ABL-independent IM-resistant CML cell lines and patient samples

Next, we sought to identify the PKC family member(s) responsible for the increased PKC activity. The qRT-PCR results in Figure 2.7 a show that *PRKCH*, which encodes PKCη, was upregulated in nearly all IMSG KD K562 cell lines. Similar results were obtained with a second shRNA targeting each IMSG (Figure

2.8 a). Immunoblot analysis confirmed that PKCη protein levels were also increased in the IMSG KD K562 cell lines (Figure 2.8 b).

As a first step toward understanding the basis by which IMSGs regulate *PRKCH* expression, we further analyzed one of the IMSGs, *ELF5*, a known transcriptional repressor (Chakrabarti et al., 2012; Escamilla-Hernandez et al., 2010). We used a chromatin immunoprecipitation assay and found that ELF5 was directly bound at the transcription start site of *PRKCH* (Figure 2.9 a), consistent with the results of a study analyzing ELF5 occupancy genome-wide (Kalyuga et al., 2012). Moreover, we found that expression of a *PRKCH* promoter-luciferase reporter construct was increased by *ELF5* knockdown and, conversely, decreased by ectopic expression of *ELF5* (Figure 2.9 b and c). Thus, ELF5 is a direct transcriptional repressor of *PRKCH*, explaining why decreased ELF5 levels result in increased *PRKCH* expression.

To verify that increased PKCη expression is responsible for the IM resistance, we derived K562 cell lines that over-expressed *PRKCH* (K562/*PRKCH* cells) to varying degrees. In several K562/*PRKCH* cell lines, PKCη levels were comparable to those found in IMSG KD K562 cells (Figure 2.10 a). The elevated *PRKCH* expression resulted in a 10–20-fold increase in IM resistance (Figure 2.7 b). Conversely, knockdown of *PRKCH* abrogated the IM resistance of representative IMSG KD K562 cell lines (Figure 2.10 b).

To determine the clinical relevance of these results, we analyzed *PRKCH* mRNA levels in IM-resistant CML patient samples harboring wild-type BCR-ABL. As a control, we also analyzed *PRKCH* mRNA levels in IM-resistant CML patient samples that contained a known IM-resistance mutation in BCR-ABL (Table 2.2). The results in Figure 2.7 c show that *PRKCH* mRNA levels were significantly (P<0.01) higher in IM-resistant CML patient samples containing wild-type BCR-ABL compared to those with mutant BCR-ABL. In addition, we found that the average expression of three IMSGs (*CLEC5A*, *ELF5*, and *WNT7B*) was significantly (P<0.01, <0.05, <0.05, respectively) lower in IM-resistant CML patient samples containing wild-type BCR-ABL compared to those with mutant BCR-ABL (Figure 2.7 d). Moreover, in all 11 IM-resistant CML patient samples containing wild-type BCR-ABL, at least one IMSG was down-regulated >2-fold, and in 9/11 samples at least one IMSG was down-regulated >5-fold relative to the average expression in IM-resistant mutant BCR-ABL samples (Table 2.3). Finally, the results in Figure 2.7 e show that knockdown of *PRKCH* increased IM sensitivity of leukemic cells from BCR-ABL-independent IM-resistant CML patients.

PKCη increases RAF/MEK/ERK signaling through phosphorylation and activation of CRAF

We next sought to understand in greater detail how PKCη increased RAF/MEK/ERK signaling. Figure 2.7 f shows that even a relatively modest

knockdown of *PRKCH* in IM-sensitive K562 cells decreased both phosphorylated MEK and ERK1/2 (see also Figure 2.11 a) and increased IM sensitivity (Figure 2.10 b). Conversely, K562/*PRKCH* cells had increased levels of both phosphorylated MEK and ERK1/2 (Figure 2.7 f). Most importantly, K562/*PRKCH* cells maintained high levels of phosphorylated MEK and ERK1/2 after IM treatment (Figure 2.7 f).

The finding that PKCη affected both phosphorylated MEK and ERK1/2 indicated that PKCη functioned upstream of MEK by, for example, stimulating RAF activity. There are three known RAF kinases: ARAF, BRAF, and CRAF (Wellbrock et al., 2004). We found that in K562/*PRKCH* cells, knockdown of *CRAF*, but not *ARAF* or *BRAF*, decreased phosphorylatedERK1/2 (Figure 2.7 g and Figure 2.11 b). Most importantly, in IM-treated K562/*PRKCH* cells, knockdown of *CRAF*, but not *ARAF* or *BRAF*, resulted in loss of sustained phosphorylation of ERK1/2.

To determine whether CRAF was a direct substrate of PKCη, we derived a glutathione-S-transferase (GST) fusion-protein containing a CRAF peptide bearing a potential PKC phosphorylation site at S497/S499 (Carroll and May, 1994; Kolch et al., 1993). The *in vitro* kinase assay in Figure 2.7 h shows that wild-type PKCη, but not a kinase-dead mutant (K384R) (Suzuki et al., 2009), could phosphorylate the CRAF S497/S499 site. Our results are consistent with

several previous findings including phosphorylation of CRAF by PKC isoforms (Cai et al., 1997; Carroll and May, 1994; Kolch et al., 1993; Schonwasser et al., 1998; Sozeri et al., 1992) and reduced activity of a CRAF S497A/S499A mutant (Cai et al., 1997; Kolch et al., 1993).

IM and a MEK inhibitor synergistically kill BCR-ABL-independent IM-resistant CML cells

The results presented above show that BCR-ABL-independent IM resistance can result from increased *PRKCH* expression, leading to sustained RAF/MEK/ERK signaling after IM treatment. An implication of this conclusion is that simultaneous inhibition of BCR-ABL and RAF/MEK/ERK signaling might efficiently kill BCR-ABL-independent IM-resistant CML cells. To investigate this possibility, we analyzed the effect of combining IM treatment with the FDA-approved MEK inhibitor trametinib (also called GSK1120212). We found that treatment with both IM and trametinib had a substantially greater effect than either drug alone in killing K562/*PRKCH* cells (Figure 2.12 a), representative IMSG KD K562 cell lines (Figure 2.12 b), and BCR-ABL+ mouse primary bone marrow cells over-expressing *Prkch* (Figure 2.12 c). In most instances, the effect of combined drug treatment was synergistic. The modest effect of trametinib alone on K562 cell lines likely reflects stimulation of RAF/MEK/ERK signaling by BCR-ABL. Finally, treatment with both IM and trametinib had a significantly (P<0.01) greater effect than either drug alone in killing primary leukemic cells from BCR-ABL-

independent IM-resistant CML patients (Figure 2.12 d and Figure 2.13 a), Moreover, these leukemic cells were killed more effectively by combined treatment with IM and trametinib than by IM and a JAK-STAT or PI3K inhibitor, and neither of these latter two drug combinations were significantly more effective than IM alone (Figure 2.13 b).

IM and a MEK inhibitor prolong survival in mouse models of BCR-ABL-independent IM-resistant CML

Based upon the cell culture results, we analyzed the ability of this drug combination to prolong survival in mouse models of BCR-ABL-independent IM-resistant CML. Briefly, mouse primary bone marrow cells were transduced with a retrovirus co-expressing BCR-ABL and either *Prkch* (Figure 2.14 a) or an shRNA targeting one of two representative IMSGs, *Clec5a* or *Elf5* (Figure 2.14 b-d), followed by transplantation into lethally irradiated syngeneic mice. We found that combined treatment with IM and trametinib was substantially more effective than either drug alone at suppressing leukemic progression, as evidenced by a reduced white blood cell count (Figure 2.12 e and f), and prolonged survival (Figure 2.12 g and h).

***PRKCH* modulates proliferation of BCR-ABL+ cells, disease progression, and IM sensitivity**

The finding that knockdown of *PRKCH* in K562 cells reduced phosphorylated ERK1/2 (Figure 2.7 f) raised the possibility that *PRKCH* might modulate the

proliferation and survival of BCR-ABL+ cells and thus affect disease progression. To investigate this possibility, we transduced mouse primary bone marrow cells with a retrovirus co-expressing BCR-ABL and a *Prkch* shRNA (Figure 2.15 a**)**. *Prkch* knockdown decreased phosphorylated ERK1/2, similar to the results in K562 cells. Figure 2.15 b shows that knockdown of *Prkch* (Figure 2.16 a) reduced the ability of untreated BCR-ABL+ mouse primary bone marrow cells to form colonies in methylcellulose (see also Figure 2.16 b). Moreover, the colony formation assay in Figure 2.15 c shows that knockdown of *Prkch* markedly increased the IM sensitivity of BCR-ABL+ mouse primary bone marrow cells.

We next transplanted the *Prkch* KD bone marrow cells into syngeneic mice to induce CML-like disease and analyzed the effect of *Prkch* knockdown on leukemic progression. We found that in untreated mice *Prkch* knockdown resulted in a lower white blood cell count (Figure 2.15 d), reduced spleen size (Figure 2.15 e), decreased infiltration of the lung and spleen by leukemic cells (Figure 2.15 f), and an increase in survival (Figure 2.15 g). Thus, in the absence of IM treatment, *PRKCH* promotes disease progression, although this effect may be relatively minor. More importantly, knockdown of *Prkch* markedly increased survival of IM-treated mice with CML-like disease (Figure 2.15 g).

IM-resistant murine and human CML stem cells contain high levels of *PRKCH*

We considered the possibility that *PRKCH* might contribute to the intrinsic resistance of CML stem cells to IM. To investigate this idea, we induced CML-like disease in mice and isolated BCR-ABL+ murine stem cells (Lin-Sca1+Kit+), progenitor cells (Lin-) and mature cells (Lin+Gr1+) by fluorescence activated cell sorting (FACS) (Hamilton et al., 2012; Neering et al., 2007). The qRT-PCR results in Figure 2.17 a show that IM-resistant murine CML stem cells ((Hamilton et al., 2012; Zhang et al., 2010; Zhang et al., 2012) and see below) had substantially higher expression of *Prkch* compared to murine CML progenitor and mature cells, both of which are IM-sensitive ((Hamilton et al., 2012; Li et al., 2012) and Figure 2.18).

We next asked whether *PRKCH* expression was also high in human CML stem cells. We isolated CML stem cells (CD34+CD38-) and CML progenitor cells (CD34+CD38+) (Corbin et al., 2011; Jiang et al., 2007; Lobo et al., 2007) from newly diagnosed CML patients. The qRT-PCR results in Figure 2.17 b show that IM-resistant human CML stem cells ((Bhatia et al., 2003; Chomel et al., 2011; Corbin et al., 2011; Graham et al., 2002; Pellicano et al., 2014) and see below) had substantially higher expression of *PRKCH* compared to human CML progenitor cells, which are IM-sensitive (Corbin et al., 2011; Jiang et al., 2007). Analysis of a published expression profiling study comparing highly enriched human CML stem and progenitor cell populations (Gerber et al., 2013) revealed similar differences in *PRKCH* expression (Figure 2.17 c). Microarray analysis

indicates that *PRKCH* expression is much higher in hematopoietic stem cells than in mature myeloid cells (Bagger et al., 2013; Konuma et al., 2011), suggesting that high *PRKCH* expression may be a marker of stemness.

High *Prkch* expression contributes to the IM resistance of CML stem cells

We performed several experiments to determine whether the high *Prkch* expression in murine CML stem cells contributes to their IM resistance. We first assessed the contribution of *Prkch*, and as a comparison BCR-ABL, to RAF/MEK/ERK signaling in murine CML stem cells. *Prkch* KD bone marrow cells were isolated from leukemic mice, permeabilized and incubated with an antibody against phosphorylated ERK1/2 or, as a negative control, IgG isotype antibody, and then analyzed by FACS to determine the phosphorylated ERK1/2 levels in CML progenitor and stem cells. Figure 2.19 a shows that knockdown of *Prkch* reduced phosphorylated ERK1/2 in both CML progenitor and stem cells (see also Figure 2.20 a).

To evaluate the role of BCR-ABL, bone marrow cells were isolated from leukemic mice and treated with either IM or trametinib, and phosphorylated ERK1/2 was monitored as described above. Figure 2.19 b shows, as expected, that trametinib reduced phosphorylated ERK1/2 in both CML progenitor and stem cells (see also Figure 2.20 b). In contrast, IM reduced phosphorylated ERK1/2 in IM-sensitive CML progenitor cells, but not in IM-resistant CML stem cells.

Collectively, these results indicate that in CML stem cells, PKCη has a more prominent role than BCR-ABL in promoting RAF/MEK/ERK signaling.

We next performed a series of experiments to determine whether *Prkch* affects survival of CML stem cells after IM treatment. In the first experiment, mouse primary bone marrow cells were transduced with a retrovirus co-expressing BCR-ABL and either *Prkch* or a control NS shRNA, followed by transplantation into lethally irradiated syngeneic mice. BCR-ABL+ murine stem cells (Lin-Sca1+Kit+) were isolated from the mice and IM sensitivity determined in a colony formation assay. The results in Figure 2.19 c show that *Prkch* knockdown markedly increased the IM sensitivity of CML stem cells. In the second experiment, mice with CML-like disease were treated with either vehicle or IM in parallel for two weeks, and then sacrificed at the same time followed by quantification of CML stem cells by FACS analysis. Figure 2.19 d shows, as expected, that IM treatment had little effect on the number of CML stem cells expressing a control NS shRNA, confirming that murine CML stem cells are IM-resistant. In contrast, IM treatment markedly reduced *Prkch* KD CML stem cells. Annexin V staining revealed that IM treatment induced a higher level of apoptosis in *Prkch* KD compared to control CML stem cells (Figure 2.21 a and b). Finally, combined treatment with IM and trametinib synergistically killed murine CML stem cells (Figure 2.19 e), which was due, at least in part, to the induction of apoptosis (Figure 2.21 c and d). By contrast, treatment with IM and trametinib

had negligible effect on normal murine hematopoietic stem cells (Figure 2.22 a).

Knockdown of *PRKCH* also increased the IM sensitivity of IM-resistant human CML stem cells (Figure 2.19 f). Moreover, treatment with both IM and trametinib had a substantially greater effect than either drug alone in killing human CML stem cells (Figure 2.19 g), and a negligible effect on normal human hematopoietic CD34+ cells and hematopoietic stem cells (CD34+CD38-) (Figure 2.22 b). Collectively, these results indicate that *PRKCH* is expressed at relatively high levels in both mouse and human CML stem cells and this contributes to their IM resistance.

DISCUSSION

In this study, we have identified a molecular pathway whose increased activity promotes BCR-ABL-independent IM resistance and also contributes to the IM resistance of CML stem cells. Our major conclusions are summarized in the schematic model in Figure 2.23 and discussed below. In typical IM-sensitive CML cells, BCR-ABL is the major contributor to RAF/MEK/ERK signaling. Thus, treatment with IM substantially reduces RAF/MEK/ERK signaling, leading to inhibition of proliferation and induction of apoptosis. In BCR-ABL-independent IM-resistant CML cells, elevation of PKCη, due to decreased expression of one or more IMSGs, results in phosphorylation and activation of CRAF, thereby augmenting RAF/MEK/ERK signaling. After treatment with IM, RAF/MEK/ERK signaling is sustained, resulting in drug resistance.

A previous study analyzing IM resistance resulting from mutations in BCR-ABL found that IM treatment "paradoxically" increased RAF/MEF/ERK signaling through a RAS-directed pathway (Packer et al., 2011). Although the IM resistance mechanism we describe, like that in (Packer et al., 2011), involves increased RAF/MEK/ERK signaling, there are several important differences. For example, in our experiments the increased RAF/MEK/ERK signaling is not dependent upon RAS but rather initiated by PKCη, is constitutive and not induced by IM, and, as discussed below, is also relevant to the intrinsic IM resistance of CML stem cells. In addition, several reports have described experimentally derived BCR-ABL-

independent IM-resistant CML cell lines in which RAF/MEK/ERK signaling is increased by a mechanism that was not determined (Aceves-Luquero et al., 2009; Hentschel et al., 2011; Nambu et al., 2010), or have provided other evidence that RAF/MEK/ERK signaling can contribute to IM resistance (Chang et al., 2007; Chu et al., 2004; Mizuchi et al., 2005; Pellicano et al., 2011).

The mechanistic basis by which IMSGs regulate *PRKCH* expression is largely unknown. We showed that one of the IMSGs, *ELF5*, is directly bound at the transcription start site of *PRKCH*, and can decrease *PRKCH* expression. Thus, ELF5 is a direct transcriptional repressor of *PRKCH*, explaining why decreased ELF5 levels result in increased *PRKCH* expression. Whether other IMSGs function directly or indirectly to regulate *PRKCH* expression remained to be determined.

It is likely that our RNAi screen, like other large-scale RNAi screens (Mullenders and Bernards, 2009), was not saturating, and thus there are probably other IMSGs and regulators of *PRKCH* expression that remain to be identified. Our results suggest that a variety of diverse perturbations can increase *PRKCH* expression. A previous expression profiling study revealed that the level of *PRKCH* in CML cells increased after one week of IM treatment (Bruennert et al., 2009), perhaps due to selection of and enrichment for cells with high *PRKCH* expression. This finding may also be explained by induction of *PRKCH* expression by IM treatment, although we found in IMSG KD K562 cell lines and CML stem cells that

PRKCH is highly expressed in the absence of IM. In addition to its role in IM resistance, we found that elevated *Prkch* expression also accelerates disease progression in a mouse model of CML. Consistent with this idea, in a previous expression profiling study, *PRKCH* levels were found to increase during disease progression in CML patients. In the same study, the expression of seven of nine IMSGs analyzed decreased during disease progression (Radich et al., 2006).

The IM-resistance mechanism we describe is therapeutically targetable, which we demonstrate by showing that combined treatment with IM and the FDA-approved MEK inhibitor trametinib synergistically kills BCR-ABL+ IMSG KD cells and prolongs survival in several mouse models of BCR-ABL-independent IM-resistant CML. However, analysis of patient-derived CML cell lines suggests there may be variable responsiveness to MEK inhibition (Jing et al., 2012). Our results are also relevant to another current challenge of CML treatment: the intrinsic resistance of CML stem cells to IM. We found that both human and murine CML stem cells contain high levels of *PRKCH* and provide evidence that this is responsible, at least in part, for their IM resistance. We further showed that the high *PRKCH* levels in CML stem cells promote RAF/MEK/ERK signaling, which helps explain why CML stem cells are not dependent upon BCR-ABL for survival (Corbin et al., 2011; Hamilton et al., 2012). Collectively, these results provide a rationale for our finding that CML stem cells, but not normal hematopoietic stem cells, are efficiently killed by

combined treatment with IM and trametinib, and suggest a therapeutic strategy for their eradication.

MATERIALS AND METHODS

Cell lines and culture

BCR-ABL+ positive human CML cell lines K562 (ATCC), K562R (kindly provided by Nicholas J. Donato, University of Michigan) and KYO-1 (Leibniz Institute DSMZ-German Collection of Microorganisms and Cell Cultures; ACC 601) were maintained in RPMI 1640 medium containing 10% fetal bovine serum (FBS), 4 mM L-glutamine, 100 units/ml penicillin, and 100 µg/ml streptomycin. 32D/BCR-ABL cells (kindly provided by Tomasz Skorski, Temple University) were maintained in RPMI 1640 with 10% FBS.

RNAi screen

The RNAi Consortium (TRC) lentiviral human shRNA library (Open Biosystems/Thermo Scientific) was obtained through the University of Massachusetts RNAi Core facility. Twenty-two lentivirus pools, each comprising ~5000 shRNA clones, were generated with titers of ~$2x10^7$ cfu/ml, as previously described (Gazin et al., 2007). $2x10^6$ K562 cells were transduced at a multiplicity of infection <1 with the lentiviral stocks in 6-well plates, and 2 days later puromycin selected (1 µg/ml) for 5 days. Cells were then treated with 20 µM IM (LC Laboratories) for 7 days, and washed twice with fresh medium until >99% of control cells (those expressing a non-silencing shRNA) died off. Surviving cells from all shRNA pools were combined and allowed to recover in IM-free medium with 1 µg/µl puromycin for 4 days. Live cells were sorted out with a Dead Cell

Removal kit (Miltenyi Biotec) and harvested, and genomic DNA was prepared for sequencing identification of the integrated shRNA as previously described (Gazin et al., 2007).

Cell viability assay

To validate candidates, K562 or KYO-1 cells were stably transduced with a lentivirus carrying an individual shRNA (clone IDs are listed in Table 2.4) and puromycin selected for 5 days. $2.5x10^3$ IMSG KD K562 cells or $1x10^4$ IMSG KD KYO-1 cells were plated in 96-well plates, and IM (10 μM for K562 cells or 0.1 μM for KYO-1 cells) or vehicle (DMSO) was added for 3 days. MTT reagent (Promega) or Alamar Blue (Invitrogen) was added to each well in 1:10 volume and incubated, and absorbance at 570 nm was recorded using a VICTOR^3 (PerkinElmer) or SpectraMAX M5 (Molecular Devices) plate reader.

For other cell viability assays, IMSG KD K562 cells or K562/*PRKCH* cells were treated for 3 days with a range of IM concentrations as indicated (Figure 2.1 e and Figure 2.7 b), or 0.1 μM IM, 1.5 nM trametinib or both (Figure 2.12 a and b), and analyzed as described above. For Figure 2.1 e and Figure 2.7 b and Figure 2.5, data were plotted in GraphPad Prism and a dose response curve was fit with nonlinear regression to calculate $IC50^{IM}$. For Figure 2.1 f, IMSG KD K562 cells were treated with 10 μM IM or 500 nM dasatinib (ChemieTeK), and cell viability was analyzed as described above. The curve was fit with linear regression, and correlation coefficient was calculated using GraphPad Prism 6.

Colony formation assay

For Figure 2.1 d, mouse primary bone marrow cells were harvested from CML mice as described below, and subjected to two rounds of infection with a mouse IMSG shRNA lentivirus (clone IDs are listed in Table 2.4). Two days later, $5x10^4$ IMSG KD cells were mixed with cytokine-free methylcellulose-based medium (MethoCult M3234; STEMCELL Technologies) and 0.5 μM IM and plated in 35 mm dishes. Colonies were counted under a brightfield microscope at day 7. For Figure 2.12 c, primary bone marrow cells were transduced for two rounds with a retrovirus expressing *Prkch*, generated by PCR amplifying mouse *Prkch* cDNA (an MGC clone; Open Biosystems/Thermo Scientific) using forward (5'-ATAGGTTAACGCCACCATGTCGTCCGG CACGATGA-3') and reverse (5'-ATAGGAATTCCTACAGTTGCAATTCCGGTGA-3') primers, digesting the PCR product with HpaI and EcoRI, and cloning it into MSCV-IRES-GFP (Addgene plasmid 20672). Two days after transduction, $5x10^4$ cells were mixed with methylcellulose and 0.5 μM IM, 2 nM trametinib (ChemieTek) or both. For Figure 2.15 b and c, primary bone marrow cells were collected from *Prkch* knockdown CML mice (generated using a retrovirus co-expressing BCR-ABL and a *Prkch* shRNA; see below), and $1x10^5$ cells were plated in methylcellulose in the absence (Figure 2.15 b) or presence of 0.1 μM IM (Figure 2.15 c). For Figure 2.19 c, primary bone marrow cells were collected from either NS or *Prkch* knockdown CML mice, BCR-ABL+ murine stem cells (Lin-Sca1+Kit+) were

isolated from the mice by FACS, and IM sensitivity determined as described above for Figure 2.15 b and c.

Immunoblot analysis

After 5 days puromycin selection, ~1x10^6 IMSG KD K562 cells were plated into 6-well dishes and treated with 10 μM IM for 36 hours. Cells were harvested and lysed with RIPA buffer (10x, 200 mM HEPES pH 6.8, 1400 mM NaCl, 25 mM $MgCl_2$, 25 mM $CaCl_2$, 10% NP40, and 5% sodium deoxycholate) plus phosphatase (Sigma) and protease inhibitors (Roche). Blots were probed with the following primary antibodies, all obtained from Cell Signaling Technology: BCR-ABL PathScan (p-BCR-ABL, p-STAT5, p-CRKL) (#5300S), total BCR-ABL (#2862S), p-ERK1/2 (#4377S), total ERK1/2 (#4695S), t-STAT5 (#9358S), p-AKT (#4060S), t-AKT (#4685S), p-SFK (#2105S), t-LYN (#2796S), t-CRKL (#3182S), p-MARCKS (#8722S), t-MARCKS (#5607S), ARAF (#4432S), BRAF (#9433S), CRAF (#9422S). The PKCη antibody (Santa Cruz Technology; C-15) was diluted in 5% skim milk at 1:150. The β-actin antibody (Sigma; AC-74) was diluted in 5% BSA at 1:5000. Blots were developed with Pico/Femato super signal (Sigma) and visualized using autoradiography or a Bio-Rad ChemiDoc MP Imaging System.

RNA preparation and qRT-PCR

Total RNA was isolated from cells using TriPure Isolation Reagent (Roche) followed by treatment with turbo DNase (Ambion) to remove contaminating genomic DNA. Reverse transcription was performed using MMLV reverse transcriptase (Zhao et al.) followed by qPCR with Fast SYBR Green Master Mix (Applied Biosystems) and primers listed in Table 2.5. The expression of each gene was normalized to that of *GAPDH*. Knockdown efficiency was calculated relative to that obtained with a control non-silencing shRNA.

In vitro kinase assay

A plasmid expressing Flag-tagged PKCη was generated by PCR amplifying *PRKCH* from a cDNA clone (Open Biosystems/Thermo Scientific) and cloning the PCR product into expression vector p3xFlag-Myc-CMV-25 (Sigma). The kinase-dead K384R mutant was generated by PCR-based site-directed mutagenesis using PfuTurbo DNA polymerase (Agilent). Plasmids were transfected individually into 293T cells, and proteins were immunopurified from cell lysate using an anti-Flag antibody (Sigma). In vitro phosphorylation reactions were set up in a 20 µl reaction volume as follows: 1 µl ^{32}P-γ-ATP (10 mCi), 1 µl 10 µM ATP, 0.2 mM microcystin, 4 µl 5X kinase buffer [23 mM MOPS, 11.5 mM β-glycerophosphate, 23 mM $MgCl_2$, 4.6 mM EGTA, 1.8 mM EDTA, 0.25 mM DTT (pH 7.0)], 60 nM purified Flag-PKCη diluted in 1X kinase buffer, and 10 µM substrate (GST or GST fused to a peptide corresponding to amino acids 491-505 of CRAF, purified from *E. coli*) diluted in 1X kinase buffer. Reactions were

incubated for 30 min at 30°C and stopped using 2X Laemmli Sample Buffer. Incorporation of the radiolabel into the peptide was monitored by autoradiography.

Flow cytometry analysis

Fifteen days after induction of CML-like disease (see below), bone marrow cells were flushed out of mouse femur and tibia bones with RBC lysis buffer (155 mM NH_4Cl, 12 mM $NaHCO_3$, 0.1 mM EDTA), spun down at 1,000 rpm for 10 min, and washed once with PBS. 2-5x10^6 cells from each sample were aliquoted for staining. A cocktail of primary antibodies [APC-conjugated Sca-1 antibody (eBioscience), PE-conjugated c-Kit antibody (eBioscience) and Biotin-conjugated Lineage antibody cocktail (Miltenyi Biotec)] was added to each sample in a total volume of 100 µl, incubated on ice for 30 min, washed once by adding PBS (1 ml) and spin down at 1,000 rpm for 10 min. The secondary antibody (APC-eFluor780-conjugated Straptavidin; eBioscience) was added in a total volume of 100 µl, incubated for 20 min on ice, and then washed once with PBS. FACS analysis was performed immediately using an LSR II flow cytometer (BD Biosciences). The Lin+ population was separated from the Lin- population by magnetic beads (Miltenyi Biotec). GFP+Lin-Sca1+Kit+ and GFP+Lin- cells (hereafter referred to as Lin-Sca1+Kit+ and Lin- cells) were then FACS sorted from the Lin- population, and GFP+Lin+Gr1+ cells (hereafter referred to as Lin+Gr1+ cells) were FACS sorted from the Lin+ population.

For Lin-Sca1+Kit+ apoptosis staining, 5 µl Annexin-V antibody [eFluor450-conjugated Annexin V (eBioscience)] was added to each sample after the last wash and incubated for 20 min in the dark at room temperature. Samples were washed once, and 2 µl 7AAD (eBioscience) was added within 4 h before FACS analysis.

For intracellular phosphorylated ERK1/2 analysis, bone marrow cells isolated from leukemic mice were treated with 5 µM IM or 10 nM trametinib for 3 hours, fixed in 4% paraformaldehyde (Electron Microscopy Sciences) for 10 min at 37°C, washed twice with wash buffer (0.05% BSA in 1x PBS), spun down, and resuspended in 100 µl wash buffer. Ice-cold methanol (900 µl) was added to the cells while gently vortexing to reach a final concentration of 90% methanol for permeabilization. Samples were incubated on ice for 30 min, washed twice, and resuspended in 100 µl wash buffer. IgG control antibody (Cell Signaling) was added (at 1:100 dilution) for 10 min at room temperature for blocking, followed by addition of 2 µl conjugated IgG control (Pacific Blue-conjugated IgG^{XP} Rabbit mAb, Cell Signaling) or phospho-ERK antibody (Pacific Blue-conjugated P-p44/42(T202/Y204)^{XP} Rabbit mAb, Cell Signaling). Samples were gently mixed and incubated at room temperature for 1 hour. Thirty minutes after the start of the incubation, a cocktail of primary antibodies for cell surface markers was added, incubated for a further 30 min, washed once with PBS, and incubated with the secondary antibody for 20 min on ice. Samples were then washed once with

wash buffer prior to FACS analysis. Relative phosphorylated ERK1/2 staining was calculated by first subtracting the IgG background staining and then normalizing the absolute fluorescence intensity (median) of the treatment group (*Prkch* knockdown or IM or TM treatment) to that of the control group (NS shRNA or DMSO).

Construction of BCR-ABL/shRNA or BCR-ABL/*Prkch* co-expression plasmids

shRNAs were subcloned from an effective TRC *Elf5* or *Clec5a* shRNA plasmid (see Table 2.4) into the MluI site downstream of GFP in the retroviral vector MSCV-BCR-ABL-IRES-GFP (Li et al., 1999) (using forward [5'-ATAGACGCGTTTCTTGGCTTTATATATCTTGTGG-3'] and reverse [5'-ATAGACGCGTCAAAGTGGATCTCTGCTGTC-3'] primers, where underlining indicates the MluI site) to ensure the shRNA would be expressed in the same transcript as BCR-ABL and GFP. Similarly, mouse *Prkch* cDNA was subcloned into MSCV-BCR-ABL-IRES-GFP as described above to generate an MSCV-BCR-ABL-IRES-mPRKCH-IRES-GFP triple gene expression construct. Virus titer was tested in NIH 3T3 cells. Briefly, $5x10^4$ cells were plated in each well of a 6-well plate, and virus was added at 1:1 dilution with fresh DMEM medium (10% FBS) plus Polybrene (Qiagen) and then cultured for 48 hours. FACS was performed to analyze GFP percentage. Only those viruses showing ≥90% infection were used for in vivo CML induction.

Mouse models of CML

Mice with CML-like disease were generated as previously described (Li et al., 1999). Briefly, wild-type male C57BL/6 mice 6–8 weeks of age (Jackson Laboratory) were tail-vein injected with 5-fluorouracil (200 mg/kg; Sigma) for 4 days to enrich for slow-cycling hematopoietic stem cells. At day 5, bone marrow cells were harvested and pre-incubated overnight in the presence of IL-3, IL-6 and SCF (all from PeproTech) to increase infection efficiency. At days 6 and 7, bone marrow cells were infected with a BCR-ABL retrovirus by co-sedimentation method at 3,000 rpm for 90 min at room temperature. Four hours after the second round of retroviral infection, $0.5x10^6$ bone marrow cells were injected into the tail vein of syngeneic recipient mice that had been lethally irradiated (twice at 550 R). Mice were randomly allocated to each group after bone marrow transplantation.

For drug treatment, mice were orally gavaged twice a day with IM (dissolved in filtered ddH_2O [vehicle]) at 100 mg/kg and/or once a day with trametinib (dissolved in 0.5% hydroxypropylmethycellulose and 0.2% Tween-80 in filtered ddH_2O [vehicle]) at 2 mg/kg.

White Blood Count

Peripheral blood (~25 µl) was collected from mouse tail veins into Microtainer tubes (BD Biosciences), and analyzed using a Hemavet 950 FS (Drew Scientific, Inc) cell counter within 3 hours after blood collection.

Acquisition and storage of CML patient samples

After informed consent in accordance with IRB-approved protocols, bone marrow aspirate or peripheral blood samples were collected from CML patients. For samples provided by the Druker lab and Emory University, mononuclear cells were isolated by Ficoll gradient and, depending on the number of viable cells available, cells were stored as pellets or guanidinium thiocynate (GTC) lysates (resuspended in Qiagen RLT lysis buffer + β-mercaptoethanol) at -80°C, or resuspended in fetal bovine serum (FBS) + 10% DMSO, frozen slowly overnight, and then transferred to liquid nitrogen for long-term storage. For samples provided by UMMS, white blood cells were isolated by red cell lysis, and cells were resuspended in FBS + 10% DMSO, frozen slowly overnight, and then transferred to liquid nitrogen for long-term storage. All samples were provided in a de-identified manner. Samples from normal donors were purchased from a commercial vendor (AllCells or Lonza).

Analysis of human CML patient samples

To analyze gene expression in IM-sensitive and IM-resistant CML patient samples, RNA was obtained in the form of purified RNA or extracted

independently from GTC lysate or Trizol stock, and qRT-PCR was performed as described above.

To culture primary cells derived from CML patients and normal individuals for functional experiments, frozen patient cells were first warmed for 10 min at 37°C. 1 ml of pre-warmed thawing medium (IMDM with 5% FBS, 0.1 mg/ml DNase, and 400 U/ml heparin) was added slowly, followed by 10 ml of wash medium (IMDM with 5% FBS, 0.1mg/ml DNase). After passing through a 70 μm filter, cells were spun at 300 g for 10 min. Cell pellets were then resuspended in an adequate amount of culture medium (IMDM with 20% BIT [STEM CELL technology], 20 ng/ml IL-3, 20 ng/ml IL-6, 20 ng/ml FLT3, 100 ng/ml G-CSF, and 100 ng/ml SCF [PeproTech]) and incubated overnight at 37°C. Cells were then either directly used, or further enriched for the CD34+ population using CD34 MicroBead Kit UltraPure (Miltenyi Biotec).

For *PRKCH* knockdown, a volume of *PRKCH* shRNA-GFP lentivirus equal to the volume of cells was used to infect cells at 2,000 g for 90 min at room temperature. After culturing for an additional 16-24 hours, cells were pelleted at 300 g for 10 min and resuspended in culture medium with 1% of initial cytokines, a more physiologically relevant concentration. Cells were then treated with DMSO, 5 μM IM, 5 nM trametinib, or both drugs for 4 days. The cell viability of the target population was then calculated by multiplying the percentage of target

population, which was obtained by FACS analysis, and the total number of live cells, which was determined by trypan blue staining.

To analyze *PRKCH* expression in human CML stem cells (CD34+CD38-) and progenitor cells (CD34+CD38+), freshly thawed CML cells or CD34+-enriched CML cells were directly stained for CD34 and CD38 cell surface markers. The target population was isolated by FACS and total RNA was extracted by Trizol for qRT-PCR analysis as described above. For bioinformatic analysis, CEL files were downloaded from Gene Expression Omnibus (GEO accession GSE43754), and *PRKCH* expression analysis was performed using the R program 'RMA' in the BioConductor 'oligo' package (Carvalho and Irizarry, 2010) with full probeset annotation.

Chromatin immunoprecipitation

K562 cells ($1x10^7$) were crosslinked with 1% formaldehyde for 12 min at room temperature, followed by addition of 0.125 mM glycine for 10 min. Cells were washed twice and lysed in ChIP lysis buffer (50 mM HEPES pH 8.0, 150 mM NaCl, 1 mM EDTA, 0.1%Na-deoxycholate, 1% TritonX-100, 0.1%SDS, plus protease inhibitor) for 15 min on ice. The lysate was sonicated for 12 rounds (30 seconds on, 1 minute 30 seconds off, power output 6.0) using Sonicator 3000 (Qsonica), and clarified by centrifugation. 50 µl 50% protein-G agarose bead slurry was used to pre-clear 5 mg of chromatin for over 4 hours at 4°C. For ChIP

experiments, 500 µg pre-cleared chromatin were incubated overnight with either 5 µg anti-ELF5 antibody ((N-20) X, Santa Cruz) or IgG, followed by addition of 50 µl 50% protein-G agarose bead slurry and incubation for 4 hours at 4°C. Beads were pelleted by centrifugation and washed twice with ChIP lysis buffer, once with high salt lysis buffer (ChIP lysis buffer adjusted to 1M NaCl), thrice with LiCl wash buffer (50 mM HEPES pH 8.0, 250 mM LiCl, 1 mM EDTA, 0.5% deoxycholate, 0.5% NP40, plus protease inhibitor), and once with Tris-EDTA buffer. After the last wash, the supernatant was removed and 400 µl elution buffer (1% SDS, 0.1% $NaHCO_3$) was added and incubated for 15 min at 65°C with occasional vortexing. Beads were pelleted, and the supernatant was transferred to a new tube and reverse-crosslinked overnight at 65°C. RNase A (2 µl of 10 mg/ml) was added to each ChIP sample and incubated for 1 hour at 37°C, followed by addition of 5 µl Protease K (20 mg/ml, Promega) and incubation for 2 hours at 55°C. DNA was phenol:chloroform extracted and isopropanol precipitated, and subjected to qPCR with the following primers: TSS-for (5'-AGGAGGAGAAGCAAGAGGAG-'3') and TSS-rev (5'-CCGACCGTCCCTTCCAAG-3'), 500-for (5'-GACCTTTCCTGCTCTATGTG-3') and 500-rev (5'-CTGCAGAGGCTAATTACACAG-3'), and 1000-for (5'-CATAGCAGCGTAGGCTAAAA G-3') and 1000-rev (5'-CGGAAGAAATTGCCTCTTCTAG-3'). Fold enrichment was calculated by setting the IgG control to a value of 1.

Luciferase reporter assays

A 2 kb genomic DNA region upstream of the *PRKCH* transcription start site was PCR amplified from a BAC clone (RP11-1069E8) using forward and reverse primers (5'-ATAGGCTAGCGTTCTGAACAGGGCCTTAGAG-3' and 5'-ATAGAAGCTTGATGCGGACCCTCAAATAGC-3', respectively), digested with NheI and HindIII, and ligated into the firefly luciferase reporter vector PGL4.14[luc2/Hygro] (Promega). 2 µg of this reporter and 40 ng of pRL-TK Renilla luciferase control reporter vector (Promega) were co-transfected into *ELF5* knockdown or *ELF5*-overexpressing K562 cells by electroporation. After 48 hours of culturing, cells were lysed and centrifuged. Supernatants were incubated with luciferase substrate (Promega), and the luciferase activity was recorded by VICTOR^3 (PerkinElmer) plate reader.

Statistics

All quantitative data were collected from experiments performed in at least triplicate, and expressed as mean ± standard deviation. Animal experiments were expressed as mean +/- standard error of the mean. Statistical analyses were performed using R, a system for statistical computation and graphics (Ihaka and Gentleman, 1996). Relative cell viability data and cell death data were first arcsine transformed to homogenize the variance. Colony number and cell number data were first log transformed. Levene's test was performed to test for homogeneity of variance. When the assumption of homogeneity of variances was

met, ANOVA was performed followed by predetermined contrasts within the ANOVA framework. When the assumption was violated, a non-parametric counterpart of ANOVA (Kruskal–Wallis test for completely randomized design or Friedman rank sum test for randomized complete block design) was performed. In some instances, *P* values were adjusted to counteract the problem of multiple comparisons (Benjamini and Hochberg, 1995). Significant differences were considered when $P<0.05$; $*P\leq0.05$ and $**P\leq0.01$.

Statistical analysis for drug synergy was performed using R (Ihaka and Gentleman, 1996) to assess whether the combined effects from IM and trametinib were additive (responses were equal to the sum of the single-drug effects), synergistic (greater than the sum of the single-drug effects) or antagonistic (less than the sum of the single-drug effects). Two-way analysis of variance (ANOVA) was used to test for the main effects of IM and trametinib and their interaction on cell viability and apoptosis. Benjamini and Hochberg (BH)-adjusted *P* value was calculated to counteract the problem of multiple comparisons (Benjamini and Hochberg, 1995). The difference between observed effects and the expected additive effects for the cell lines exposed to both drugs were compared as previously described (Slinker, 1998). The difference was estimated as the interaction coefficient in ANOVA. For cell viability, if there was a significant positive difference (interaction coefficient > 0 and BH-adjusted *P* value < 0.05), then the impact from the combined drugs was classified as antagonism;

if there was a significant negative difference (interaction coefficient < 0 and BH-adjusted *P* value < 0.05), then the impact from the combined drugs was classified as synergistic; if there was no significant difference, then the impact from the combined drugs was classified as additive. For apoptosis, if there was a significant positive difference, then the impact from the combined drugs was classified as synergism; if there was a significant negative difference, then the impact from the combined drugs was classified as antagonism.

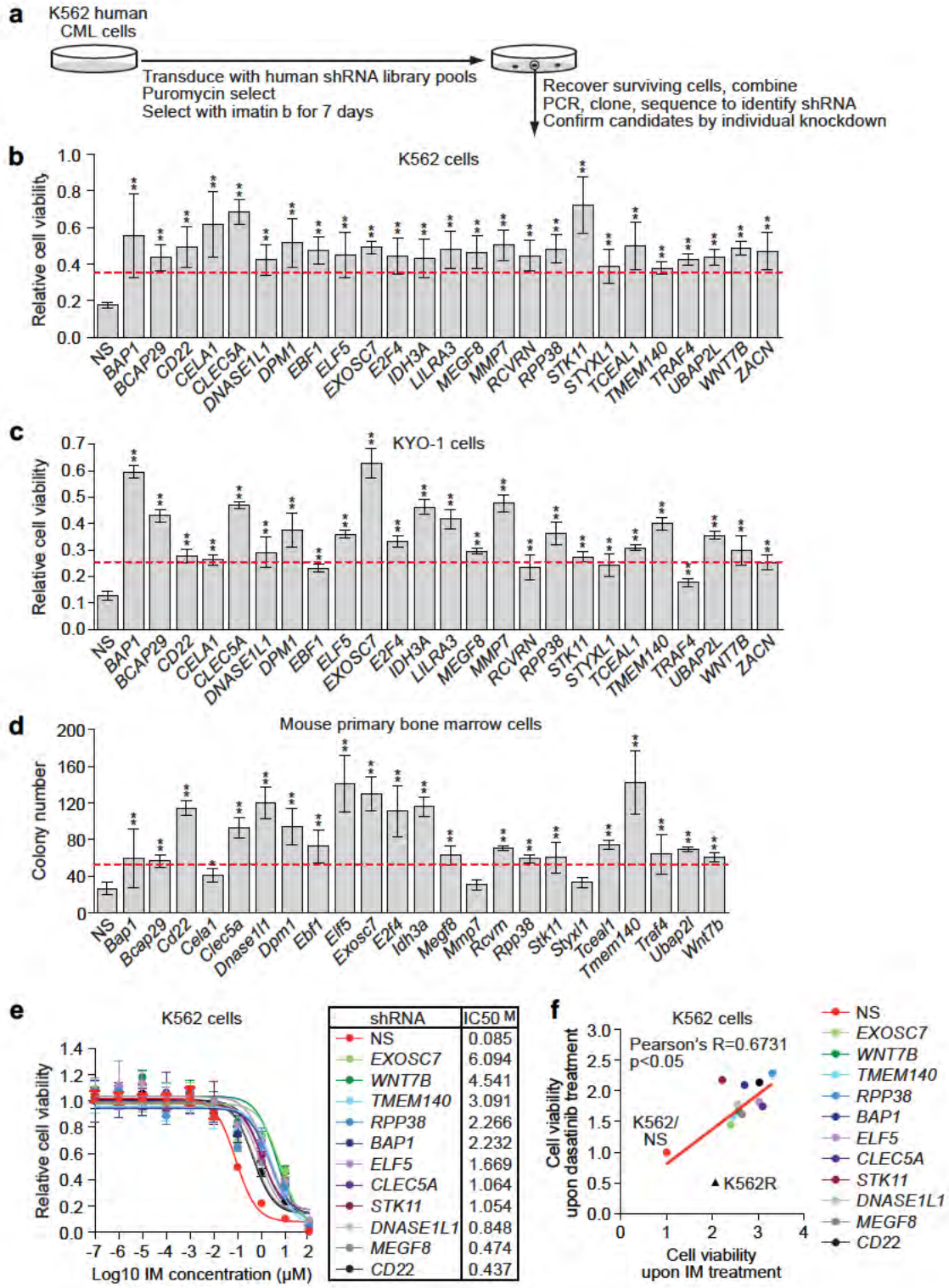

Figure 2.1. A large-scale shRNA screen identifies IMSGs.

Figure 2.1. A large-scale shRNA screen identifies IMSGs. (**a**) Schematic summary of the screen. (**b**) Relative viability of IMSG KD K562 cells in the presence of IM, as measured by MTT assay (n=4). The results were normalized to that obtained with DMSO-treated cells, which was set to 1. IMSG shRNAs that conferred >2-fold increase in cell survival (indicated by the red line) relative to the NS control shRNA were considered positive. (**c**) Relative viability of IMSG KD KYO-1 cells in the presence of IM, as measured by MTT assay (n=4). The results were normalized and positives determined as described in (b). (**d**) Colony formation assay monitoring survival of BCR-ABL+ mouse primary bone marrow cells expressing an IMSG shRNA in the presence of IM (n=3). IMSG shRNAs that conferred >2-fold increase in colony number (indicated by the red line) relative to the NS control shRNA were considered positive. (**e**) Relative $IC50^{IM}$ of IMSG KD K562 cells (n=4). (**f**) Cell viability, as measured by MTT assay, of IMSG KD K562 cells treated with 500 nM dasatinib or 10 μM IM for 3 days (n=4). K562 cells expressing an NS shRNA (K562/NS) and IM-resistant K562 cells (K562R) were analyzed as controls. Data are represented as mean ± SD. *$P \leq 0.05$, **$P \leq 0.01$.

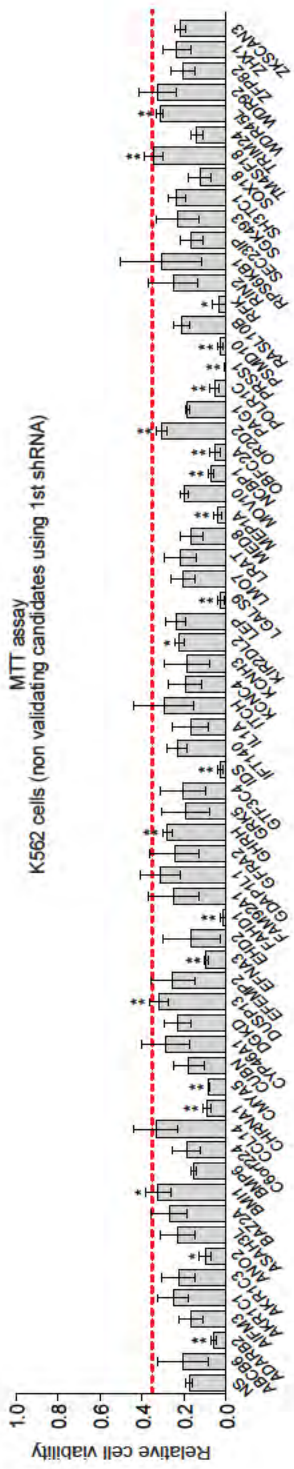

Figure 2.2 IM sensitivity of non-validating candidates isolated from the primary shRNA screen.

Figure 2.2 IM sensitivity of non-validating candidates isolated from the primary shRNA screen. MTT assay showing relative viability of IMSG KD K562 cells in the presence of IM. The results were normalized to that obtained with DMSO-treated cells, which was set to 1. The red line indicates a 2-fold increase in cell survival relative to that of the non-silencing (NS) control shRNA; none of the shRNAs shown here were considered positive. The NS control is the same as that used in Figure 2.1 b. Data are represented as mean ± SD (n=4). *$P \leq 0.05$, **$P \leq 0.01$.

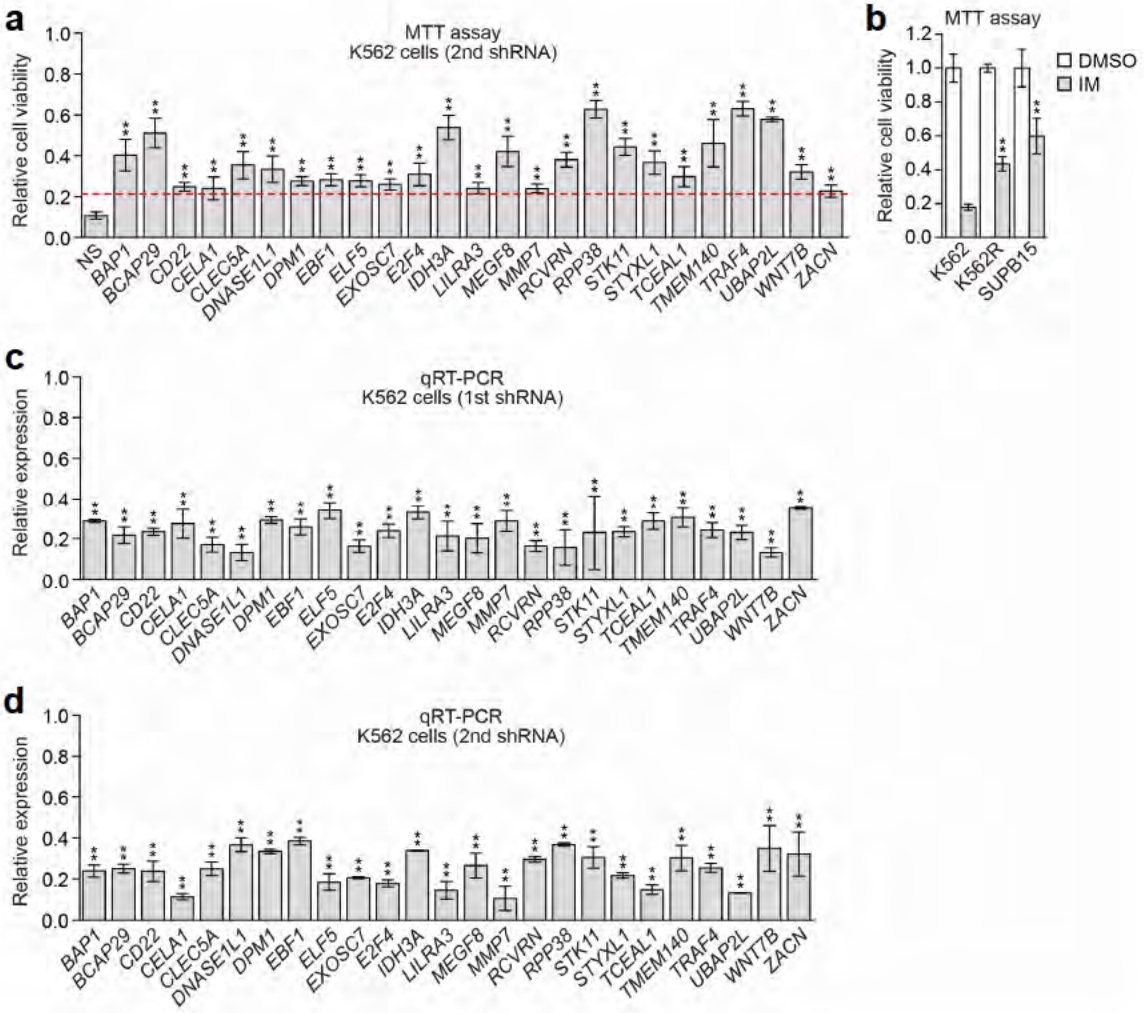

Figure 2.3. Confirmation of validating candidates using a second shRNA. (**a**) MTT assay showing relative viability of IM-treated K562 cells expressing a second IMSG shRNA unrelated to that isolated in the primary screen and used in Figure 2.1 b (n=4). The results were normalized as described in Figure 2.1 b. IMSG shRNAs that conferred >2-fold increase in cell survival (indicated by the red line) relative to that of the NS control shRNA were considered positive. (**b**) MTT assay showing relative viability of IM-sensitive K562 cells and IM-resistant K562R and SUPB15 cells treated with 10 μM IM (n=4). The results were normalized to that obtained with DMSO-treated cells, which was set to 1. (**c and d**) qRT-PCR analysis monitoring knockdown efficiencies, in K562 cells, of IMSG shRNAs isolated from the primary screen (b; n=3) or a second, unrelated IMSG shRNA (c; n=3). Data are represented as mean ± SD. **P*≤0.05, ***P*≤0.01.

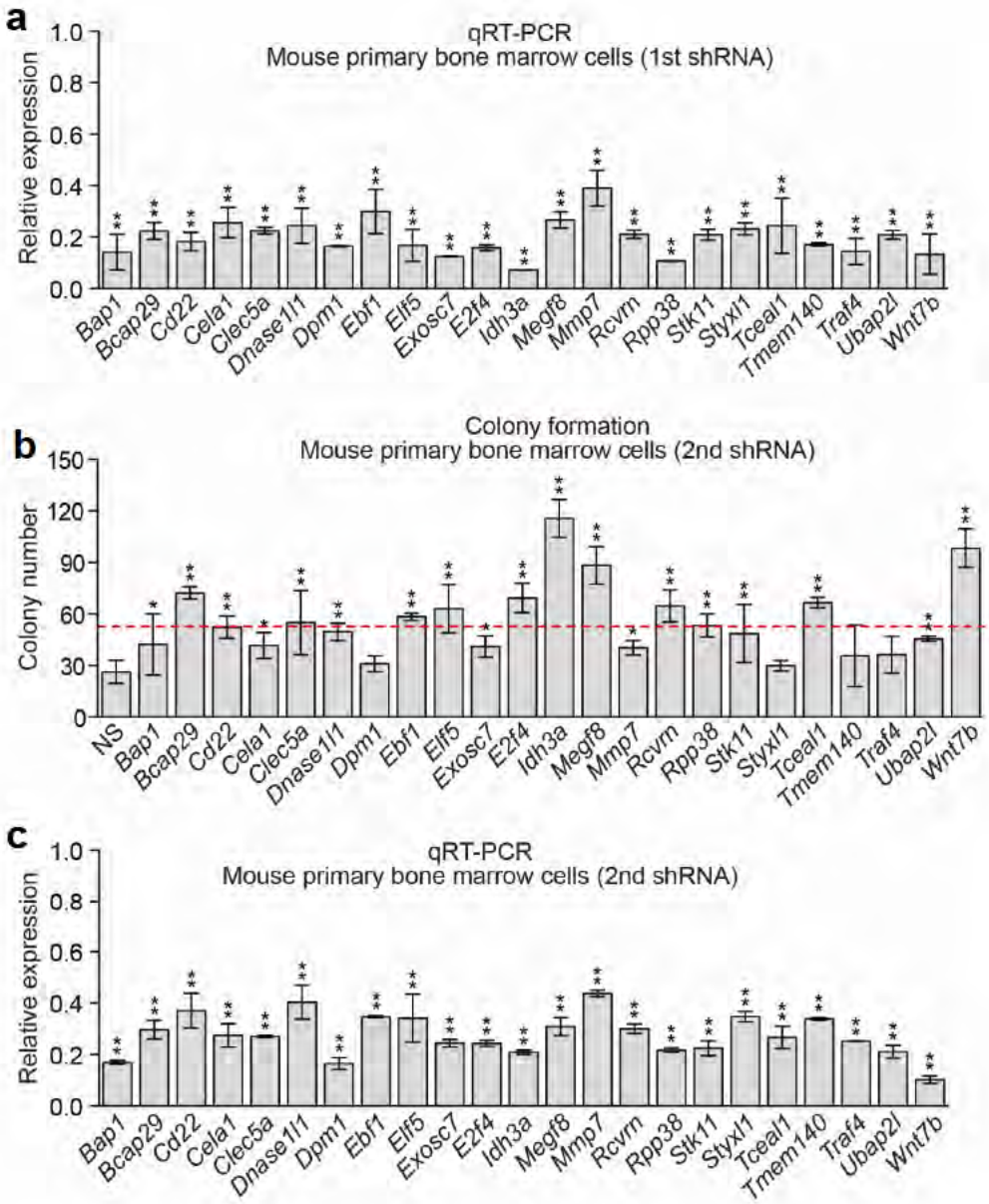

Figure 2.4. IM sensitivity after candidate IMSG knockdown in mouse primary bone marrow cells.

Figure 2.4. IM sensitivity after candidate IMSG knockdown in mouse primary bone marrow cells. (**a**) qRT-PCR analysis monitoring knockdown efficiencies of mouse IMSG shRNAs in mouse primary bone marrow cells (n=3). (**b**) Colony formation assay monitoring survival of BCR-ABL+ mouse primary bone marrow cells expressing an IMSG shRNA in the presence of IM (n=3). IMSG shRNAs that conferred >2-fold increase in colony formation relative to that of the NS control shRNA (indicated by the red line) were considered positive. (**c**) qRT-PCR analysis monitoring knockdown efficiencies, in mouse primary bone marrow cells, of a second set of mouse IMSG shRNAs unrelated to those used in (A) but the same as those used in (b) (n=3). Data are represented as mean ± SD. *$P \leq 0.05$, **$P \leq 0.01$.

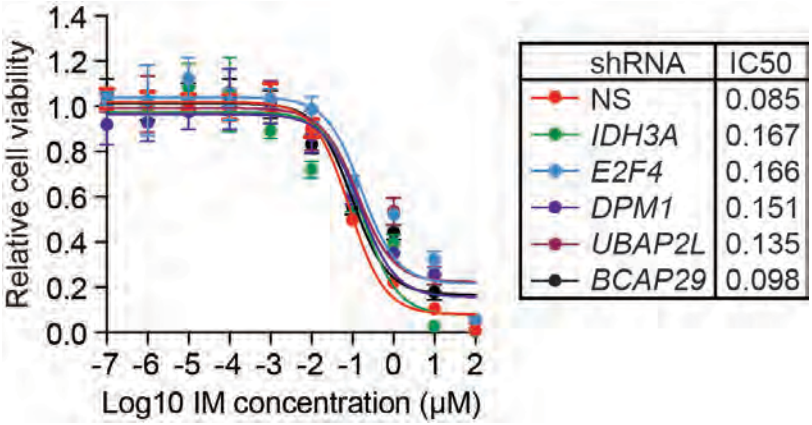

Figure 2.5. Relative IC50^{IM} of candidate IMSG KD K562 cells. The NS control used here is the same as that used in Figure 2.1 e, which was derived from the same experiment. Data are represented as mean ± SD (n=4).

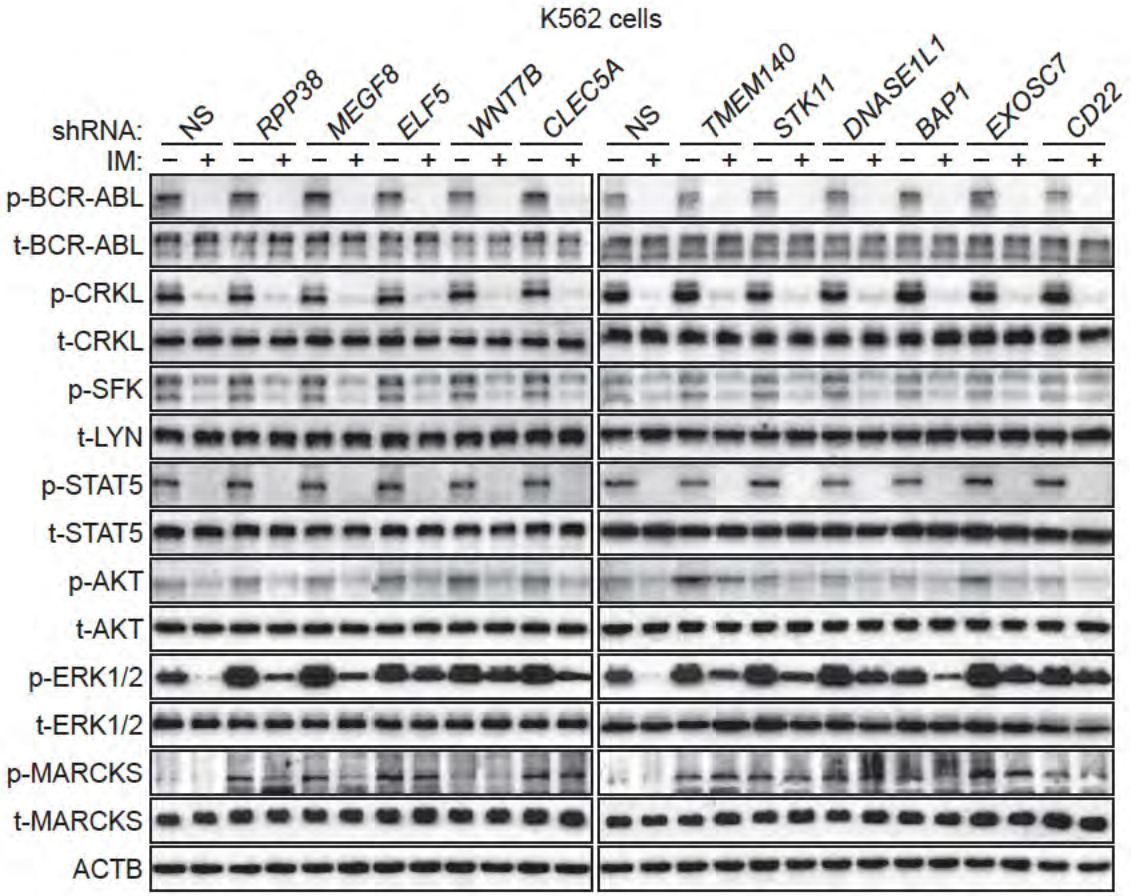

Figure 2.6. Knockdown of IMSGs in BCR-ABL+ cells results in sustained RAF/MEK/ERK signaling after IM treatment. Immunoblot analysis monitoring the activity of BCR-ABL (as measured by phosphorylated (p) and total (t) BCR-ABL and CRKL), SFKs (p-SFK and t-LYN), JAK/STAT (p- and t-STAT5), PI3K/AKT (p- and t-AKT), MEK/ERK (p- and t-ERK1/2), and PKC (p- and t-MARCKS) pathways in IMSG KD K562 cells treated in the presence or absence of IM. β-actin (ACTB) was monitored as a loading control.

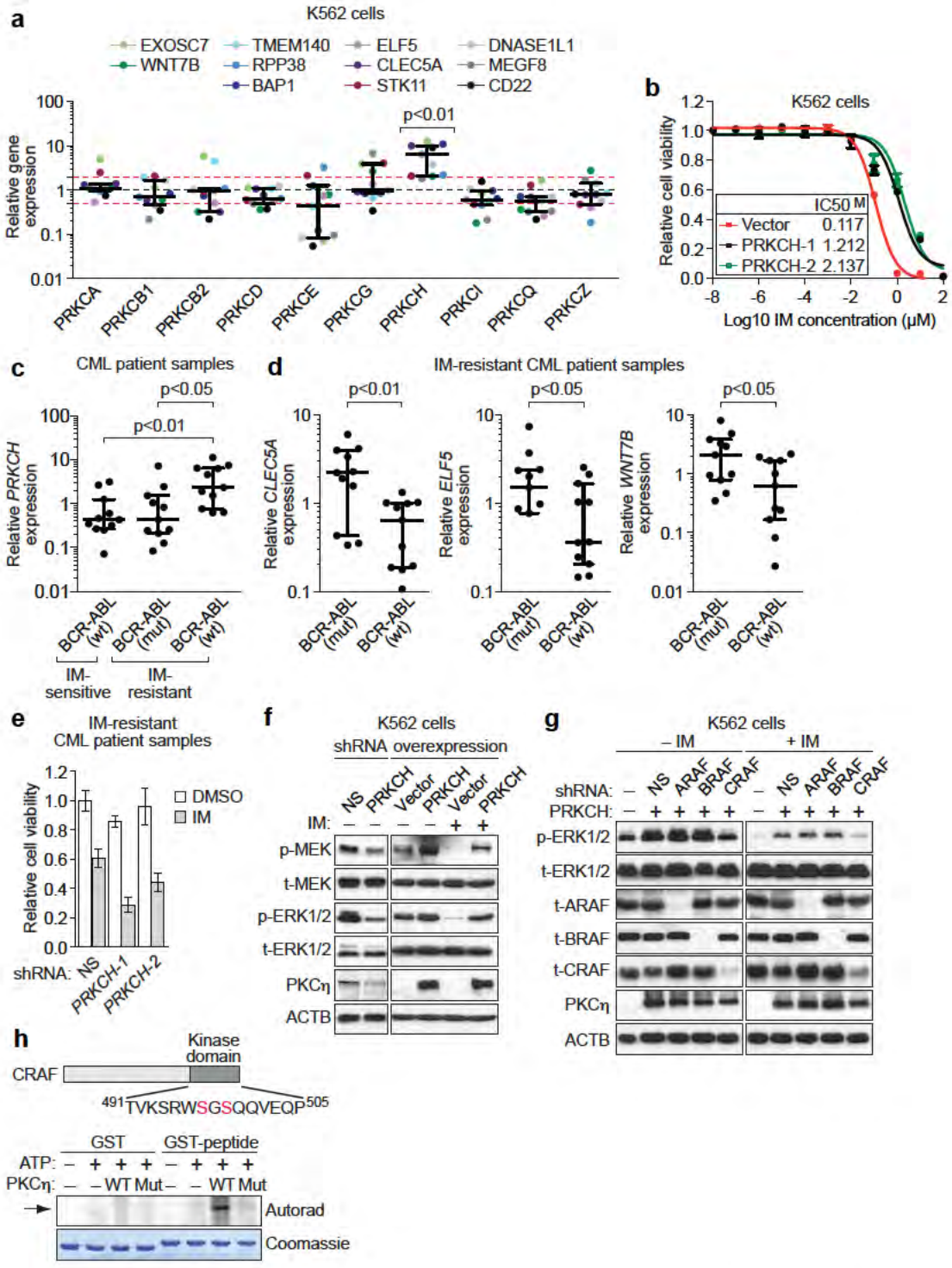

Figure 2.7. IMSG knockdown increases RAF/MEK/ERK signaling through upregulation of PKCη, an activator of CRAF.

Figure 2.7. IMSG knockdown increases RAF/MEK/ERK signaling through upregulation of PKCη, an activator of CRAF. (**a**) qRT-PCR analysis monitoring expression of different *PKC* isotypes in IMSG KD K562 cells. Each colored dot represents an individual IMSG KD K562 cell line. Error bars indicate median with interquartile range. The results were normalized to that obtained with the NS control shRNA, which was set to 1. The red lines indicate >2-fold change in gene expression relative to that obtained with the NS shRNA. (**b**) Relative $IC50^{IM}$ in K562 cells expressing empty vector and in two independently derived K562 clonal cell lines ectopically expressing *PRKCH* (n=4). Data are represented as mean ± SD. (**c**) qRT-PCR analysis monitoring expression of *PRKCH* in BCR-ABL wild-type IM-sensitive patient samples (n=11), and BCR-ABL mutant (n=11) or BCR-ABL wild-type (n=11) IM-resistant CML patient samples. Error bars indicate median with interquartile range. (**d**) qRT-PCR analysis monitoring expression of three IMSGs in BCR-ABL mutant (n=11) or BCR-ABL wild-type (n=11) IM-resistant CML patient samples. For *ELF5*, BCR-ABL mutant (n=9). Error bars indicate median with interquartile range. (**e**) Relative viability, as measured by trypan blue cell counting, of primary leukemic cells from BCR-ABL independent IM-resistant CML patient samples (n=5) expressing a NS or *PRKCH* shRNA and treated with DMSO or IM. The results were normalized to that obtained with DMSO-treated cells expressing a NS shRNA, which was set to 1. Data are represented as mean ± SEM. **P*≤0.05, ***P*≤0.01. (**f**) Immunoblot analysis monitoring RAF/MEK/ERK activity (as measured by p- and t-MEK and p- and t-ERK1/2) in *PRKCH* KD K562 cells (left) and in K562/*PRKCH-1* cells in the absence or presence of IM (right). (**g**) Immunoblot analysis monitoring p- and t-ERK1/2 levels in K562/*PRKCH-1* cells expressing an *ARAF*, *BRAF* or *CRAF* shRNA, treated with DMSO or IM for 1 h. (**h**) (Tsai et al.) Schematic of CRAF showing the kinase domain bearing a potential PKC phosphorylation site at S497/S499. (Bottom) *In vitro* phosphorylation assay. Wild-type (WT) or kinase-dead mutant (Mut; K384R) PKCη was used in an *in vitro* phosphorylation reaction containing either GST or a GST-CRAF(aa491-505) fusion-protein. The phosphorylated product was visualized by autoradiography. The Coomassie-stained gel shows the abundance of each protein.

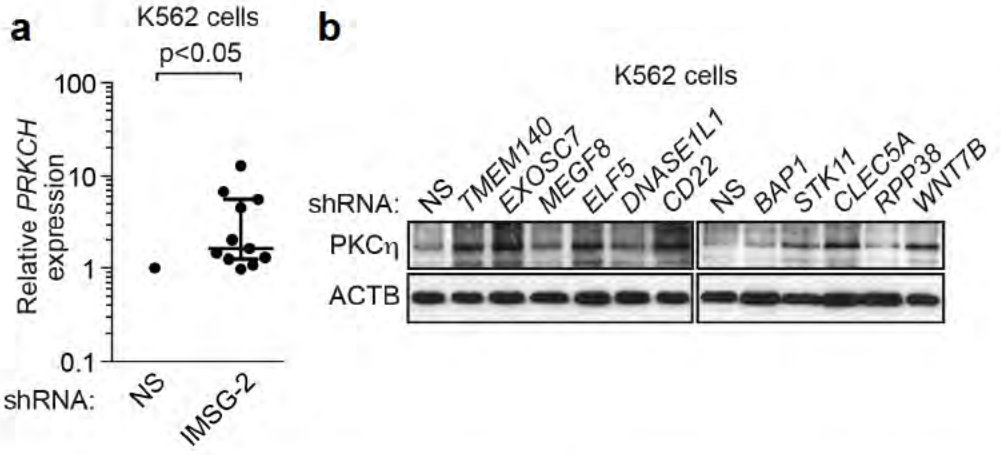

Figure 2 8. Increased *PRKCH* and PKCη after IMSG knockdown in K562 cells. (**a**) qRT-PCR analysis monitoring expression of *PRKCH* in K562 cells expressing a second IMSG shRNA unrelated to that used in Figure 2.7 a The results were normalized to that obtained with the NS control shRNA which was set to 1 The scatter dot plot shows the median line with interquartile range. (**b**) Immunoblot analysis showing the level of PKCη in IMSG KD K562 cells. β-actin (ACTB) was monitored as a loading control.

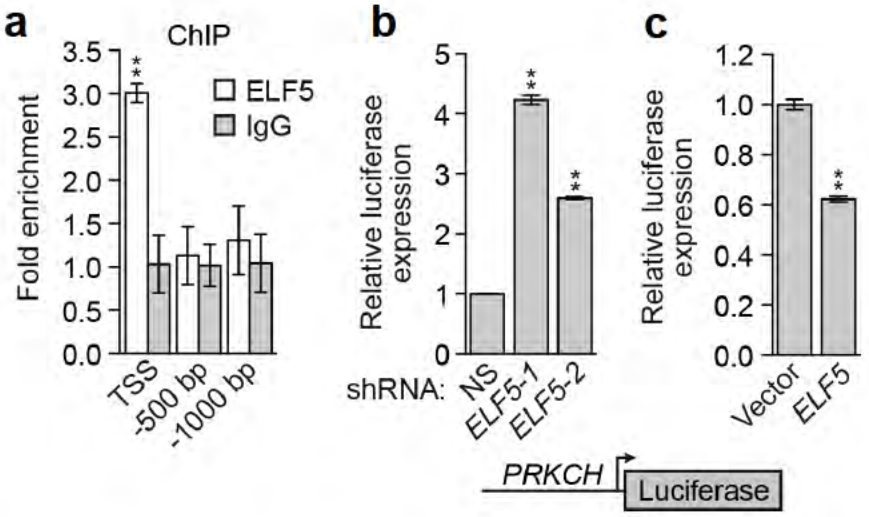

Figure 2.9. Direct transcriptional repression of *PRKCH* by ELF5. (**a**) Chromatin immunoprecipitation assay monitoring binding of ELF5 to the *PRKCH* promoter at the transcription start site (TSS) and at 500 and 1000 bp upstream of the TSS (n=3). The results were normalized to that obtained with an IgG control antibody, which was set to 1 (**b and c**) Expression of a luciferase reporter driven by the *PRKCH* promoter in K562 cells expressing a NS shRNA or one of two unrelated *ELF5* shRNAs (b; n=3) or in K562 cells ectopically expressing *ELF5* or, as a control, empty vector (c; n=3). Shown are firefly luciferase activities normalized to that of *Renilla* luciferase. Data are represented as mean ± SD. **P*≤0.05, ***P*≤0.01.

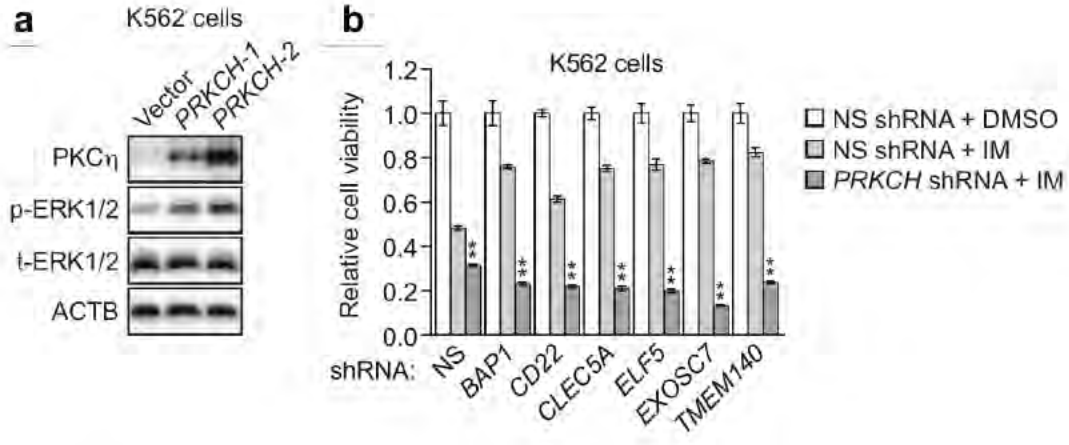

Figure 2.10. Confirmation of elevated PKCη levels in K562/*PRKCH* cells and role of *PRKCH* in IM resistance. (**a**) Immunoblot analysis showing the levels of PKCη and phosphorylated and total ERK1/2 (p-ERK1/2 and t-ERK1/2, respectively) in K562 cells expressing empty vector and in two independently derived K562 clonal cell lines ectopically expressing *PRKCH*. **(b)** MTT assay measuring relative viability of representative IMSG KD K562 cell lines expressing a NS or *PRKCH* shRNA, and treated in the presence or absence of IM. Data are represented as mean ± SD (n=4). Asterisks indicate comparisons between the two IM-treated samples. **P*≤0.05, ***P*≤0.01.

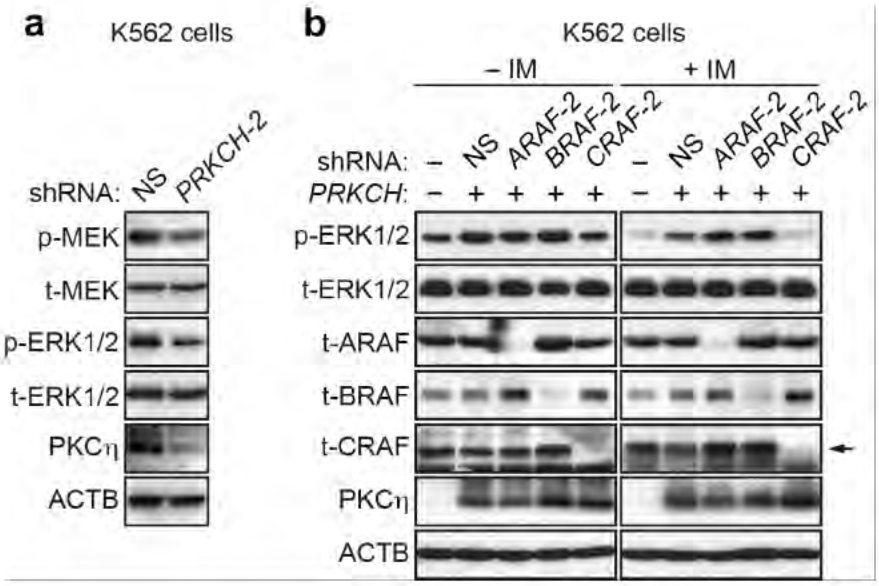

Figure 2.11. Confirmation that PKCη functions through CRAF to increase RAF/MEK/ERK signaling. (**a**) Immunoblot analysis showing RAF/MEK/ERK activity (as measured by p- and t-MEK and p- and t-ERK1/2) in K562 cells expressing a second *PRKCH* shRNA unrelated to that used in Figure 2.7 f. The level of PKCη was monitored as a control. β-actin (ACTB) was monitored as a loading control. (**b**) Immunoblot analysis showing p- and t-ERK1/2 levels in K562/*PRKCH-1* cells, treated in the absence or presence of IM, expressing a second *ARAF*, *BRAF* or *CRAF* shRNA unrelated to that used in Figure 2.7 g. The levels of total (t-) ARAF, BRAF and CRAF, and PKCη were monitored as controls. ACTB was monitored as a loading control.

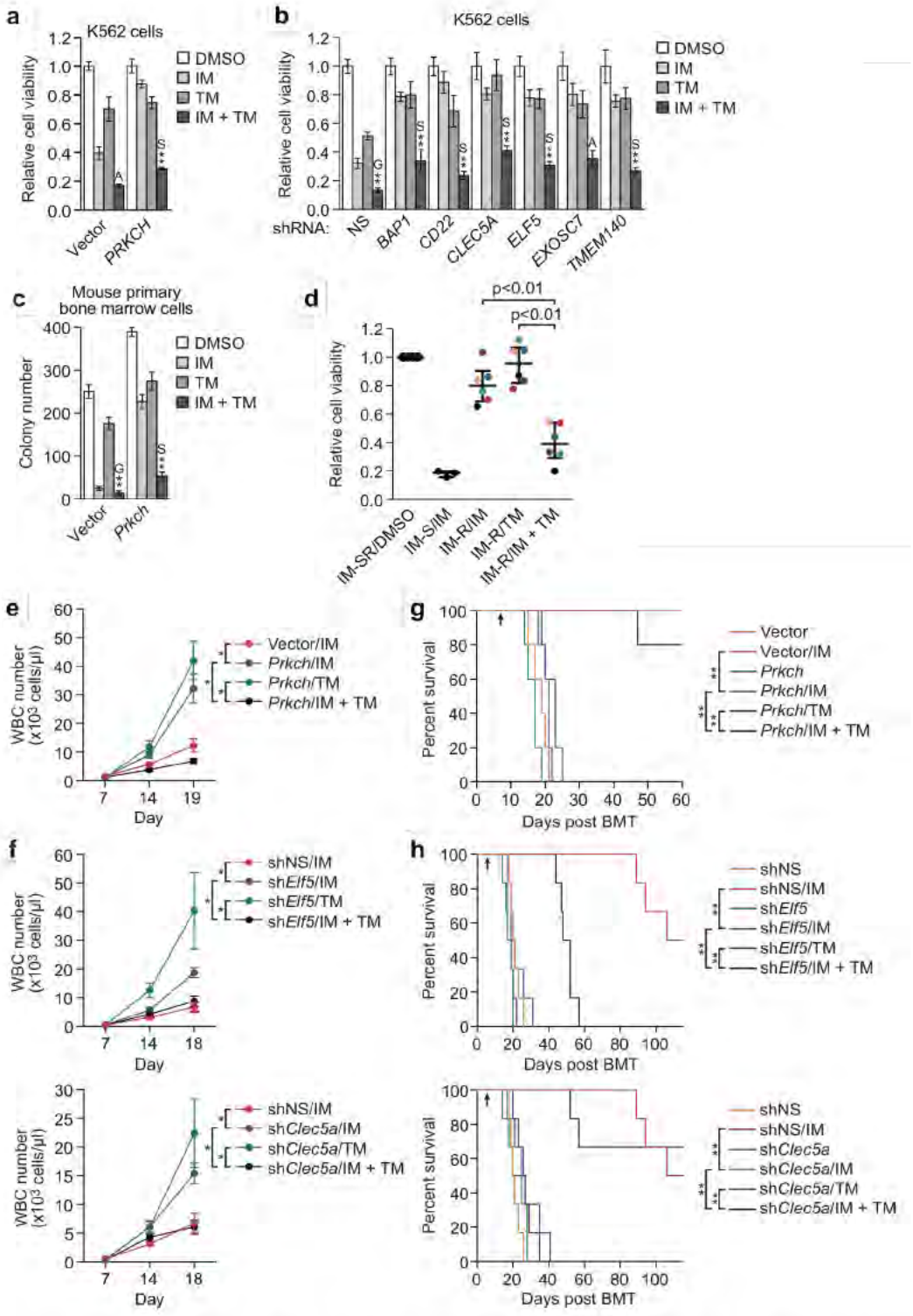

Figure 2.12. Combined treatment with IM and a MEK inhibitor has beneficial effects.

Figure 2.12. Combined treatment with IM and a MEK inhibitor has beneficial effects. (**a and b**) Cell viability, as measured by MTT assay, of K562/*PRKCH-1* (a; n=4) or IMSG KD K562 cells (b; n=3 or 4) treated with 0.1 μM IM, 1.5 nM trametinib (TM) or a combination of the two drugs, as indicated. The results were normalized to that observed with DMSO, which was set to 1. Data are represented as mean ± SD. Asterisks indicate comparisons between the combined drug treatment and single drug treatments. Combined drug treatment was synergistic (S), additive (A) or antagonistic (G). (**c**) Colony formation assay monitoring survival of BCR-ABL+ mouse primary bone marrow cells ectopically expressing *Prkch* and treated with IM, TM or a combination, as described in (a) (n=3). Data are represented as mean ± SD. (**d**) Relative viability, as measured by trypan blue cell counting, of primary leukemic cells from BCR-ABL-independent IM-sensitive (n=3) or -resistant (n=6) CML patients treated with 5 μM IM, 5 μM TM or a combination. The results were normalized to those obtained by DMSO treatment of the same samples [IM-S or IM-R (IM-SR)], which was set to 1. Error bars indicate median with interquartile range. Matched samples from the same patient are indicated by dots of the same color. (**e and f**) White blood cell (WBC) count of leukemic mice derived by transplantation of BCR-ABL+ mouse primary bone marrow cells ectopically expressing *Prkch* (e) or knocked down for an IMSG (F), and treated at day 7 with either IM, TM or a combination of the two drugs as indicated (n=4 or 5 mice per group). Data are represented as mean ± SEM. The same NS control is used in the two graphs shown in (f), which were derived from a single experiment. (**g and h**) Kaplan-Meier survival curves of leukemic mice derived as described in (E and F). The indicated cohorts of mice (n=5 for *Prkch* overexpression and n=6 for IMSG knockdown) were treated with either vehicle, IM (100 mg/kg twice a day), TM (2 mg/kg once a day), or both IM and TM by oral gavage starting at day 7 (indicated by the arrow). The same NS control is used in the curves shown in (H), which were derived from a single experiment. *$P \leq 0.05$, **$P \leq 0.01$.

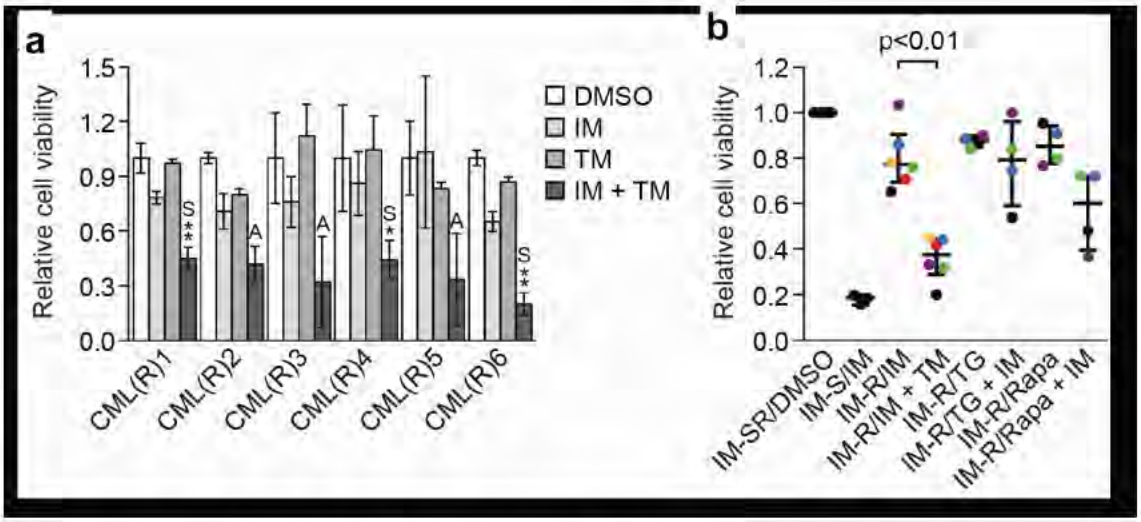

Figure 2.13. Comparison of combined treatment with IM and trametinib to IM and a JAK-STAT or PI3K inhibitor. (**a**) Cell viability, as measured by trypan blue cell counting, of primary leukemic cells from BCR-ABL-independent IM-resistant CML patients (n=6) treated with DMSO. 5 μM IM, 5 μM TM or a combination of the two drugs was used as indicated. The results were normalized to that observed with DMSO, which was set to 1. Data are represented as mean ± SD. The data are the same as those shown in Figure 2.12 d, but plotted to show the results for each individual patient sample. Asterisks indicate comparisons between the combined drug treatment and single drug treatments. Combined drug treatment was synergistic (S) or additive (a). (**b**) Relative viability, as measured by trypan blue cell counting, of leukemic cells from IM-sensitive CML patient samples (n=3), BCR-ABL-independent IM-resistant CML patients treated with 5 μM IM, 5 μM TM or a combination (n=6), or BCR-ABL-independent IM-resistant CML patients treated with 0.5 μM TG101348 (TG, a JAK-STAT inhibitor) or 10 nM rapamycin (Rapa, a PI3K inhibitor) alone or in combination with 5 μM IM (n=4). The results were normalized to those obtained by DMSO treatment of the same samples, which was set to 1. Error bars indicate median with interquartile range. Matched samples from the same patient are indicated by dots of the same color. Samples IM-SR/DMSO, IM-S/IM, IM-R/IM and IM-R/IM + TM are the same as those in Figure 2.12 d and are shown to facilitate comparison. The results presented here and in Figure 2.12 d were derived from a single experiment. For statistical significance, only comparisons between double treatments and IM alone were made.

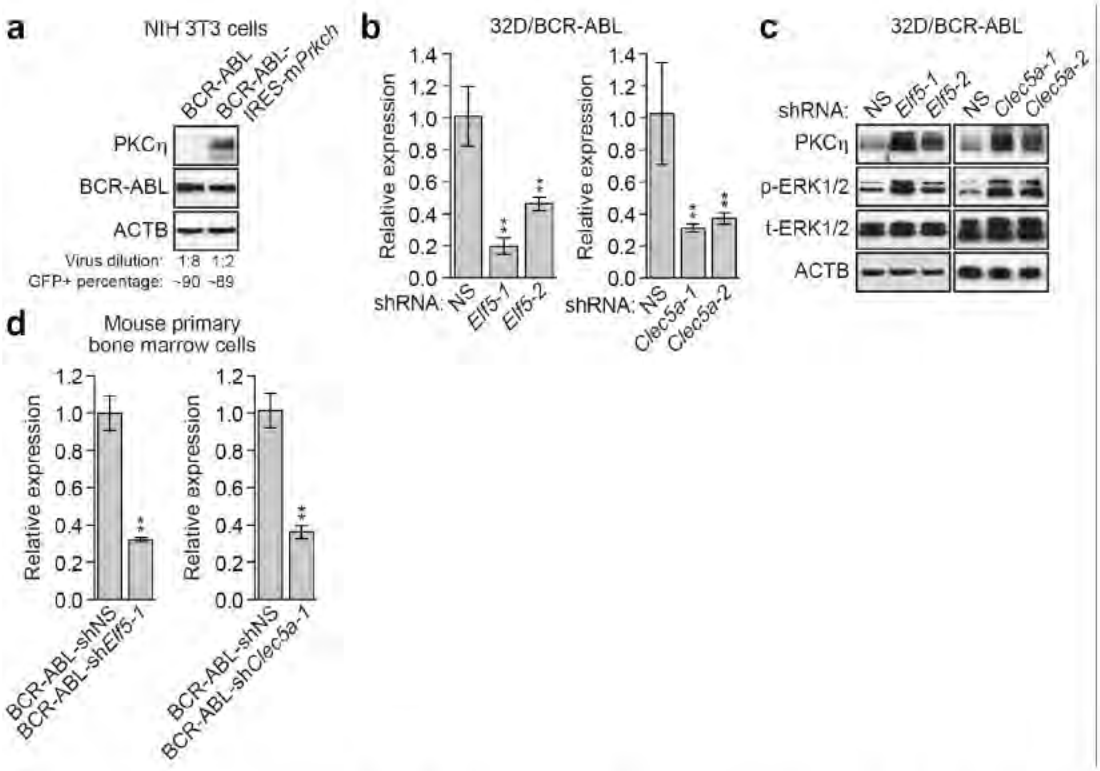

Figure 2.14. Effectiveness of retroviruses co-expressing BCR-ABL and either *PRKCH* or an *Elf5* or *Clec5a* shRNA. (**a**) Immunoblot analysis monitoring levels of PKCη and BCR-ABL in NIH 3T3 cells transduced with a retrovirus expressing BCR-ABL or one co-expressing BCR-ABL and murine *Prkch*. The percentage of GFP+ cells obtained was similar using both retroviruses, demonstrating equivalent virus titers. The same virus titers were used for transduction of primary mouse bone marrow cells. (**b**) qRT-PCR analysis monitoring knockdown efficiencies in 32D/BCR-ABL cells of one of two unrelated *Elf5* (left) or *Clec5a* (right) shRNAs. Data are represented as mean ± SD (n=3). **P*≤0.05, ***P*≤0.01. (**c**) Immunoblot analysis monitoring levels of PKCη and phosphorylated and total ERK1/2 (p-ERK1/2 and t-ERK1/2, respectively) in 32D/BCR-ABL cells expressing an NS, *Elf5* or *Clec5a* shRNA. (**d**) qRT-PCR analysis monitoring knockdown efficiencies of *Elf5* (left) and *Clec5a* (right) in mouse primary bone marrow cells transduced with a retrovirus co-expressing BCR-ABL and either an *Elf5* or *Clec5a* shRNA. The most effective *Elf5* shRNA (*Elf5-1*) and *Clec5a* shRNA (*Clec5a-1*), as determined by the results in (B), were used here and in Figure 2.12 f-h. Data are represented as mean ± SD (n=3). **P*≤0.05, ***P*≤0.01.

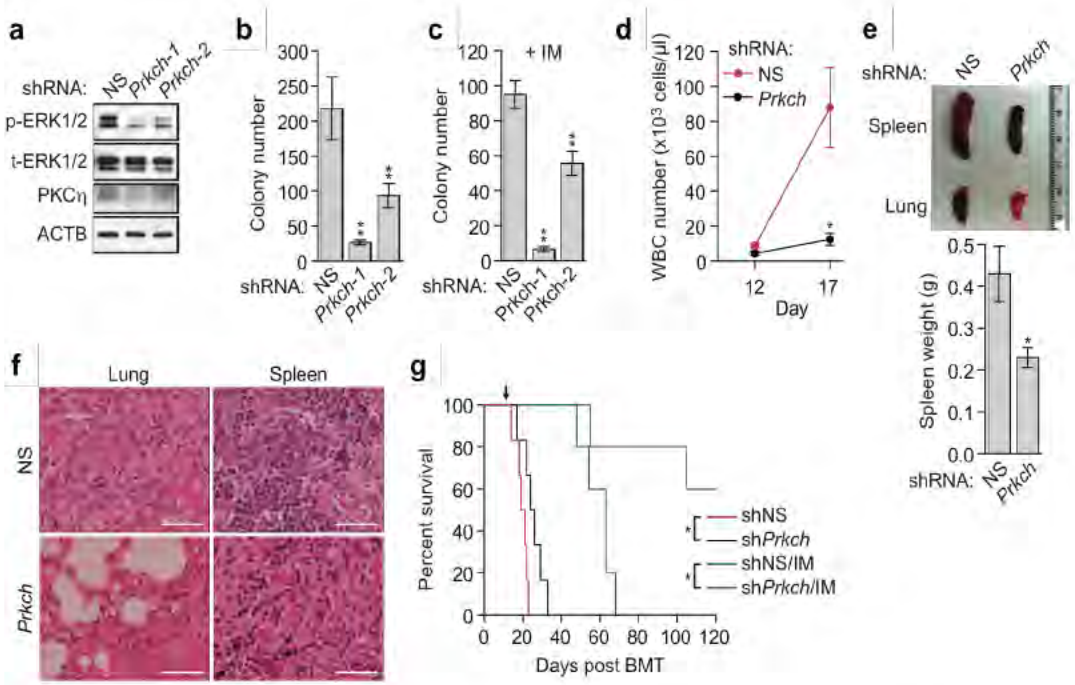

Figure 2.15. *PRKCH* modulates proliferation of BCR-ABL+ cells, disease progression, and IM-sensitivity. (**a**) Immunoblot analysis monitoring p- and t-ERK1/2 levels in BCR-ABL+ mouse primary bone marrow cells expressing an NS shRNA or one of two *Prkch* shRNAs. (**b**) Colony formation assay after knockdown of *Prkch* in BCR-ABL+ mouse primary bone marrow cells (n=3). Data are represented as mean ± SD. (**c**) Colony formation assay monitoring survival of BCR-ABL+ mouse primary bone marrow cells expressing a NS or one of two *Prkch* shRNAs and treated with 0.1 μM IM. Data are represented as mean ± SD. (**d**) WBC count of leukemic mice derived by transplantation of *Prkch* KD BCR-ABL+ mouse primary bone marrow cells (n=4 or 5). Data are represented as mean ± SEM. (**e**) (Tsai et al.) Representative spleen and lung images of leukemic mice derived as described in (d). Mice were sacrificed at day 17. (Bottom) Spleen weight of mice (n=4). Data are represented as mean ± SEM. (**f**) Hematoxylin and eosin (H&E) staining of spleen and lung sections from leukemic mice derived as described in (D). Scale bars, 50 μm. (**g**) Kaplan-Meier survival curve of untreated leukemic mice (n=6) or leukemic mice treated with IM at day 14 (indicated by the arrow) (n=5), derived as described in (D). **P*≤0.05, ***P*≤0.01.

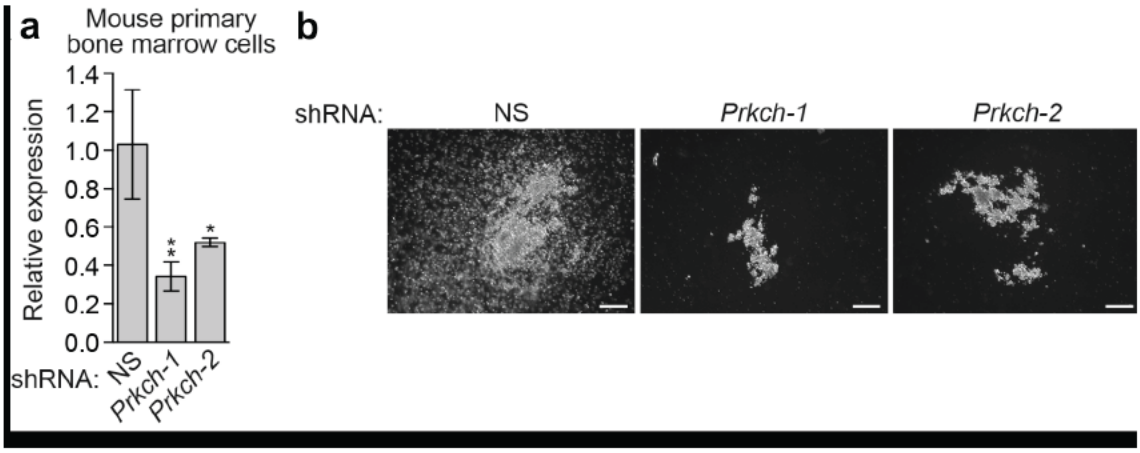

Figure 2.16. Decreased colony formation after knockdown of *PRKCH* in BCR-ABL+ cells. (**a**) qRT-PCR analysis monitoring knockdown efficiency of *Prkch* in mouse primary bone marrow cells expressing two unrelated *Prkch* shRNAs. The results were normalized to that obtained with a NS control, which was set to 1. Data are represented as mean ± SD (n=3). **P*≤0.05, ***P*≤0.01. (**b**) Micrograph showing typical colonies of BCR-ABL+ mouse primary bone marrow cells expressing a NS shRNA or one of two unrelated *Prkch* shRNAs. Scale bar, 100 μm.

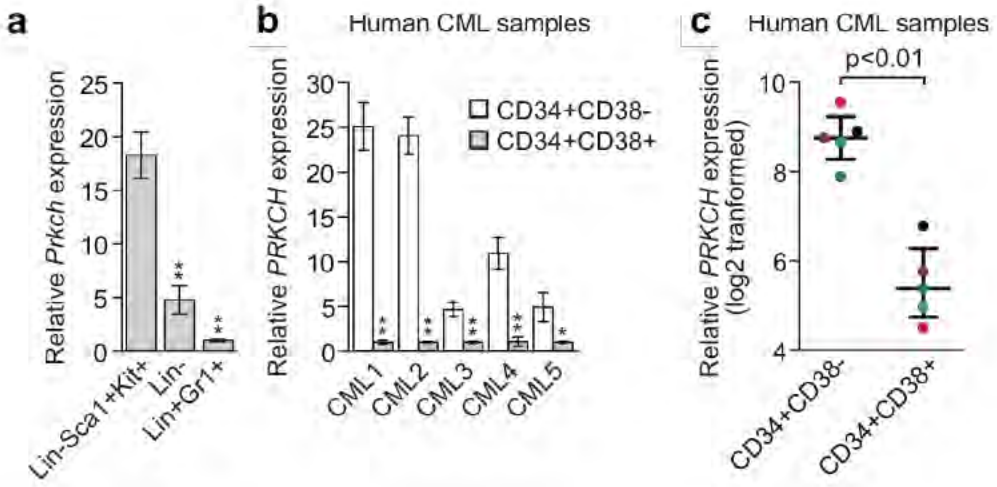

Figure 2.17. IM-resistant murine and human CML stem cells contain high levels of *PRKCH*. (**a**) qRT-PCR analysis monitoring *Prkch* expression in BCR-ABL+ murine CML stem cells (Lin-Sca1+Kit+), progenitor cells (Lin-) and mature cells (Lin+Gr1+) (n=3). Data are represented as mean ± SD. (**b**) qRT-PCR analysis monitoring *PRKCH* expression in human CML stem cells (CD34+CD38-) and progenitor cells (CD34+CD38+) isolated from CML patient samples (n=5). Data are from three technical replicates and are means ± SD. (**c**) *PRKCH* expression in CD34+CD38- and CD34+CD38+ cells, mined from a previous expression profiling study (Gerber et al., 2013). Matched samples from the same patient are indicated by dots of the same color. Error bars indicate median with interquartile range. *$P \leq 0.05$, **$P \leq 0.01$.

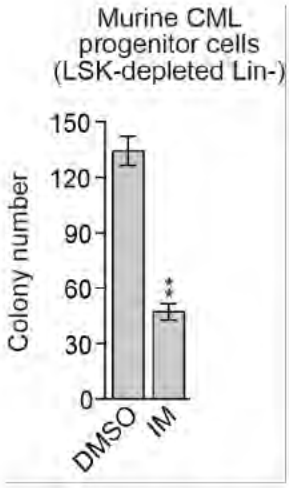

Figure 2.18. Confirmation of IM sensitivity of murine CML progenitor cells. Colony formation assay monitoring survival of BCR-ABL+ murine progenitor cells (Lin-Sca1+Kit+-depleted Lin- cells) expressing a NS shRNA and treated with DMSO or 0.1 μM IM (n=3). Data are represented as mean ± SD. As a comparison, see Figure 2.19 c, which shows the results of a similar analysis of IM-resistant murine CML stem cells. **P*≤0.05, ***P*≤0.01.

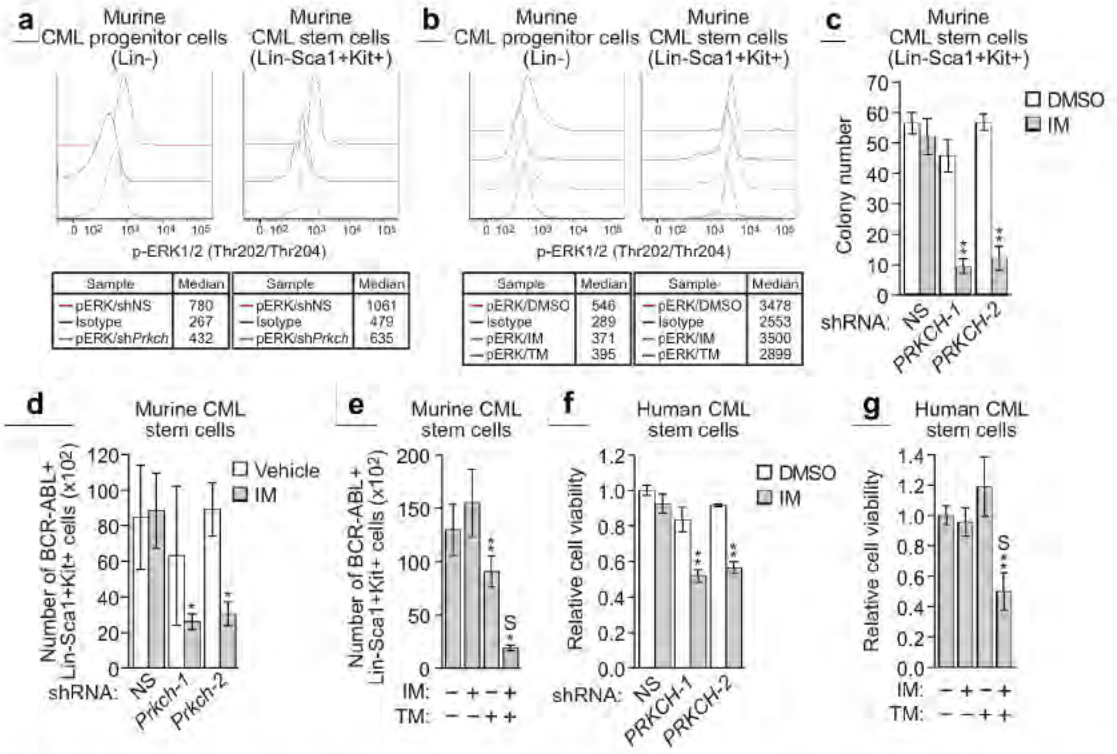

Figure 2.19. High *Prkch* levels contribute to the IM resistance of CML stem cells. (**a**) Intracellular phosphorylated ERK1/2 levels in Lin- and Lin-Sca1+Kit+ BCR-ABL+ *Prkch* KD or control bone marrow cells. As a negative control, cells were incubated with a conjugated IgG isotype antibody. (**b**) Intracellular phosphorylated ERK1/2 levels in Lin- and Lin-Sca1+Kit+ BCR-ABL+ bone marrow cells treated with DMSO, IM or trametinib. (**c**) Colony formation assay monitoring survival of BCR-ABL+ murine stem cells expressing a NS or one of two *Prkch* shRNAs and treated with 0.1 μM IM (n=3). Data are represented as mean ± SD. (**d**) FACS determination of the number of BCR-ABL+ Lin-Sca1+Kit+ bone marrow cells expressing a NS or *Prkch* shRNA after IM treatment of mice (n=4 or 5). Data are represented as mean ± SEM. (**e**) FACS determination of the number of BCR-ABL+ Lin-Sca1+Kit+ bone marrow cells after treatment of mice with vehicle (n=10), IM (n=12), TM (n=10) or both IM and TM (n=12). Data are represented as mean ± SEM. Asterisks indicate comparisons between the combined drug treatment and single drug treatments. Combined drug treatment was synergistic (S). (**f**) Relative viability, as measured by trypan blue cell counting, of BCR-ABL+ human CML stem cells (CD34+CD38-) expressing a NS or *Prkch* shRNA and treated with DMSO or IM (n=3). Data are represented as mean ± SEM. (**g**) Relative viability of BCR-ABL+ human CML stem cells treated with DMSO, IM, TM or a combination of drugs (n=3). Data are represented as mean ± SEM. **P*≤0.05, ***P*≤0.01.

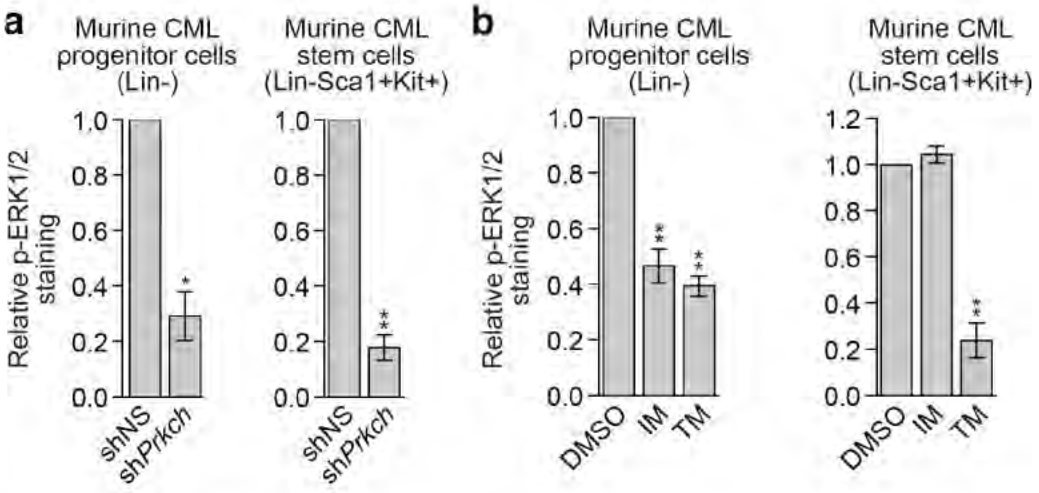

Figure 2.20. Quantification of phosphorylated ERK1/2 in CML progenitor and stem cells. (**a**) Intracellular phosphorylated ERK1/2 levels in Lin- and Lin-Sca1+Kit+ BCR-ABL+ *Prkch* KD or control bone marrow cells (n=3). The results were background corrected and then normalized to that obtained with the NS control shRNA, which was set to 1. Data are represented as mean ± SEM. (**b**) Intracellular phosphorylated-ERK1/2 levels in Lin- and Lin-Sca1+Kit+ BCR-ABL+ bone marrow cells treated with DMSO, IM or trametinib. (n=4). The results were background corrected and then normalized to that obtained with DMSO, which was set to 1. Data are represented as mean ± SEM. **P*≤0.05, ***P*≤0.01. These results accompany the representative experiment shown in Figure 2.19 a and b.

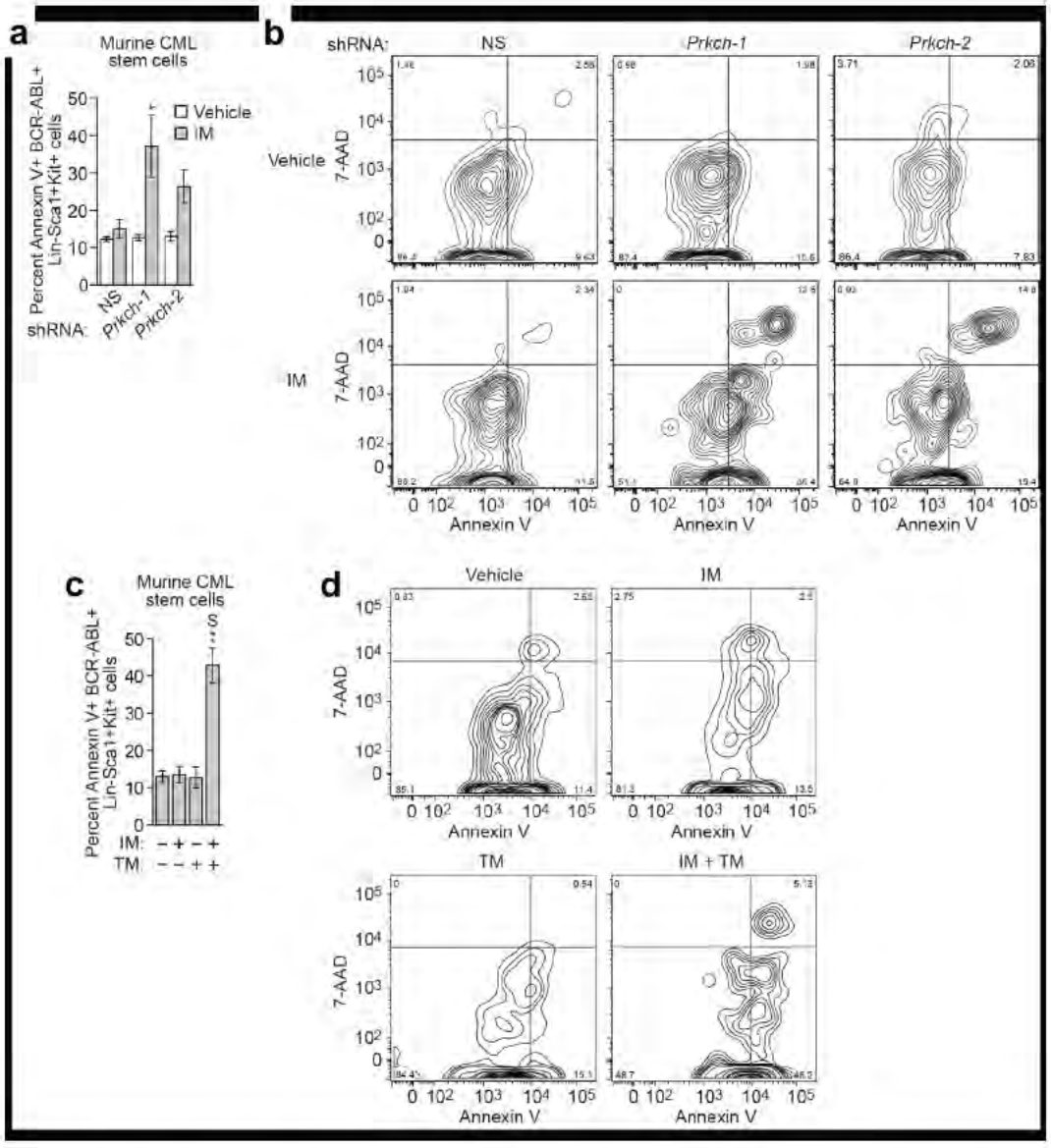

Figure 2.21. Synergistic induction of apoptosis in murine CML stem cells by IM and trametinib.

Figure 2.21. Synergistic induction of apoptosis in murine CML stem cells by IM and trametinib. (**a**) Apoptosis assay. CML mice (n=5) were orally gavaged with vehicle or IM. BCR-ABL+ bone marrow cells were stained with a Lin/Sca1/Kit antibody cocktail, then with Annexin V and 7-AAD followed by FACS. Data are represented as mean ± SEM. (**b**) FACS analysis showing representative Annexin V/7-AAD staining of murine CML stem cells expressing a NS shRNA or one of two unrelated *Prkch* shRNAs isolated from mice treated with vehicle or IM. These data provided the basis for the bar graph in (a). (**c**) Apoptosis assay. Mice were orally gavaged with vehicle (n=6), IM (n=6), TM (n=5) or both (n=5). BCR-ABL+ bone marrow cells were stained as described in (a). Data are represented as mean ± SEM. (**d**) FACS analysis showing representative Annexin V/7-AAD staining of murine CML stem cells isolated from mice treated with vehicle, IM, TM or a combination of IM and TM. These data provided the basis for the bar graph in (c). *$P \leq 0.05$, **$P \leq 0.01$.

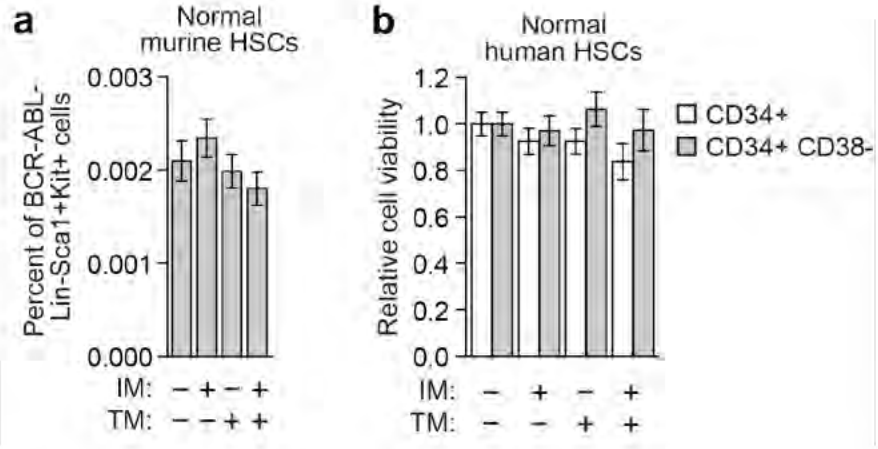

Figure 2.22. Effect of IM and trametinib on normal hematopoietic stem cells. (**a**) FACS determination of the percentage of normal (BCR-ABL-) murine Lin-Sca1+Kit+ bone marrow cells after treatment with vehicle (n=21), IM (n=21), TM (n=9) or both IM and TM (n=9). Data are represented as mean ± SEM. (**b**) Relative viability, as measured by trypan blue cell counting, of normal human hematopoietic CD34+ cells and hematopoietic stem cells (CD34+CD38-) treated with DMSO, IM, TM or a combination of drugs (n=4). The results were normalized to that obtained in cells treated with DMSO, which was set to 1. Data are represented as mean ± SD. **P*≤0.05, ***P*≤0.01.

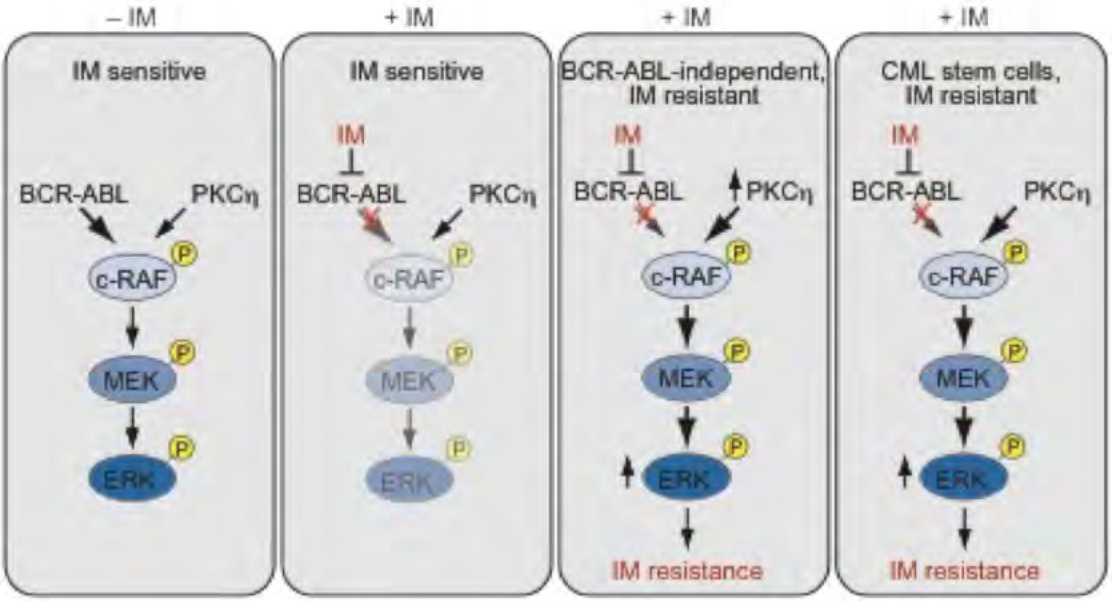

Figure 2.23. Elevated PKCη levels lead to IM resistance in CML and CML stem cells. Relative contributions of BCR-ABL and PKCη to RAF/MEK/ERK signaling are indicated by arrow size and shading.

Biological process	Gene symbol	Gene name
Cell signaling	*CLEC5A*	C-type lectin domain family 5, member A
	STK11	Serine/threonine kinase 11
	WNT7B	Wingless-type MMTV integration site family, member 7B
DNA/RNA metabolism	*DNASE1L1*	Deoxyribonuclease I-like 1
	EXOSC7	Exosome component 7
	RPP38	Ribonuclease P/MRP 38kDa subunit
Protein metabolism	*BAP1*	BRCA1 associated protein-1 (ubiquitin carboxy-terminal hydrolase)
Transcriptional regulation	*ELF5*	E74-like factor 5 (ets domain transcription factor)
Immunity	*CD22*	CD22 molecule
Unknown	*MEGF8*	Multiple EGF-like-domains 8
	TMEM140	Transmembrane protein 140

Table 2.1. List of 11 IMSGs obtained from the genome-wide RNAi screen. All candidates were validated with a second, unrelated shRNA. Knockdown conferred IM resistance in BCR-ABL-transformed primary bone marrow cells and increased $IC50^{IM}$ greater than 5-fold in K562 cells.

Sample ID	Source	BCR-ABL mutation	CML phase	Origin	IM resistant /sensitive
WT-1	Druker lab, OHSU Knight Cancer Institute	–	CP	Bone marrow	Resistant
WT-2	Druker lab, OHSU Knight Cancer Institute	–	CP	Bone marrow	Resistant
WT-3	Druker lab, OHSU Knight Cancer Institute	–	CP	Bone marrow	Resistant
WT-4	Druker lab, OHSU Knight Cancer Institute	–	CP	Bone marrow	Resistant
WT-5	Hematology Bank, Winship Cancer Institute	–	My BP	Bone marrow	Resistant
WT-6	Hematology Bank, Winship Cancer Institute	–	CP	Bone marrow	Resistant
WT-7	Hematology Bank, Winship Cancer Institute	–	My BP	Bone marrow	Resistant
WT-8	Hematology Bank, Winship Cancer Institute	–	CP	Bone marrow	Resistant
WT-9	Hematology Bank, Winship Cancer Institute	–	CP	Bone marrow	Resistant
WT-10	Hematology Bank, Winship Cancer Institute	–	CP	Peripheral blood	Resistant
WT-11	Hematology Bank, Winship Cancer Institute	–	CP	Peripheral blood	Resistant
Mut-1	Druker lab, OHSU Knight Cancer Institute	G250E	CP	Bone marrow	Resistant
Mut-2	Druker lab, OHSU Knight Cancer Institute	M244V	AP	Bone marrow	Resistant
Mut-3	Druker lab, OHSU Knight Cancer Institute	Y253F	CP	Peripheral blood	Resistant
Mut-4	Druker lab, OHSU Knight Cancer Institute	T315I	BC	Leukapheresis	Resistant
Mut-5	Druker lab, OHSU Knight Cancer Institute	T315I	AP	Peripheral blood	Resistant
Mut-6	Hematology Bank, Winship Cancer Center	T315I, E255R	My BP	Bone marrow	Resistant
Mut-7	Hematology Bank, Winship Cancer Center	F317L	Ly BP	Bone marrow	Resistant
Mut-8	Hematology Bank, Winship Cancer Center	T315I	CP	Bone marrow	Resistant
Mut-9	Hematology Bank, Winship Cancer Center	T315I	CP	Bone marrow	Resistant
Mut-10	Hematology Bank, Winship Cancer Center	T315I	CP	Bone marrow	Resistant
Mut-11	Hematology Bank, Winship Cancer Center	F317L	CP	Peripheral blood	Resistant
CML(R)1	Department of Pathology, UMMS	–	CP	Peripheral blood	Resistant
CML(R)2	Department of Pathology, UMMS	–	CP	Peripheral blood	Resistant
CML(R)3	Druker lab, OHSU Knight Cancer Institute	–	CP	Bone marrow	Resistant
CML(R)4	Druker lab, OHSU Knight Cancer Institute	–	CP	Bone marrow	Resistant
CML(R)5	Druker lab, OHSU Knight Cancer Institute	–	CP	Bone marrow	Resistant
CML(R)6	Druker lab, OHSU Knight Cancer Institute	–	BC	Peripheral blood	Resistant
WT-1	Hematology Bank, Winship Cancer Institute	–	CP	Peripheral blood	Sensitive
WT-2	Hematology Bank, Winship Cancer Institute	–	CP	Peripheral blood	Sensitive
WT-3	Hematology Bank, Winship Cancer Institute	–	CP	Peripheral blood	Sensitive
WT-4	Hematology Bank, Winship Cancer Institute	–	CP	Bone marrow	Sensitive
WT-5	Department of Pathology, UMMS	–	CP	Bone marrow	Sensitive
WT-6	Department of Pathology, UMMS	–	CP	Bone marrow	Sensitive
WT-7	Department of Pathology, UMMS	–	CP	Bone marrow	Sensitive
WT-8	Department of Pathology, UMMS	–	CP	Peripheral blood	Sensitive
WT-9	Department of Pathology, UMMS	–	CP	Peripheral blood	Sensitive
WT-10	Department of Pathology, UMMS	–	CP	Peripheral blood	Sensitive
WT-11	Department of Pathology, UMMS	–	CP	Peripheral blood	Sensitive
CML(S)1	Department of Pathology, UMMS	–	CP	Peripheral blood	Sensitive
CML(S)2	Department of Pathology, UMMS	–	CP	Peripheral blood	Sensitive
CML(S)3	Druker lab, OHSU Knight Cancer Institute	–	CP	Bone marrow	Sensitive
CML(S)4	Druker lab, OHSU Knight Cancer Institute	–	CP	Bone marrow	Sensitive
CML(S)5	Druker lab, OHSU Knight Cancer Institute	–	CP	Bone marrow	Sensitive

[1]WT, BCR-ABL wild-type; Mut, BCR-ABL kinase domain mutant.
[2]AP, accelerated phase; BC, blast crisis; CP, chronic phase; Ly BP, lymphoid blast crisis phase; My BP, myeloid blast crisis phase.

Table 2.2. List of CML patient samples used in this study.

Sample ID	Relative expression											
	BAP1	***CD22***	***CLEC5A***	***DNASE1L1***	***ELF5***	***EXOSC7***	***MEGF8***	***RPP38***	***STK11***	***TMEM140***	***WNT7B***	***PRKCH***
WT-1	0.498	3.723	13.781	1.231	9.882	1.299	3.806	0.541	0.607	3.559	15.608	0.204
WT-2	1.294	5.749	2.379	1.198	8.263	3.765	9.764	1.872	2.876	7.013	10.095	0.688
WT-3	1.086	0.651	12.468	1.058	1.963	3.295	0.915	0.784	1.710	1.780	1 552	0.176
WT-4	0.723	1.042	1.828	1.401	1.208	5.210	1.713	7.357	.0842	0.478	1.191	0.858
WT-5	0.437	0.976	2.717	1.268	0.953	.0332	1.431	0.437	3.192	0.503	4.125	0.116
WT-6	1.222	0.655	2.400	0.918	0.790	1.807	0.696	2.904	2.692	0.404	1 341	0.287
WT-7	7.906	16.193	22 845	2.368	13.862	0.195	5.888	5.464	1.770	3.420	96.887	2.075
WT-8	5.844	3.436	3.760	2.744	13.486	2.027	3.055	1.708	5.362	3.521	10.836	1.735
WT-10	0.574	0.569	7.508	0.852	1.954	2.260	1.537	0.102	0.795	0.438	2 595	2.107
WT-11	3.589	2.881	12.961	1.870	5.556	0.682	15.511	7.422	1.651	8.578	31.855	0.565
WT-12	1.509	2.863	2.445	1.921	5.634	1.999	3.179	0.611	2.273	1.422	1 549	0.208

Table 2.3. Relative expression of IMSGs in IM-resistant BCR-ABL-wt CML patient samples. Relative expression was calculated by determining the average expression of a given gene in all 11 mutant BCR-ABL patient samples, and dividing by the expression of the gene in the individual wild-type BCR-ABL sample. Thus, the value represents the fold down-regulation in wild-type BCR-ABL samples.

Human Gene	First shRNA	Second shRNA
ABCB6	TRCN0000060318	
ADARB2	TRCN0000051893	
AIFM3	TRCN0000064545	
AKR1C1	TRCN0000036544	
AKR1C3	TRCN0000026540	
ANO2	TRCN0000138764	
ARAF	TRCN0000000571	TRCN0000000568
ASAH3L	TRCN0000050685	
BAP1	TRCN0000007373	TRCN0000007372
BAZ2A	TRCN0000015571	
BCAP29	TRCN0000060447	TRCN0000060444
BMI1	TRCN0000020158	
BMP6	TRCN0000058615	
BRAF	TRCN0000006291	TRCN0000006292
C6orf224	TRCN0000140490	
CCL14	TRCN0000057850	
CD22	TRCN0000057623	TRCN0000057625
CELA1	TRCN0000003679	TRCN0000003681
CHRNA1	TRCN0000060992	
CLEC5A	TRCN0000054035	TRCN0000054034
CMYA5	TRCN0000129695	
CRAF	TRCN0000001067	TRCN0000001068
CUBN	TRCN0000055649	
CYP46A1	TRCN0000063810	
DGKD	TRCN0000000672	
DNASE1L1	TRCN0000049688	TRCN0000049690
DPM1	TRCN0000036188	TRCN0000036186
DUSP13	TRCN0000003064	
EBF1	TRCN0000013828	TRCN0000013830
EFEMP2	TRCN0000053336	
EFNA3	TRCN0000058722	
EHD2	TRCN0000053473	
ELF5	TRCN0000013875	TRCN0000013877
EXOSC7	TRCN0000051072	TRCN0000051070
E2F4	TRCN0000013809	TRCN0000013810
FAHD1	TRCN0000050068	
FAM92A1	TRCN0000136349	
GDAP1L1	TRCN0000136540	
GFRA2	TRCN0000060710	
GHRH	TRCN0000083152	
GRK5	TRCN0000000842	
GTF3C4	TRCN0000013402	
IDH3A	TRCN0000027270	TRCN0000027310
IDS	TRCN0000051546	
IFT140	TRCN0000147721	

Table 2.4. List of clone IDs for shRNAs obtained from Open Biosystems /Thermo Scientific.

IL1A	TRCN0000059211	
ITCH	TRCN0000002087	
KCNC4	TRCN0000044942	
KCNH3	TRCN0000044593	
KIR2DL2	TRCN0000061458	
LEP	TRCN0000058353	
LGALS9	TRCN0000057446	
LILRA3	TRCN0000056945	TRCN0000056946
LMO7	TRCN0000006490	
LRAT	TRCN0000035998	
MED8	TRCN0000052951	
MEGF8	TRCN0000055555	TRCN0000055554
MEP1A	TRCN0000050903	
MMP7	TRCN0000051847	TRCN0000051844
MOV10	TRCN0000049978	
NCBP1	TRCN0000059506	
OBFC2A	TRCN0000134695	
OR2D2	TRCN0000060969	
PAG1	TRCN0000123270	
POLR1C	TRCN0000052904	
PRKCH	TRCN0000006296	TRCN0000006295
PRSS1	TRCN0000052119	
PSMD10	TRCN0000058074	
RASL10B	TRCN0000047610	
RCVRN	TRCN0000053264	TRCN0000053263
RFK	TRCN0000037600	
RIN2	TRCN0000062647	
RPP38	TRCN0000049875	TRCN0000049876
RPS6KB1	TRCN0000003162	
SEC23IP	TRCN0000064955	
SGK493	TRCN0000037531	
SH3TC1	TRCN0000062611	
SOX18	TRCN0000017449	
STK11	TRCN0000000408	TRCN0000000409
STYXL1	TRCN0000003054	TRCN0000003052
TCEAL1	TRCN0000013415	TRCN0000013413
TM4SF18	TRCN0000122444	
TMEM140	TRCN0000138719	TRCN0000138320
TRAF4	TRCN0000034239	TRCN0000034241
TRIM24	TRCN0000021262	
UBAP2L	TRCN0000007681	TRCN0000007679
WDR45L	TRCN0000148944	
WDR92	TRCN0000053730	
WNT7B	TRCN0000061877	TRCN0000061875
ZACN	TRCN0000060205	TRCN0000060204
ZFP82	TRCN0000016086	
ZHX1	TRCN0000020354	
ZKSCAN3	TRCN0000017750	

Table 2.4. List of clone IDs for shRNAs obtained from Open Biosystems /Thermo Scientific. (Continued)

Mouse Gene		
Bap1	TRCN0000030719	TRCN0000030721
Bcap29	TRCN0000099810	TRCN0000099811
Cd22	TRCN0000067945	TRCN0000067946
Cela1	TRCN0000092406	TRCN0000092407
Clec5a	TRCN0000067713	TRCN0000067715
Dnase1l1	TRCN0000108731	TRCN0000108730
Dpm1	TRCN0000111999	TRCN0000111996
Ebf1	TRCN0000086578	TRCN0000086580
Elf5	TRCN0000081940	TRCN0000081938
Exosc7	TRCN0000051070	TRCN0000051068
E2f4	TRCN0000085633	TRCN0000085634
Idh3a	TRCN0000041785	TRCN0000041786
Megf8	V3LMM_497156	V3LMM_457695
Mmp7	TRCN0000031250	TRCN0000031251
Prkch	TRCN0000022812	TRCN0000022811
Rcvrn	TRCN0000053267	V3LMM_504872
Rpp38	TRCN0000099598	TRCN0000099599
Stk11	TRCN0000024146	TRCN0000024147
Styxl1	TRCN0000071409	TRCN0000071412
Tceal1	TRCN0000108607	TRCN0000108608
Tmem140	TRCN0000177850	TRCN0000178239
Traf4	TRCN0000067747	TRCN0000067743
Ubap2l	TRCN0000007677	TRCN0000007679
Wnt7b	TRCN0000071779	TRCN0000071780

Table 2.4 List of clone IDs for shRNAs obtained from Open Biosystems /Thermo Scientific. (Continued)

	Forward primer sequence (5' → 3')	**Forward primer sequence (5' → 3')**
Human Gene		
BAP1	ATCTGGGTCCTGTCATCAGC	GCTGCCTTGGATTGGTCTG
BCAP29	AACTAGTAGAAGACCAGGAG	CGAAAGTCTCTCTGACTGC
CD22	CACCTCAATGACAGTGGTCAG	TGGATCGGATACCCATAGCAG
CELA1	TCCAGCTCCTCCTACTGG	CAGAATACTTGCCATTCACC
CLEC5A	AGGTGGCGTTGGATCAACAA	TTAGGCCAATGGTCGCACAG
DNASE1L1	CTGCACACCACTCCTAAGGC	CAGGCGCTTTTTGGTCAGT
DPM1	ATGGATGCTGATCTCTCACACC	CCATTTCCTTTGTAGCGAGTTCC
EBF1	CCTGGTGTTGTGGAAGTCACA	GCTCAACGAACCCACCATC
ELF5	GCTGATTCCAACTGCTTGAAAAC	CAGTTTTCTTCAGGAGATAGAAGC
EXOSC7	CCAAATGAAGGCTACTTGGAGT	TAGAGGGTGTTAGCGATCTCG
E2F4	ATCGGGCTAATCGAGAAAAAGTC	TGCTGGTCTAGTTCTTGCTCC
IDH3A	AGCCGGTCACCCATCTATGAA	TAGAGACACATGGTCGGACAT
LILRA3	GCTCACTCAGCTCCAACC	TCACCAGCCTTGGATTCG
LYN	TTCTGGTCTCCGAGTCACTCA	GCCGTCCACTTAATAGGGAACT
MEGF8	CGCCTGTCTTCGTCACGTC	CTGCTGAAAGGTGAGCAAGT
MMP7	GTGGAGTGCCAGATGTTGC	ATCGATCCACTGAATATGCG
PRKCH	GTGACTTGATGTTCCACATTCAG	ATTGTCCAGTTTCAGATCTCTATAG
RCVRN	CACGCCGGAAAAGCGAGC	GGATCAGTCGCAGAATTTCC
RPP38	GACTTTGTGGACGAAGTAAGAGC	GCTTTCCAGAGGTTCAGTCTC
STK11	CTGCAAGCAGCAGTGAGG	AACCGGCAGGAAGACTGAG
STYXL1	GACCCCAAGATTCAGAAGG	TCCGGGGAATCTTCTATCC
TCEAL1	TCGTTCTCGCCCGCAATTTAG	GATAAGGACGGCTCCGTTTTG
TMEM140	TCGGCTTCTATAACTTCTGCCT	CTGTTGCACTGGGCTAGGAG
TRAF4	TGCCTATCCGCTGCATCC	TTCATGGGGCAGCGATTAGC
UBAP2L	ATAGCAGCGGCAATACGTGG	GAAGACACATTAGAGGCAGTGAA
WNT7B	GAAGCAGGGCTACTACAACCA	CGGCCTCATTGTTATGCAGGT
ZACN	GAGAGGGGAACAGCGAGAG	CAGTCTCAGGCCAGCTTCTC
Mouse Gene		
Bap1	TAGTCCTCCCAGCAAATGTAAG	GTCTTCCTCCTCCTGCATAG
Bcap29	TTCTGTCTGCCCTTTATTCCTCC	TCTTACTTCTCTCACGGCATCT
Cd22	AAGCTGGATGTCCATTATGCTC	TCTGTAGGAGGTGACGTCTG
Cela1	TCTGGATGCCAGGGTGATTC	TATTCATCCAGGAAATGTAAGCAG
Mclec5a	GAAACTGGGATTTTCACCAAGG	TCCTGAAGATACTTCAGTTTCTC
Dnase1l1	TATGTGTATATCTACAGGTCTGAC	ACCACACTTGGAAGAGTTTTGC
Dpm1	GTAATTTTGATATTGTCTCTGGAAC	CTTCTTTTCGGTATAATCTGAAGC
Ebf1	CTCACCCTATGCCATTGTGC	CGAAAGCACTCTTCTGTTTCAC
Elf5	TGCCTTTGAGCATCAGACAG	TACTGGTCGCAGCAGAATTG
Exosc7	GTGATGACCTTGGCACAGAG	CATTCCAGCAGCAGCACATC
E2f4	ACATCTGAGATTGCAGTGAGTG	TACTACTATCCAGCAGTGCAG
Idh3a	TGGGTGTCCAAGGTCTCTC	CTCCCACTGAATAGGTGCTTTG
Megf8	CTGCCAGTGTTCTAGGAAACTAC	ATGTGAGTAACGGCCACTAGG
Mmp7	TGAGGACGCAGGAGTGAAC	CGTCCTTTGTAAGACTGAAGTC
Prkch	TCCGGCACGATGAAGTTCAAT	TACGCTCACCGTCAGGTAGG
Rcvrn	ACGACGTAGACGGCAATGG	CCGCTTTTCTGGGGTGTTTT

Table 2.5. List of primer sequences used for quantitative real-time RT-PCR.

Rpp38	CTTCTGCTCAGGGTTTTCAAG	ATGTCTTCTCTCTCCAAGGTG
Stk11	AGTATGACTGTAGTGCCCTAC	CAGGACCTGTCCAGGCAC
Styxl1	CTGCTTTTCTGCGAGCCAAC	TGTCGTTTTGATCGGACATCC
Tceal1	GTATCCGCCCTCAATTCATAG	CTCCGTTTTGCCTTCCAATGC
Tmem140	CAGCGTTGGTTTTTGTCTCCC	GAGGAGAGCGTAGAACATCAG
Traf4	CCCGGCTTCGACTACAAGTTC	TCAGGGCATTTGAAGACTCCT
Ubap2l	TGCTACAACTTCAGGAAAAGCTC	GTCTGGAGCATCTGTAAATCATC
Wnt7b	CCCGATGCCATCATTGTGATC	GTAGGGAGTCGAGAGGCTG

Table 2.5. List of primer sequences used for quantitative real-time RT-PCR. (Continued)

CHAPTER III: SINGLE-CELL RNA-SEQ REVEALS A TARGETABLE IMATINIB-RESISTANCE PATHWAY IN LEUKEMIC STEM CELLS

ABSTRACT

Chronic myeloid leukemia (CML) is a hematopoietic malignancy that is predominantly caused by a chromosomal translocation that leads to expression of the oncogenic fusion protein BCR-ABL(Faderl et al., 1999). The first-line treatment for CML is the BCR-ABL inhibitor imatinib mesylate (IM). CML, like several other malignancies, is propagated by a small population of stem cells whose eradication is required to achieve long-term remission and cure(Dean et al., 2005; Graham et al., 2002). Unfortunately, CML stem cells (CMLSCs) do not depend on BCR-ABL activity for survival and are thus not eliminated by IM treatment(Corbin et al., 2011; Hamilton et al., 2012). Pro-survival genes that are preferentially expressed in CMLSCs compared to normal hematopoietic stem cells (HSCs) represent potential therapeutic targets for selectively eradicating CMLSCs. However, the discovery of such preferentially expressed genes has been hampered by the inability to completely separate CMLSCs from HSCs(Jiang et al., 2008), which display the same set of surface markers(Carter et al., 2010; Sloma et al., 2010). To overcome this challenge, and to minimize confounding effects of individual differences in gene expression profiles(Cheung et al., 2003), here we perform single-cell RNA-seq on CMLSCs and HSCs that were isolated from the same patient and distinguished based on the presence or

absence of BCR-ABL. Among genes preferentially expressed in CMLSCs is *PIM2*, which encodes a pro-survival serine-threonine kinase that phosphorylates and inhibits the pro-apoptotic protein BAD(Yan et al., 2003). We show that IM resistance of CMLSCs is due, at least in part, to maintenance of BAD phosphorylation by PIM2. Combined treatment with IM and a PIM2 inhibitor synergistically increases apoptosis of CMLSCs, suppresses colony formation, and significantly prolongs survival in a mouse CML model with a negligible effect on HSCs. Importantly, BCR-ABL independent IM-resistant CML cells are also sensitive to this combination therapy. Our results reveal a therapeutically targetable mechanism of IM resistance in CMLSCs and bulk CML cells. The experimental approach we describe can be generally applied to other malignancies that harbor oncogenic fusion proteins or other characteristic genetic markers.

RESULTS

To distinguish CMLSCs and HSCs, which display the same set of surface markers (CD34+CD38-CD90+CD45RA-)(Carter et al., 2010; Sloma et al., 2010), we first captured ~600 CD34+CD38-CD90+CD45RA- cells (~200 from each of three CML patient samples) and then used single-cell nested PCR to detect the presence (CMLSCs) or absence (HSCs) of the BCR-ABL transcript (Figure 3.1 a and Figure 3.2). Once CMLSCs and HSCs had been identified, we then carried out single-cell RNA-seq on ~48 CMLSCs and ~48 HSCs from each patient.

Typically, we obtained ~2.5 million mapped reads (>70% average mapping efficiency) and detected ~5,000 genes (transcript per million [TPM]>1) per cell (Figure 3.1 b and Figure 3.3 a-c). To ensure quality of the analysis, we excluded those cells with low-sequencing depth (fewer than 0.5 million mapped reads) and low coverage (<2,000 genes). Comparison of our single-cell RNA-seq data to published RNA-seq results from HSCs(Woll et al., 2014) revealed that both CMLSCs and HSCs have an HSC-like signature (Figure 3.1 c). Notably, there were substantial differences in HSC and CMLSC gene expression patterns among the three CML patients (Figure 3.3 d), underscoring the contribution of individual variation.

Previous single-cell RNA-seq studies have found that the average gene expression of as few as 30 single cells highly correlates with that of the

population control typically derived from >10,000 cells(Shalek et al., 2014). Because our analysis involved a pure population that consisted of a relatively small number of cells, we asked whether our small sample size was sufficient to mimic a larger population control. Consistent with the previous studies, we found that random sampling with increasing number of cells achieved a high correlation at ~30 cells (Figure 3.3 e), confirming the validity of using ~48 cells to represent each population group.

The correlation of overall gene expression among single cells from the same patient ranged from 0.27–0.61 with a median of 0.43, indicative of significant heterogeneity (Figure 3.1 d and Figure 3.3 f). Notably, the inter-patient correlation was significantly lower than the intra-patient correlation (Figure 3.1 d and Figure 3.3 f). Thus, there was greater heterogeneity between CML patients than between CMLSCs and HSCs of the same patient, which could also be visualized by multidimensional scaling (MDS) (Figure 3.1 e). The MDS analysis also revealed that the CMLSC and HSC populations could not be clearly distinguished from one another, indicating that BCR-ABL did not substantially affect global gene expression.

Despite the heterogeneity of the gene expression pattern, we were able to identify genes that were significantly more highly expressed in CMLSCs than in HSCs (Figure 3.4a, Figure 3.5a). About 50% of these differentially expressed

genes had modest total expression levels (10<TPM≤100) (Figure 3.4b and Figure 3.5b). Two cell surface markers, CD33 and CD47, were expressed at significantly higher levels in CMLSCs than in HSCs and could potentially be used to isolate CMLSCs (Figure 3.4c). Gene Set Enrichment Analysis (GSEA) revealed that compared to HSCs, CMLSCs preferentially expressed genes associated with active cell division (Figure 3.4d).

Systematic inter-patient comparison revealed that one of genes preferentially expressed in CMLSCs compared to HSCs was *PIM2* (Figure 3.4c). Intra-patient comparison confirmed that *PIM2* was more highly expressed in CMLSCs compared to HSCs in all three CML patients (Figure 3.4e). We also found that in mice, *Pim2* was expressed at a significantly higher level in BCR-ABL-positive CML Lin-Sca1+Kit+ (LSK) cells and long-term HSCs than in their normal BCR-ABL-negative counterparts (Figure 3.6).

PIM2 is a member of a family of serine/threonine protein kinase found to have oncogenic potential in several malignancies(Nawijn et al., 2011). PIM kinases promote cell survival by phosphorylating the pro-apoptotic BH3-only protein BAD at S112(Yan et al., 2003). Phosphorylation of BAD prevents it from interacting with and inhibiting anti-apoptotic BCL-2 family proteins, thereby promoting cell survival(Yang et al., 1995). The availability of small molecule PIM

inhibitors(Keeton et al., 2014) and the finding that *Pim*$^{-/-}$ mice are viable and fertile(Mikkers et al., 2004), makes PIM2 an attractive therapeutic target.

Previous studies have shown that IM treatment of IM-sensitive CML cells leads to reduced phosphorylation of BAD, which is responsible, at least in part, for cell death(Kuroda et al., 2006). The IM resistance of CMLSCs raised the question of whether BAD phosphorylation was maintained following IM treatment. To address this issue, we FACS sorted IM-resistant CMLSCs and, as a control, IM-sensitive CML progenitors from patient samples and performed intra-cellular staining for phosphorylated BAD (pBAD). As an additional control we also analyzed IM-sensitive human CML K562 cells(Andersson et al., 1979). Consistent with previous studies(Kuroda et al., 2006), we found that IM treatment of IM-sensitive CML progenitors and K562 cells resulted in a substantial decrease of pBAD levels (Figure 3.4f, left and middle panels). By contrast, IM treatment of CMLSCs did not significantly affect pBAD levels (Figure 3.4f, right panel and Figure 3.7). Notably, however, treatment with a small molecule PIM family inhibitor, AZD1208(Keeton et al., 2014), substantially reduced pBAD levels in CMLSCs, CML progenitors and K562 cells (Figure 3.4f and Figure 3.7).

IM is not a PIM2 inhibitor, raising the question of why PIM2 fails to maintain pBAD levels following IM treatment of IM-sensitive CML cells. Previous studies have shown that *PIM2* expression is promoted by STAT5(Adam et al.,

2015). Because the JAK/STAT pathway is downstream of and stimulated by BCR-ABL(Sillaber et al., 2000), we hypothesized that BCR-ABL upregulates PIM2, and thus IM treatment would result in reduced PIM2 levels. Consistent with this hypothesis, PIM2 levels were much higher in BCR-ABL-transformed mouse Ba/F3 (Ba/F3-BCR-ABL) cells than in parental Ba/F3 cells (Figure 3.8 a). Moreover, treatment of Ba/F3-BCR-ABL cells with IM led to a large reduction in PIM2 levels (Figure 3.8 a). Likewise, IM treatment of K562 cells and CML progenitors significantly reduced *PIM2* mRNA (Figure 3.4g) and PIM2 protein levels (Figure 3.8 b). Finally, inhibition of the JAK/STAT pathway by the small molecule inhibitor pimozide(Nelson et al., 2011) also resulted in decreased PIM2 levels in Ba/F3-BCR-ABL (Figure 3.8 c) and K562 cells (Figure 3.8 d).

By contrast to the results in IM-sensitive CML cells, IM treatment of IM-resistant human CMLSCs and mouse CML LSK cells did not significantly reduce *PIM2* levels (Figure 3.4 g and Figure 3.8 e, f). Intracellular staining of phosphorylated CRKL, a cellular marker of BCR-ABL activity(ten Hoeve et al., 1994), confirmed complete inhibition of BCR-ABL activity by IM in CMLSCs (Figure 3.8 g). Consistent with our results, mining of two published expression profiling studies(Zhang et al., 2013; Zhang et al., 2010) revealed that IM treatment did not affect *PIM2* levels in human CMLSCs (Figure 3.8 h, i). However, RNA interference-mediated knockdown of *BCR-ABL* with a short hairpin RNA (shRNA) resulted in reduced *PIM2* levels (Figure 3.8 j, k). Thus in

CMLSCs *PIM2* expression and its regulation of the BAD/BCL-2 pathway is dependent upon BCR-ABL but independent of BCR-ABL kinase activity.

The results described above suggested that PIM2 could be a therapeutic target for elimination of CMLSCs and we performed a series of experiments to test this idea. We found that RNA interference-mediated knockdown of *PIM2* with a short hairpin RNA (shRNA) sensitized CMLSCs to IM treatment (Figure 3.9 a), which was due, at least in part, to increased apoptosis (Figure 3.9 b and Figure 3.10 a). Similar results were obtained when PIM2 was inhibited with AZD1208 (Figure 3.9 c, d and Figure 3.10 b). Notably, combined treatment with IM and AZD1208 had synergistic effects on cell viability and apoptosis (Figure 3.9 c, d). In addition, combined treatment with IM and AZD1208 synergistically suppressed colony formation of human primary CML CD34+ cells (Figure 3.9 e and Figure 3.10 c), and long-term culture initiation cells (Figure 3.9 f). Notably, however, the combined drug treatment had negligible effect on viability of HSCs (Figure 3.9 g).

A recent study demonstrated selected elimination of CML stem cells with dual targeting of p53 and c-Myc signaling(Abraham et al., 2016). However, this strategy is not evaluated in most primitive CD34+CD38-CD90+ CMLSCs(Zhang et al., 2016). We therefore performed a side-by-side comparison using the combination of PIM2 inhibitor and IM versus the combination of p53 activator (RITA) and c-Myc inhibitor (CPI-203). Our combination proved to be equally

effective in killing CD34+ CML cells and CD34+CD38- CMLSCs while demonstrating significantly higher efficacy in killing most primitive CD34+CD38-CD90+ CMLSCs (Figure 3.11). We also think our strategy could be superior in treating those CML patients harboring p53 mutation, for whom the combination of p53 activator and c-Myc inhibitor may not work.

We next asked whether combined IM and AZD1208 treatment could eradicate CMLSCs in an established mouse model of CML (Figure 3.12 a). We found that two weeks of combined treatment with IM and AZD1208 significantly delayed the relapse of CML disease compared to either drug along or vehicle-treated mice (Figure 3.13 a). FACS analysis demonstrated that combined drug treatment synergistically increased apoptosis in the CML LSK population (Figure 3.13 b and Figure 3.12 b), and significantly reduced the total number of CML LSK cells (Figure 3.13 c), short-term HSCs and long-term HSCs (Figure 3.13 d), but spared normal LSK cells (Figure 3.13 e).

To confirm the effect of combined IM and AZD1208 treatment on CMLSCs, we harvested bone marrow from CML mice treated with vehicle, one drug, or both drugs, and transplanted an equal number of total CML cells into secondary recipients (see Figure 3.12 a). We found that expansion of CML cells in the peripheral blood was significantly slower in mice treated with both drugs (Figure 3.12 c). Most importantly, mice receiving bone marrow from donors

treated with IM and AZD1208 survived significantly longer (Figure 3.13 f), indicative of a reduced number of transplantable CMLSCs.

From both literature and previous work of our group (Hurtz et al., 2011; Jiang et al., 2007; Ma et al., 2014), we realized that bulk CML cells with BCR-ABL independent IM resistance and CMLSCs could share the same IM resistance mechanisms. We sought to understand if targeting PIM2 could sensitize BCR-ABL independent IM resistant CML cells as well. Knocking down PIM2 or pharmacologically inhibiting PIM2 function significantly increased IM induced apoptosis in and reduced cell viability of an *in vitro* established BCR-ABL independent/ mutation-free IM resistant cell line, K562R cells (Figure 3.14 a-c). We further demonstrated that combined treatment with IM and AZD1208 markedly kills primary cells from BCR-ABL independent IM resistant CML patients (Figure 3.14 d). Overall, these evidences emphasized that PIM2 is required for maintenance of BCR-ABL independent IM resistance.

CONCLUSIONS

Our major conclusions are summarized in the model of Figure 3.13 g and discussed below. In IM-sensitive CML cells, BCR-ABL promotes *PIM2* expression, and inhibition of BCR-ABL by IM results in reduced levels of *PIM2*, decreased pBAD, and cell death. In IM-resistant CMLSCs, IM treatment does not lead to a reduction in PIM2 levels or loss of pBAD, and survival is maintained by anti-apoptotic BCL-2 family members. Our model is consistent with previous studies showing that a pan-BCL-2 inhibitor can sensitize CMLSCs to IM, demonstrating a role for the BCL-2 pro-survival pathway in IM resistance(Airiau et al., 2012; Goff et al., 2013). Most importantly, we have shown that IM resistance of CMLSCs and bulk CML cells can be overcome by combining IM with a PIM2 inhibitor to inactivate BCL2-mediated pro-survival. Our results reveal a therapeutically targetable mechanism of IM resistance in CMLSCs and bulk CML cells. Interestingly, a recent study reported that the pan-PIM inhibitor SGI-1776 enhances the ability of IM to induce apoptosis in IM-sensitive CML cells(Curi et al., 2015). Notably, however, this study did not investigate the effects of SGI-1776 on IM-resistant CMLSCs.

Although *PIM2* expression is increased in CMLSCs compared to HSCs, suggesting upregulation by BCR-ABL, paradoxically IM treatment does not reduce *PIM2* expression. Consistent with our results, previous studies have identified several genes that are up- or down-regulated in BCR-ABL-positive cells

but whose expression is not normalized by IM treatment(Chen et al., 2009; Chen et al., 2014; Zhang et al., 2012). One possibility is that these genes are up- or down-regulated by BCR-ABL, but their expression is maintained through a mechanism that is independent of BCR-ABL kinase activity and thus is not affected by IM. Consistent with this possibility, we find that *PIM2* expression is decreased when BCR-ABL protein levels are reduced, either through shRNA-mediated knockdown of BCR-ABL in CMLSCs (Figure 3.8 k), or through tetracycline-induced loss of BCR-ABL in mouse LSK cells (Figure 3.6 c). Further elucidation of such BCR-ABL kinase-independent mechanisms may provide insight into the basis of IM-resistance in CMLSCs.

Pro-survival genes that are preferentially expressed in cancer cells are potential therapeutic targets. In principle, such genes can be identified by comparing gene expression profiles of normal and cancer cells. However, this strategy is often impeded by the inability to completely separate normal and cancer cells and the confounding effect of individual variation in gene expression profiles. Here, using CML as a model system, we describe a novel strategy by which HSCs and CMLSCs can be distinguished based on the presence or absence of a characteristic genetic marker, BCR-ABL. Moreover, by comparing single-cell RNA-seq results of HSCs and CMLCs isolated from the same patient we eliminate the potential masking effect of often substantial differences in gene expression among individuals(Cheung et al., 2003). The experimental approach

we have described can be generally applied to other malignancies that harbor oncogenic fusion proteins or other characteristic genetic markers.

MATERIALS AND METHODS

CML patient samples

Frozen samples isolated from patients with chronic phase CML (Table 3.1) were obtained from the UMass Cancer Center Tissue Bank, Department of Pathology, or the Druker Lab at Oregon Health and Science University Knight Cancer Institute, which procured samples with approval from the Institutional Review Board (Gazin et al., 4422). Human CML samples were selected on the basis of sample availability and a requirement to achieve statistical significance. Samples were thawed at 37°C. To avoid clumping during centrifugation, cells were immediately transferred to 20 ml IMDM medium (STEMCELL Technologies) containing 20% fetal bovine serum (Atlanta Biologicals) and 0.1 mg ml^{-1} DNaseI (Sigma) and incubated in a 37°C water bath for 15-20 min. Cells were then pelleted at 300*g* for 10 min, and either stained for HSC isolation or subjected to cell culture (see below).

Single-cell RNA-seq

Samples were enriched for CD34+ cells using magnetic beads (Miltenyi Biotech). CD34+ cells were then stained with Pacific Blue-conjugated CD34 (cat. no. 48-0349), APC-conjugated CD38 (cat. no. 17-0389), PE-conjugated CD90 (cat. no. 12-0909), and FITC-conjugated CD45RA (cat. no. 11-0458) antibodies, and 7-AAD (all from eBioscience). The HSC population (CD34+CD38-CD90+CD45RA-) was then sorted at single-cell mode into 96-well plates containing lysis buffer (4

µl of 0.2% TritonX-100, 2 U μl^{-1} RNase in nuclease-free water). Plates were immediately spun at 800 g for 1 min and put on dry ice. Single HSC lysates were processed immediately for cDNA synthesis according to a revised Smart-seq2 protocol(Picelli et al., 2014; Trombetta et al., 2014). Samples were processed immediately after collection or within two weeks to avoid severe degradation.

To identify wells that had successfully captured single cells, cDNAs were analyzed for expression of two housekeeping genes, *B2M* and *GAPDH*, by qPCR (see Table 3.2 for primer sequences). The quality of cDNA was also evaluated using an Agilent 2100 Bioanalyzer. Only cDNAs showing expression of housekeeping genes and the expected fragment distribution (peaking at ~2 kb, with minimal noisy peaks below 500 bp; see Figure 3.2) were used for subsequent experiments. The typical concentration of cDNA obtained ranged from 0.1–11 ng μl^{-1} in a volume of 20 µl.

For library construction, cDNAs were diluted to 0.1–0.3 ng μl^{-1} and barcoded following the Smart-seq2 protocol using a Nextera XT Index Kit (Illumina). A multiplexed library was generated using a Nextera XT DNA Library Prep Kit (Illumina). The fragment distribution of a typical library is shown in Figure 3.2. Before deep sequencing, the amplifiable fraction of the library was quantified using a KAPA Library Quantification Lit (Kapa Biosystems) according to the

manufacturer's instructions. Finally, 2x75 bp paired-end deep-sequencing was performed using an Illumina NextSeq 500 instrument.

Single-cell RNA-seq data analysis

Raw reads from the RNA-seq experiment were first assessed for their quality using fastqc (version 0.10.1) (http://www.bioinformatics.babraham.ac.uk/projects/fastqc), followed by alignment to the reference human genome (hg19) using tophat (version 2.0.14)(Kim et al., 2013), with default settings except the parameter read-mismatches was set to 2. HTseq-count (version 0.6.1p1)(Anders et al., 2015) was used to quantify gene expression. Cells with <500,000 aligned reads or <2000 expressed genes (at least 1 count per million [CPM]) were excluded from subsequent analysis. The remaining 283 cells were used for identifying differentially expressed genes between BCR-ABL- and BCR-ABL+ cells using the Voom method of Bioconductor package limma (version 3.26.5)(Law et al., 2014) after TMM (trimmed mean of M-values) normalization(Robinson and Oshlack, 2010). Genes with a Benjamini-Hochberg (BH)(Benjamini and Hochberg, 1995) adjusted *P*-value < 0.01 and fold change > 1.5 were considered as significantly (both statistically and biologically) differentially expressed genes. In addition, differential gene expression analysis for individual patients (Figure 3.4 e) was conducted with the Tuxedo suite(Trapnell et al., 2012), i.e., Cufflinks (version 2.2.1)(Trapnell et al., 2010) for assembling transcript and quantifying gene

expression as FPKM (Fragments Per Kilobase of transcript per Million mapped reads), and Cuffdiff2 for differential expression analysis and *P*-value determination. RSEM (version RSEM/1.2.11)(Hentschel et al., 2011; Li and Dewey, 2011) was used to calculate TPMs (Transcripts Per Million).

The HSC signature was defined as a set of genes differentially expressed in HSCs (Lin-CD34+CD38-CD90+CD45RA-) compared to non-stem cells, i.e. MEP and GMP (fold change > 2, $P < 0.001$) in the dataset GSE55689(Woll et al., 2014) using limma package(Law et al., 2014). The MDS plot of Figure 3.1 e was generated using limma package(Law et al., 2014). Heatmap and Venn diagrams were drawn with pheatmap and Vennerable packages, respectively. For the pie chart of Figure 3.4, the number of genes in each category was first calculated in each individual cell (see Figure 3.3 b), and then all the cells were combined to obtain the average distribution.

Nested PCR to identify BCR-ABL transcripts in single cells

Two-step nested PCR was performed as follows using primers listed in Table 3.2. The first round of PCR (10 µl total volume, 1 µl of undiluted single-cell cDNA as template) consisted of 1 cycle of 95°C for 3 min; 25 cycles of 95°C for 30 sec, 58°C for 30 sec, and 68°C for 30 sec; extension at 68°C for 5 min; and 4°C hold. The second round of qPCR (10 µl total volume, 1 µl of 10x diluted first-round

PCR product as template) consisted of 1 cycle of 95°C for 3 min; 40 cycles of 95°C for 3 sec and 60°C for 30 sec.

Gene Set Enrichment Analysis (GSEA)

GSEA was performed using GSEAPreranked module from GSEA v2.2.2 package(Mootha et al., 2003; Subramanian et al., 2005) with all genes pre-ordered based on log2 fold change. GSEA analysis was performed using the gene set: EGUCHI_CELL_CYCLE_RB1_TARGETS (systematic name: M4455).

Ultra-low cell number qRT-PCR

Due to the scarcity of the CMLSC population, it is usually difficult to collect enough cells from a frozen CML patient sample for qRT-PCR. To generate cDNA from ~200 cells, we employed a modified single-cell Smart-seq2 protocol. First, to accommodate the volume of sorted cells (<0.6 µl), the lysis buffer volume was increased from 4 µl to 8 µl, and the reaction volume was doubled in all subsequent steps. Second, rather than using 20 rounds post-amplification cycles for single-cell cDNA synthesis, only 15 rounds were used for 200 cells. To ensure all qRT-PCR experiments were carried out under the same conditions, the method was not only used for analysis of *PIM2* expression in CMLSCs (CD34+CD38-CD90+ [Figure 3.4 g] and CD34+CD38- [Figure 3.8 e)] cells), but also in CML progenitor (CD34+CD38+) cells (Figure 3.4 g), and mouse CML LSK cells (Figure 3.6 c and 3.8 f) and LT-HSCs (Figure 3.6 d).

CML patient sample culturing

Cell pellets were re-suspended in binding buffer (1x PBS with 0.2% BSA and 2 mM EDTA) to enrich for bulk live cells or CD34+ cells alone. Cells were then cultured in IMDM medium plus 20% BSA, insulin and transferrin (Ma et al.) (STEMCELL Technologies) and the following cytokines: 100 ng ml^{-1} SCF, 100 ng ml^{-1} G-CSF, 20 ng ml^{-1} FLT3L, 20 ng ml^{-1} IL-3, and 20 ng ml^{-1} IL-6 (all from Prospec). For imatinib-induced apoptosis and cell viability experiments, cells were cultured in the presence of cytokines for 24 h, then cells were switched to IMDM plus 20% BIT with less than 10% of cytokines for the rest of culturing. From our FACS analysis (see Figure 3.2), we found that the HSC population (CD34+CD38-CD90+CD45RA-) was almost exclusively CD34+CD38-CD90+, which has also been used previously to define HSCs[(Zhang et al., 2016)]. We therefore used CD34+CD38-CD90+ cells as an alternative for CMLSCs in the functional experiments for convenient FACS analysis.

Phospho-flow analysis

Human primary CD34+ cells were cultured for 2 days to expand the population, and then IM-sensitive CML progenitor cells (CD34+CD38+) and IM-resistant CMLSCs (CD34+CD38- and CD34+CD38-CD90+) were FACS sorted and further cultured for ~16 h in the presence of DMSO, IM (ChemieTek; 5 μM), or AZD1208 (Active Biochem; 5 μM). K562 cells (ATCC) were cultured for ~16 h in the presence of DMSO, IM (5 μM), or AZD1208 (5 μM). Cells were then collected,

fixed, and processed as previously described(Ma et al., 2014) for staining of PE-conjugated phospho-BAD (S112) (cat. no. 11865) and PE-conjugated rabbit IgG (cat. no. 5742) (both from Cell Signaling Technology). To assess efficient inhibition of BCR-ABL activity by IM, K562 or FACS sorted CMLSCs, were treated for 4 h with DMSO or IM, and then processed as above and stained with Alexa Fluor 488 conjugated pCRKL antibody (cat. no. 560789, BD Biosciences) and Alexa Fluor 488 conjugated IgG (cat. no. 557703, BD Biosciences). Fixed cells were used either immediately, or stored at 4°C for two weeks.

Immunoblot analysis

Ba/F3-BCR-ABL cells were generated by transducing Ba/F3 (originally purchased from ATCC) cells with a lentiviral vector expressing doxycycline-inducible BCR-ABL (constructed by replacing the shRNA cassette and TurboRFP reporter in pTRIPZ [GE Dharmacon] with BCR-ABL[p210]). Cells were maintained in RPMI plus 10% fetal bovine serum in the presence of 1 µg/ml doxycycline (Sigma). To assay PIM2 expression upon BCR-ABL or JAK/STAT inhibition, Ba/F3-BCR-ABL cells were subjected to doxycycline withdrawal, or treatment with 5 µM IM or 0, 5 or 10 µM pimozide (Calbiochem). K562 cells were treated with 10 µM IM or 0, 2, 5 or 10 µM pimozide. After ~16 h of treatment, protein extracts were prepared and analyzed by immunoblotting for PIM2 (human PIM2: Cell Signaling Technology, cat. no. 4730; mouse PIM2: Santa Cruz, sc-13514) and ACTB (Sigma, cat. no. A2228).

shRNA-mediated knockdown in primary CML samples and K562R cells

Bulk live patient cells were enriched using a Dead Cell Removal Kit (Miltenyi Biotec) and cultured overnight at 37°C. For PIM2 knockdown, cells were transduced with a pLKO-GFP lentivirus (constructed by excising the puromycin-resistance gene from pLKO.1 [Addgene plasmid #10878] and replacing it with PCR-amplified GFP) carrying either a control non-silencing shRNA or human *PIM2* shRNA (TRCN0000001629 and TRCN0000001630) using two rounds of spin infection, with ~12-16 h in between. Cells were further cultured for 24 h to allow for expression of the shRNA. Cells were treated with IM (5 μM) for an additional 24 h for apoptosis analysis or 48 h for cell viability determination. For BCR-ABL knockdown, cells were transduced with pLKO-GFP carrying a non-silencing or *BCR-ABL* shRNA (TRCN0000000790). Following two rounds of spin infection, cells were further cultured for 48 h and then FACS sorted to isolate CD34+CD38- cells. Conventional qRT-PCR was performed to analyze expression of *BCR-ABL* and *PIM2*. For K562R cells, one round of viral transduction is enough to achieve >90% infection rate. Cells were cultured in RPMI1640 + 10% FBS, and drug treatment started at day 4.

Relative cell viability and apoptosis assays

Bulk primary human cells were stained with PE-cy7-conjugated CD34 (cat. no. 25-0349), APC-conjugated CD38, and PE-conjugated CD90 antibodies, Pacific

Blue-conjugated Annexin V, and 7-AAD, and immediately analyzed by FACS. For relative cell viability, the percentage of the HSC fraction was determined by FACS analysis, and the total cell number was determined by trypan blue cell counting. The number of viable cells was determined as [Total viable cell number] x [percentage of CMLSCs]. For mouse CML LSK cells, apoptosis and viability were determined as previously described(Ma et al., 2014). For analysis of mouse ST-HSCs and LT-HSCs, total mouse bone marrow cells were stained with a cocktail of primary antibodies [APC-conjugated Sca-1 (cat. no. 17-5981), PE-conjugated c-Kit (cat. no. 12-1171), Pacific blue-conjugated CD48 (cat. no. 48-0481), PE-cy7-conjugated CD150 (cat. no. 25-1502) antibodies (all from eBioscience), and Biotin-conjugated Lineage antibody cocktail (Miltenyi Biotec)], followed by staining with APC-eFluor780-conjugated streptavidin secondary antibody (eBioscience; cat. no. 47-4317) as previously described(Ma et al., 2014). Representative staining is shown in Figure 3.6 a. After initially culturing for 24 h, cells were treated with DMSO, IM (5 μM), AZD1208 (5 μM) or a combination of IM and AZD1208 for an additional 24 h for apoptosis analysis or 48 h for cell viability determination.

To perform side-by-side comparison of combination therapies, we used a fixed concentration of IM (5uM) and AZD1208(5uM), and the combination of p53 activator (RITA,) and c-Myc inhibitor (CPI-203) at three highest concentrations

as listed in Abraham SA et al, *Nature*, 2016. FACS analysis was done and cell viability was determined at either 48 hour or 72 hour treatment.

Colony formation and LTC-IC assays

For colony formation assays, ~500 CD34+ cells or bulk cells with equivalent number of CD34+ cells were plated on 35 mm dishes in MethoCult H4435 Enriched medium supplemented with recombinant human cytokines (STEMCELL Technologies). Total colonies were counted at day 14.

For LTC-IC assays, M2-10B4 mouse fibroblast cells (ATCC) were irradiated with ~8,000 cGy, and then plated on collagen-coated 35 mm dishes and incubated overnight. ~3,000 CD34+ cells or bulk cells containing equivalent number of CD34+ cells were plated in MyeloCult H5100 medium (STEMCELL Technologies) with hydrocordisone (STEMCELL Technologies) with weekly half medium change for 6 weeks according to the manufacturer's protocol. Cells were collected and plated in MethoCult H4535 medium (STEMCELL Technologies) containing DMSO, IM (5 μM), AZD1208 (5 μM) or a combination of IM and AZD1208, and assayed for colony formation as described above.

CML mice

All animal protocols were approved by the Institution Animal Care and Use Committee at UMMS (A-2300). Animal sample sizes were selected based on precedent established from previous publications and an understanding that at

least n=5 is generally required to achieve statistical significance. Mice were randomly allocated to each group for drug treatment after bone marrow transplantation, and were subsequently analyzed in a non-blinded fashion. Animals were excluded from the study based on pre-established criteria (death within 10 days with no evidence of enlarged spleen, indicative of bone marrow engraftment failure); based on these criteria, one mouse in the IM+AZD1208-treated group was excluded (Figure 3.13 c-e).

CML was induced in male 6-8 week old C57BL/6 mice (The Jackson Laboratory) using retrovirus transduction as previously described(Ma et al., 2014; Zhang et al., 2016). At day 7 of bone marrow transplantation, mice were randomly grouped (n=5 per group) and treated with vehicle (0.5% hydroxypropylmethycellulose and 0.2% Tween-80 in filtered ddH_2O), IM (100 mg kg^{-1}), AZD1208 (30 mg kg^{-1}, resuspended in H_2O and sonicated to disrupt clumps, then resuspended in 0.5% hydroxypropylmethycellulose and 0.2% Tween-80 in filtered ddH_2O) or a combination of IM and AZD1208 for about 2 weeks until the first vehicle-treated mouse died. Mice were monitored for survival.

For apoptosis and stem cell viability analysis, CML mice (n=6 per group) were treated for 2 weeks, and sacrificed to harvest bone marrow cells for analysis as described previously(Ma et al., 2014). BCR-ABL+ (GFP+) and BCR-

ABL- (GFP-) mouse stem cells (Lin-Sca1+Kit+) were isolated from the mice by FACS as described previously(Ma et al., 2014). For secondary transplantation, all the bone marrow cells from the same group of mice were combined, and the percentage of GFP-positive cells was determined by FACS. An equal number of total bone marrow cells were transplanted into lethally irradiated secondary recipients. Mice were monitored for accumulation of CML cells (GFP+ cells) in peripheral blood and survival.

To analyze *Pim2* expression in CML LSK cells and LT-HSCs (Figure 3.6 c and 3.8 f), Tet-off SCL-tTA/BCR-ABL transgenic mice were used, which were bred as previously described(Koschmieder et al., 2005). To induce CML, BCR-ABL transgenic mice were subjected to tetracycline-water withdrawal starting at 8 weeks old, and CML development was monitored by FACS analysis of peripheral Gr1+/Mac1+ cells, which typically reached 20-30% after 2 weeks of induction. Mice were treated with vehicle or imatinib (100 mg kg^{-1}) for 2 more weeks and then sacrificed, and bone marrow was collected for FACS sorting of LSK cells and LT-HSCs. To revert the CML phenotype, CML mice were re-administered with tetracycline water (0.5g L^{-1}) for 4 weeks to suppress BCR-ABL expression, CML reversion was monitored by FACS analysis of peripheral Gr1+/Mac1+ cells. As a normal control, mice of the same age but maintained with tetracycline-water since birth were used. Ultra-low cell number qRT-PCR was used to determine *Pim2* expression.

Statistical Analysis

To achieve statistical significance, all qRT-PCR data were collected from experiments performed in technical triplicate; each experiment was repeated at least twice and statistically significant results were obtained in independent biological replicates. Differences between groups were assayed using a two-tailed student *t*-test using GraphPad Prism. In cases where the assumption of the *t*-test was not valid a non-parametric statistical method was used (e.g., Mann-Whitney test). Significant differences were considered when $P<0.05$. Data are presented as mean ± SD or SEM, as indicated in the legend.

Statistical analysis for drug synergy was performed using R, a system for statistical computation and graphics(Ihaka and Gentleman, 1996), to assess whether the combined effects from IM and AZD1208 were synergistic (greater than the sum of the single-drug effects) or non-synergistic. The number of surviving cells were log transformed before performing two-way analysis of variance (ANOVA) to test the main effect and the interaction of the two drugs with Randomized Complete Block Design or Completely Randomized Design. The percentage of viable cells was transformed using logit function followed by two-way analysis of variance (ANOVA) with the Randomized Complete Block Design or Completely Randomized Design, and the BH-adjusted *P*-value was

calculated to counteract the problem of multiple comparisons(Benjamini and Hochberg, 1995).

To determine whether or not IM and AZD1208 exerted synergistic impacts on decreasing cell survival, we compared the difference between observed effects with the expected additive effects for the mouse/patient samples exposed to both drugs(Slinker, 1998). The difference was estimated as the interaction coefficient in the ANOVA. If there was a significant negative difference (i.e., interaction coefficient < 0 and BH adjusted *P*-value < 0.05), then the impact from the combined drugs was classified as synergistic; otherwise, the impact from the combined drugs was classified as non-synergistic. For apoptosis, if there was a significant positive difference, then the impact from the combined drugs was classified as synergistic; otherwise, the impact from the combined drugs was classified as non-synergistic. When there was no statistically significant synergistic effect, combined drug treatments were compared with imatinib treatment alone using a pre-determined contrast under the framework of ANOVA.

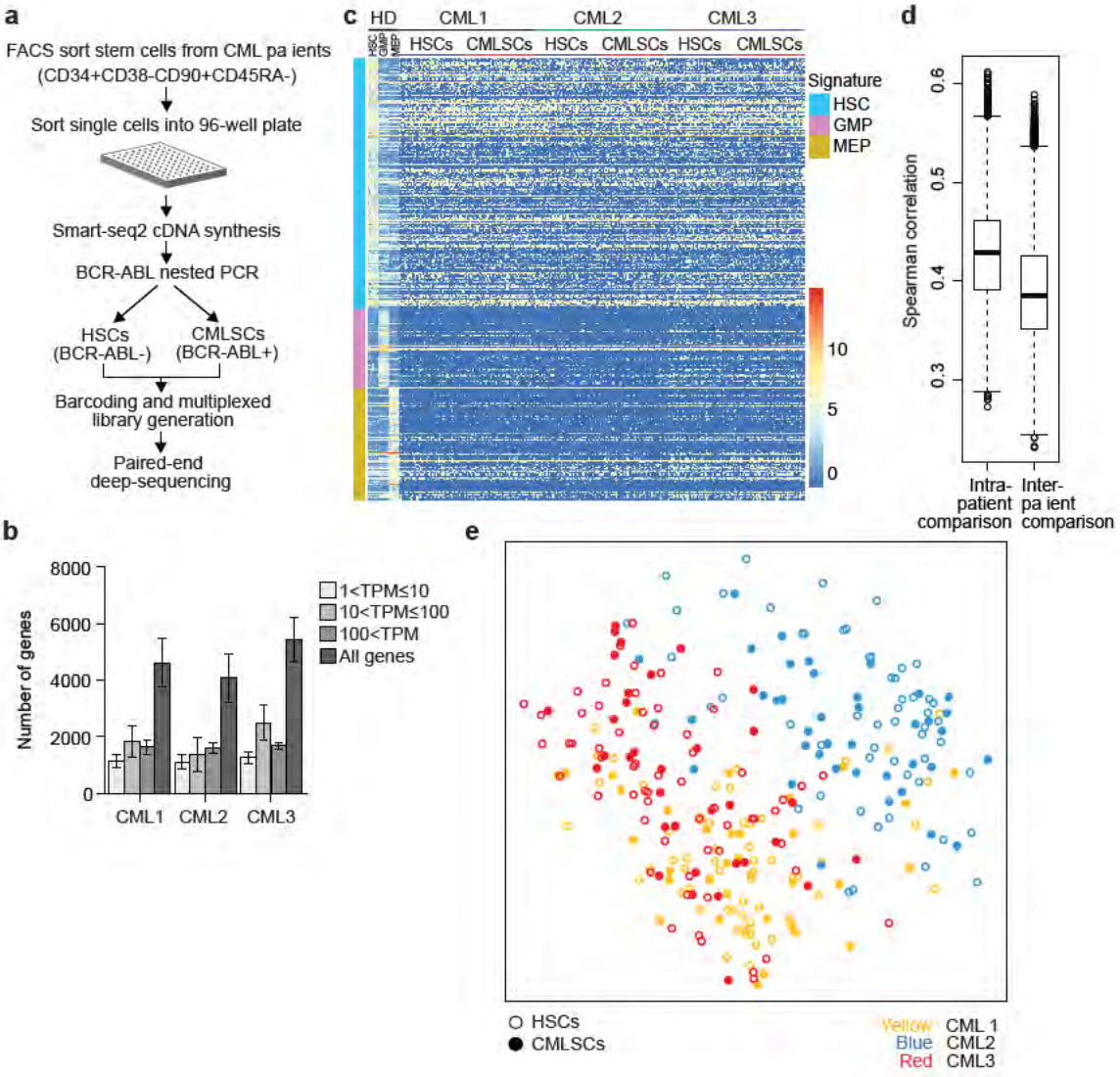

Figure 3.1. Single-cell RNA-seq analysis of CMLSCs and HSCs.

Figure 3.1. Single-cell RNA-seq analysis of CMLSCs and HSCs. a, Schematic of the single-cell RNA-seq analysis. **b**, Number of genes expressed at a low (1<TPM≤10), modest (10<TPM≤100), or high (100<TPM) level in single CMLSCs and HSCs isolated from three CML patients. Error bars indicate SD; n=~96 biological replicates. **c**, Gene expression signature in single HSCs and CMLSCs. A published RNA-seq dataset from HSCs, granulocyte-macrophage progenitors (GMPs), and megakaryocyte-erythrocyte progenitors (MEPs) was used to define an HSC-specific gene signature, and all 283 single-cell RNA-seq data were mapped to this signature. **d**, Box plot showing the distribution of the Spearman correlation coefficient of the global transcription profile of every pair of single cells within the same patient (intra-patient correlation) and between any pair of cells from different patients (inter-patient correlation). HSCs and CMLSCs were analyzed separately and then combined. Boxed areas span the first to the third quartile, and whiskers represent maximum or minimum observations within 1.5 inter-quartile range (IQR). $P < 0.001$. **e**, Multidimensional scaling plot showing the inter-relationship of gene expression profiles of 283 single HSCs and CMLSCs from three CML patients. The distance between any two cells reflects the similarity of their expression profiles.

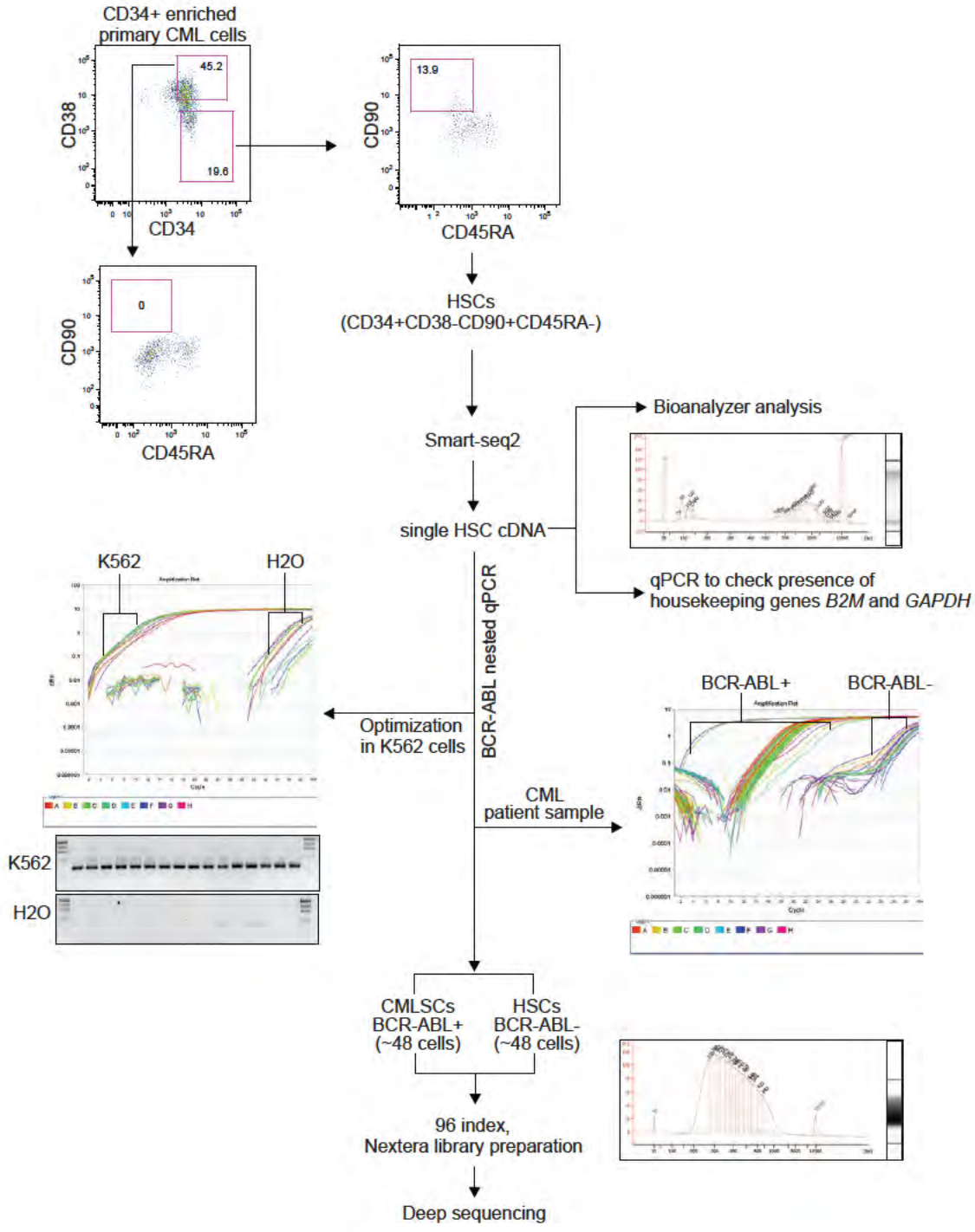

Figure 3.2. Single-cell RNA-seq workflow

Figure 3.2. Single-cell RNA-seq workflow. Primary CML patient samples were enriched for CD34+ cells using magnetic beads. Enriched CD34+ cells were stained with CD34, CD38, CD90, and CD45RA cell surface markers, and single HSCs (CD34+CD38-CD90+CD45RA-) were collected and converted into cDNA using a revised Smart-seq2 protocol. cDNA quality was checked on a Bioanalyzer; a representative single HSC cDNA size distribution is shown in the inset on the top right. qPCR was performed to detect the expression of housekeeping genes *B2M* and *GAPDH*. Because the expression level of BCR-ABL is typically low in primary CML cells, particularly in the stem cell population from chronic phase CML patients, nested PCR was performed to enhance specificity and sensitivity for detection of BCR-ABL. Nested qPCR for BCR-ABL was first optimized in human CML K562 cells. Briefly, cDNAs were prepared from 16 single K562 cells and, following confirmation of expression of housekeeping genes, two-step nested PCR was carried out to detect BCR-ABL. The inset on the bottom left shows that all 16 single K562 cells showed positive amplification (>1,000-fold over background) with no detectable signal in the water (H2O) control, confirming the validity of this approach. Nested qPCR was then performed for single HSCs from CML patients. For every plate of single cells (~96 cells), 16 water control samples were also included; if any of the water controls was positive, the nested PCR was discarded and repeated. Typically, 70~80% of single HSCs showed a positive BCR-ABL signal, which had a ~1,000-fold reduced intensity compared to control K562 cells; a typical amplification from a plate of single HSCs is shown (inset, middle right). For each sample, we analyzed ~200 single cells and could obtain 40~60 HSCs that were negative for BCR-ABL. We combined ~96 BCR-ABL+ and BCR-ABL- cells to generate a cDNA library for deep-sequencing; a representative 96 index cDNA library size distribution is shown in the inset on the bottom right.

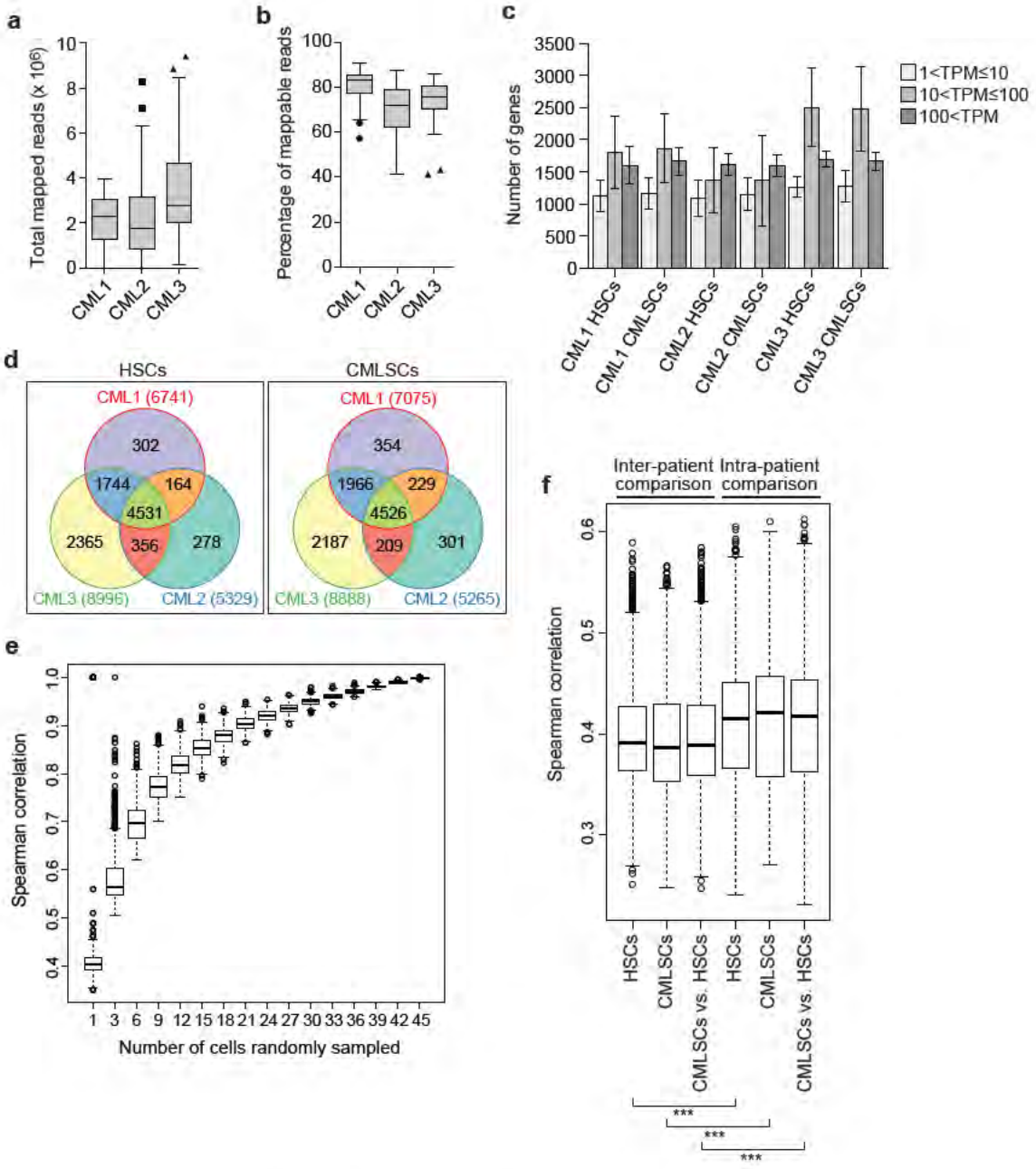

Figure 3.3. Quality controls for single-cell RNA-seq data.

Figure 3.3. Quality controls for single-cell RNA-seq data. a,**b**, Box plots showing the number of total mapped reads (a) or the percentage of mappable reads (b) in all single HSCs and CMLSCs from each CML sample. Boxed areas span the first to the third quartile, and whiskers represent maximum or minimum observations within 1.5 inter-quartile range (IQR). **c**, Number of genes expressed at a low (1<TPM≤10), modest (10<TPM≤100), or high (100<TPM) level across all single cells in each patient. The results from BCR-ABL+ and BCR-ABL- cells are presented separately. Error bars indicate s.d.; n=~48 biological replicates. **d**, Venn diagrams showing the number of common detectable genes in HSCs and CMLSCs from three CML patients. A detectable gene is defined as one with TPM>1 in more than 50% of single cells. **e**, Box plot showing the distribution of the Spearman correlation coefficient of the global transcription profile of an increasing number of randomly sampled HSCs from the CML1 patient sample. The results show that the correlation reaches above 0.9 at ~30 cells. Boxed areas span the first to the third quartile, and whiskers represent maximum or minimum observations within 1.5 IQR. **f**, Box plot showing the distribution of the Spearman correlation coefficient of the global transcription profile of every pair of single cells within the same patient (intra-patient correlation) and between any pair of cells from different patients (inter-patient correlation). The results from BCR-ABL+ and BCR-ABL- cells were analyzed separately. Boxed areas span the first to the third quartile, and whiskers represent maximum or minimum observations within 1.5 IQR. ****P*<0.001.

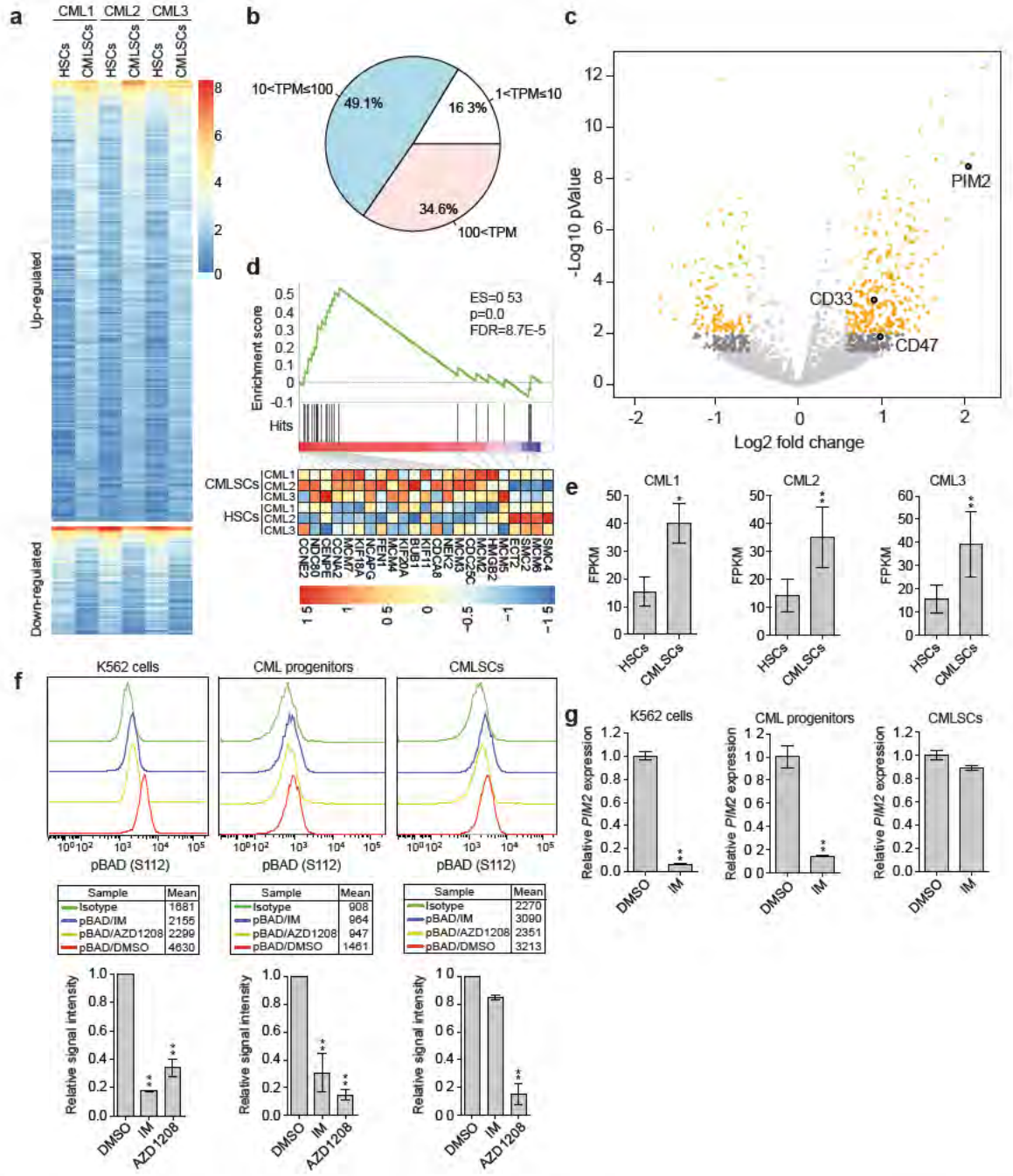

Figure 3.4. IM resistance in CMLSCs is due to PIM2-mediated maintenance of BAD phosphorylation.

Figure 3.4. IM resistance in CMLSCs is due to PIM2-mediated maintenance of BAD phosphorylation. **a**, Heatmap showing the population average of differentially expressed genes between all single HSCs and CMLSCs in three CML patients. Only those differentially expressed genes with adjusted $P<0.01$ and fold change ≥2 are shown. **b**, Pie chart showing the average distribution of differentially expressed genes at low ($1<TPM\leq10$), modest ($10<TPM\leq100$), and high ($100<TPM$) levels in all single cells. **c**, Volcano plot showing the significance (y-axis) and differential expression (x-axis) for all genes identified by the RNA-seq analysis. Genes with $P<0.01$, fold change>1.5 and average (CPM)>1 are highlighted in yellow, genes with $0.01\leq P<0.05$, fold change>1.5 and average (CPM)>1 are in dark grey, and genes that are not significantly changed are indicated by light grey. **d**, GSEA showing CMLSCs are significantly enriched for genes involved in cell cycle progression. The heatmap shows individual gene expression from both CMLSCs and HSCs from three CML patients. ES, enrichment score, FDR, false discovery rate. **e**, FPKM value of *PIM2* from intra-patient comparison in three CML samples. Error bars indicate SEM; n=~48 biological replicates. **f**, Phospho-flow analysis showing intra-cellular staining of pBAD (S112) levels in DMSO, IM, or AZD1208 treated K562 cells, CML progenitor cells (CD34+CD38+), and CMLSCs (CD34+CD38-CD90+). IgG was used for control staining. The upper panel shows a representative staining histogram for each population and the mean value of the population. The lower panel shows the quantification of n=3 biological replicates. Error bars indicate SEM. **g**, qRT-PCR monitoring *PIM2* expression following IM treatment in K562 cells, CML progenitors, and CMLSCs (CD34+CD38-CD90+). Error bars indicate SD; n=3 technical replicates of a representative experiment (out of two independent experiments). S denotes the combined drug treatment was synergistic. *$P \leq 0.05$, **$P \leq 0.01$.

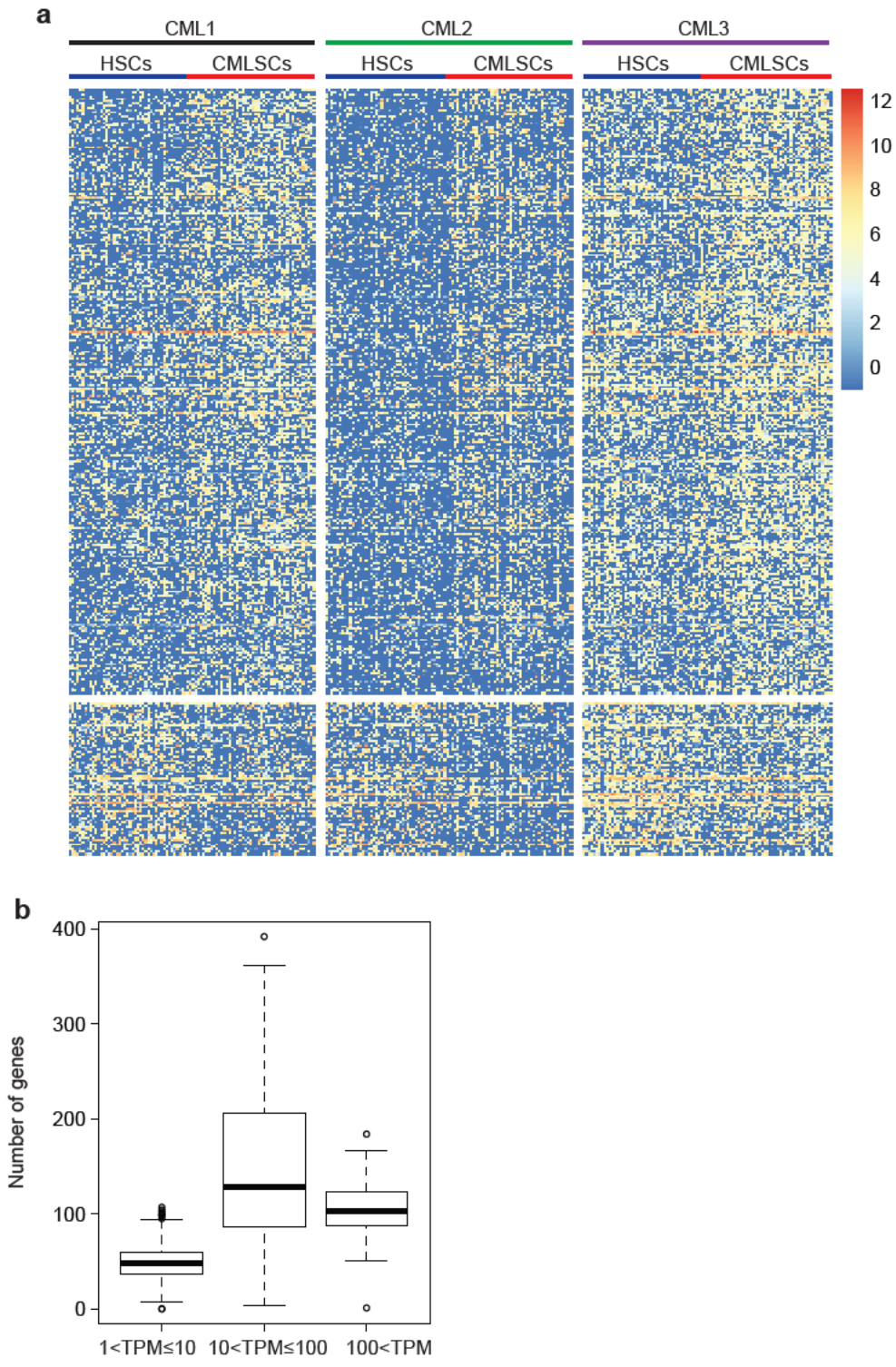

Figure 3.5. Gene expression patterns and statistics in single cells.

Figure 3.5. Gene expression patterns and statistics in single cells. a, Heatmap showing the differentially expressed genes of 283 individual single HSCs (BCR-ABL-) and CMLSCs (BCR-ABL+) in three CML patients. Only those differentially expressed genes with adjusted $P < 0.01$ and fold-change ≥2 are shown. **b**, Box plot showing the distribution of the number of differentially expressed genes (P <0.01 and logFC≥1) at a low (1<TPM≤10), modest (10<TPM≤100), or high (100<TPM) level in all single cells. Boxed areas span the first to the third quartile, and whiskers represent maximum or minimum observations within 1.5 IQR.

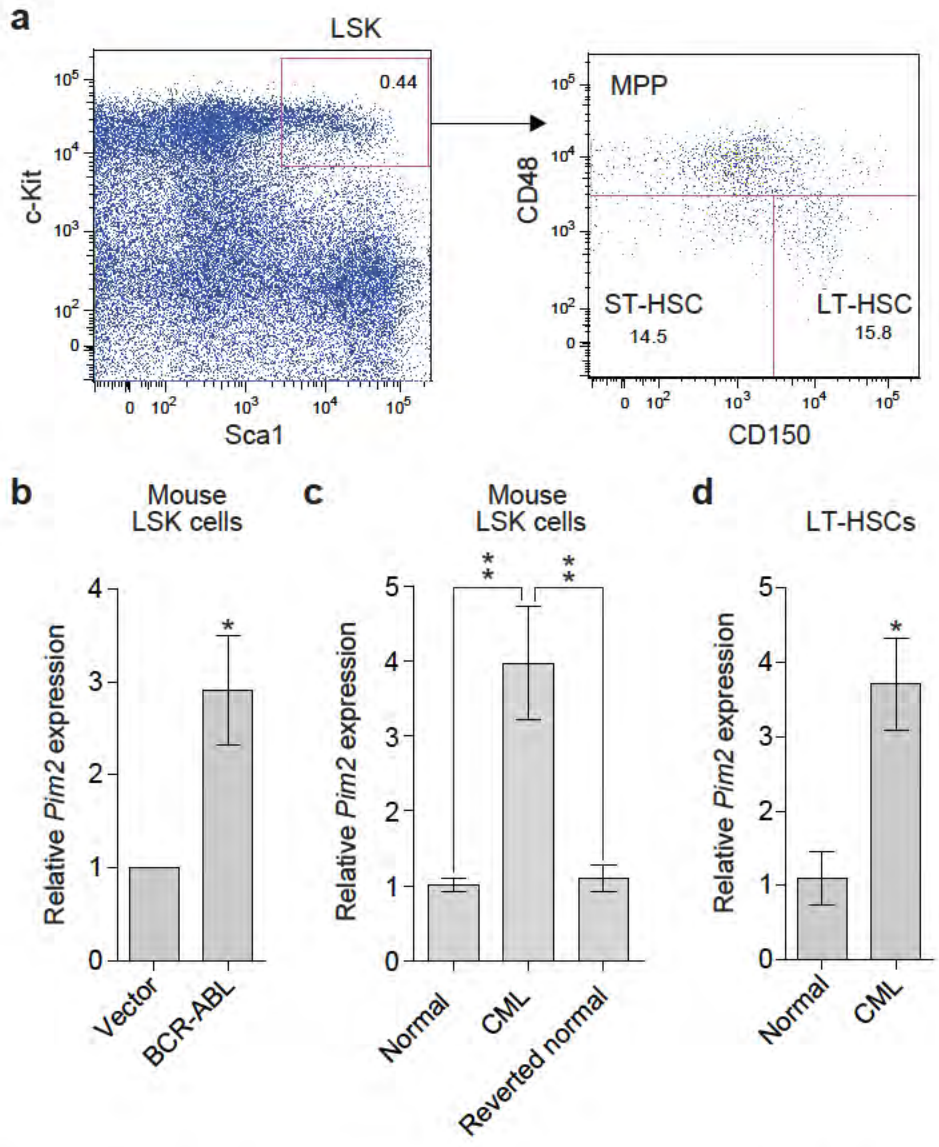

Figure 3.6. *Pim2* expression is elevated in mouse CMLSCs.

Figure 3.6*. Pim2* expression is elevated in mouse CMLSCs. a, FACS plot showing the gating of murine Lin-Sca1+Kit+ (LSK) cells, multi-potent progenitor (MPP, LSKCD48+CD150-) cells, short-term HSCs (ST-HSC, LSKCD48-CD150-), and long-term HSCs (LT-HSC, LSKCD48-CD150+). **b**, qRT-PCR analysis showing relative *Pim2* mRNA levels in murine LSK cells expressing vector or BCR-ABL; the data were mined from a published expression profiling study (GSE10912[Chen et al., 2009]). Error bars indicate SD; n=2 biological replicates**. c**, qRT-PCR analysis showing relative *Pim2* mRNA levels in murine LSK cells from normal mice (Tet-off SCL-tTA/BCR-ABL transgenic mice given tetracycline-water since birth), CML mice (Tet-off SCL-tTA/BCR-ABL transgenic mice subjected to tetracycline-water withdrawal at 8 weeks of age), or reverted normal mice (Tet-off SCL-tTA/BCR-ABL transgenic mice subjected to tetracycline-water withdrawal from 8-12 weeks of age, then given tetracycline-water for 4 weeks to revert CML phenotype). Error bars indicate SEM; n=4 mice per group. **d**, qRT-PCR analysis showing the relative *Pim2* mRNA level in LT-HSCs from control (normal) and BCR-ABL transgenic mice. Error bars indicate SEM; n=3 mice per group.

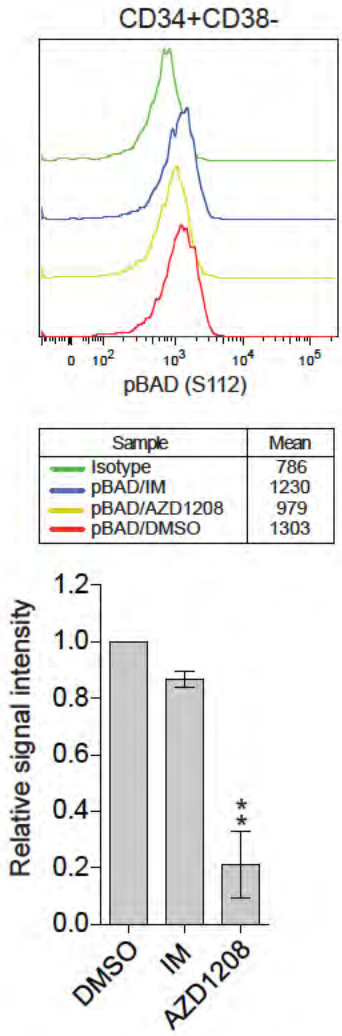

Figure 3.7. Treatment with AZD1208 reduces pBAD levels in CD34+CD38- CMLSCs. Phospho-flow analysis showing intra-cellular staining of pBAD (S112) levels in DMSO, IM, or AZD1208 treated CMLSCs (CD34+CD38-). IgG was used for control staining. The upper panel shows a representative staining histogram for each population and the mean value of population. The lower panel shows the quantification of n=3 biological replicates. Error bars indicate SEM.

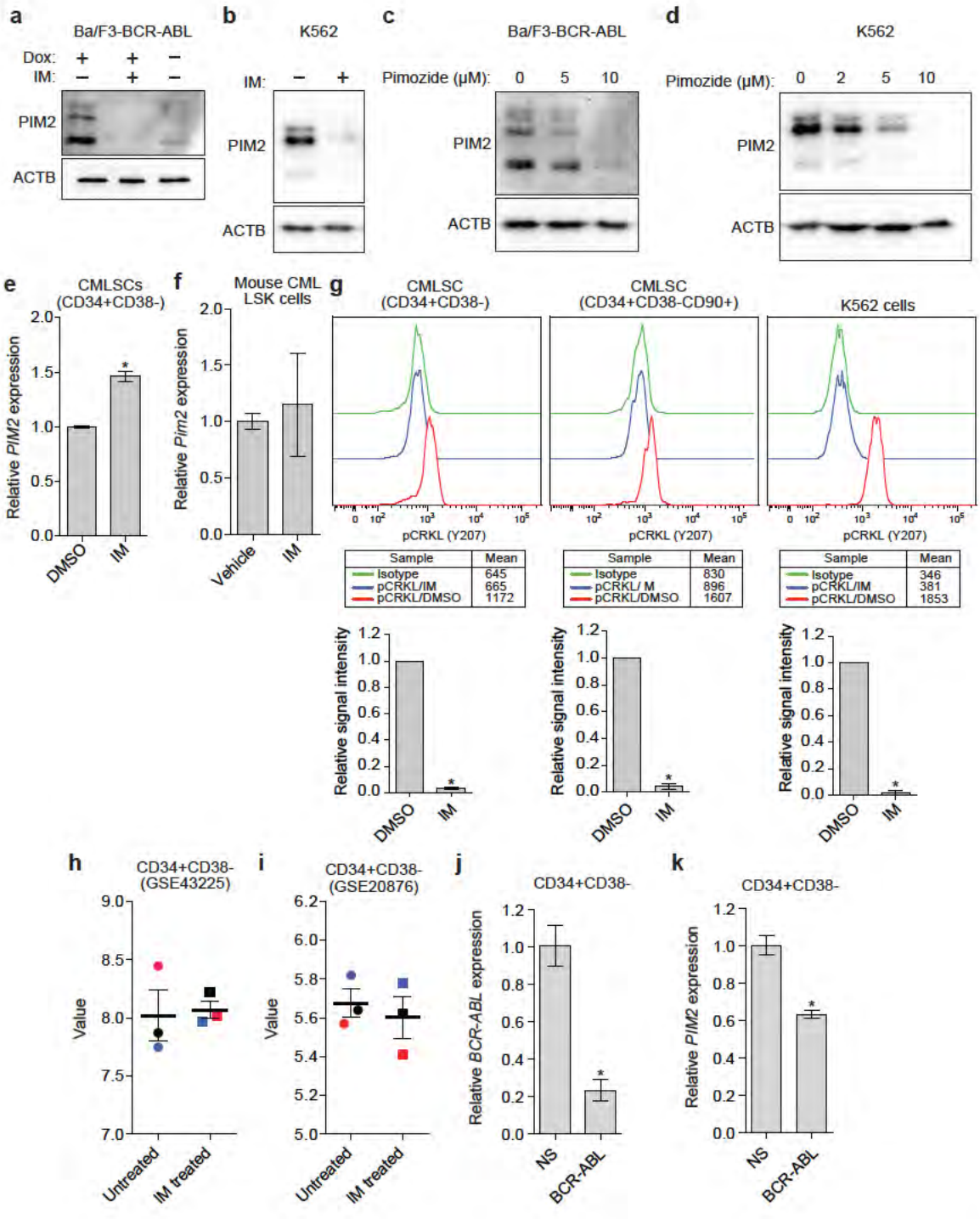

Figure 3.8. *Pim2* expression is regulated by BCR-ABL and the JAK/STAT5 pathway, and is not affected by IM treatment in CMLSCs.

Figure 3.8. *Pim2* expression is regulated by BCR-ABL and the JAK/STAT5 pathway, and is not affected by IM treatment in CMLSCs. a, Immunoblot showing PIM2 levels in Ba/F3 cells expressing a doxycycline inducible BCR-ABL fusion protein. Cells were maintained in doxycycline (Dox) and subjected to Dox withdrawal or treatment with IM. β-actin (ACTB) was monitored as a loading control. **b**, Immunoblot showing PIM2 levels in K562 cells in the absence or presence of IM. The results of (a) and (b) show that PIM2 expression depends on BCR-ABL kinase activity. **c,d,** Immunoblots showing PIM2 levels in Ba/F3-BCR-ABL cells (c) or K562 cells (d) treated with the STAT5 inhibitor, pimozide. The results of (c) and (d) show that PIM2 expression is regulated by the JAK/STAT5 pathway. **e**, qRT-PCR analysis showing relative *PIM2* mRNA levels in DMSO and imatinib-treated primary CML CD34+CD38- cells. Error bars indicate SD; n=3 technical replicates of a representative experiment (out of two experiments). **f**, qRT-PCR analysis showing relative *Pim2* mRNA levels upon IM treatment in LSK cells from CML mice. CML mice were treated with vehicle or IM for two weeks, bone marrow was harvested, and LSK cells were sorted by FACS. Error bars indicate SEM; n=3 mice per group. **g**, Phospho-flow analysis showing intra-cellular staining of phosphorylated CRKL (pCRKL) (Y207) levels in CMLSCs (CD34+CD38-, CD34+CD38-CD90+), or as a control K562 cells, treated with DMSO or IM (5 μM). IgG was used for control staining. The upper panel shows a representative staining histogram for each population and the mean value of the population. The lower panel shows the quantification of n=3 biological replicates. Error bars indicate SEM. The results show that IM treatment completely abolishes BCR-ABL activity. **h**,**i**, Relative *PIM2* mRNA levels in CD34+CD38- CMLSCs treated in the presence or absence of IM. The data were mined from published expression profiling studies GSE43225[(Zhang et al., 2013)] (h) and GSE20876[(Zhang et al., 2010)] (i). Matched samples from the same patient are indicated by dots of the same color. Error bars indicate s.d.; n=3 biological replicates. The results shown that *PIM2* expression is not affected by IM treatment in CD34+CD38- CMLSCs. **j**,**k**, qRT-PCR analysis in CD34+CD38- CMLSCs monitoring expression of *BCR-ABL* (j) or *PIM2* (k) following knockdown of BCR-ABL. Error bars indicate SD; n=3 technical replicates. ***P* ≤ 0.01, **P* ≤ 0.05.

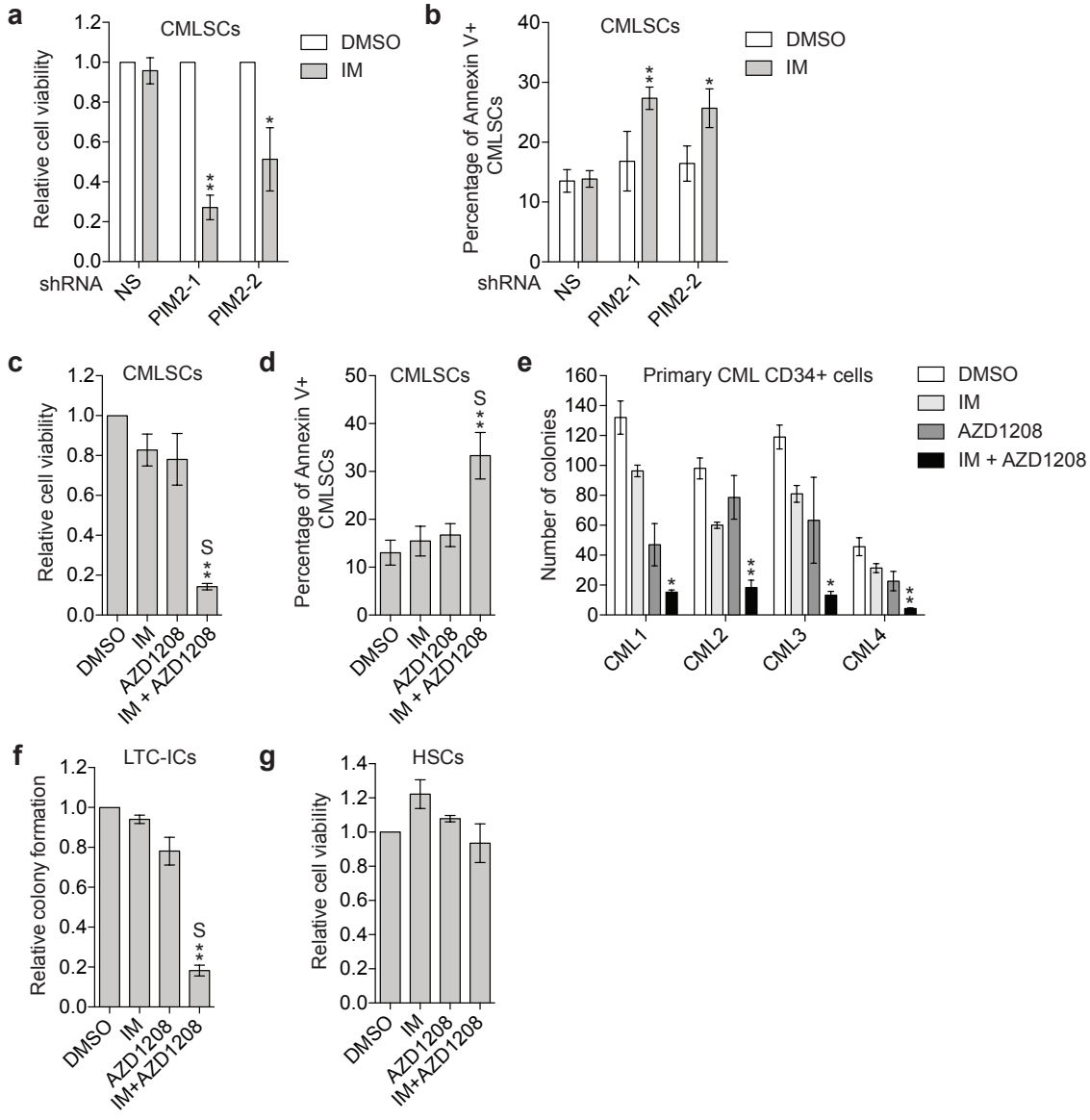

Figure 3.9. Impairment of PIM2 function by shRNA or small molecule inhibitor sensitizes CMLSCs to IM treatment.

Figure 3.9. Impairment of PIM2 function by shRNA or small molecule inhibitor sensitizes CMLSCs to IM treatment. a,**b**, Relative cell viability (a) or apoptosis (b) of CMLSCs from CML patient samples expressing an NS or *PIM2* shRNA and treated with DMSO or IM. In (a), the results were normalized to that obtained in DMSO-treated cells, which was set to 1. Error bars indicate SEM; n=4 biological replicates. **c**,**d**, Relative cell viability (c) and apoptosis (d) of CMLSCs from CML patient samples treated with DMSO, IM, AZD1208 or a combination of both drugs. Error bars indicate SEM; n=4 biological replicates. **e**, Colony formation assay of human primary CML cells treated with DMSO, IM, AZD1208 or a combination of IM and AZD1208. Error bars indicate SD; n=3 technical replicates. **f**, Colony formation and LTC-IC assay of post-culture primary CML cells treated with IM, AZD1208 or a combination of both drugs. Error bars indicate SEM; n=3 biological replicates. **g**, Relative cell viability of normal HSCs from healthy donors treated with DMSO, IM, AZD1208 or both drugs. Error bars indicate SEM; n=3 biological replicates. S denotes the combined drug treatment was synergistic. *$P \leq 0.05$, **$P \leq 0.01$.

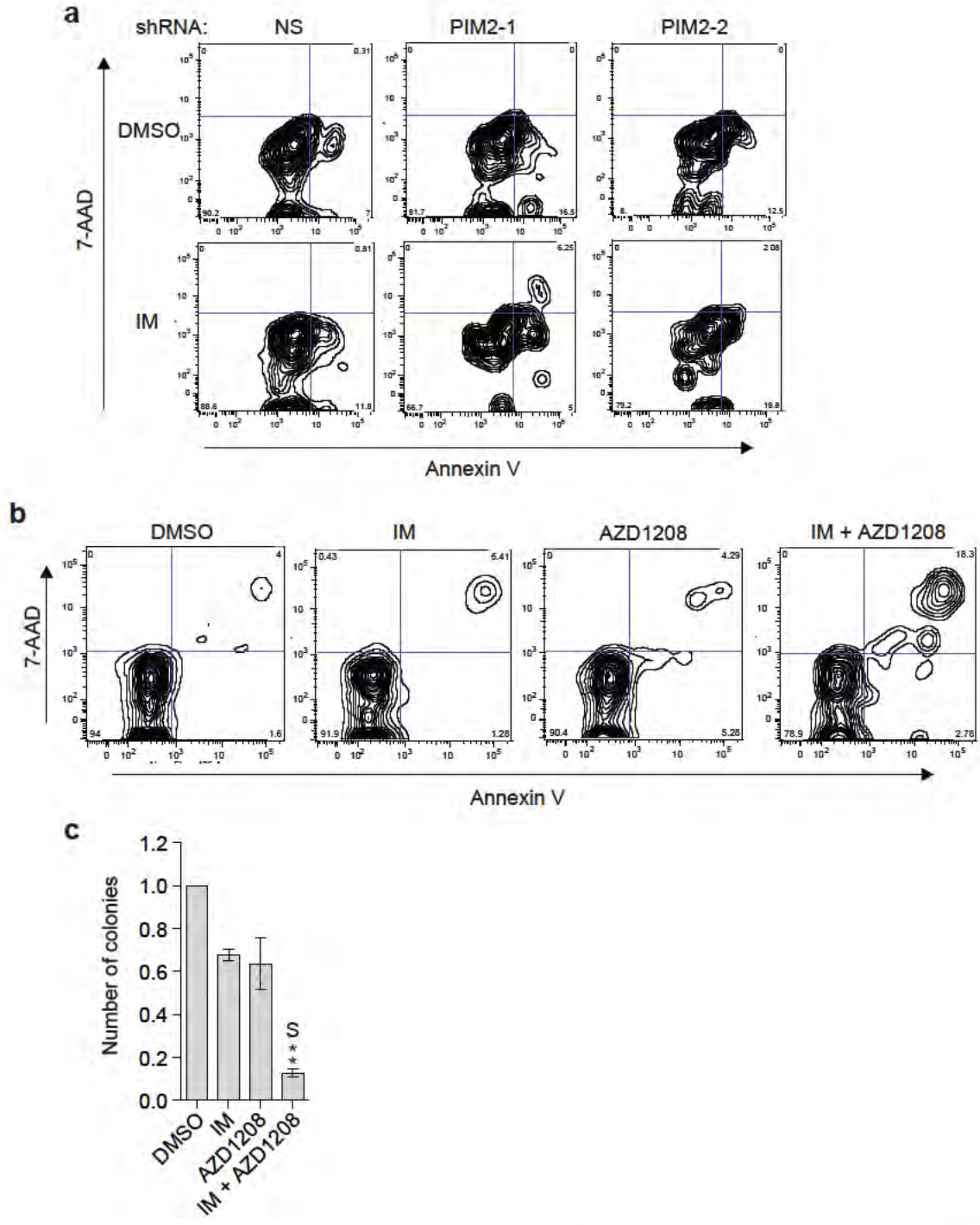

Figure 3.10. FACS analyses for Figure 3.9 b and d, and synergy analysis for Figure 3.9 e.

Figure 3.10. FACS analyses for Figure 3.9 b and d, and synergy analysis for Figure 3.9 e. a, FACS analysis showing representative Annexin V/7-AAD staining of DMSO- or IM-treated human CML stem cells expressing a NS shRNA or one of two unrelated PIM2 shRNAs. These data provided the basis for the bar graph in Figure 3.9 b. **b**, FACS analysis showing representative Annexin V/7-AAD staining of human CMLSCs treated with DMSO, IM, AZD1208 or a combination of IM and AZD1208. These data provided the basis for the bar graph in Figure 3.9 d. **c**, Colony formation assay of human primary CML cells treated with DMSO, IM, AZD1208 or a combination of IM and AZD1208. To perform synergy analysis, the data from 4 individual CML patients (shown in Figure 3.9 e) were combined and normalized by setting DMSO treatment to 1. Error bars indicate SEM; n=4 biological replicates. S denotes the combined drug treatment was synergistic. $^{**}P \leq 0.01$.

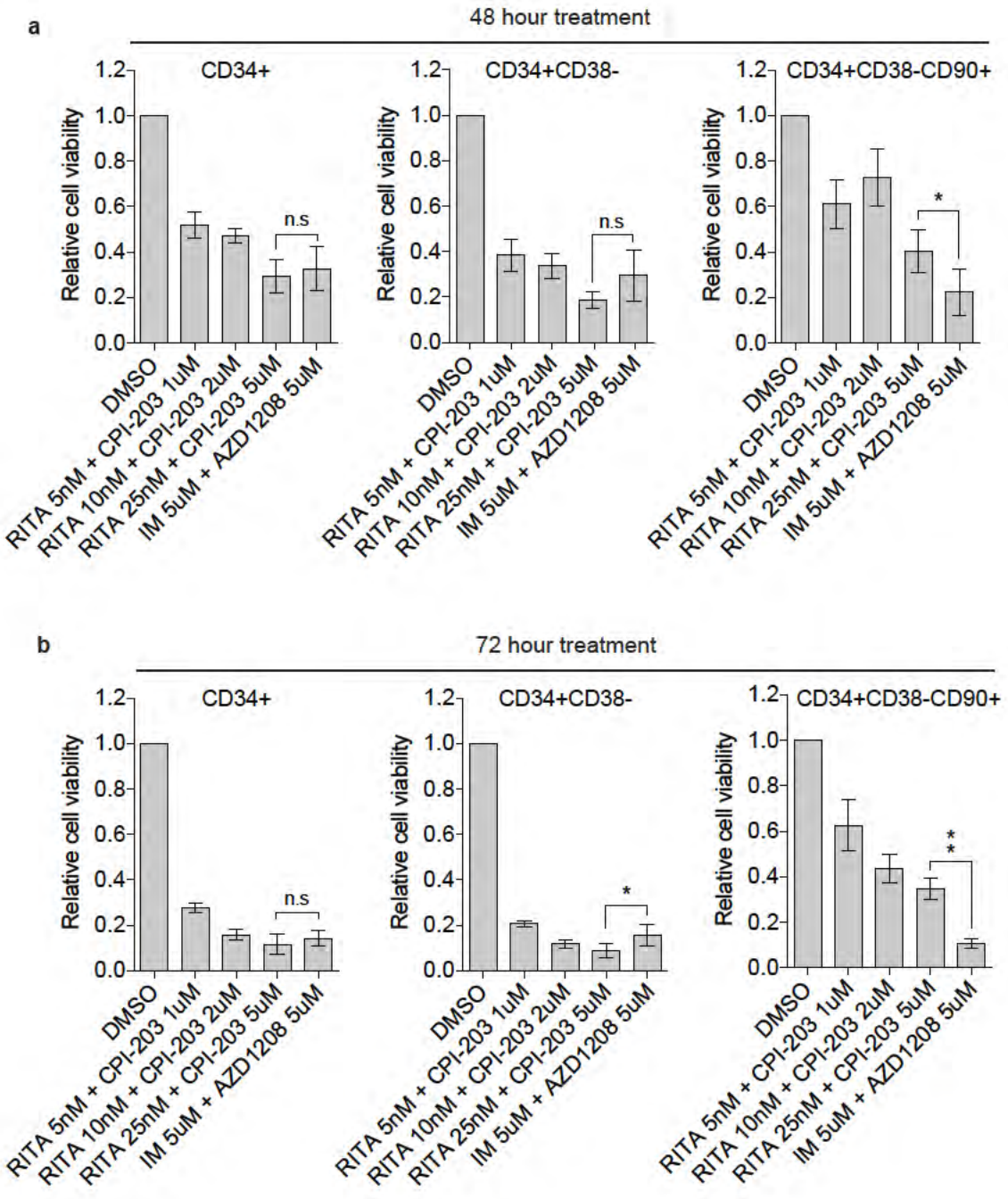

Figure 3.11. Side by side comparison of combination therapy using IM and PIM2 inhibitor versus p53 activator and c-Myc inhibitor in primary CML cells.

Figure 3.11. Side by side comparison of combination therapy using IM and PIM2 inhibitor versus p53 activator and c-Myc inhibitor in primary CML cells. Relative cell viability of total CD34+ CML cells, CD34+CD38- CMLSCs, and CD34+CD38-CD90+ CMLSCs was determined after either 48 hours (a) or 72 hours (b) treatment with either a combination of RITA (p53 activator) and CPI-203 (c-Myc inhibitor) at various concentrations or a combination of AZD 1208 and IM. The results were normalized to that obtained in DMSO-treated cells, which was set to 1. Error bars indicate SEM; n=4 biological replicates. $^{**}P \leq 0.01$, $^{*}P \leq 0.05$, n.s means not significant.

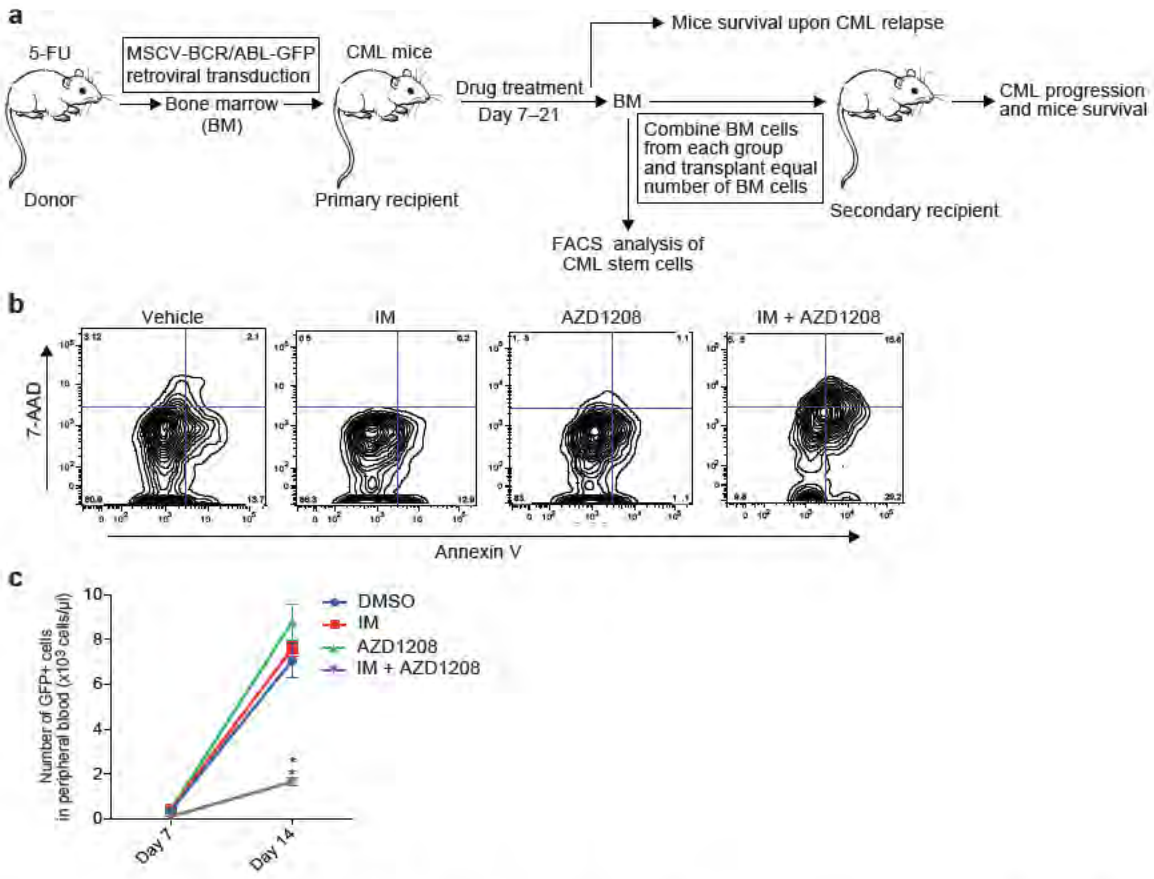

Figure 3.12. Experimental schematic and additional supporting data for CML animal experiments. a, Schematic of the animal experiments. CML was induced in mice using a retroviral transduction model. Seven days after bone marrow transplantation, CML mice were treated for two weeks with vehicle, IM, AZD1208, or a combination of IM and AZD1028. After drug discontinuation, some CML mice were sacrificed to harvest bone marrow cells to either analyze CML stem cell apoptosis and viability or transplanted into secondary recipients to monitor engraftment and animal survival. The remaining primary transplant CML mice were continuously monitored for disease relapse and animal survival. **b**, FACS analysis showing representative Annexin V/7-AAD staining of murine CML stem cells isolated from mice treated with vehicle, IM, AZD1208, or a combination of IM and AZD1208. These data provided the basis for the bar graph in Figure 3.13 b. **c**, Expansion of CML (GFP+) cells in the peripheral blood of secondary recipient mice after receiving bone marrow cells from primary transplant mice treated with vehicle (n=5), IM (n=5), AZD1208 (n=5), or a combination of IM and AZD1028 (n=5). Error bars indicate SEM. $^{**}P \leq 0.01$.

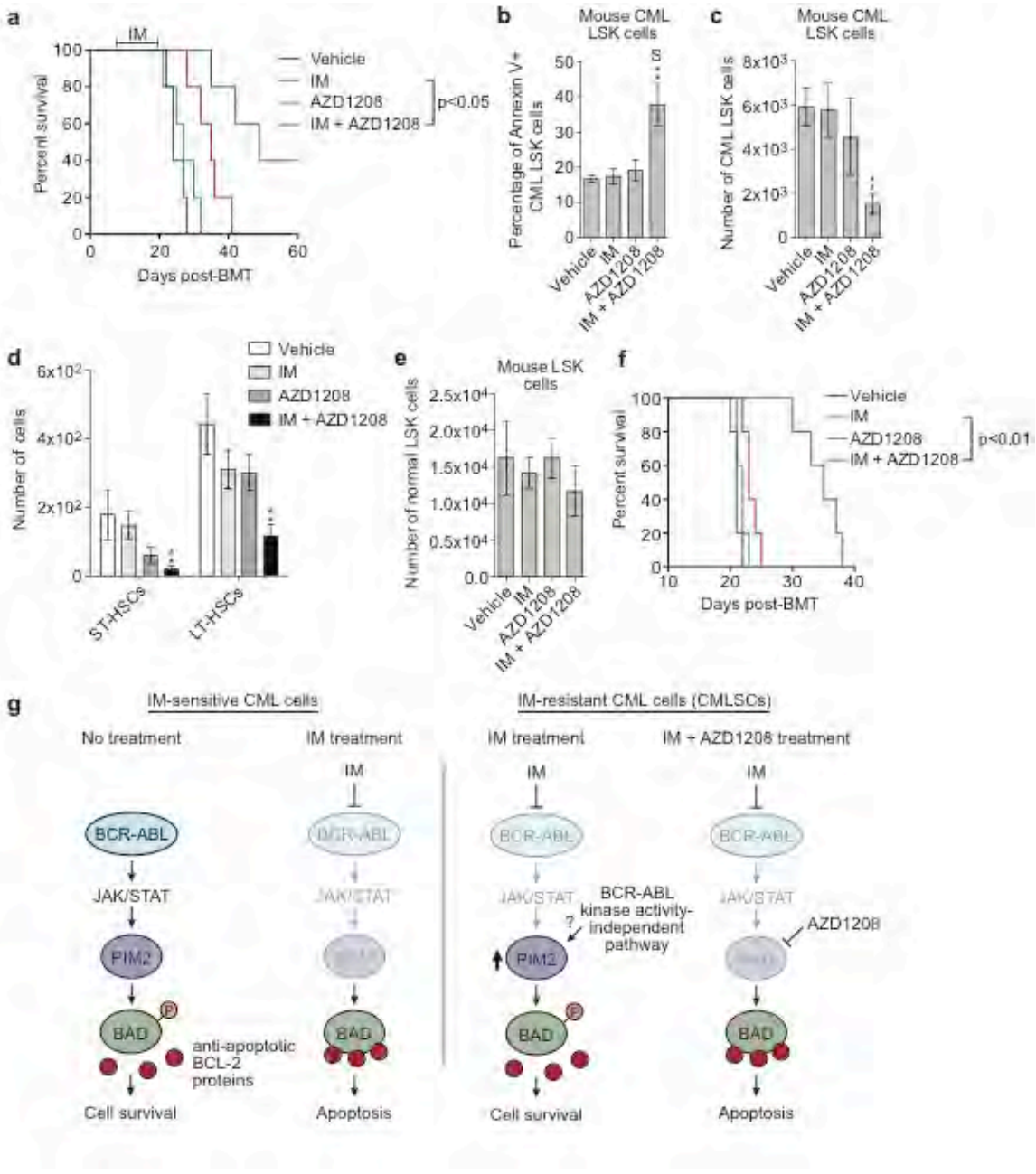

Figure 3.13. Combined treatment with IM and the PIM2 inhibitor AZD1208 significantly prolongs survival in a mouse CML model.

Figure 3.13. Combined treatment with IM and the PIM2 inhibitor AZD1208 significantly prolongs survival in a mouse CML model. a, Kaplan-Meier survival curve of CML mice (n=5 per group) treated for two weeks (days 7-21) with vehicle, IM, AZD1208 or a combination of both drugs. **b**, Annexin-V staining monitoring apoptosis of CML LSK cells from CML mice treated with vehicle (n=10), IM (n=9), AZD1208 (n=10) or a combination of IM and AZD1208 (n=9). **c-e** FACS determination of the number of CML (GFP+) LSK cells (c), CML (GFP+) short-term HSCs (ST-HSCs) and long-term HSCs (LT-HSCs) (d), or normal (GFP-) LSK cells (e) after treatment of mice with vehicle (n=6), IM (n=6), AZD1208 (n=6), or both IM and AZD1208 (n=5). **f**, Kaplan-Meier survival curve showing CML engraftment and progression in secondary transplant mice (n=5) with bone marrow cells from each group of primary transplant CML mice shown in (a). Error bars indicate SEM. *$P \leq 0.05$, **$P \leq 0.01$.

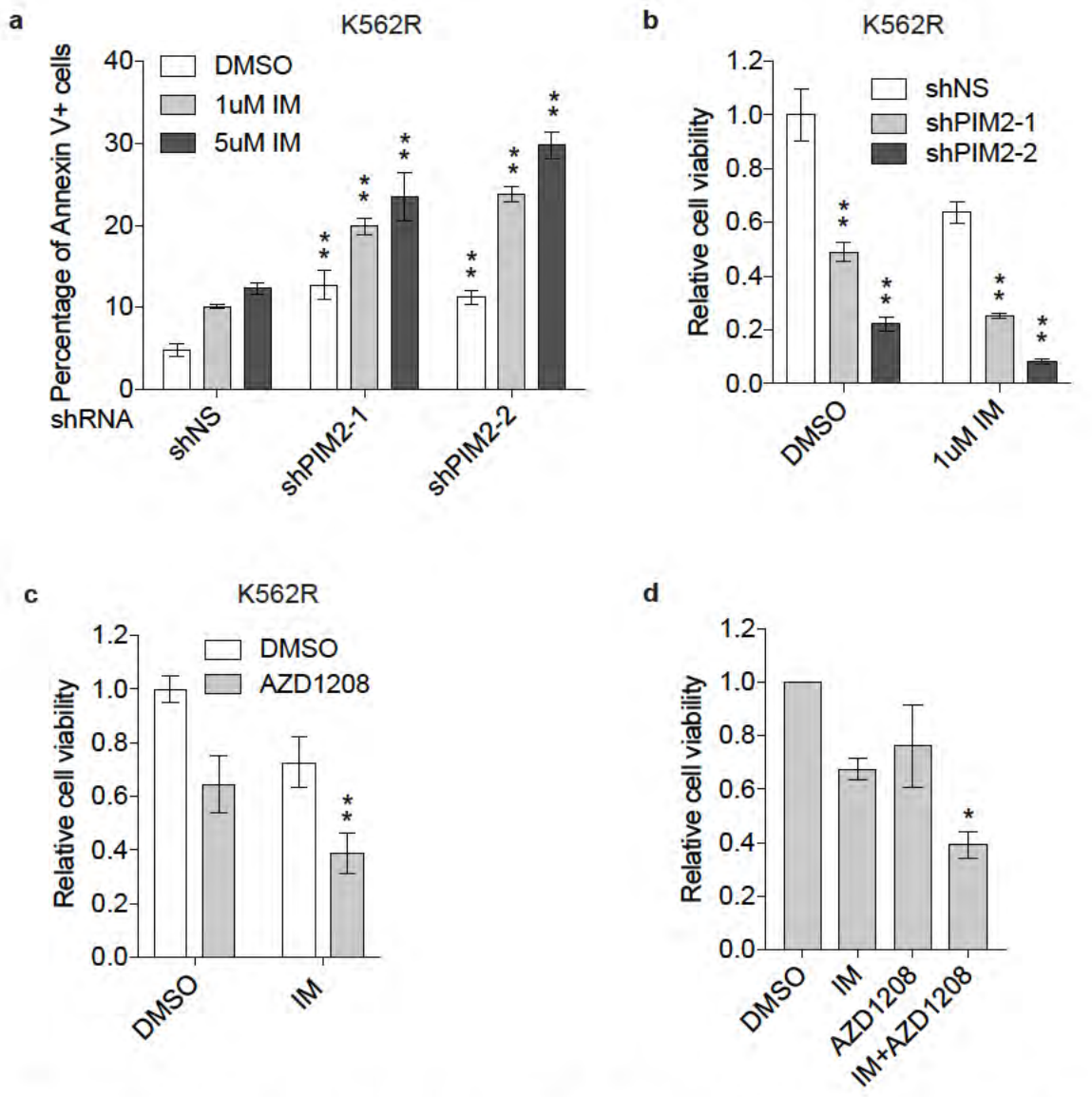

Figure 3.14. Combined therapy with IM and AZD1208 kills BCR-ABL independent IM-resistant CML cells.

Figure 3.14. Combined therapy with IM and AZD1208 kills BCR-ABL independent IM-resistant CML cells. Apoptosis(a) or cell viability(b) of K562R cells expressing an NS or *PIM2* shRNA and treated with DMSO or IM. Statistical analysis was performed between each *PIM2* shRNA and NS shRNA expressing cells in either DMSO or IM treated condition. In (b), the results were normalized to that obtained in DMSO-treated NS shRNA expressing cells, which was set to 1. Error bars indicate SD; n=4 technical replicates. c, Cell viability of K562R cells treated with DMSO, IM (1uM), AZD1208 (1uM) or a combination of both drugs. Error bars indicate SD; n=4 technical replicates. d, Cell viability of primary CML cells with BCR-ABL independent IM resistance upon treatment with DMSO, IM (5uM), AZD1208 (5uM) or a combination of both drugs. Error bars indicate SEM; n=3 biological replicates. In (c) and (d), statistical analysis was performed between IM treated group and combination treated group. $^{**}P \leq 0.01$, $^{*}P \leq 0.05$.

Sample ID	Source[1]	CML phase	BCR-ABL mutation status	Origin	Application	
					Single-cell RNA seq	Functional assay
CML1	UMass	Newly-diagnosed chronic phase	Wild-type	Bone marrow	●	●
CML2	OHSU	Newly-diagnosed chronic phase	Wild-type	Bone marrow	●	
CML3	UMass	Newly-diagnosed chronic phase	Wild-type	Bone marrow	●	●
CML4	UMass	Newly-diagnosed chronic phase	Wild-type	Bone marrow		●
CML5	UMass	Newly-diagnosed chronic phase	Wild-type	Bone marrow		●
CML6	UMass	Newly-diagnosed chronic phase	Wild-type	Bone marrow		●
CML7	UMass	Newly-diagnosed chronic phase	Wild-type	Bone marrow		●
CML8	UMass	Resistant to IM (Gleevec)	Wild-type	Bone marrow		●
CML9	UMass	Resistant to IM (Gleevec)	Wild-type	Bone marrow		●
CML10	UMass	Resistant to IM (Gleevec)	Wild-type	Peripheral Blood		●

[1] UMass, UMass Cancer Center Tissue Bank; OHSU, Druker Lab, OHSU Knight Cancer Institute.

Table 3.1 List of human CML patient samples used in this study.

Gene	Forward primer (5'→ 3')	Reverse primer (5'→3')
BCR-ABL (1st round)	GCAGCAGAAGAAGTGTTTCAG	CCGGAGCTTTTCACCTTTAG
BCR-ABL (2nd round)*	CATTCCGCTGACCATCAATAA	AACGAGCGGCTTCACTCAGA
B2M	GTATGCCTGCCGTGTGAAC	AAAGCAAGCAAGCAGAATTTGG
GAPDH	TGCACCACCAACTGCTTAGC	GGCATGGACTGTGGTCATGAG
PIM2 (human)	CTGACTTTGATGGGACAAGG	GAATCTCCTGGTCCCTCTC
Pim2 (mouse)	ATCTCGCGACACCAGTACCAT	GATTAGGGCACAGCAATCTGG

* Published in ref. (Chu et al., 2005)

Table 3.2 List of primers used for qPCR and nested PCR analysis.

CHAPTER IV: CRISPR-CAS9 MEDIATED SATURATED MUTAGENESIS SCREEN IN BCR-ABL PREDICTS CLINICAL TKI RESISTANT MUTATIONS

ABSTRACT

Understanding the mechanism of drug resistant mutations should improve the ability to generate therapeutics with reduced susceptibility to resistance. In vitro analyses of mutations provide a promising approach, but previous analyses of BCR-ABL mutations inserted at stochastic locations in the genome identified many mutations that increased tolerance to drug but that were rarely observed in patients. We developed a high-throughput CRISPR-Cas9 mediated approach to analyze the effects of systematic libraries of BCR-ABL point mutations at a consistent genomic location. Using bulk competitions with a deep-sequencing readout, we analyzed the effects of hundreds of mutations in parallel under multiple drug conditions. The effects of mutations on growth with and without inhibitor were critical for predicting clinical resistant mutations, many of which were cancer adaptive in the absence of drug pressure. The strategy we have developed can be applied to many different oncogenes and should be more useful than previous approaches for interpreting patient mutations and for evaluating resistance susceptibility in the development of new therapeutics.

INTRODUCTION

Drug resistance limits the effectiveness of many therapeutic strategies with a tremendous impact on patients that develop resistance (Gottesman, 2002; Holohan et al., 2013). Drug resistance has been challenging to address in part because it is difficult to predict the mutations that will contribute to patient health. In vitro screens of drug resistant mutations in many target proteins, including BCR-ABL, often identify many more resistant mutations than are observed in patients (Azam et al., 2003). One potential reason for the discrepancy between in vitro identified BCR-ABL resistant mutations and those observed in patients is that most previous *in vitro* analyses introduced mutations using viral transduction, which integrates mutations stochastically. The genomic location of a gene can have a large effect on its expression level that can in turn have a large effect on phenotype (Day et al., 2000). In our own previous analyses of mutations in oncogenic BRAF using transduction (Wagenaar et al., 2014), we observed that multiple independent measurements (>4) were required to confidently distinguish mutations that consistently caused resistance from those that exhibited resistance in occasional replicates. These observations motivated us to develop strategies that would provide higher confidence in understanding drug resistant mutations, and would be improved for predicting the impacts of mutations on drug resistance in patients.

We chose to focus on BCR-ABL because inhibitors to this oncogene are effective at curing many patients, and where resistance has been observed it is frequently associated with direct mutations in BCR-ABL itself (Gorre et al., 2001; Soverini et al., 2011). Thus, the prediction of the impact of BCR-ABL mutations on patients most likely has a high potential to provide information to guide the development of new therapeutics.

To improve the consistency and efficiency of *in vitro* screens, we developed an approach that we refer to as BIG (Barcoded Introns in the Genome) EMPIRIC (Exceedingly Meticulous and Parallel Investigation of Randomized Individual Codons). We previously developed EMPIRIC to analyze hundreds to thousands of mutations encoded on plasmids in yeast (Hietpas et al., 2011; Mishra et al., 2016), as well as in reverse engineered viruses (Jiang et al., 2016), and randomly integrated oncogenes in mammalian cells in culture (Wagenaar et al., 2014). EMPIRIC experiments are a type of mutational scanning approach (Fowler and Fields, 2014) that focuses on individual amino acid changes, which are often the most relevant to mammalian genetic disorders including cancer.

In our previous EMPIRIC studies in yeast and reverse engineered viruses, we observed strong reproducibility between independent measurements of the impact of amino acid changes. We observed far greater variation between independent measurements in the analyses of randomly integrated variants of

BRAF in mammalian cells, and multiple independent measurements were necessary to distinguish signal from noise. BIG EMPIRIC was designed to provide both reduced variation through the targeting of mutations to a consistent genomic location using CRISPR-Cas9 (Cong et al., 2013; Horvath and Barrangou, 2010), and multiple independent measurements for each amino acid change by utilizing a barcoding strategy (Figure 4.1). Of note, the use of multiple barcodes for each amino acid variant provides internal independent measurements within each experimental replicate.

RESULTS

Towards the goal of sampling hundreds of Bcr-Abl mutations in the same experiment, we extensively optimized a CRISPR-Cas9 integration strategy (Figure 4.1, Figure 4.2, Figure 4.3 & Methods). We utilized Ba/F3 cells because of their conditional dependence on Bcr-Abl function in the absence of exogenously supplied IL-3 (Daley and Baltimore, 1988). We transduced a non-functional Bcr-AblΔKD (lacking the kinase domain) and utilized CRISPR-Cas9 to site specifically introduce the AblKD to generate full-length Bcr-Abl and induce expression of a GFP marker (Figure 4.1 b). We used a donor template with DsRed to optimize homology-directed repair (HDR) efficiency (Figure 4.1 c, Figure 4.3 and Methods) and were able to achieve 8% HDR efficiency, which represented successful genetic modification of 10^5 cells. For 10-fold representation of mutant libraries, we estimate that this would be sufficient to screen up to 10,000 mutations in a single reaction. As part of the HDR optimization process, we tested dozens of clonal cell lines to identify a clone (C7) that when rescued with the wildtype AblKD produced a response to TKI treatment that resembled the response of CML cells (Figure 4.4). In this cell line that we refer to as Ba/F3-BcrAblΔKD, we observed that Bcr-AblΔKD was integrated at a single genomic location within transcriptionally active chromatin (see Methods, Figure 4.5). To facilitate multiple independent measurements for each amino acid change in AblKD mutant libraries, we introduced a short intron containing a barcode (Figure 4.1). We designed the barcode sequence to avoid

sequences that would disturb intron splicing (see Methods, Figure 4.6). The frequency of mutations that we observed integrated into the genome closely matched the frequency in the donor library (Figure 4.1 d and Figure 4.7), indicating that integration was not strongly biased by the mutations.

We initially investigated the experimental fitness effects of mutants at the gatekeeper position (Figure 4.8 a). Cells with the T315X library were grown without IL-3 for three days, then split and grown for a further three days with and without Bcr-Abl inhibitors. Based on next-generation sequencing of barcodes we determined the frequency of each amino acid at position 315 at the time of IL-3 withdrawal and at the end of the experiment. The effects of mutations on growth without IL-3 provide a readout of Bcr-Abl function without inhibitors. Most amino acid changes at position 315 caused a functional defect (Figure 4.8 b). Five mutations increased Bcr-Abl function, including the T315I mutation that is known to cause resistance (Gorre et al., 2001). Supporting these observations, mutations corresponding to T315I and T315M have been reported to increased kinase function in c-Abl and/or c-Src (Azam et al., 2008).

In replicate growth competitions, strong correlation (R^2=0.93) was observed between estimates of Bcr-Abl function (Figure 4.7 b). We estimated the effects of mutations on drug binding by comparing relative growth of mutants in the presence and absence of imatinib, similar to what is done in traditional IC-50

measurements. All mutations at position 315 compromised drug binding based on this analysis (Figure 4.8 b). The observation that few gatekeeper mutations have been observed in patients (Zabriskie et al., 2014) indicates that alterations in drug binding without consideration of function may be misleading with regard to clinical relevance. In principle, the combined effects of mutations on Bcr-Abl function and drug binding will be under selection in patients. In our experiments, these combined effects provide the strongest advantage (Figure 4.8 b) for four different amino acid changes (L,M,I,E). Among these mutations, only T315I is accessible by a single nucleotide change, which is the most common form of mutation in cancer (Vogelstein et al., 2013). The T315I mutation was the most frequently observed mutation in imatinib resistant patients (Shah and Sawyers, 2003), suggesting that consideration of mutational accessibility and combined effects on function and drug binding can provide clinically relevant predictions.

The combined effects of mutations on function and drug binding were further investigated with additional inhibitors at varying concentrations (Figure 4.8 c). Six amino acid changes at position 315 (L,M,I,V,Q,E) demonstrated greater combined effects than the parental Bcr-Abl. Five of these (L,M,I,Q,E) exhibited increasingly adaptive responses with elevated imatinib concentration (Figure 4.8 c), indicating our measurements are capturing relevant aspects of drug selection. We also examined selection in the presence of dasatinib (Figure 4.9) and ponatinib (Figure 4.8 c), which was designed to counteract the T315I mutation

(O'Hare et al., 2009). Consistent with its design, we observed that T315I could be inhibited by ponatinib. However, four mutations(L,M,Q,E) at position 315 were increasingly adaptive with higher ponatinib concentrations.

Next, a panel of individual mutations were analyzed in isolation (Figure 4.10) to further probe the relationships between our bulk analyses and traditional IC-50 measurements. We chose mutations at position 315 that exhibited strong growth effects and strong combined effects (L,M,I,E), as well as the T315C mutation that exhibited a slight growth defect and a mild combined benefit. Of note, all of these mutations exhibited strong imatinib benefits in our bulk competitions (Figure 4.10b, upper panel). Consistent with our bulk observations, all five mutants had IC-50's to imatinib that were shifted by similar amounts relative to parental Bcr-Abl. The IC-50 results alone indicate that the T315C mutation would be a viable resistant mutation. However, our bulk competitions indicate that T315C causes a negative growth effect in the absence of drug pressure (Figure 4.8 b). These observations highlight the potential utility of observing growth effects in understanding the evolution of drug resistance in cancer.

To explore how these amino acid changes might evolve, we examined the number of nucleotide substitutions and the potential single step pathways (Figure 4.8 d). Of the six amino acid changes at position 315 that appear adaptive to imatinib (L,M,I,V,Q,E), only T315I is accessible by a single base substitution, the

most accessible type of mutation (Vogelstein et al., 2013). In principle, the prevalence of T315I in patient isolates (Jones et al., 2009) could be due to mutational accessibility and/or adaptive potential. Our data indicate similar adaptive potential with imatinib for L,M, I, and E at position 315, with L, M, and E having slightly greater adaptive potential than I at high imatinib concentrations (Figure 4.8 c). These observations suggest that mutational probabilities have a strong influence on the evolution of drug resistance in Bcr-Abl. In high concentrations of both imatinib and ponatinib, T315M and T315E were the most adaptive (Figure 4.8 c). T315M is accessible by a fitness increase path, while T315E cannot be accessed by single nucleotide substitutions without going through a maladaptive intermediate (Figure 4.8 d). The observed advantage of M relative to I at position 315 is greater under ponatinib treatment compared to imatinib, indicating that a mutational pathway from T to I to M may be likely in patients transitioned from imatinib to ponatinib therapy. Consistent with this hypothesis, T315M has recently been reported to evolve from T315I during ponatinib treatment of a patient that had previously failed imatinib therapy (Zabriskie et al., 2014).

Our findings above highlight the potential of our approach to identify clinically relevant resistant mutational pathways. We then examined a larger region encompassing positions 311-319 of Bcr-Abl that flank the gatekeeper residue (Figure 4.11). To assess the reliability of this higher throughput experiment, we

compared results for position 315 with our single position experiment. We observed a strong correlation between these experiments (R^2=0.95, Figure 4. 7 c) indicating that both experiments provide accurate measurements of selection pressures acting on these mutations.

To investigate structure-function relationships in Bcr-Abl in the absence of inhibitors, we examined how the growth effects of mutations map to protein structure. Different positions exhibited strikingly distinct patterns of functional sensitivity to mutation. At position 316 every amino acid substitution caused a strong defect, while at position 319 all amino acid changes exhibited small impacts on function (Figure 4.11 a). These sensitivities were generally consistent with inferences from structure. For example, the glutamate at position 316, which is sensitive to amino acid changes, makes multiple hydrogen bonds (Figure 4.12) that cannot be recovered by any other side chain. In contrast, the side chain of position 319 is oriented towards solvent such that amino acid changes can be tolerated without directly disrupting structure (Figure 4.12).

The conformational dynamics of Bcr-Abl are known to play an integral role in activation and inhibitor binding (Agafonov et al., 2014; Aleksandrov and Simonson, 2010). Additionally, mutation of the gatekeeper residue is thought to activate tyrosine kinases by stabilizing the hydrophobic spine, characteristic of the active protein conformation (Azam et al., 2008). Using molecular dynamics

simulations (10 ns), we tested the stability of the inactive and active kinase states for seven mutations identified in our screens. Five of the mutations (F311L, T315I, T315E, T315M, & F317L) provided a positive growth effect (Figure 4.8 b and Figure 4.11 a), while the other mutations (T315K & T315A) had varying negative growth effects (Figure 4.8 b). The simulations reveal that neither state is substantially perturbed by any of the mutations (Figure 4.13). These results suggest that the varied functional effects of these mutations are due to conformational dynamics, rather than gross structural incompatibilities. However, due to the slow kinetics of these conformational transitions (~100 μs), exploring the effects of these mutations on protein dynamics is beyond the scope of the work presented here (Shukla et al., 2014).

We observed many mutations that provided a growth advantage in the absence of drug (Figure 4.11 a). The observation of adaptive mutations indicates that Bcr-Abl kinase function is linked to Ba/F3 growth rate and can be increased by many mutations, suggesting that the parental kinase activity of Abl may not have been subjected to stringent positive selection. Consistent with these observations, we speculate that signaling proteins such as kinases may be subject to balancing selection when too much or too little signaling is deleterious for organism fitness. This idea is consistent with observations that hyperactive kinases including Bcr-Abl often lead to senescence in primary cells (Mooi and Peeper, 2006).

In the presence of imatinib, the fitness advantage of Bcr-Abl mutations were mediated by both drug binding and growth effects (Figure 4.11 a). The mutations with the strongest combined effects were located at position 315, which is consistent with mutations at this position evolving as the most commonly observed imatinib resistant mutations in clinical samples (Jones et al., 2009). Encouraged by this observation, we investigated if the combined effects in our screen together with mutational probabilities could predict clinical observations of imatinib resistance. Amino acid changes with the greatest combined effects and accessible by a single base change in our screen were ranked (Figure 4.11 b). We developed a predictive resistance score based on the combined effects we observed and mutational probabilities. The predictive resistance score correlates with observed prevalence in patients (Figure 4.11 c). Together, these observations indicate that kinase mutational scans can provide clinically relevant information.

CONCLUSIONS

Here, we have demonstrated an approach to quantitatively interrogate the effect of point mutations on cell fitness across various conditions by leveraging the advantages of saturated mutant library generation, high-fidelity CRISPR-Cas9 mediated library integration through HDR and high-throughput sequencing readout. Conventional mutagenesis study typically involves viral delivery of mutant library. However, random or “safe-harbor” virus integration fails to recapitulate the native chromatin context and ensure uniform transcription regulation for all the mutants, leading to inconsistent and noisy gene expression of individual variants(Day et al., 2000). Given that gene expression level changes caused by factors, such as copy number variation, also significantly affect cell fitness(Ciriello et al., 2013; Gadzicki et al., 2005; Willyard, 2015), this shortcoming markedly compromises the accuracy of the resulting measurement of mutational impact. A saturated mutagenesis approach using CRISPR-Cas9 was recently reported to overcome these drawbacks (Findlay et al., 2014). However, this works harnesses the unique feature of splicing junction and small size of *BRCA1* exon 18 and *DBR1* exon 2, which does not apply to majority of coding region and poses strong limits on its application. With a unique intron based barcoding strategy and a systematic method optimizing HDR efficiency, our approach significantly expanded the randomized DNA region up to 1kb, and offers a more flexible way to study almost any gene of interest, particularly oncogenes involved in cancer.

We showed that our approach could quantitatively interpret the functional consequence of hundreds of BCR-ABL mutations at once. IC50, the gold standard to assessing drug resistance, depicts the effect of mutations on inhibitor binding, and has been widely used to predict therapeutic response of mutants. However, the question remains unsolved how to associate resistant BCR-ABL mutations identified from various *in vitro* high throughput mutagenesis screens with their actual clinical relevance(Azam et al., 2003; Ray et al., 2007). IC50 itself seems not to be a reliable way for this purpose based on our study. In contrast, a combined effect of both cell growth and inhibitor binding provides better estimation of the likelihood of individual mutation emerging from patients under TKI therapy. Nevertheless, an accurate estimation could only be achieved by taking into account the variable nucleotide substitution rate and the number of accessible single-base mutational pathways. As a proof of principle, we assessed those mutations within 311-319 region from patients treated with Imatinib and obtained marked association between our prediction and clinical data, suggesting a predictive power of this approach.

While there is sufficient clinical data on BCR-ABL mutations, such information is still largely missing for other oncogenes, such as EGFR and BRAF, that are widely associated with cancer and that could be targeted by small molecules. The mutations observed to cause resistance in patients are often not clear until drugs are utilized clinically. In the case of HIV-1 protease, it was shown

previously that inhibitors confined to the space that the substrate would occupy can reduce resistance(Nalam et al., 2013). This pioneering work demonstrates that research on resistance mechanism has the capability to inform drug development. It also highlights the need for additional approaches such as the one presented here to analyze drug resistance mutations (e.g., when all of the relevant structures are not known).

MATERIALS AND METHODS

Reagents

Px330 vector was a gift from Mike Browsky lab. pTRIPZ vector was obtained from shRNA core facility at UMass Medical School. PUC19 vector was a gift from Lucio Castilla lab. BCR antibody (cat. No. 3902) was purchased from Cell Signaling Technology. Imatinib (cat. No. CT-IM001) and Dasatinib (cat.no. CT-DS001) were purchased from ChemieTek Ponatinib was purchased from LC labs (cat.no. P-7022). Eelectroporation kit V(cat.no. VCA-1003) was purchased from Lonza. Doxycycline (cat.no. D9891) was purchased from Sigma.

Cell lines and cell culture

All Ba/F3 cell lines were maintained RPMI 1640 medium containing 10% fetal bovine serum (FBS), 4 mM L-glutamine, 100 units/ml penicillin, and 100 µg/ml streptomycin. Parental Ba/F3 cell culture was supplemented with 10ng/ml IL-3, and clonal Ba/F3 cell containing doxycycline inducible BCR-ABL was supplemented with 1ug/ml of doxycycline unless otherwise stated.

Reporter plasmid construction

The reporter construct was generated by removing the BCR-ABL kinase domain, such that in the absence of CRISPR-Cas9 cutting there would be an in-frame proximal downstream stop codon, thereby producing a truncated non-functional protein product containing BCR and a short region of ABL (Figure 4.2 and Figure

4.3). A PAM element (NGG) was engineered 3 nucleotides away from the junction, either upstream (BCR) or downstream (ABL), to create functional target sites that are not present in the endogenous BCR-ABL sequence. SgRNA-mediated CRISPR-Cas9 cutting results in complete separation of the BCR and ABL fragments. To monitor the rate of CRISPR-Cas9 double strand break (DSB) formation, we introduced GFP linked to ABL through a 2A peptide such that non-homologous end joining (NHEJ)-mediated mutagenesis at this locus will create indels, a portion of which will lead to in-frame expression of ABL and 2A-GFP. The BCR-ABL fusion protein was also put under control of a doxycycline-regulated promoter for tight and quantitative control of BCR-ABL expression.

Cutting efficiency of Cas9 could be affected by the base-pairing properties of sgRNA and its target DNA sequence (Doench et al., 2014). Therefore, we constructed three different versions of BCR-ABL reporter and two sgRNAs for each reporter to identify the most active combination.

pTRIPZ vector was re-engineered by removing shRNA and TurboRed cassette removed and replaced with multiple cloning sites. Two PCR reactions were performed using phusion polymerase (cat.no. M0530, NEB) to amplify BCR region and ABL (Δkinase domain) region based on the reporter design, then PCR product is purified and fused together into pTRIPZ vector using Gibson assembly (cat.no. E2611, NEB).

Reporter cell line generation

pTRIPZ reporter plasmids was packaged into low-titer lentivirus and transduced into Ba/F3 cells. After 3 days of culturing, cells were subjected to puromycin selection, and continuously expanded for ~1 week. Cells were then collected, stained for 7AAD and single live cell were sorted at sterile condition into each well in 96-well plate containing culture medium with IL-3 and extra antibiotics (ciprofloxin). After 7~10 days of expanding without medium change, usually~50% of well will have colonies growing up. Colonies were then transferred into 24 well plate and cultured in IL-3 supplemented medium with 1ug/ml of Doxycycline for additional 48 hours. ~50 colonies from each reporter construct were then harvested for fusion protein expression analysis using western blots. The top 5 colonies with highest fusion protein expression were considered to be most accessible to Cas9/Crisper and saved for subsequent HDR analysis.

HDR optimization

To optimize HDR efficiency, we used a donor template containing an in-frame DsRed (~600bp) flanked by homology arms (Figure 4.3). Successful HDR events will lead to both in-frame DsRed and GFP expression, and therefore HDR efficiency could be accurately estimated by the percentage of GFP+/DsRed+ cells (Figure 4.3).

First, we generated BCR-DsRed-ABL containing donor plasmids. Specifically, we replaced the kinase domain region with DsRed in BCR-ABL, short linker sequence was added to ensure in-frame expression of BCR-DsRed-ABL. Then, we performed PCR reactions with primers binding on either side of DsRed at different distance, 0.4kb, 0.8kb, 1.2kb, 1.5kb, 2kb, and 2.5kb, to generate PCR products with different homology arm length. Then these PCR products were fused into a small PUC19 vector using Sequence and Ligation Independent Cloning (Klein et al.) method to achieve the final donor plasmid.

We then selected three clonal lines with similar expression of BCR-ABL fusion protein, one clone from each reporter lines. Then used 1.2kb homology arm donor plasmid and 10 ug of total plasmid (1:3 ratio of Cas9/Crispr:donor plasmid), and we found HRC reporter and sgRNA C2 gave the highest HDR rate(Figure 4.3). Then we further optimized the homology arm length, and found 2kb homology sequence on both arms offers the best HDR rate (Figure 4.3). Next, we tested multiple clonal HRC BCR-ABL reporter clones and found variation in HDR efficiency (Figure 4.3), which is likely due to chromatin accessibility of reporter insertion site. We selected the HRC Clone 7(C7) and further optimized the ratio of sgRNA and donor template. Ba/F3 cells have high tolerance to large amount of plasmids, however, more than 20ug of total plasmid sometimes leads to significant portion of cell death (Figure 4.3). Therefore, we performed all our

following experiments using a ratio of 1:5 of sgRNA:Donor template, with a total amount of 20ug. We often manage to obtain 5~8% of HDR rate.

Transfection was conducted using standard electroporation reaction(Lonza Kit V) with 2 million cells each reaction. A library with 1x10^4 variants could be efficiently incorporated with a minimal 5% HDR rate and a typical 10-fold coverage. By scaling up the electroporation reactions and with optimal 10% HDR rate, confident screening of a large library of 10^5~10^6 variants could be easily achieved.

Verification of single chromatin locus integration of reporter gene

Genomic DNA was extracted from reporter cell line C7, digested overnight with a 4-cutter restriction enzyme CviQI, and then ligated to adaptors. Then, nested PCR was performed using KAPA HiFi DNA polymerase (cat.no. KK2602.) to amplify the joint region of the reporter construct and genomic DNA from both 5' and 3' end (Figure 4.5). PCR product from the clone that yield single PCR band on agarose gel was then cloned into TA vector and sequenced to identify the specific genomic location.

T315x and T311-319x HDR donor library construction

Site saturation libraries were generated using a cassette ligation strategy in a bacterial cloning plasmid and transferred to mammalian specific plasmid

constructs as previously described(Wagenaar et al., 2014). The T315X site saturation library was generated with a NNN codon at position 315, while the 311-319 library utilized NNK codons.

To facilitate specific recovery of inserted mutants, we further modified the donor template plasmid by inserting the human *Beta*-globin intron 2(~130bp) downstream of the BCR-ABL kinase domain to accommodate a set of barcodes as an alternative for specific identification of BCR-ABL mutants using deep-sequencing (Figure 4.6). To ensure optimal splicing context is preserved to guarantee efficient splicing and protein expression, we inserted the intron between the two guanines of the CAGG sequence at~120bp downstream of the kinase domain. The barcodes(NMYRMYNMYRMYNMYRMYNM) were inserted between the 5' splicing donor site and branch site, and also designed to avoid interference of normal splicing context, i.e., the 5' splicing donor, 3' splicing acceptor and branching (A) site. (Figure 4.6).

By using CRISPR-Cas9-HDR to introduce donor plasmid with or without intron into the reporter cell line, we can see expression of BCR-ABL in both cases, indicating successfully splicing has happened (Figure 4.6). Previously, it was reported that a mini-intron could increase protein expression, potentially by stabilizing pre-mRNA. However, we did not notice dramatic difference in expression level of BCR-ABL.

Library introduction and drug treatment

Day 1, one million of BaF3 reporter cells were cultured initially in T75 flask for 3 days in the presence of IL3 but without doxycycline. Day 4, cells were collected, pelleted and re-suspended in 15ml of IL3 containing fresh medium for every 10 million cells, cultured for additional 24 hours. Day 5, cells were collected for electroporation using optimal parameters defined above.

Day 6, cells were transferred from 12-well plate into T25 with fresh medium, and doxycycline was added at this moment. Day 8, cells were pelleted, washed twice in IL3-free medium. An aliquot of cells(1~2 million) were saved as baseline control sample. The remaining cells were cultured in IL-3-free and doxycycline containing medium in T75 for additional 3 days, unless otherwise stated. Day 11, cells were collected and treated with DMSO, TKI, or a combination of drugs. Day 14, all cells were collected and saved for genomic DNA extraction. All samples should be pelleted and saved at -80 if not used immediately.

Genomic DNA extraction and Nested PCR

Cell pellet were thawed and re-suspended in DNA extraction buffer(100mM Tris pH8.0, 5mM EDTA, 1%SDS, 200mM NaCl)+ 5ul of protease K and digested at 55 degree for 4 hours. Then genomic DNA were extracted using phenol:cloriform method, and kept at -20.

For 1st round of PCR, 2ug of total genomic DNA was used as template, 2mM Mg_2Cl was added to ensure the high efficiency of polymerase. 1ul of 10uM primer (PE1, GFP_r), the PCR reaction was carried out using KAPA HIFI DNA polymerase. In 25ul reaction volume.

Cycling condition:

95°C 3min

98°C 20s

58°C 15s

72°C 2:30min

additional cycles 22x

72°C 5min

4°C cool

5ul of PCR product was checked on 1% agrose gel. All samples should yield a ~2.5kb band, the band from baseline control sample should be barely seen(<10% library integration), while the rest of sample should give a nice band(~100% library integration.)

For the 2nd round of PCR, 1ul of 1st round PCR product was used as template, 1ul of 10uM primer (Index 1,2,3,…15, PE1) (see Table 4.1 for the list of nested PCR primers). The PCR reaction was carried out by switching to Phusion polymerase to avoid further amplification of 1st round PCR.

Cycling condition:

95°C 3min

98°C 20s

58°C 15s

72°C 20s

additional cycles 9x

72°C 5min

4°C cool

5ul of PCR product was checked on 2.5% agrose gel. All samples should yield a ~200bp band, the band from baseline control sample should be visible now, but still relatively faint compared to other samples. Final PCR products purified by silica column (Zymo Research).

Library preparation and deep-sequencing:

Library sample created by blending equimolar amounts of purified PCR products and then purifying by silica column (Zymo Research. Concentration of the library sample was determined by qPCR using Illumina Library Quantification kit (KAPA Biosystems). Libraries with 20% PhiX control (Illumina) were sequenced on either a MiSeq or NextSeq sequencer (Illumina).

Fitness and drug resistance analysis

Deep sequencing results were processed by custom perl scripts. First, sequences with Phred scores >10 containing the constant region of the PCR

products were extracted from the fastq file. Extracted sequences were then parsed based on the sample ID added in the 2nd round of PCR; IDs correspond to the growth condition the PCR product was generated from. Next, counts for each unique barcode were generated for each condition/sample ID. Barcodes were then decoded using the subassembly file described in the T315x and T311-319x HDR donor library construction section. Finally, counts for barcodes corresponding to the same codon or amino acid mutation were merged.

The mutant frequencies for each condition were analyzed in three ways. First, the ratio of the 'Day 9, -IL-3, DMSO' to the 'Day 3, +IL-3' samples were log2 transformed and normalized to the wild-type synonyms. This analysis highlights the effect each mutant has solely on cell growth in the absence of any inhibitor. The second analysis looks at the effect each mutant has on inhibitor resistance. This is done by taking the ratio of the 'Day 9, -IL-3, Inhibitor' to the 'Day 9, -IL-3, DMSO' samples, then log 2 transforming and normalizing to wild-type synonyms. Finally, the ratio of the 'Day 9, -IL-3, Inhibitor' to the 'Day 3, +IL-3' looks at the combined growth and resistance effect of each mutant.

Mutational probability for each a.a. pair in Figure 4.11c was calculated with the following equation:

$$\sum_{0}^{n} \text{Score of combined effects x Single base mutational rate}$$

n = Number of single base mutational paths for each a.a. pair

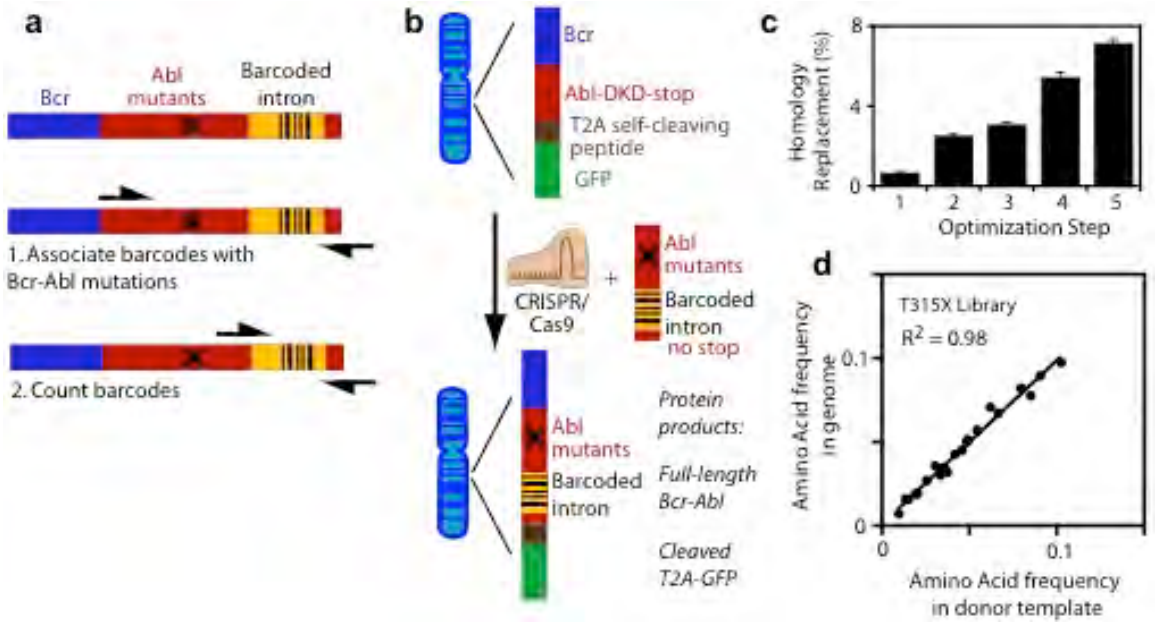

Figure 4.1. Optimized CRISPR/Cas9 strategy efficiently chromosomally integrates barcoded Bcr-Abl libraries. a, Prior to genomic integration, Abl mutations were generated by site saturation mutagenesis and specifically associated with unique barcodes inserted into an engineered intron through a paired end sequencing reaction. b, CRISPR/Cas9 strategy to insert barcoded libraries of Bcr-Abl mutants into a consistent genomic location. Transduction was used to insert a defective Bcr-Abl allele into the genome. A CRISPR/Cas9 strategy was utilized to introduce barcoded libraries of Abl mutations. Successful homologous replacement generates an intact Bcr-Abl gene and rescues expression and rescues the expression of GFP. c, The efficiency of homologous replacement was increased from initial levels (step 1) by optimization of the synthetic guide RNA and donor template sequences (step 2), homology arm length (step 3), clonal cell line (step 4), and the amount of guide RNA and donor template (step 5). Error bars represent the standard deviation of three independent experiments. d, The frequency of a library of site saturation mutations at the gatekeeper position (T315X) integrated into the genome was similar to the frequency of these mutations in the donor template, indicating efficient incorporation of mutants into a consistent genomic location.

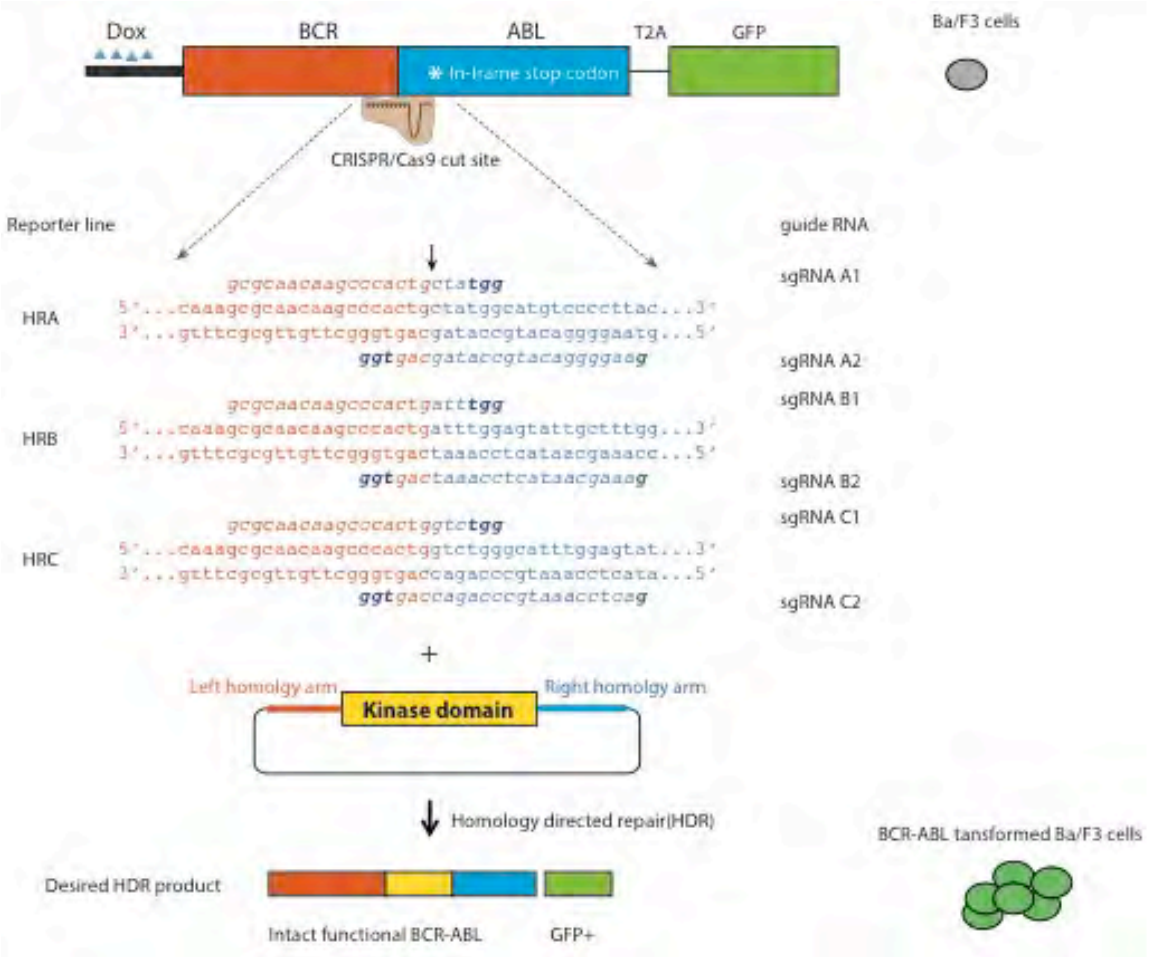

Figure 4.2. Design of CRISPR/Cas9 mediated saturated mutagenesis system. Illustration of doxycycline inducible BCR-ABL(ΔKinase Domain) 2A-GFP reporter construct for CIRSPR/Cas9 mediated saturated mutagenesis. A stop codon was put immediately downstream of the BCR-ABL junction to terminate transcription and prevent GFP expression. Three reporter constructs were generated, varying in the junction region as shown in the DNA sequence. Two separate sgRNAs of opposite orientation were designed to recognize each junction and mediate Cas9 cutting right at the junction as the arrow pointed. With supplement of a donor plasmid containing the wildtype kinase domain flanked by homology arms, homology directed repair(HDR) pathway could facilitate incorporation of the wildtype kinase domain, restoring BCR-ABL kinase function to promote IL-3 independent growth of Ba/F3 cells and driving GFP expression.

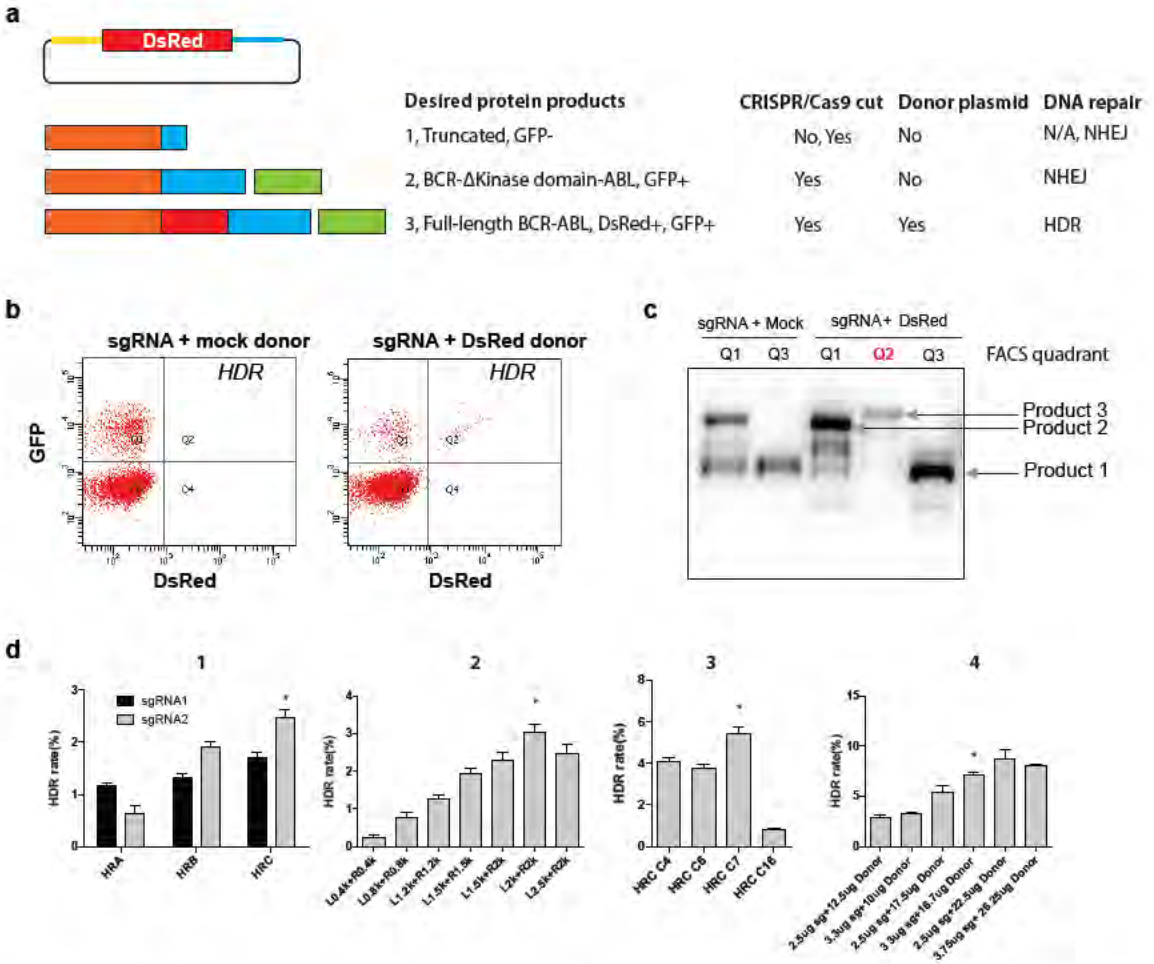

Figure 4.3 Optimization of homology directed repair rate in reporter cell line. a, Schematic diagram showing the DsRed-containing donor plasmid, and expected protein product after repair of CRISPR/Cas9 induced genomic lesion. b, FACS plot showing cell population distribution after CRISPR/Cas9 cutting in the absence or presence of DsRed-containing donor plasmid. Cell population undergone successful HDR express both DsRed and GFP. C, Western blot showing expression of the desired protein product in cell population isolated from corresponding quadrant in FACS plot in panel B. Product, 1,2,3, correspond to the description in panel A. D, Optimization of four parameters to maximize HDR rate: 1, Combination of target sequence and sgRNA; 2, Homology arm length; 3, Variation of clonal cells; 4, Ratio and total amount of sgRNA and donor plasmid.

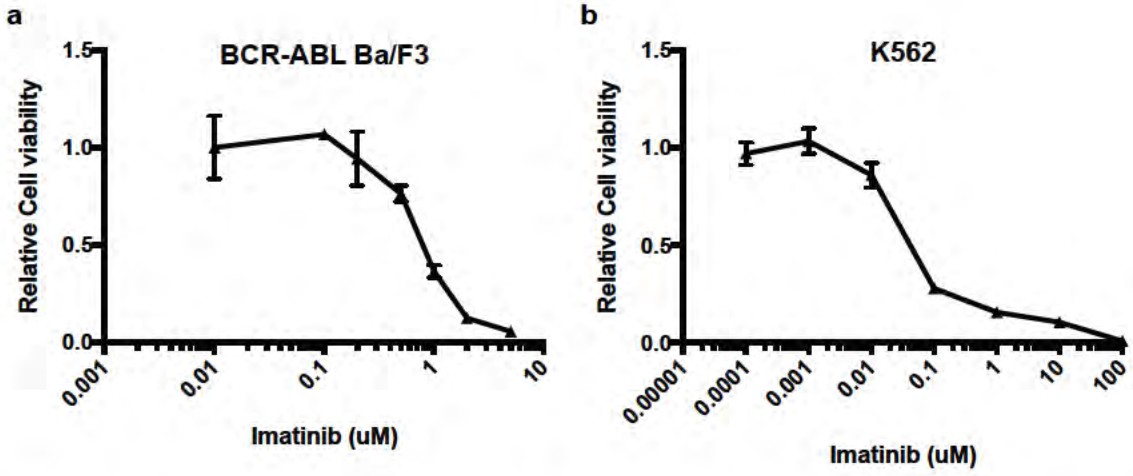

Figure 4.4. Response of BCR-ABL transformed Ba/F3 cells to imatinib. BCR-ABL transformed Ba/F3 cells(a) or K562 CML cells(b) were cultured with increasing concentration of imatinib for 3 days, relatively cell viability was determined by MTT assay.

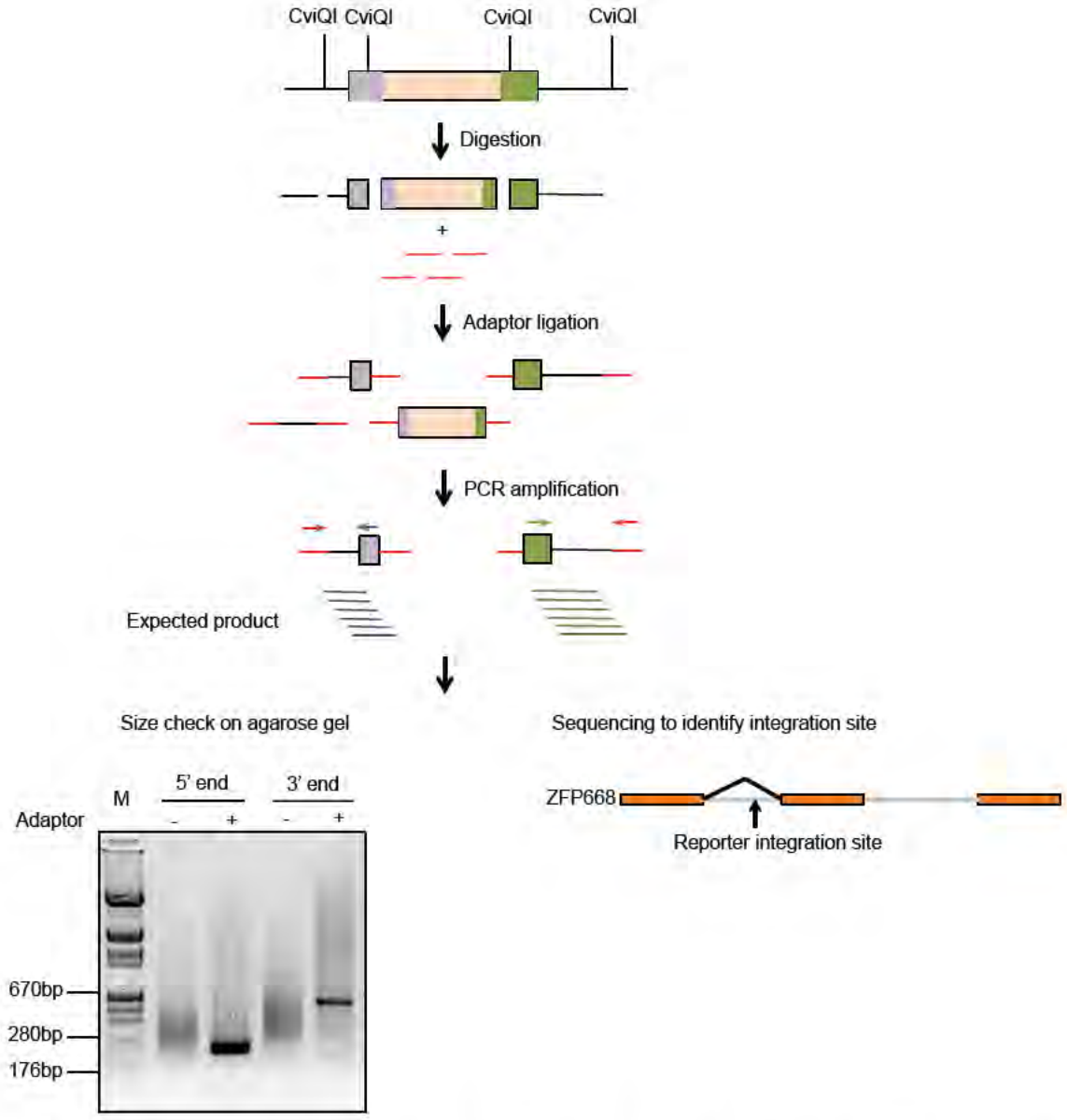

Figure 4.5. Validation of single chromatin locus integration. Illustration of procedures to identify reporter integration site. Genomic DNA was extracted and digested with a 4-cutter restriction enzyme CviQI, ligated to adaptors and PCR amplified using primers specific to either 3'LTR or 5'LTR and the adaptor. As shown in the agarose gel, single integration event results in a single PCR product. Sanger sequencing of the PCR products indicates integration of the reporter in the first intron of mouse gene ZFP668.

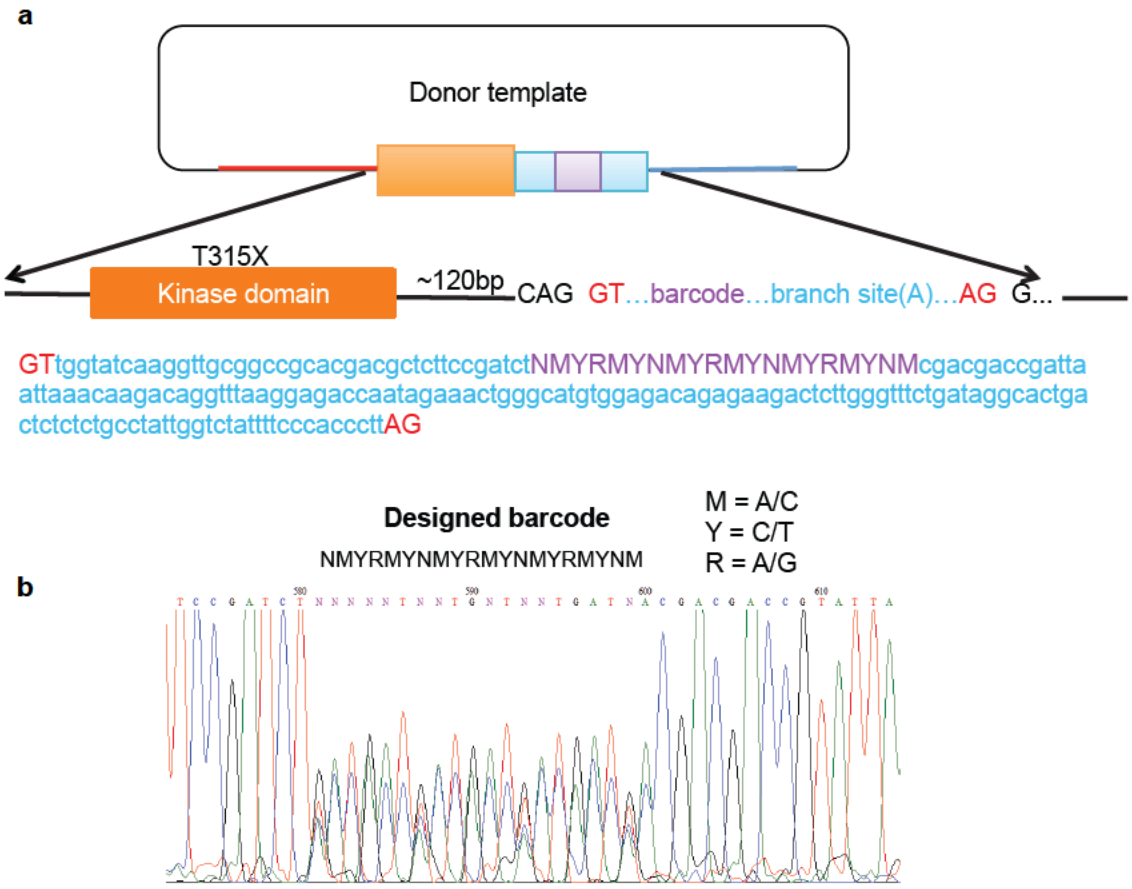

Figure 4.6. Donor template design and barcoding strategy. a, Illustration of key components of donor template and corresponding DNA sequences. Human β-globin mini-intron was inserted ~120 bp downstream of kinase domain, in an optimal splicing DNA context(CAG GT AG G). Splicing donor and acceptor sites were marked in red, intron in cyan, and barcode in purple. b, Sanger sequencing confirms successful incorporation of barcodes at desired location.

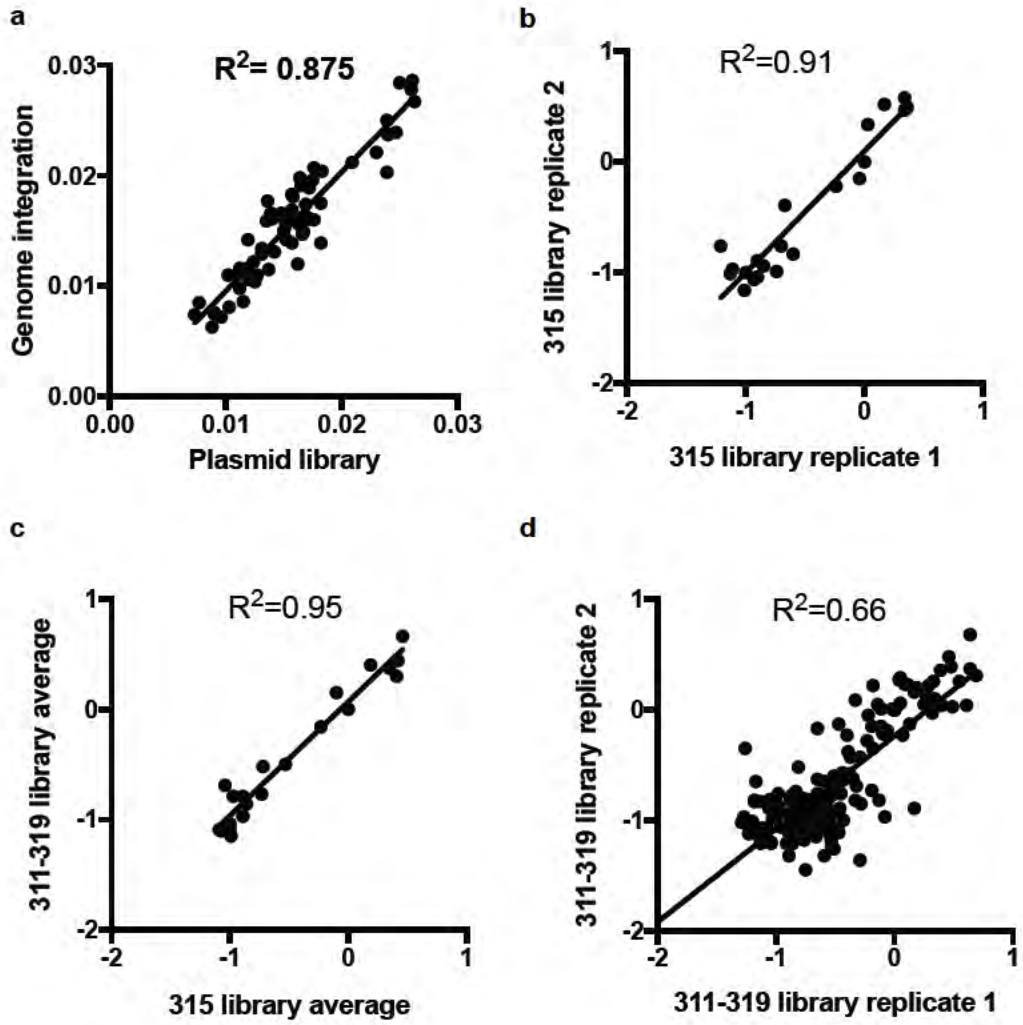

Figure 4.7. Experimental reproducibility. a, Correlation of donor plasmid library and genomic integration of the library at codon level. b, Correlation of growth effect of T315x mutants in two biological replicates. c, Correlation of growth effect of T315x mutants in 315x library and 311-319x library. d, Correlation of growth effect of all amino acid mutants in two replicates of 311-319x library.

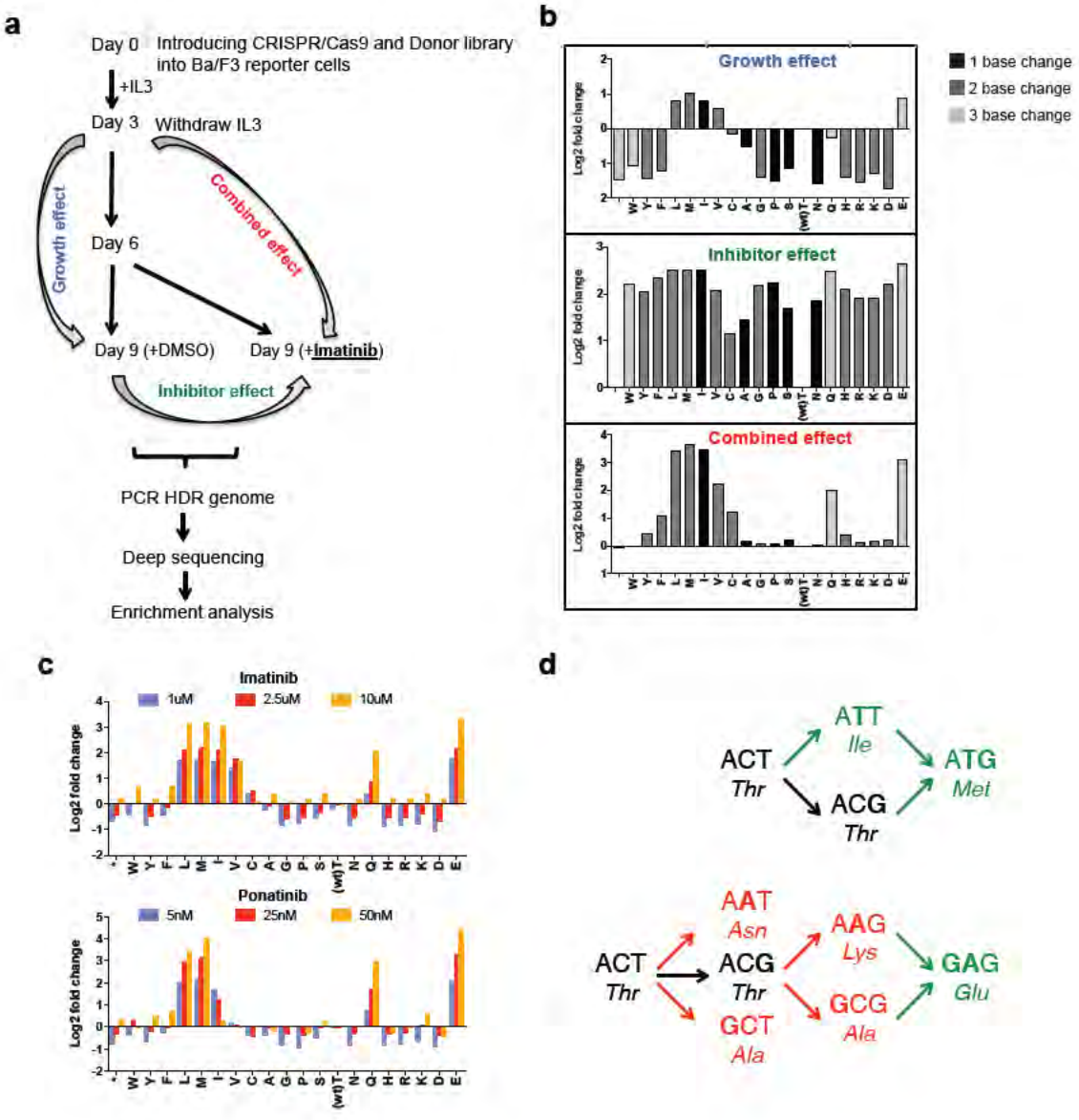

Figure 4.8. Fitness of 315 mutations under various selection pressure.

Figure 4.8. Fitness of 315 mutations under various selection pressure. a, Flow chart showing the experimental procedures using CRISPR-Cas9 to introduce 315x library into reporter Ba/F3 cell line, and subsequent selection of mutations under growth selection and inhibitor selection. Samples at various stage were collected for PCR and deep-sequencing to study mutant enrichment. Three comparisons were performed, Day9 + DMSO vs Day 3 represents “growth effect”, Day 9 + Imatinib vs day 9 + DMSO represents “inhibitor effect”, Day 9 + Imatinib vs Day 3 represents “combined effect”. b, Enrichment analysis of 315 mutants in growth effect, inhibitor effect and combined effect. Mutations that are accessible through single base change were marked in black, two bases change in dark grey, and three base change in light grey. c, Enrichment analysis of 315 mutants in combined effect at different concentration of Imatinib or Ponatinib. d, Single base mutational pathway from Thr to Met or Glu. Mutations with increase fitness were marked in green, decrease fitness in red, near neutral mutation in black.

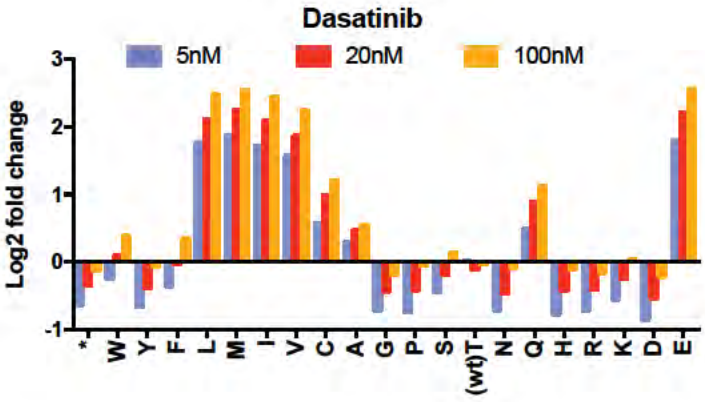

Figure 4.9. Combined effect of T315 mutants in response to Dasatinib.

a

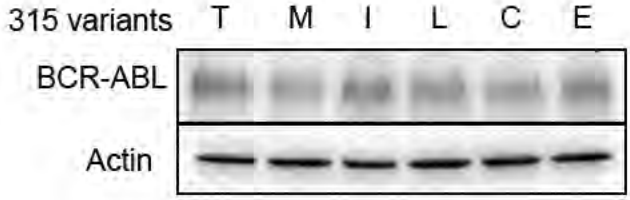

b

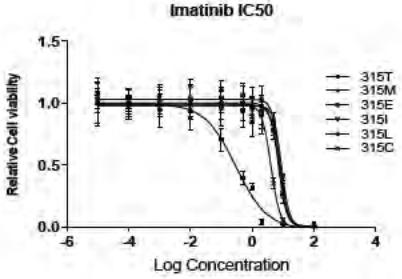

T315X	$IC50^{IM}$ uM
315T	0.3018
315M	7.823
315E	7.154
315I	8.968
315L	7.439
315C	4.073

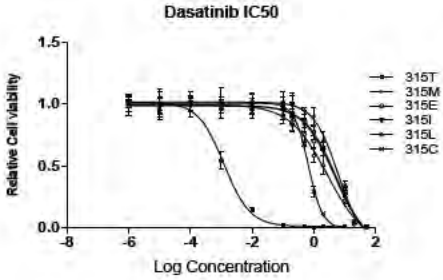

T315X	$IC50^{Da}$ uM
315T	0.001245
315M	5.891
315E	4.693
315I	5.277
315L	2.778
315C	0.6715

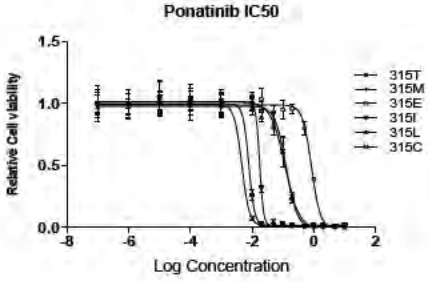

T315X	$IC50^{Po}$ uM
315T	0.0079
315M	0.1288
315E	0.8449
315I	0.01774
315L	0.1168
315C	0.004694

Figure 4.10. TKI resistance of individual T315X mutations. a, Western blots showing consistent expression level of individual T315 mutants at 1ug/ml of doxycycline. b, IC50 values of individual T315 mutants for Imatinib, Dasatinib, and Ponatinib.

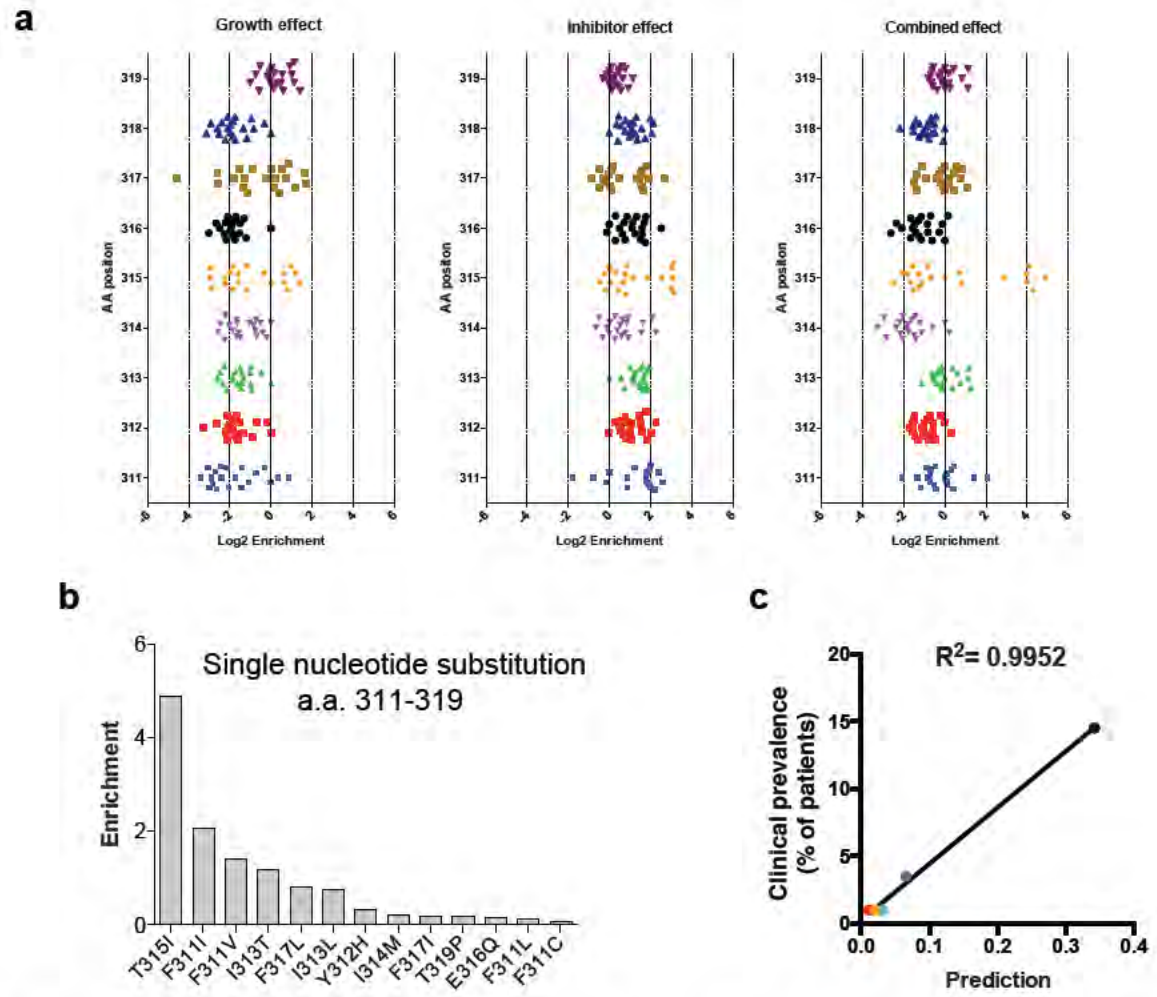

Figure 4.11. Estimating clinical prevalence of BCR-ABL mutations. a, Enrichment analysis of all possible amino acid mutations at each a.a. position in 311-319 region. Growth effect, inhibitor effect and combined effect analysis was carried out as before. Each group comprises 20 dots, representing all possible a.a variants, wildtype a.a was set as 0. b, Ranking of all enriched a.a mutations in 311-319 region that could be achieved through single nucleotide substitution from the corresponding wildtype codon. c, Correlation of predicted probability of 5 mutations and their clinical prevalence.

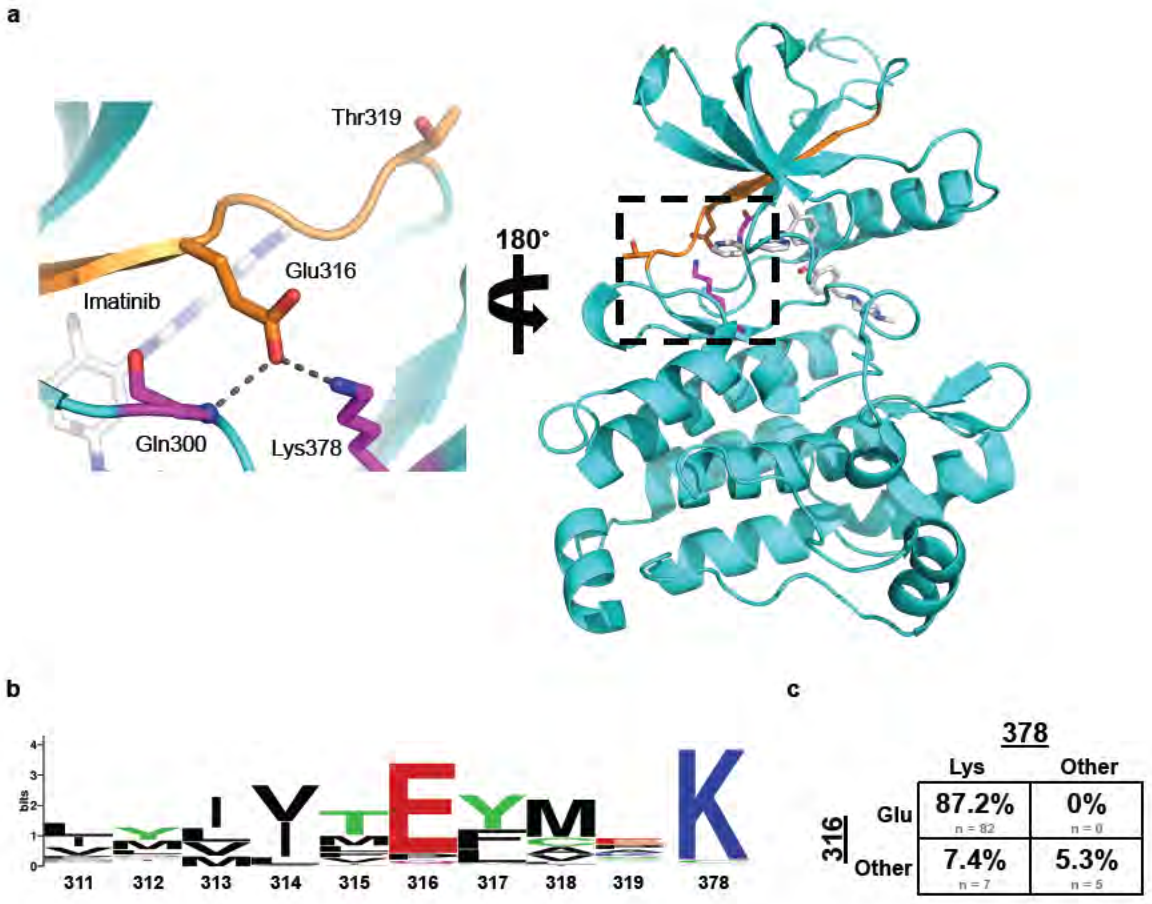

Figure 4.12. Structure and Sequence Analysis of 311-319 Region. a. Bcr-abl structure in the inactive/closed state with imatinib (PDB ID: 1OPJ). Imatinib shown as ball and sticks in GRAY. Residues 311-319 highlighted in ORANGE. Amino acids interacting with carboxyl of Glu316 are highlighted in PURPLE. Insert shows hydrogen bonding between Glu316's carboxyl group and the main chain amide of Gln300 and the amine of Lys378. b, Sequence conservation of residues 311-319 and 378 based on the alignment of 94 Tyrosine Kinases (downloaded from kinase.com). Plot highlights the coevolution between positions 316 and 378. Logo generated using WebLogo (weblogo.berkeley.edu/). c, Coevolution of residue identity at positions 316 and 378. Calculated from residue frequencies in alignment of 94 Tyrosine Kinases.

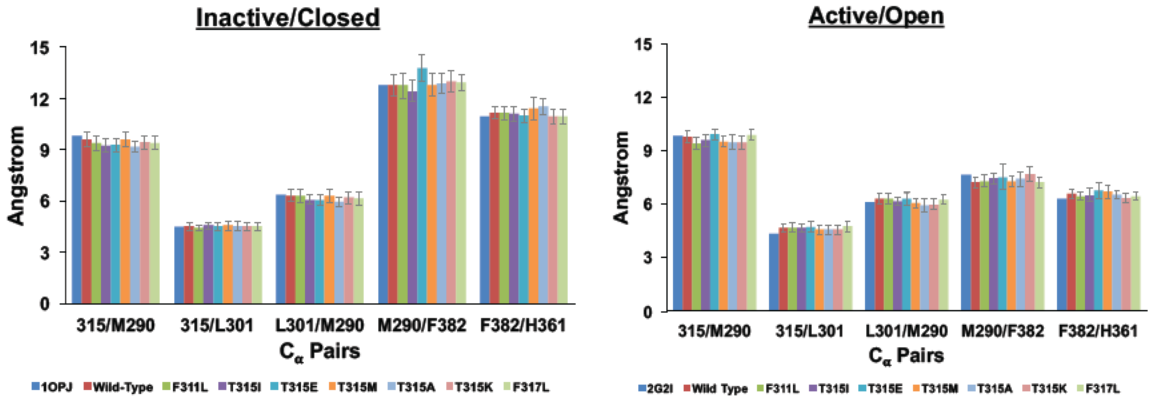

Figure 4.13. Hydrophobic Spine C_αDistances from Molecular Dynamics Simulations. Distances between C_αs of the hydrophobic spine (M290, L301, H361, F382) and gatekeeper position (315) for 10 ns molecular dynamics simulations of selected mutants started from the indicated conformation.

Primer	Sequence
PE1	AATGATACGGCGACCACCGAGATCTACACTCTTTCCCTACACGACGCTCTTCCGATCT
GFR_R	TCGTCCTTGAAGAAGATGGTG
Index 1	CAAGCAGAAGACGGCATACGAGATattactcgTCTCTGTCTCCACATGCCCA
Index 2	CAAGCAGAAGACGGCATACGAGATtccggagaTCTCTGTCTCCACATGCCCA
Index 3	CAAGCAGAAGACGGCATACGAGATcgctcattTCTCTGTCTCCACATGCCCA
Index 4	CAAGCAGAAGACGGCATACGAGATgagattccTCTCTGTCTCCACATGCCCA
Index 5	CAAGCAGAAGACGGCATACGAGATattcagaaTCTCTGTCTCCACATGCCCA
Index 6	CAAGCAGAAGACGGCATACGAGATgaattcgtTCTCTGTCTCCACATGCCCA
Index 7	CAAGCAGAAGACGGCATACGAGATctgaagctTCTCTGTCTCCACATGCCCA
Index 8	CAAGCAGAAGACGGCATACGAGATtaatgcgcTCTCTGTCTCCACATGCCCA
Index 9	CAAGCAGAAGACGGCATACGAGATcggctatgTCTCTGTCTCCACATGCCCA
Index 10	CAAGCAGAAGACGGCATACGAGATtccgcgaaTCTCTGTCTCCACATGCCCA
Index 11	CAAGCAGAAGACGGCATACGAGATtctcgcgcTCTCTGTCTCCACATGCCCA
Index 12	CAAGCAGAAGACGGCATACGAGATagcgatagTCTCTGTCTCCACATGCCCA
Index 13	CAAGCAGAAGACGGCATACGAGATcagatccaTCTCTGTCTCCACATGCCCA
Index 14	CAAGCAGAAGACGGCATACGAGATtgtgaccaTCTCTGTCTCCACATGCCCA
Index 15	CAAGCAGAAGACGGCATACGAGATacagtggtTCTCTGTCTCCACATGCCCA

Table 4.1. List of primers for nested PCR

CHAPTER V: DISCUSSION AND FUTURE PERSPECTIVES

In this thesis work, I have employed CML as a model, and studied three major aspects of drug resistance, namely, BCR-ABL mutation based resistance which blocks drug-target interaction, BCR-ABL independent drug resistance, which is caused by activation of parallel survival pathway, and drug insensitivity of cancer stem cells.

Despite the findings from current thesis work, many interesting areas remain to be explored:

Genetic screens to study drug resistant genes

In addition to PRKCH mediated maintenance of MAPK pathway discovered from my work, activation or maintenance of other pro-survival or anti-apoptotic pathways, including PI3K/AKT(Quentmeier et al., 2011), JAK/STAT(Warsch et al., 2011), LYN kinase(Donato et al., 2003), have been reported to contribute to BCR-ABL independent IM resistance. Interestingly, all these pathways are directly regulated by, and act downstream of BCR-ABL(Weisberg et al., 2007). This raises the question how many different ways CML cells could employ to circumvent BCR-ABL inhibition induced cell death?

“Oncogene addiction” has been a long established theory behind the scene of current targeted therapy(Weinstein and Joe, 2006). Cell viability is a status maintained by equilibrium of survival and death signals. Loss of oncogenic input

will lead to immediate loss of activity of multiple survival pathways, which reduces the apoptotic threshold. In the context of BCR-ABL, IM treatment results in suppression of phosphorylation of CRKL, SRC kinases, loss of MAPK, JAK/STAT and PI3K activity as early as 4 hour in vitro(Ma et al., 2014). When treated long enough, cells will pass the “point of no return” and enter apoptosis.

However, each signaling pathway is not linear, but rather part of a complicated signaling network(Bhalla and Iyengar, 1999). It is not uncommon that change of a proximal or even distal signaling node will lead to alteration of dynamics and kinetics of signal dampening caused by rapid loss of activation signal due to BCR-ABL inhibition. For example, MAPK pathway, although is known as a linear cascade due to the scaffold proteins(Kolch, 2005). Activation of RAF protein could be either through RAS(Leevers et al., 1994), or other kinases such as PKC(Kolch et al., 1993). Additionally, there are three different RAF proteins, ARAF, BRAF, and CRAF(Marais et al., 1997), and three different RAS isoforms, NRAS, HRAS and KRAS(Malumbres and Barbacid, 2003). Different combination of RAS and RAF is another layer of regulation that is not directly affected by BCR-ABL. Other than this positive regulatory mechanism, MAPK pathway activity is also maintained by serine/threonine phosphatases, such as PP2A(Silverstein et al., 2002).

RNAi based knockdown or CRISPR-Cas9 mediated knockout genetic screens offer unprecedented tools to reveal those negative regulators that could potentially lead to resistance(Moffat et al., 2006; Wang et al., 2014). Recently developed CRISPRa and CRISPRi technology would be useful for complete evaluation of both potential positive and negative regulators(Gilbert et al., 2014).

One caveat is that most genetic screens could only be performed in established cell lines, which might have accumulated additional mutations that may not exist in primary cancer cells. Also, primary cancer cells are often a mixed lineage, for example, CML is a stem cell based malignancy, and BCR-ABL could exist in all hematopoietic lineages. Performing genetic screens in a single clonal cell line from a defined lineage may not provide the entire picture. Some types of primary cells are difficult to transduce, the delivery of whole genome RNAi or CRISPR library could be a big challenge. In this scenario, customized small size sublibraries, such as kinome that target all kinases, phosophatome that target all phosphatase, epigenome that target all epigenetic regulators could be used instead. Transduced primary cells could then be transplanted back to humanized or syngeneic mice for expansion and therapy based selection. Any gene revealed in this way might be more clinically relevant.

Drug resistance mechanisms of Leukemic Stem Cells

IM insensitivity of CML stem cell is an interesting phenomenon but also represent a major challenge for the whole cancer therapeutic field—eliminating cancer stem cells(Reya et al., 2001). Mounting evidence has shown that cancer stem cells are resistant to a variety of therapies(Dean et al., 2005). Acquirement of stem cell property is enough to lead to such resistance, as exampled by the epithelial-mesenchymal transition (EMT) process in which cancer cells with epithelial morphology are sensitive to cancer drugs but become resistant once acquired mesenchymal morphology(Doherty et al., 2016; Tam et al., 2013). This phenomenon highlights the immediate need to understand the effects of stem cell signaling characteristics on drug resistance other than the typical properties such as self-renewal and quiescence.

In CML stem cells, genes including Alox5 and Pim2 have been found to be up-regulated compared to normal HSCs, however, IM treatment fails to restore their expression back to endogenous level(Chen et al., 2009). In contrast, PIM2 expression is highly dependent on BCR-ABL activity in CML cell lines, inhibition of BCR-ABL activity by IM completely abolishes PIM2 expression. Such evidence indicates the presence of leukemic stem-cell specific gene regulation in CML stem cells, and also raises the question why some genes are deregulated in CML stem cells but this deregulation is unable to be reversed by inhibiting BCR-ABL kinase function. One hypothesis is that BCR-ABL possesses other functional domains that can exert kinase independent effect on gene regulation. In addition,

such deregulated genes are adapted and maintained by stem cell specific signaling pathways once stimulated by BCR-ABL.

Our results using TET-off BCR-ABL transgenic mice model provides certain clues for this hypothesis. After withdrawal of tetracycline (TET) water and induction of BCR-ABL expression, mice develop CML and CML stem cells have increased PIM2 expression. By adding back TET water, BCR-ABL expression is suppressed, CML is reversed, and PIM2 expression was restored to the endogenous level. However, the detailed mechanisms why inhibiting BCR-ABL activity alone fails to inhibit PIM2 expression, and how BCR-ABL protein contributes to gene regulation in CML stem cells remain open questions.

Cancer cell heterogeneity and drug resistance

Cell heterogeneity is gradually recognized as a universal feature of normal and cancerous tissue(Altschuler and Wu, 2010). The advent of single cell RNA-seq technology also greatly facilitated the process of systematically evaluating population heterogeneity and revealing rare cell types(Grun et al., 2015; Johnson et al., 2015; Narsinh et al., 2011; Patel et al., 2014). In our single cell study of CML stem cell versus normal HSCs, we showed that both normal HSC and CML stem cells possess extensive gene expression heterogeneity. Presence of BCR-ABL is thought to cause significant changes in many gene expression patterns as revealed by previous transcriptome studies(Juric et al., 2007; Nowicki et al.,

2003). However, we found in our study that both CML stem cells and normal HSCs from CML patients display a gene expression pattern highly consistent with normal HSCs (Figure 3.1 c). In MDS plot, global gene expression differences caused by BCR-ABL expression seems to be minimal and masked by the population heterogeneity, as evidence by the inability to completely separate BCR-ABL- cells from BCR-ABL+ cells (Figure 3.1 e). Interestingly, cells from each individual patient closely aggregate together, regardless of BCR-ABL status, indicating greater contribution of genetic background to gene expression pattern than BCR-ABL expression. Conventional gene expression studies often use bulk cell population with a mixed population of cancer and normal cells from a group of patients or healthy donors. Given the large effect of genetic background on gene expression pattern(Whitney et al., 2003), the conventional analysis for differential gene expression could lead to large variation(up to 50 folds variation) in the expression of certain genes, which could account for 30% of total transcriptome(Cheung et al., 2003). Therefore, we propose using single cell RNA-seq coupled with unique molecular markers, BCR-ABL in the case of CML, as a novel strategy to study cancer specific gene expression between phenotypically indistinguishable cancer and normal cells. This could be particularly useful leukemia study since the leukemic and normal cells typically possess the same set of pre-defined cell surface markers(Sloma et al., 2010). In solid tumors, laser capture microdissection(LCM) could be used to pick individual

cells in a confined area(Frumkin et al., 2008), and perform similar studies accordingly.

In addition, cell heterogeneity also contributes to origination of rare resistant cells during drug treatment(Burrell and Swanton, 2014; Dexter and Leith, 1986). A well-known example in CML field is the establishment of resistant K562 cell line(K562R) by treating sensitive K562 cells with increasing concentration of IM(Donato et al., 2003). K562R cells are no longer sensitive to BCR-ABL inhibition, but rather shifted its dependence to Lyn kinase as shown by markedly Lyn overexpression in K562R cells compared to K562S cells(Donato et al., 2003). Importantly, the final resistant clone does not harbor BCR-ABL mutations, it suggests rewiring and adaption of cell signaling network during prolonged drug treatment. Additional examples include the establishment of LAMA84R cells(le Coutre et al., 2000) and KCL22R cells(Puttini et al., 2006). The feasibility to establish such resistant cell lines without drug target mutation strongly argue for the existence of cell signaling or gene expression heterogeneity even within a clonal population. Recent single cell study of T cells in response to LPS also proposed the idea of gene expression bimodality in a homogenous population(Shalek et al., 2013; Shalek et al., 2014). Daniel Haber's group isolated circulating breast cancer cells, and showed that even isolated single HER2- cell could acquire HER2+ phenotype after a minimal 4 cell divisions(Jordan et al., 2016). Such intrinsic heterogeneity and bimodal gene

expression could underlie the emergence of drug resistant population. Drug treatment and prolonged cell survival due to insufficient death signal likely enriched and promoted the expansion of a minor cell population possessing beneficial gene expression signatures. This could be particularly true for primary cancer cells that are continuously supported by additional survival signals, such as cytokines or secondary messengers(Chen et al., 2016), from tumor cell microenvironment or stem cell niche.

Despite the compelling evidence of cell population heterogeneity, the underlying cause remains elusive. It is still under debate whether cell cycle stage has a large contribution to the degree of cell heterogeneity(2016; Buettner et al., 2015; McDavid et al., 2016). Recently developed Div-seq from Zhang and Regev lab presents a unique advantage in resolving this debate by studying cells at predefined cell cycle stages(Habib et al., 2016). Again, there remain significant technical challenges in most of the single cell RNA-seq protocols(Saliba et al., 2014). One of the challenges is that many protocols, such as Smart-seq, require significant amount of post-amplification, which may lead to a false positive bimodal gene expression or exaggerated gene expression variation among single cells. However, bimodal expression of many genes have also been confirmed by RNA-FISH in Regev and Haber's paper(Jordan et al., 2016; Shalek et al., 2013), indicating this is still a true phenomenon.

Evolution of oncogene during drug selection

Current cellular proteins are thought to have been subjected over millions year of evolution and selection(Chothia and Gough, 2009). In terms of kinases, however, such adaption may be different from maximal activity(Arnold, 2009). When most of the mutations could cause functional defects, it has been shown that mutation of c-Abl and c-Src at gate keeper position from T to I or M could further increase their kinase activity and leading to transformation of transduced Ba/F3 cells overtime(Azam et al., 2008). This is supported by the crystal structure study that such mutations could promote the assembly of active confirmation, while proteins with wildtype residues are subjected to extensive post-translational modifications as sophisticated regulation of kinase activity(Azam et al., 2008).

Our saturated mutagenesis study in BCR-ABL kinase domain revealed that a number of such mutations could lead to increased BCR-ABL activity, and these mutations are typically associated with drug resistance. Those that could be achieved by single nucleotide substitution are also frequently observed in drug resistant CML or Ph+ ALL patients(Soverini et al., 2011). More interestingly, a couple of mutations in 311-319 region, T315I and F317L, could be identified from patients prior to IM treatment, indicating clonal expansion and selection due to increased fitness/kinase function(Shah et al., 2002).

Since most of drugs are designed to specifically target one particular kinase conformation, either by inhibiting active conformation or locking it in an inactive conformation, mutations that block drug binding and/or promote kinase activity will easily lead to drug resistance. It is surprising that around 17% of BCR-ABL mutations in 311-319 region have positive effect on cell growth. However, previous mutagenesis screening fails to reveal such properties of these mutations due to the inherent drawbacks of their screening technologies, including variable gene expression caused by random retroviral integration in the genome.

The novel screen strategy developed in the current study harnesses the CRISPR-Cas9 genome editing and HDR mechanism to introduce mutant library into a single chromatin locus for consistent gene expression. In addition, the mini-intron based barcoding strategy offers a simple tool to perform up to 20 biological replicates in a single run, thus significantly increasing the robustness and reproducibility of the results. This novel screening platform could be easily adapted for any oncogene of interest and expanded to cover the whole ORF for a particular oncogene. Since most of the small molecule inhibitor takes years from its first development to pre-clinical evaluation till final clinical trials(Novac, 2013), it would be of great help if we can predict clinical resistance beforehand in order to facilitate next-generation drug development. The screening platform we developed here could be employed in the pre-clinical stage to study the protein-

drug interaction, and systematically evaluate mutation fitness during therapy. For example, if a group of such mutations fall into a particular category, say, that promote the assembly of a particular protein conformation, the next-generation drug development could be initiated immediately to target this unique conformation and suppress drug resistance.

Future cancer therapy

In the current era of targeted cancer therapy, small molecules have played a critical role due to its ease of manufacturing and administration(Zhang et al., 2009). As exampled by TKI, small molecule cancer drugs have significantly prolonged cancer patients' overall survival and saved millions of lives(Bower et al., 2016; Gerber, 2008; Robert et al., 2015; Topalian et al., 2014). However, targeting a single oncogene, even though it is strongly addicted by cancer cells, the intrinsic hypermutation rate and heterogeneity in cell signaling pathways and gene expression pattern in cancer cells will lead to adaption of cancer cells and rewired signaling network overtime(Pawson and Warner, 2007). In this case, drug resistance has been and will always be unavoidable. Recently, chimeric antigen receptor T cells(CAR-T cells) were developed to treat refractory B-ALL by engineering cytotoxic T cells to target B cell-specific CD19 antigen. This enforced engagement leads to constant T cell proliferation and activation cytotoxic program to kill CD19-expressing cells. CAR-T therapy showed great clinical efficacy and sustained maintenance of leukemia remission(Kalos et al.,

2011). However, clinical cases resistant to CAR-T therapy have been reported, and the mechanism was found to be mutation or loss of CD19 expression(Sotillo et al., 2015), suggesting cancer cells are still finding ways to adapt and evade immunotherapy. Although drug-targeting specificity enhances safety, capability to counteract upcoming changes of cancer cells and heterogeneity is compromised.

Cancer evolution is a multi-step process, and includes clonal selection and expansion. In light of this, targeting multiple pathways using small molecules could significantly increase the cell death rate and prevent cells from accumulating additional mutations that may lead to subsequent resistance. Such combination therapy will greatly reduce the chance of resistance by suppressing clonal expansion events in the early period. In addition, our immune system has evolved to recognize and fight theoretically all hazardous signals, tuning body's own immune system to directly combat cancer or maintain disease remission, probably in combination with small molecule-based targeted therapy could also be a critical way to manage evolving changes of cancer.

BIBLIOGRAPHY

(1997). Interferon alfa versus chemotherapy for chronic myeloid leukemia: a meta-analysis of seven randomized trials: Chronic Myeloid Leukemia Trialists' Collaborative Group. Journal of the National Cancer Institute *89*, 1616-1620.

(2016). Reply to The contribution of cell cycle to heterogeneity in single-cell RNA-seq data. Nature biotechnology *34*, 593-595.

Abraham, S.A., Hopcroft, L.E., Carrick, E., Drotar, M.E., Dunn, K., Williamson, A.J., Korfi, K., Baquero, P., Park, L.E., Scott, M.T.*, et al.* (2016). Dual targeting of p53 and c-MYC selectively eliminates leukaemic stem cells. Nature *534*, 341-346.

Aceves-Luquero, C.I., Agarwal, A., Callejas-Valera, J.L., Arias-Gonzalez, L., Esparis-Ogando, A., del Peso Ovalle, L., Bellon-Echeverria, I., de la Cruz-Morcillo, M.A., Galan Moya, E.M., Moreno Gimeno, I.*, et al.* (2009). ERK2, but not ERK1, mediates acquired and "de novo" resistance to imatinib mesylate: implication for CML therapy. PLoS One *4*, e6124.

Adam, K., Lambert, M., Lestang, E., Champenois, G., Dusanter-Fourt, I., Tamburini, J., Bouscary, D., Lacombe, C., Zermati, Y., and Mayeux, P. (2015). Control of Pim2 kinase stability and expression in transformed human haematopoietic cells. Bioscience reports *35*.

Aderem, A. (1992). The MARCKS brothers: a family of protein kinase C substrates. Cell *71*, 713-716.

Agafonov, R.V., Wilson, C., Otten, R., Buosi, V., and Kern, D. (2014). Energetic dissection of Gleevec's selectivity toward human tyrosine kinases. Nature structural & molecular biology *21*, 848-853.

Airiau, K., Mahon, F.X., Josselin, M., Jeanneteau, M., Turcq, B., and Belloc, F. (2012). ABT-737 increases tyrosine kinase inhibitor-induced apoptosis in chronic myeloid leukemia cells through XIAP downregulation and sensitizes CD34(+) CD38(-) population to imatinib. Experimental hematology *40*, 367-378 e362.

Al-Hajj, M., Wicha, M.S., Benito-Hernandez, A., Morrison, S.J., and Clarke, M.F. (2003). Prospective identification of tumorigenic breast cancer cells. Proceedings of the National Academy of Sciences of the United States of America *100*, 3983-3988.

Aleksandrov, A., and Simonson, T. (2010). A molecular mechanics model for imatinib and imatinib:kinase binding. Journal of computational chemistry *31*, 1550-1560.

Altschuler, S.J., and Wu, L.F. (2010). Cellular heterogeneity: do differences make a difference? Cell *141*, 559-563.

An, X., Tiwari, A.K., Sun, Y., Ding, P.R., Ashby, C.R., Jr., and Chen, Z.S. (2010a). BCR-ABL tyrosine kinase inhibitors in the treatment of Philadelphia chromosome positive chronic myeloid leukemia: a review. Leukemia research *34*, 1255-1268.

An, X., Tiwari, A.K., Sun, Y., Ding, P.R., Ashby, C.R., Jr., and Chen, Z.S. (2010b). BCR-ABL tyrosine kinase inhibitors in the treatment of Philadelphia

chromosome positive chronic myeloid leukemia: a review. Leukemia research *34*, 1255-1268.
Anders, S., Pyl, P.T., and Huber, W. (2015). HTSeq--a Python framework to work with high-throughput sequencing data. Bioinformatics *31*, 166-169.
Andersson, L.C., Nilsson, K., and Gahmberg, C.G. (1979). K562--a human erythroleukemic cell line. International journal of cancer *23*, 143-147.
Arnold, F.H. (2009). How proteins adapt: lessons from directed evolution. Cold Spring Harbor symposia on quantitative biology *74*, 41-46.
Azam, M., Latek, R.R., and Daley, G.Q. (2003). Mechanisms of autoinhibition and STI-571/imatinib resistance revealed by mutagenesis of BCR-ABL. Cell *112*, 831-843.
Azam, M., Seeliger, M.A., Gray, N.S., Kuriyan, J., and Daley, G.Q. (2008). Activation of tyrosine kinases by mutation of the gatekeeper threonine. Nature structural & molecular biology *15*, 1109-1118.
Bagger, F.O., Rapin, N., Theilgaard-Monch, K., Kaczkowski, B., Thoren, L.A., Jendholm, J., Winther, O., and Porse, B.T. (2013). HemaExplorer: a database of mRNA expression profiles in normal and malignant haematopoiesis. Nucleic Acids Res *41*, D1034-1039.
Benjamini, Y., and Hochberg, Y. (1995). Controlling the false discovery rate: a practical and powerful approach to multiple testing. J Roy Statist Soc Ser B *57*, 289-300.
Berns, K., Hijmans, E.M., Mullenders, J., Brummelkamp, T.R., Velds, A., Heimerikx, M., Kerkhoven, R.M., Madiredjo, M., Nijkamp, W., Weigelt, B.*, et al.* (2004). A large-scale RNAi screen in human cells identifies new components of the p53 pathway. Nature *428*, 431-437.
Bhalla, U.S., and Iyengar, R. (1999). Emergent properties of networks of biological signaling pathways. Science *283*, 381-387.
Bhamidipati, P.K., Kantarjian, H., Cortes, J., Cornelison, A.M., and Jabbour, E. (2013). Management of imatinib-resistant patients with chronic myeloid leukemia. Therapeutic advances in hematology *4*, 103-117.
Bhatia, R., Holtz, M., Niu, N., Gray, R., Snyder, D.S., Sawyers, C.L., Arber, D.A., Slovak, M.L., and Forman, S.J. (2003). Persistence of malignant hematopoietic progenitors in chronic myelogenous leukemia patients in complete cytogenetic remission following imatinib mesylate treatment. Blood *101*, 4701-4707.
Bjerkvig, R., Tysnes, B.B., Aboody, K.S., Najbauer, J., and Terzis, A.J. (2005). Opinion: the origin of the cancer stem cell: current controversies and new insights. Nature reviews Cancer *5*, 899-904.
Bonnet, D., and Dick, J.E. (1997). Human acute myeloid leukemia is organized as a hierarchy that originates from a primitive hematopoietic cell. Nature medicine *3*, 730-737.
Bower, H., Bjorkholm, M., Dickman, P.W., Hoglund, M., Lambert, P.C., and Andersson, T.M. (2016). Life Expectancy of Patients With Chronic Myeloid Leukemia Approaches the Life Expectancy of the General Population. Journal of

clinical oncology : official journal of the American Society of Clinical Oncology *34*, 2851-2857.
Bruennert, D., Czibere, A., Bruns, I., Kronenwett, R., Gattermann, N., Haas, R., and Neumann, F. (2009). Early in vivo changes of the transcriptome in Philadelphia chromosome-positive CD34+ cells from patients with chronic myelogenous leukaemia following imatinib therapy. Leukemia *23*, 983-985.
Buettner, F., Natarajan, K.N., Casale, F.P., Proserpio, V., Scialdone, A., Theis, F.J., Teichmann, S.A., Marioni, J.C., and Stegle, O. (2015). Computational analysis of cell-to-cell heterogeneity in single-cell RNA-sequencing data reveals hidden subpopulations of cells. Nature biotechnology *33*, 155-160.
Burrell, R.A., and Swanton, C. (2014). Tumour heterogeneity and the evolution of polyclonal drug resistance. Molecular oncology *8*, 1095-1111.
Cai, H., Smola, U., Wixler, V., Eisenmann-Tappe, I., Diaz-Meco, M.T., Moscat, J., Rapp, U., and Cooper, G.M. (1997). Role of diacylglycerol-regulated protein kinase C isotypes in growth factor activation of the Raf-1 protein kinase. Molecular and cellular biology *17*, 732-741.
Canaani, E., Gale, R.P., Steiner-Saltz, D., Berrebi, A., Aghai, E., and Januszewicz, E. (1984). Altered transcription of an oncogene in chronic myeloid leukaemia. Lancet *1*, 593-595.
Carroll, M.P., and May, W.S. (1994). Protein kinase C-mediated serine phosphorylation directly activates Raf-1 in murine hematopoietic cells. The Journal of biological chemistry *269*, 1249-1256.
Carter, B.Z., Mak, D.H., Cortes, J., and Andreeff, M. (2010). The elusive chronic myeloid leukemia stem cell: does it matter and how do we eliminate it? Seminars in hematology *47*, 362-370.
Carvalho, B.S., and Irizarry, R.A. (2010). A framework for oligonucleotide microarray preprocessing. Bioinformatics *26*, 2363-2367.
Chakrabarti, R., Hwang, J., Andres Blanco, M., Wei, Y., Lukacisin, M., Romano, R.A., Smalley, K., Liu, S., Yang, Q., Ibrahim, T.*, et al.* (2012). Elf5 inhibits the epithelial-mesenchymal transition in mammary gland development and breast cancer metastasis by transcriptionally repressing Snail2. Nature cell biology *14*, 1212-1222.
Chang, J.S., Santhanam, R., Trotta, R., Neviani, P., Eiring, A.M., Briercheck, E., Ronchetti, M., Roy, D.C., Calabretta, B., Caligiuri, M.A.*, et al.* (2007). High levels of the BCR/ABL oncoprotein are required for the MAPK-hnRNP-E2 dependent suppression of C/EBPalpha-driven myeloid differentiation. Blood *110*, 994-1003.
Charlesworth, B., Morgan, M.T., and Charlesworth, D. (1993). The effect of deleterious mutations on neutral molecular variation. Genetics *134*, 1289-1303.
Chen, Q., Boire, A., Jin, X., Valiente, M., Er, E.E., Lopez-Soto, A., Jacob, L.S., Patwa, R., Shah, H., Xu, K.*, et al.* (2016). Carcinoma-astrocyte gap junctions promote brain metastasis by cGAMP transfer. Nature *533*, 493-498.
Chen, Y., Hu, Y., Zhang, H., Peng, C., and Li, S. (2009). Loss of the Alox5 gene impairs leukemia stem cells and prevents chronic myeloid leukemia. Nature genetics *41*, 783-792.

Chen, Y., Peng, C., Abraham, S.A., Shan, Y., Guo, Z., Desouza, N., Cheloni, G., Li, D., Holyoake, T.L., and Li, S. (2014). Arachidonate 15-lipoxygenase is required for chronic myeloid leukemia stem cell survival. The Journal of clinical investigation *124*, 3847-3862.
Cheung, V.G., Conlin, L.K., Weber, T.M., Arcaro, M., Jen, K.Y., Morley, M., and Spielman, R.S. (2003). Natural variation in human gene expression assessed in lymphoblastoid cells. Nature genetics *33*, 422-425.
Chomel, J.C., Bonnet, M.L., Sorel, N., Bertrand, A., Meunier, M.C., Fichelson, S., Melkus, M., Bennaceur-Griscelli, A., Guilhot, F., and Turhan, A.G. (2011). Leukemic stem cell persistence in chronic myeloid leukemia patients with sustained undetectable molecular residual disease. Blood *118*, 3657-3660.
Chothia, C., and Gough, J. (2009). Genomic and structural aspects of protein evolution. The Biochemical journal *419*, 15-28.
Chu, S., Holtz, M., Gupta, M., and Bhatia, R. (2004). BCR/ABL kinase inhibition by imatinib mesylate enhances MAP kinase activity in chronic myelogenous leukemia CD34+ cells. Blood *103*, 3167-3174.
Chu, S., Xu, H., Shah, N.P., Snyder, D.S., Forman, S.J., Sawyers, C.L., and Bhatia, R. (2005). Detection of BCR-ABL kinase mutations in CD34+ cells from chronic myelogenous leukemia patients in complete cytogenetic remission on imatinib mesylate treatment. Blood *105*, 2093-2098.
Colicelli, J. (2010). ABL tyrosine kinases: evolution of function, regulation, and specificity. Sci Signal *3*, re6.
Cong, L., Ran, F.A., Cox, D., Lin, S., Barretto, R., Habib, N., Hsu, P.D., Wu, X., Jiang, W., Marraffini, L.A.*, et al.* (2013). Multiplex genome engineering using CRISPR/Cas systems. Science *339*, 819-823.
Corbin, A.S., Agarwal, A., Loriaux, M., Cortes, J., Deininger, M.W., and Druker, B.J. (2011). Human chronic myeloid leukemia stem cells are insensitive to imatinib despite inhibition of BCR-ABL activity. The Journal of clinical investigation *121*, 396-409.
Cortes, J., Jabbour, E., Kantarjian, H., Yin, C.C., Shan, J., O'Brien, S., Garcia-Manero, G., Giles, F., Breeden, M., Reeves, N.*, et al.* (2007). Dynamics of BCR-ABL kinase domain mutations in chronic myeloid leukemia after sequential treatment with multiple tyrosine kinase inhibitors. Blood *110*, 4005-4011.
Cortes, J.E., Kantarjian, H., Shah, N.P., Bixby, D., Mauro, M.J., Flinn, I., O'Hare, T., Hu, S., Narasimhan, N.I., Rivera, V.M.*, et al.* (2012). Ponatinib in refractory Philadelphia chromosome-positive leukemias. The New England journal of medicine *367*, 2075-2088.
Curi, D.A., Beauchamp, E.M., Blyth, G.T., Arslan, A.D., Donato, N.J., Giles, F.J., Altman, J.K., and Platanias, L.C. (2015). Pre-clinical evidence of PIM kinase inhibitor activity in BCR-ABL1 unmutated and mutated Philadelphia chromosome-positive (Ph+) leukemias. Oncotarget *6*, 33206-33216.
Daley, G.Q., and Baltimore, D. (1988). Transformation of an interleukin 3-dependent hematopoietic cell line by the chronic myelogenous leukemia-specific

P210bcr/abl protein. Proceedings of the National Academy of Sciences of the United States of America *85*, 9312-9316.
Daley, G.Q., Van Etten, R.A., and Baltimore, D. (1990). Induction of chronic myelogenous leukemia in mice by the P210bcr/abl gene of the Philadelphia chromosome. Science *247*, 824-830.
Daley, G.Q., Van Etten, R.A., and Baltimore, D. (1991). Blast crisis in a murine model of chronic myelogenous leukemia. Proceedings of the National Academy of Sciences of the United States of America *88*, 11335-11338.
Danial, N.N., and Rothman, P. (2000). JAK-STAT signaling activated by Abl oncogenes. Oncogene *19*, 2523-2531.
Dash, A.B., Williams, I.R., Kutok, J.L., Tomasson, M.H., Anastasiadou, E., Lindahl, K., Li, S., Van Etten, R.A., Borrow, J., Housman, D.*, et al.* (2002). A murine model of CML blast crisis induced by cooperation between BCR/ABL and NUP98/HOXA9. Proceedings of the National Academy of Sciences of the United States of America *99*, 7622-7627.
Day, C.D., Lee, E., Kobayashi, J., Holappa, L.D., Albert, H., and Ow, D.W. (2000). Transgene integration into the same chromosome location can produce alleles that express at a predictable level, or alleles that are differentially silenced. Genes & development *14*, 2869-2880.
Dean, M., Fojo, T., and Bates, S. (2005). Tumour stem cells and drug resistance. Nature reviews Cancer *5*, 275-284.
Deininger, M., Buchdunger, E., and Druker, B.J. (2005). The development of imatinib as a therapeutic agent for chronic myeloid leukemia. Blood *105*, 2640-2653.
Deininger, M.W., Goldman, J.M., and Melo, J.V. (2000). The molecular biology of chronic myeloid leukemia. Blood *96*, 3343-3356.
Dexter, D.L., and Leith, J.T. (1986). Tumor heterogeneity and drug resistance. Journal of clinical oncology : official journal of the American Society of Clinical Oncology *4*, 244-257.
Dhut, S., Dorey, E.L., Horton, M.A., Ganesan, T.S., and Young, B.D. (1988). Identification of two normal bcr gene products in the cytoplasm. Oncogene *3*, 561-566.
Dierov, J., Dierova, R., and Carroll, M. (2004). BCR/ABL translocates to the nucleus and disrupts an ATR-dependent intra-S phase checkpoint. Cancer cell *5*, 275-285.
Doench, J.G., Hartenian, E., Graham, D.B., Tothova, Z., Hegde, M., Smith, I., Sullender, M., Ebert, B.L., Xavier, R.J., and Root, D.E. (2014). Rational design of highly active sgRNAs for CRISPR-Cas9-mediated gene inactivation. Nature biotechnology *32*, 1262-1267.
Doherty, M.R., Smigiel, J.M., Junk, D.J., and Jackson, M.W. (2016). Cancer Stem Cell Plasticity Drives Therapeutic Resistance. Cancers *8*.
Donato, N.J., Wu, J.Y., Stapley, J., Gallick, G., Lin, H., Arlinghaus, R., and Talpaz, M. (2003). BCR-ABL independence and LYN kinase overexpression in

chronic myelogenous leukemia cells selected for resistance to STI571. Blood *101*, 690-698.
Donato, N.J., Wu, J.Y., Stapley, J., Lin, H., Arlinghaus, R., Aggarwal, B.B., Shishodia, S., Albitar, M., Hayes, K., Kantarjian, H.*, et al.* (2004). Imatinib mesylate resistance through BCR-ABL independence in chronic myelogenous leukemia. Cancer research *64*, 672-677.
Druker, B.J. (2002). Inhibition of the Bcr-Abl tyrosine kinase as a therapeutic strategy for CML. Oncogene *21*, 8541-8546.
Druker, B.J., Tamura, S., Buchdunger, E., Ohno, S., Segal, G.M., Fanning, S., Zimmermann, J., and Lydon, N.B. (1996). Effects of a selective inhibitor of the Abl tyrosine kinase on the growth of Bcr-Abl positive cells. Nature medicine *2*, 561-566.
Duy, C., Hurtz, C., Shojaee, S., Cerchietti, L., Geng, H., Swaminathan, S., Klemm, L., Kweon, S.M., Nahar, R., Braig, M.*, et al.* (2011). BCL6 enables Ph+ acute lymphoblastic leukaemia cells to survive BCR-ABL1 kinase inhibition. Nature *473*, 384-388.
Eck, M.J., and Manley, P.W. (2009). The interplay of structural information and functional studies in kinase drug design: insights from BCR-Abl. Current opinion in cell biology *21*, 288-295.
Eisterer, W., Jiang, X., Christ, O., Glimm, H., Lee, K.H., Pang, E., Lambie, K., Shaw, G., Holyoake, T.L., Petzer, A.L.*, et al.* (2005). Different subsets of primary chronic myeloid leukemia stem cells engraft immunodeficient mice and produce a model of the human disease. Leukemia *19*, 435-441.
Escamilla-Hernandez, R., Chakrabarti, R., Romano, R.A., Smalley, K., Zhu, Q., Lai, W., Halfon, M.S., Buck, M.J., and Sinha, S. (2010). Genome-wide search identifies Ccnd2 as a direct transcriptional target of Elf5 in mouse mammary gland. BMC molecular biology *11*, 68.
Eyre-Walker, A., and Keightley, P.D. (2007). The distribution of fitness effects of new mutations. Nature reviews Genetics *8*, 610-618.
Fabian, J.R., Daar, I.O., and Morrison, D.K. (1993). Critical tyrosine residues regulate the enzymatic and biological activity of Raf-1 kinase. Molecular and cellular biology *13*, 7170-7179.
Faderl, S., Talpaz, M., Estrov, Z., O'Brien, S., Kurzrock, R., and Kantarjian, H.M. (1999). The biology of chronic myeloid leukemia. The New England journal of medicine *341*, 164-172.
Fefer, A., Cheever, M.A., Thomas, E.D., Boyd, C., Ramberg, R., Glucksberg, H., Buckner, C.D., and Storb, R. (1979). Disappearance of Ph1-positive cells in four patients with chronic granulocytic leukemia after chemotherapy, irradiation and marrow transplantation from an identical twin. The New England journal of medicine *300*, 333-337.
Feng, J., Park, J., Cron, P., Hess, D., and Hemmings, B.A. (2004). Identification of a PKB/Akt hydrophobic motif Ser-473 kinase as DNA-dependent protein kinase. The Journal of biological chemistry *279*, 41189-41196.

Findlay, G.M., Boyle, E.A., Hause, R.J., Klein, J.C., and Shendure, J. (2014). Saturation editing of genomic regions by multiplex homology-directed repair. Nature *513*, 120-123.
Fowler, D.M., and Fields, S. (2014). Deep mutational scanning: a new style of protein science. Nature methods *11*, 801-807.
Frumkin, D., Wasserstrom, A., Itzkovitz, S., Harmelin, A., Rechavi, G., and Shapiro, E. (2008). Amplification of multiple genomic loci from single cells isolated by laser micro-dissection of tissues. BMC biotechnology *8*, 17.
Fu, X., Fu, N., Guo, S., Yan, Z., Xu, Y., Hu, H., Menzel, C., Chen, W., Li, Y., Zeng, R.*, et al.* (2009). Estimating accuracy of RNA-Seq and microarrays with proteomics. BMC genomics *10*, 161.
Fujii, R., Kitaoka, M., and Hayashi, K. (2004). One-step random mutagenesis by error-prone rolling circle amplification. Nucleic acids research *32*, e145.
Gaj, T., Gersbach, C.A., and Barbas, C.F., 3rd (2013). ZFN, TALEN, and CRISPR/Cas-based methods for genome engineering. Trends in biotechnology *31*, 397-405.
Gaziev, D., Galimberti, M., Polchi, P., Angelucci, E., Giardini, C., Baronciani, D., Andreani, M., Persini, B., Erer, B., Sodani, P.*, et al.* (2002). Fate of chronic myeloid leukemia patients treated with allogeneic bone marrow transplantation or chemotherapy and/or interferon at a single center: long-term results. Bone marrow transplantation *29*, 1-8.
Gazin, C., Wajapeyee, N., Gobeil, S., Virbasius, C.M., and Green, M.R. (2007). An elaborate pathway required for Ras-mediated epigenetic silencing. Nature *449*, 1073-1077.
Gerber, D.E. (2008). Targeted therapies: a new generation of cancer treatments. American family physician *77*, 311-319.
Gerber, J.M., Gucwa, J.L., Esopi, D., Gurel, M., Haffner, M.C., Vala, M., Nelson, W.G., Jones, R.J., and Yegnasubramanian, S. (2013). Genome-wide comparison of the transcriptomes of highly enriched normal and chronic myeloid leukemia stem and progenitor cell populations. Oncotarget *4*, 715-728.
Gertz, J., Varley, K.E., Davis, N.S., Baas, B.J., Goryshin, I.Y., Vaidyanathan, R., Kuersten, S., and Myers, R.M. (2012). Transposase mediated construction of RNA-seq libraries. Genome research *22*, 134-141.
Gilbert, L.A., Horlbeck, M.A., Adamson, B., Villalta, J.E., Chen, Y., Whitehead, E.H., Guimaraes, C., Panning, B., Ploegh, H.L., Bassik, M.C.*, et al.* (2014). Genome-Scale CRISPR-Mediated Control of Gene Repression and Activation. Cell *159*, 647-661.
Giotopoulos, G., van der Weyden, L., Osaki, H., Rust, A.G., Gallipoli, P., Meduri, E., Horton, S.J., Chan, W.I., Foster, D., Prinjha, R.K.*, et al.* (2015). A novel mouse model identifies cooperating mutations and therapeutic targets critical for chronic myeloid leukemia progression. The Journal of experimental medicine *212*, 1551-1569.

Gobeil, S., Zhu, X., Doillon, C.J., and Green, M.R. (2008). A genome-wide shRNA screen identifies GAS1 as a novel melanoma metastasis suppressor gene. Genes & development *22*, 2932-2940.
Goff, D.J., Court Recart, A., Sadarangani, A., Chun, H.J., Barrett, C.L., Krajewska, M., Leu, H., Low-Marchelli, J., Ma, W., Shih, A.Y.*, et al.* (2013). A Pan-BCL2 inhibitor renders bone-marrow-resident human leukemia stem cells sensitive to tyrosine kinase inhibition. Cell stem cell *12*, 316-328.
Goldman, J.M. (2010). Chronic myeloid leukemia: a historical perspective. Seminars in hematology *47*, 302-311.
Golub, T.R., Slonim, D.K., Tamayo, P., Huard, C., Gaasenbeek, M., Mesirov, J.P., Coller, H., Loh, M.L., Downing, J.R., Caligiuri, M.A.*, et al.* (1999). Molecular classification of cancer: class discovery and class prediction by gene expression monitoring. Science *286*, 531-537.
Gorre, M.E., Mohammed, M., Ellwood, K., Hsu, N., Paquette, R., Rao, P.N., and Sawyers, C.L. (2001). Clinical resistance to STI-571 cancer therapy caused by BCR-ABL gene mutation or amplification. Science *293*, 876-880.
Gottesman, M.M. (2002). Mechanisms of cancer drug resistance. Annual review of medicine *53*, 615-627.
Graham, S.M., Jorgensen, H.G., Allan, E., Pearson, C., Alcorn, M.J., Richmond, L., and Holyoake, T.L. (2002). Primitive, quiescent, Philadelphia-positive stem cells from patients with chronic myeloid leukemia are insensitive to STI571 in vitro. Blood *99*, 319-325.
Greener, A., Callahan, M., and Jerpseth, B. (1997). An efficient random mutagenesis technique using an E. coli mutator strain. Molecular biotechnology *7*, 189-195.
Groffen, J., Stephenson, J.R., Heisterkamp, N., de Klein, A., Bartram, C.R., and Grosveld, G. (1984). Philadelphia chromosomal breakpoints are clustered within a limited region, bcr, on chromosome 22. Cell *36*, 93-99.
Grun, D., Lyubimova, A., Kester, L., Wiebrands, K., Basak, O., Sasaki, N., Clevers, H., and van Oudenaarden, A. (2015). Single-cell messenger RNA sequencing reveals rare intestinal cell types. Nature *525*, 251-255.
Gu, G., Wells, J.M., Dombkowski, D., Preffer, F., Aronow, B., and Melton, D.A. (2004). Global expression analysis of gene regulatory pathways during endocrine pancreatic development. Development *131*, 165-179.
Guertin, D.A., Stevens, D.M., Thoreen, C.C., Burds, A.A., Kalaany, N.Y., Moffat, J., Brown, M., Fitzgerald, K.J., and Sabatini, D.M. (2006). Ablation in mice of the mTORC components raptor, rictor, or mLST8 reveals that mTORC2 is required for signaling to Akt-FOXO and PKCalpha, but not S6K1. Developmental cell *11*, 859-871.
Habib, N., Li, Y., Heidenreich, M., Swiech, L., Avraham-Davidi, I., Trombetta, J.J., Hession, C., Zhang, F., and Regev, A. (2016). Div-Seq: Single-nucleus RNA-Seq reveals dynamics of rare adult newborn neurons. Science *353*, 925-928.

Hamilton, A., Helgason, G.V., Schemionek, M., Zhang, B., Myssina, S., Allan, E.K., Nicolini, F.E., Muller-Tidow, C., Bhatia, R., Brunton, V.G.*, et al.* (2012). Chronic myeloid leukemia stem cells are not dependent on Bcr-Abl kinase activity for their survival. Blood *119*, 1501-1510.
Hashimshony, T., Wagner, F., Sher, N., and Yanai, I. (2012). CEL-Seq: single-cell RNA-Seq by multiplexed linear amplification. Cell reports *2*, 666-673.
Hawley, R.G., Lieu, F.H., Fong, A.Z., and Hawley, T.S. (1994). Versatile retroviral vectors for potential use in gene therapy. Gene therapy *1*, 136-138.
Hemmings, B.A., and Restuccia, D.F. (2012). PI3K-PKB/Akt pathway. Cold Spring Harbor perspectives in biology *4*, a011189.
Hentschel, J., Rubio, I., Eberhart, M., Hipler, C., Schiefner, J., Schubert, K., Loncarevic, I.F., Wittig, U., Baniahmad, A., and von Eggeling, F. (2011). BCR-ABL- and Ras-independent activation of Raf as a novel mechanism of Imatinib resistance in CML. Int J Oncol *39*, 585-591.
Hietpas, R., Roscoe, B., Jiang, L., and Bolon, D.N. (2012). Fitness analyses of all possible point mutations for regions of genes in yeast. Nature protocols *7*, 1382-1396.
Hietpas, R.T., Jensen, J.D., and Bolon, D.N. (2011). Experimental illumination of a fitness landscape. Proceedings of the National Academy of Sciences of the United States of America *108*, 7896-7901.
Holohan, C., Van Schaeybroeck, S., Longley, D.B., and Johnston, P.G. (2013). Cancer drug resistance: an evolving paradigm. Nature reviews Cancer *13*, 714-726.
Honda, H., Fujii, T., Takatoku, M., Mano, H., Witte, O.N., Yazaki, Y., and Hirai, H. (1995). Expression of p210bcr/abl by metallothionein promoter induced T-cell leukemia in transgenic mice. Blood *85*, 2853-2861.
Honda, H., Ushijima, T., Wakazono, K., Oda, H., Tanaka, Y., Aizawa, S., Ishikawa, T., Yazaki, Y., and Hirai, H. (2000). Acquired loss of p53 induces blastic transformation in p210(bcr/abl)-expressing hematopoietic cells: a transgenic study for blast crisis of human CML. Blood *95*, 1144-1150.
Horvath, P., and Barrangou, R. (2010). CRISPR/Cas, the immune system of bacteria and archaea. Science *327*, 167-170.
Hsu, P.D., Lander, E.S., and Zhang, F. (2014). Development and applications of CRISPR-Cas9 for genome engineering. Cell *157*, 1262-1278.
Hu, Y., Swerdlow, S., Duffy, T.M., Weinmann, R., Lee, F.Y., and Li, S. (2006). Targeting multiple kinase pathways in leukemic progenitors and stem cells is essential for improved treatment of Ph+ leukemia in mice. Proceedings of the National Academy of Sciences of the United States of America *103*, 16870-16875.
Huettner, C.S., Zhang, P., Van Etten, R.A., and Tenen, D.G. (2000). Reversibility of acute B-cell leukaemia induced by BCR-ABL1. Nature genetics *24*, 57-60.
Hughes, T., Deininger, M., Hochhaus, A., Branford, S., Radich, J., Kaeda, J., Baccarani, M., Cortes, J., Cross, N.C., Druker, B.J.*, et al.* (2006). Monitoring CML patients responding to treatment with tyrosine kinase inhibitors: review and

recommendations for harmonizing current methodology for detecting BCR-ABL transcripts and kinase domain mutations and for expressing results. Blood *108*, 28-37.
Huntly, B.J., and Gilliland, D.G. (2005). Leukaemia stem cells and the evolution of cancer-stem-cell research. Nature reviews Cancer *5*, 311-321.
Huntly, B.J., Shigematsu, H., Deguchi, K., Lee, B.H., Mizuno, S., Duclos, N., Rowan, R., Amaral, S., Curley, D., Williams, I.R.*, et al.* (2004). MOZ-TIF2, but not BCR-ABL, confers properties of leukemic stem cells to committed murine hematopoietic progenitors. Cancer cell *6*, 587-596.
Hurtz, C., Hatzi, K., Cerchietti, L., Braig, M., Park, E., Kim, Y.M., Herzog, S., Ramezani-Rad, P., Jumaa, H., Muller, M.C.*, et al.* (2011). BCL6-mediated repression of p53 is critical for leukemia stem cell survival in chronic myeloid leukemia. The Journal of experimental medicine *208*, 2163-2174.
Ihaka, R., and Gentleman, R. (1996). R: A language for data analysis and graphics. J Comput Graph Stat *5*, 299-314.
Ilaria, R.L., Jr. (2004). Animal models of chronic myelogenous leukemia. Hematology/oncology clinics of North America *18*, 525-543, vii.
Ilaria, R.L., Jr., and Van Etten, R.A. (1996). P210 and P190(BCR/ABL) induce the tyrosine phosphorylation and DNA binding activity of multiple specific STAT family members. The Journal of biological chemistry *271*, 31704-31710.
Iliopoulos, D., Hirsch, H.A., Wang, G., and Struhl, K. (2011). Inducible formation of breast cancer stem cells and their dynamic equilibrium with non-stem cancer cells via IL6 secretion. Proceedings of the National Academy of Sciences of the United States of America *108*, 1397-1402.
Illmer, T., Schaich, M., Platzbecker, U., Freiberg-Richter, J., Oelschlagel, U., von Bonin, M., Pursche, S., Bergemann, T., Ehninger, G., and Schleyer, E. (2004). P-glycoprotein-mediated drug efflux is a resistance mechanism of chronic myelogenous leukemia cells to treatment with imatinib mesylate. Leukemia *18*, 401-408.
Ishikawa, F., Yasukawa, M., Lyons, B., Yoshida, S., Miyamoto, T., Yoshimoto, G., Watanabe, T., Akashi, K., Shultz, L.D., and Harada, M. (2005). Development of functional human blood and immune systems in NOD/SCID/IL2 receptor {gamma} chain(null) mice. Blood *106*, 1565-1573.
Islam, S., Kjallquist, U., Moliner, A., Zajac, P., Fan, J.B., Lonnerberg, P., and Linnarsson, S. (2011). Characterization of the single-cell transcriptional landscape by highly multiplex RNA-seq. Genome research *21*, 1160-1167.
Jabbour, E., Cortes, J., and Kantarjian, H. (2009). Nilotinib for the treatment of chronic myeloid leukemia: An evidence-based review. Core evidence *4*, 207-213.
Jabbour, E., Kantarjian, H., Jones, D., Talpaz, M., Bekele, N., O'Brien, S., Zhou, X., Luthra, R., Garcia-Manero, G., Giles, F.*, et al.* (2006). Frequency and clinical significance of BCR-ABL mutations in patients with chronic myeloid leukemia treated with imatinib mesylate. Leukemia *20*, 1767-1773.
Jiang, L., Liu, P., Bank, C., Renzette, N., Prachanronarong, K., Yilmaz, L.S., Caffrey, D.R., Zeldovich, K.B., Schiffer, C.A., Kowalik, T.F.*, et al.* (2016). A

Balance between Inhibitor Binding and Substrate Processing Confers Influenza Drug Resistance. Journal of molecular biology *428*, 538-553.
Jiang, X., Zhao, Y., Forrest, D., Smith, C., Eaves, A., and Eaves, C. (2008). Stem cell biomarkers in chronic myeloid leukemia. Disease markers *24*, 201-216.
Jiang, X., Zhao, Y., Smith, C., Gasparetto, M., Turhan, A., Eaves, A., and Eaves, C. (2007). Chronic myeloid leukemia stem cells possess multiple unique features of resistance to BCR-ABL targeted therapies. Leukemia *21*, 926-935.
Jinek, M., Chylinski, K., Fonfara, I., Hauer, M., Doudna, J.A., and Charpentier, E. (2012). A programmable dual-RNA-guided DNA endonuclease in adaptive bacterial immunity. Science *337*, 816-821.
Jing, J., Greshock, J., Holbrook, J.D., Gilmartin, A., Zhang, X., McNeil, E., Conway, T., Moy, C., Laquerre, S., Bachman, K.*, et al.* (2012). Comprehensive predictive biomarker analysis for MEK inhibitor GSK1120212. Mol Cancer Ther *11*, 720-729.
Johnson, M.B., Wang, P.P., Atabay, K.D., Murphy, E.A., Doan, R.N., Hecht, J.L., and Walsh, C.A. (2015). Single-cell analysis reveals transcriptional heterogeneity of neural progenitors in human cortex. Nature neuroscience *18*, 637-646.
Jones, D., Kamel-Reid, S., Bahler, D., Dong, H., Elenitoba-Johnson, K., Press, R., Quigley, N., Rothberg, P., Sabath, D., Viswanatha, D.*, et al.* (2009). Laboratory practice guidelines for detecting and reporting BCR-ABL drug resistance mutations in chronic myelogenous leukemia and acute lymphoblastic leukemia: a report of the Association for Molecular Pathology. The Journal of molecular diagnostics : JMD *11*, 4-11.
Jordan, C.T. (2009). Cancer stem cells: controversial or just misunderstood? Cell stem cell *4*, 203-205.
Jordan, N.V., Bardia, A., Wittner, B.S., Benes, C., Ligorio, M., Zheng, Y., Yu, M., Sundaresan, T.K., Licausi, J.A., Desai, R.*, et al.* (2016). HER2 expression identifies dynamic functional states within circulating breast cancer cells. Nature *537*, 102-106.
Juric, D., Lacayo, N.J., Ramsey, M.C., Racevskis, J., Wiernik, P.H., Rowe, J.M., Goldstone, A.H., O'Dwyer, P.J., Paietta, E., and Sikic, B.I. (2007). Differential gene expression patterns and interaction networks in BCR-ABL-positive and -negative adult acute lymphoblastic leukemias. Journal of clinical oncology : official journal of the American Society of Clinical Oncology *25*, 1341-1349.
Kacser, H., and Beeby, R. (1984). Evolution of catalytic proteins or on the origin of enzyme species by means of natural selection. Journal of molecular evolution *20*, 38-51.
Kalos, M., Levine, B.L., Porter, D.L., Katz, S., Grupp, S.A., Bagg, A., and June, C.H. (2011). T cells with chimeric antigen receptors have potent antitumor effects and can establish memory in patients with advanced leukemia. Science translational medicine *3*, 95ra73.
Kalyuga, M., Gallego-Ortega, D., Lee, H.J., Roden, D.L., Cowley, M.J., Caldon, C.E., Stone, A., Allerdice, S.L., Valdes-Mora, F., Launchbury, R.*, et al.* (2012).

ELF5 suppresses estrogen sensitivity and underpins the acquisition of antiestrogen resistance in luminal breast cancer. PLoS biology *10*, e1001461.
Kantarjian, H., Giles, F., Wunderle, L., Bhalla, K., O'Brien, S., Wassmann, B., Tanaka, C., Manley, P., Rae, P., Mietlowski, W.*, et al.* (2006). Nilotinib in imatinib-resistant CML and Philadelphia chromosome-positive ALL. The New England journal of medicine *354*, 2542-2551.
Kantarjian, H.M., Giles, F., Gattermann, N., Bhalla, K., Alimena, G., Palandri, F., Ossenkoppele, G.J., Nicolini, F.E., O'Brien, S.G., Litzow, M.*, et al.* (2007). Nilotinib (formerly AMN107), a highly selective BCR-ABL tyrosine kinase inhibitor, is effective in patients with Philadelphia chromosome-positive chronic myelogenous leukemia in chronic phase following imatinib resistance and intolerance. Blood *110*, 3540-3546.
Keeton, E.K., McEachern, K., Dillman, K.S., Palakurthi, S., Cao, Y., Grondine, M.R., Kaur, S., Wang, S., Chen, Y., Wu, A.*, et al.* (2014). AZD1208, a potent and selective pan-Pim kinase inhibitor, demonstrates efficacy in preclinical models of acute myeloid leukemia. Blood *123*, 905-913.
Kelliher, M.A., McLaughlin, J., Witte, O.N., and Rosenberg, N. (1990). Induction of a chronic myelogenous leukemia-like syndrome in mice with v-abl and BCR/ABL. Proceedings of the National Academy of Sciences of the United States of America *87*, 6649-6653.
Khorashad, J.S., Anand, M., Marin, D., Saunders, S., Al-Jabary, T., Iqbal, A., Margerison, S., Melo, J.V., Goldman, J.M., Apperley, J.F.*, et al.* (2006). The presence of a BCR-ABL mutant allele in CML does not always explain clinical resistance to imatinib. Leukemia *20*, 658-663.
Kim, C.F., Jackson, E.L., Woolfenden, A.E., Lawrence, S., Babar, I., Vogel, S., Crowley, D., Bronson, R.T., and Jacks, T. (2005). Identification of bronchioalveolar stem cells in normal lung and lung cancer. Cell *121*, 823-835.
Kim, D., Pertea, G., Trapnell, C., Pimentel, H., Kelley, R., and Salzberg, S.L. (2013). TopHat2: accurate alignment of transcriptomes in the presence of insertions, deletions and gene fusions. Genome biology *14*, R36.
Kimura, M. (1979). The neutral theory of molecular evolution. Scientific American *241*, 98-100, 102, 108 passim.
Kittler, R., Putz, G., Pelletier, L., Poser, I., Heninger, A.K., Drechsel, D., Fischer, S., Konstantinova, I., Habermann, B., Grabner, H.*, et al.* (2004). An endoribonuclease-prepared siRNA screen in human cells identifies genes essential for cell division. Nature *432*, 1036-1040.
Klein, A.M., Mazutis, L., Akartuna, I., Tallapragada, N., Veres, A., Li, V., Peshkin, L., Weitz, D.A., and Kirschner, M.W. (2015). Droplet barcoding for single-cell transcriptomics applied to embryonic stem cells. Cell *161*, 1187-1201.
Klein, C.A., Seidl, S., Petat-Dutter, K., Offner, S., Geigl, J.B., Schmidt-Kittler, O., Wendler, N., Passlick, B., Huber, R.M., Schlimok, G.*, et al.* (2002). Combined transcriptome and genome analysis of single micrometastatic cells. Nature biotechnology *20*, 387-392.

Klejman, A., Schreiner, S.J., Nieborowska-Skorska, M., Slupianek, A., Wilson, M., Smithgall, T.E., and Skorski, T. (2002). The Src family kinase Hck couples BCR/ABL to STAT5 activation in myeloid leukemia cells. The EMBO journal *21*, 5766-5774.

Kolch, W. (2005). Coordinating ERK/MAPK signalling through scaffolds and inhibitors. Nature reviews Molecular cell biology *6*, 827-837.

Kolch, W., Heidecker, G., Kochs, G., Hummel, R., Vahidi, H., Mischak, H., Finkenzeller, G., Marme, D., and Rapp, U.R. (1993). Protein kinase C alpha activates RAF-1 by direct phosphorylation. Nature *364*, 249-252.

Konopka, J.B., Watanabe, S.M., and Witte, O.N. (1984). An alteration of the human c-abl protein in K562 leukemia cells unmasks associated tyrosine kinase activity. Cell *37*, 1035-1042.

Konuma, T., Nakamura, S., Miyagi, S., Negishi, M., Chiba, T., Oguro, H., Yuan, J., Mochizuki-Kashio, M., Ichikawa, H., Miyoshi, H.*, et al.* (2011). Forced expression of the histone demethylase Fbxl10 maintains self-renewing hematopoietic stem cells. Exp Hematol *39*, 697-709 e695.

Koschmieder, S., Gottgens, B., Zhang, P., Iwasaki-Arai, J., Akashi, K., Kutok, J.L., Dayaram, T., Geary, K., Green, A.R., Tenen, D.G.*, et al.* (2005). Inducible chronic phase of myeloid leukemia with expansion of hematopoietic stem cells in a transgenic model of BCR-ABL leukemogenesis. Blood *105*, 324-334.

Krivtsov, A.V., Twomey, D., Feng, Z., Stubbs, M.C., Wang, Y., Faber, J., Levine, J.E., Wang, J., Hahn, W.C., Gilliland, D.G.*, et al.* (2006). Transformation from committed progenitor to leukaemia stem cell initiated by MLL-AF9. Nature *442*, 818-822.

Kuroda, J., Puthalakath, H., Cragg, M.S., Kelly, P.N., Bouillet, P., Huang, D.C., Kimura, S., Ottmann, O.G., Druker, B.J., Villunger, A.*, et al.* (2006). Bim and Bad mediate imatinib-induced killing of Bcr/Abl+ leukemic cells, and resistance due to their loss is overcome by a BH3 mimetic. Proceedings of the National Academy of Sciences of the United States of America *103*, 14907-14912.

Kurzrock, R., Kantarjian, H.M., Druker, B.J., and Talpaz, M. (2003). Philadelphia chromosome-positive leukemias: from basic mechanisms to molecular therapeutics. Annals of internal medicine *138*, 819-830.

Kurzrock, R., Shtalrid, M., Romero, P., Kloetzer, W.S., Talpas, M., Trujillo, J.M., Blick, M., Beran, M., and Gutterman, J.U. (1987). A novel c-abl protein product in Philadelphia-positive acute lymphoblastic leukaemia. Nature *325*, 631-635.

Laboratory, W.M.R.G. (2007). Guidelines for mutation analysis of BCR/ABL kinase domain:
Interpreting TKI-Resistance Mutations in CML Patients. WMRGL.

Lange, T., Park, B., Willis, S.G., and Deininger, M.W. (2005). BCR-ABL kinase domain mutations in chronic myeloid leukemia: not quite enough to cause resistance to imatinib therapy? Cell cycle *4*, 1761-1766.

Lathia, J.D. (2013). Cancer stem cells: moving past the controversy. CNS oncology *2*, 465-467.

Laurent, E., Talpaz, M., Wetzler, M., and Kurzrock, R. (2000). Cytoplasmic and nuclear localization of the 130 and 160 kDa Bcr proteins. Leukemia *14*, 1892-1897.
Law, C.W., Chen, Y., Shi, W., and Smyth, G.K. (2014). voom: Precision weights unlock linear model analysis tools for RNA-seq read counts. Genome biology *15*, R29.
le Coutre, P., Tassi, E., Varella-Garcia, M., Barni, R., Mologni, L., Cabrita, G., Marchesi, E., Supino, R., and Gambacorti-Passerini, C. (2000). Induction of resistance to the Abelson inhibitor STI571 in human leukemic cells through gene amplification. Blood *95*, 1758-1766.
Leevers, S.J., Paterson, H.F., and Marshall, C.J. (1994). Requirement for Ras in Raf activation is overcome by targeting Raf to the plasma membrane. Nature *369*, 411-414.
Leonard, W.J. (2001). Role of Jak kinases and STATs in cytokine signal transduction. International journal of hematology *73*, 271-277.
Lewis, I.D., McDiarmid, L.A., Samels, L.M., To, L.B., and Hughes, T.P. (1998). Establishment of a reproducible model of chronic-phase chronic myeloid leukemia in NOD/SCID mice using blood-derived mononuclear or CD34+ cells. Blood *91*, 630-640.
Li, B., and Dewey, C.N. (2011). RSEM: accurate transcript quantification from RNA-Seq data with or without a reference genome. BMC bioinformatics *12*, 323.
Li, C., Heidt, D.G., Dalerba, P., Burant, C.F., Zhang, L., Adsay, V., Wicha, M., Clarke, M.F., and Simeone, D.M. (2007). Identification of pancreatic cancer stem cells. Cancer research *67*, 1030-1037.
Li, L., Wang, L., Wang, Z., Ho, Y., McDonald, T., Holyoake, T.L., Chen, W., and Bhatia, R. (2012). Activation of p53 by SIRT1 inhibition enhances elimination of CML leukemia stem cells in combination with imatinib. Cancer cell *21*, 266-281.
Li, S., Ilaria, R.L., Jr., Million, R.P., Daley, G.Q., and Van Etten, R.A. (1999). The P190, P210, and P230 forms of the BCR/ABL oncogene induce a similar chronic myeloid leukemia-like syndrome in mice but have different lymphoid leukemogenic activity. The Journal of experimental medicine *189*, 1399-1412.
Liang, F., Han, M., Romanienko, P.J., and Jasin, M. (1998). Homology-directed repair is a major double-strand break repair pathway in mammalian cells. Proceedings of the National Academy of Sciences of the United States of America *95*, 5172-5177.
Lobo, N.A., Shimono, Y., Qian, D., and Clarke, M.F. (2007). The biology of cancer stem cells. Annu Rev Cell Dev Biol *23*, 675-699.
Lock, L.S., Royal, I., Naujokas, M.A., and Park, M. (2000). Identification of an atypical Grb2 carboxyl-terminal SH3 domain binding site in Gab docking proteins reveals Grb2-dependent and -independent recruitment of Gab1 to receptor tyrosine kinases. The Journal of biological chemistry *275*, 31536-31545.
Logue, J.S., and Morrison, D.K. (2012). Complexity in the signaling network: insights from the use of targeted inhibitors in cancer therapy. Genes & development *26*, 641-650.

Lozzio, C.B., and Lozzio, B.B. (1975). Human chronic myelogenous leukemia cell-line with positive Philadelphia chromosome. Blood *45*, 321-334.
Luo, J., Emanuele, M.J., Li, D., Creighton, C.J., Schlabach, M.R., Westbrook, T.F., Wong, K.K., and Elledge, S.J. (2009). A genome-wide RNAi screen identifies multiple synthetic lethal interactions with the Ras oncogene. Cell *137*, 835-848.
Ma, L., Shan, Y., Bai, R., Xue, L., Eide, C.A., Ou, J., Zhu, L.J., Hutchinson, L., Cerny, J., Khoury, H.J*., et al.* (2014). A therapeutically targetable mechanism of BCR-ABL-independent imatinib resistance in chronic myeloid leukemia. Science translational medicine *6*, 252ra121.
Ma, W., Giles, F., Zhang, X., Wang, X., Zhang, Z., Lee, T.S., Yeh, C.H., and Albitar, M. (2011). Three novel alternative splicing mutations in BCR-ABL1 detected in CML patients with resistance to kinase inhibitors. International journal of laboratory hematology *33*, 326-331.
MacKeigan, J.P., Murphy, L.O., and Blenis, J. (2005). Sensitized RNAi screen of human kinases and phosphatases identifies new regulators of apoptosis and chemoresistance. Nature cell biology *7*, 591-600.
Macosko, E.Z., Basu, A., Satija, R., Nemesh, J., Shekhar, K., Goldman, M., Tirosh, I., Bialas, A.R., Kamitaki, N., Martersteck, E.M*., et al.* (2015). Highly Parallel Genome-wide Expression Profiling of Individual Cells Using Nanoliter Droplets. Cell *161*, 1202-1214.
Malumbres, M., and Barbacid, M. (2003). RAS oncogenes: the first 30 years. Nature reviews Cancer *3*, 459-465.
Manley, P.W., Cowan-Jacob, S.W., and Mestan, J. (2005). Advances in the structural biology, design and clinical development of Bcr-Abl kinase inhibitors for the treatment of chronic myeloid leukaemia. Biochimica et biophysica acta *1754*, 3-13.
Marais, R., Light, Y., Paterson, H.F., Mason, C.S., and Marshall, C.J. (1997). Differential regulation of Raf-1, A-Raf, and B-Raf by oncogenic ras and tyrosine kinases. The Journal of biological chemistry *272*, 4378-4383.
Marioni, J.C., Mason, C.E., Mane, S.M., Stephens, M., and Gilad, Y. (2008). RNA-seq: an assessment of technical reproducibility and comparison with gene expression arrays. Genome research *18*, 1509-1517.
McCubrey, J.A., Steelman, L.S., Chappell, W.H., Abrams, S.L., Wong, E.W., Chang, F., Lehmann, B., Terrian, D.M., Milella, M., Tafuri, A*., et al.* (2007). Roles of the Raf/MEK/ERK pathway in cell growth, malignant transformation and drug resistance. Biochimica et biophysica acta *1773*, 1263-1284.
McDavid, A., Finak, G., and Gottardo, R. (2016). The contribution of cell cycle to heterogeneity in single-cell RNA-seq data. Nature biotechnology *34*, 591-593.
Melo, J.V. (1996). The diversity of BCR-ABL fusion proteins and their relationship to leukemia phenotype. Blood *88*, 2375-2384.
Melo, J.V., and Barnes, D.J. (2007). Chronic myeloid leukaemia as a model of disease evolution in human cancer. Nature reviews Cancer *7*, 441-453.

Mikkers, H., Nawijn, M., Allen, J., Brouwers, C., Verhoeven, E., Jonkers, J., and Berns, A. (2004). Mice deficient for all PIM kinases display reduced body size and impaired responses to hematopoietic growth factors. Molecular and cellular biology *24*, 6104-6115.
Million, R.P., and Van Etten, R.A. (2000). The Grb2 binding site is required for the induction of chronic myeloid leukemia-like disease in mice by the Bcr/Abl tyrosine kinase. Blood *96*, 664-670.
Mishra, P., Flynn, J.M., Starr, T.N., and Bolon, D.N. (2016). Systematic Mutant Analyses Elucidate General and Client-Specific Aspects of Hsp90 Function. Cell reports *15*, 588-598.
Mitchell-Olds, T., Willis, J.H., and Goldstein, D.B. (2007). Which evolutionary processes influence natural genetic variation for phenotypic traits? Nature reviews Genetics *8*, 845-856.
Mizuchi, D., Kurosu, T., Kida, A., Jin, Z.H., Jin, A., Arai, A., and Miura, O. (2005). BCR/ABL activates Rap1 and B-Raf to stimulate the MEK/Erk signaling pathway in hematopoietic cells. Biochem Biophys Res Commun *326*, 645-651.
Moffat, J., Grueneberg, D.A., Yang, X., Kim, S.Y., Kloepfer, A.M., Hinkle, G., Piqani, B., Eisenhaure, T.M., Luo, B., Grenier, J.K.*, et al.* (2006). A lentiviral RNAi library for human and mouse genes applied to an arrayed viral high-content screen. Cell *124*, 1283-1298.
Mooi, W.J., and Peeper, D.S. (2006). Oncogene-induced cell senescence--halting on the road to cancer. The New England journal of medicine *355*, 1037-1046.
Moore, N., and Lyle, S. (2011). Quiescent, slow-cycling stem cell populations in cancer: a review of the evidence and discussion of significance. J Oncol *2011*.
Mootha, V.K., Lindgren, C.M., Eriksson, K.F., Subramanian, A., Sihag, S., Lehar, J., Puigserver, P., Carlsson, E., Ridderstrale, M., Laurila, E.*, et al.* (2003). PGC-1alpha-responsive genes involved in oxidative phosphorylation are coordinately downregulated in human diabetes. Nat Genet *34*, 267-273.
Mullenders, J., and Bernards, R. (2009). Loss-of-function genetic screens as a tool to improve the diagnosis and treatment of cancer. Oncogene *28*, 4409-4420.
Naka, K., Hoshii, T., Muraguchi, T., Tadokoro, Y., Ooshio, T., Kondo, Y., Nakao, S., Motoyama, N., and Hirao, A. (2010). TGF-beta-FOXO signalling maintains leukaemia-initiating cells in chronic myeloid leukaemia. Nature *463*, 676-680.
Nalam, M.N., Ali, A., Reddy, G.S., Cao, H., Anjum, S.G., Altman, M.D., Yilmaz, N.K., Tidor, B., Rana, T.M., and Schiffer, C.A. (2013). Substrate envelope-designed potent HIV-1 protease inhibitors to avoid drug resistance. Chemistry & biology *20*, 1116-1124.
Nambu, T., Araki, N., Nakagawa, A., Kuniyasu, A., Kawaguchi, T., Hamada, A., and Saito, H. (2010). Contribution of BCR-ABL-independent activation of ERK1/2 to acquired imatinib resistance in K562 chronic myeloid leukemia cells. Cancer Sci *101*, 137-142.
Narsinh, K.H., Sun, N., Sanchez-Freire, V., Lee, A.S., Almeida, P., Hu, S., Jan, T., Wilson, K.D., Leong, D., Rosenberg, J.*, et al.* (2011). Single cell

transcriptional profiling reveals heterogeneity of human induced pluripotent stem cells. The Journal of clinical investigation *121*, 1217-1221.
Naughton, R., Quiney, C., Turner, S.D., and Cotter, T.G. (2009). Bcr-Abl-mediated redox regulation of the PI3K/AKT pathway. Leukemia *23*, 1432-1440.
Nawijn, M.C., Alendar, A., and Berns, A. (2011). For better or for worse: the role of Pim oncogenes in tumorigenesis. Nature reviews Cancer *11*, 23-34.
Neering, S.J., Bushnell, T., Sozer, S., Ashton, J., Rossi, R.M., Wang, P.Y., Bell, D.R., Heinrich, D., Bottaro, A., and Jordan, C.T. (2007). Leukemia stem cells in a genetically defined murine model of blast-crisis CML. Blood *110*, 2578-2585.
Nelson, E.A., Walker, S.R., Weisberg, E., Bar-Natan, M., Barrett, R., Gashin, L.B., Terrell, S., Klitgaard, J.L., Santo, L., Addorio, M.R.*, et al.* (2011). The STAT5 inhibitor pimozide decreases survival of chronic myelogenous leukemia cells resistant to kinase inhibitors. Blood *117*, 3421-3429.
Neviani, P., Santhanam, R., Trotta, R., Notari, M., Blaser, B.W., Liu, S., Mao, H., Chang, J.S., Galietta, A., Uttam, A.*, et al.* (2005). The tumor suppressor PP2A is functionally inactivated in blast crisis CML through the inhibitory activity of the BCR/ABL-regulated SET protein. Cancer cell *8*, 355-368.
Ngo, V.N., Davis, R.E., Lamy, L., Yu, X., Zhao, H., Lenz, G., Lam, L.T., Dave, S., Yang, L., Powell, J.*, et al.* (2006). A loss-of-function RNA interference screen for molecular targets in cancer. Nature *441*, 106-110.
Nielsen, R. (2005). Molecular signatures of natural selection. Annual review of genetics *39*, 197-218.
Novac, N. (2013). Challenges and opportunities of drug repositioning. Trends in pharmacological sciences *34*, 267-272.
Nowell PC, H.D. (1960). A minute chromosome in human chronic granulocytic leukemia. Science, 1497.
Nowicki, M.O., Pawlowski, P., Fischer, T., Hess, G., Pawlowski, T., and Skorski, T. (2003). Chronic myelogenous leukemia molecular signature. Oncogene *22*, 3952-3963.
O'Hare, T., Shakespeare, W.C., Zhu, X., Eide, C.A., Rivera, V.M., Wang, F., Adrian, L.T., Zhou, T., Huang, W.S., Xu, Q.*, et al.* (2009). AP24534, a pan-BCR-ABL inhibitor for chronic myeloid leukemia, potently inhibits the T315I mutant and overcomes mutation-based resistance. Cancer cell *16*, 401-412.
Ohkubo, T., Kamamoto, T., Kita, K., Hiraoka, A., Yoshida, Y., and Uchino, H. (1985). A novel Ph1 chromosome positive cell line established from a patient with chronic myelogenous leukemia in blastic crisis. Leukemia research *9*, 921-926.
Olivieri, A., and Manzione, L. (2007). Dasatinib: a new step in molecular target therapy. Annals of oncology : official journal of the European Society for Medical Oncology / ESMO *18 Suppl 6*, vi42-46.
Packer, L.M., Rana, S., Hayward, R., O'Hare, T., Eide, C.A., Rebocho, A., Heidorn, S., Zabriskie, M.S., Niculescu-Duvaz, I., Druker, B.J.*, et al.* (2011). Nilotinib and MEK inhibitors induce synthetic lethality through paradoxical activation of RAF in drug-resistant chronic myeloid leukemia. Cancer cell *20*, 715-727.

Paddison, P.J., Caudy, A.A., Bernstein, E., Hannon, G.J., and Conklin, D.S. (2002). Short hairpin RNAs (shRNAs) induce sequence-specific silencing in mammalian cells. Genes & development *16*, 948-958.
Paddison, P.J., Silva, J.M., Conklin, D.S., Schlabach, M., Li, M., Aruleba, S., Balija, V., O'Shaughnessy, A., Gnoj, L., Scobie, K.*, et al.* (2004). A resource for large-scale RNA-interference-based screens in mammals. Nature *428*, 427-431.
Patel, A.P., Tirosh, I., Trombetta, J.J., Shalek, A.K., Gillespie, S.M., Wakimoto, H., Cahill, D.P., Nahed, B.V., Curry, W.T., Martuza, R.L.*, et al.* (2014). Single-cell RNA-seq highlights intratumoral heterogeneity in primary glioblastoma. Science *344*, 1396-1401.
Pawson, T., and Warner, N. (2007). Oncogenic re-wiring of cellular signaling pathways. Oncogene *26*, 1268-1275.
Pear, W.S., Miller, J.P., Xu, L., Pui, J.C., Soffer, B., Quackenbush, R.C., Pendergast, A.M., Bronson, R., Aster, J.C., Scott, M.L.*, et al.* (1998). Efficient and rapid induction of a chronic myelogenous leukemia-like myeloproliferative disease in mice receiving P210 bcr/abl-transduced bone marrow. Blood *92*, 3780-3792.
Pellicano, F., Mukherjee, L., and Holyoake, T.L. (2014). Concise review: cancer cells escape from oncogene addiction: understanding the mechanisms behind treatment failure for more effective targeting. Stem Cells *32*, 1373-1379.
Pellicano, F., Simara, P., Sinclair, A., Helgason, G.V., Copland, M., Grant, S., and Holyoake, T.L. (2011). The MEK inhibitor PD184352 enhances BMS-214662-induced apoptosis in CD34+ CML stem/progenitor cells. Leukemia *25*, 1159-1167.
Pendergast, A.M., Muller, A.J., Havlik, M.H., Clark, R., McCormick, F., and Witte, O.N. (1991). Evidence for regulation of the human ABL tyrosine kinase by a cellular inhibitor. Proceedings of the National Academy of Sciences of the United States of America *88*, 5927-5931.
Picelli, S., Bjorklund, A.K., Faridani, O.R., Sagasser, S., Winberg, G., and Sandberg, R. (2013). Smart-seq2 for sensitive full-length transcriptome profiling in single cells. Nature methods *10*, 1096-1098.
Picelli, S., Faridani, O.R., Bjorklund, A.K., Winberg, G., Sagasser, S., and Sandberg, R. (2014). Full-length RNA-seq from single cells using Smart-seq2. Nature protocols *9*, 171-181.
Pluk, H., Dorey, K., and Superti-Furga, G. (2002). Autoinhibition of c-Abl. Cell *108*, 247-259.
Puttini, M., Coluccia, A.M., Boschelli, F., Cleris, L., Marchesi, E., Donella-Deana, A., Ahmed, S., Redaelli, S., Piazza, R., Magistroni, V.*, et al.* (2006). In vitro and in vivo activity of SKI-606, a novel Src-Abl inhibitor, against imatinib-resistant Bcr-Abl+ neoplastic cells. Cancer research *66*, 11314-11322.
Quentmeier, H., Eberth, S., Romani, J., Zaborski, M., and Drexler, H.G. (2011). BCR-ABL1-independent PI3Kinase activation causing imatinib-resistance. Journal of hematology & oncology *4*, 6.

Quintas-Cardama, A., Kantarjian, H.M., and Cortes, J.E. (2009). Mechanisms of primary and secondary resistance to imatinib in chronic myeloid leukemia. Cancer control : journal of the Moffitt Cancer Center *16*, 122-131.
Radich, J.P., Dai, H., Mao, M., Oehler, V., Schelter, J., Druker, B., Sawyers, C., Shah, N., Stock, W., Willman, C.L.*, et al.* (2006). Gene expression changes associated with progression and response in chronic myeloid leukemia. Proceedings of the National Academy of Sciences of the United States of America *103*, 2794-2799.
Ramskold, D., Luo, S., Wang, Y.C., Li, R., Deng, Q., Faridani, O.R., Daniels, G.A., Khrebtukova, I., Loring, J.F., Laurent, L.C.*, et al.* (2012). Full-length mRNA-Seq from single-cell levels of RNA and individual circulating tumor cells. Nature biotechnology *30*, 777-782.
Rawlings, J.S., Rosler, K.M., and Harrison, D.A. (2004). The JAK/STAT signaling pathway. Journal of cell science *117*, 1281-1283.
Redaelli, A., Bell, C., Casagrande, J., Stephens, J., Botteman, M., Laskin, B., and Pashos, C. (2004). Clinical and epidemiologic burden of chronic myelogenous leukemia. Expert review of anticancer therapy *4*, 85-96.
Ren, R. (2005). Mechanisms of BCR-ABL in the pathogenesis of chronic myelogenous leukaemia. Nature reviews Cancer *5*, 172-183.
Reya, T., Morrison, S.J., Clarke, M.F., and Weissman, I.L. (2001). Stem cells, cancer, and cancer stem cells. Nature *414*, 105-111.
Reynaud, D., Pietras, E., Barry-Holson, K., Mir, A., Binnewies, M., Jeanne, M., Sala-Torra, O., Radich, J.P., and Passegue, E. (2011). IL-6 controls leukemic multipotent progenitor cell fate and contributes to chronic myelogenous leukemia development. Cancer cell *20*, 661-673.
Robert, C., Karaszewska, B., Schachter, J., Rutkowski, P., Mackiewicz, A., Stroiakovski, D., Lichinitser, M., Dummer, R., Grange, F., Mortier, L.*, et al.* (2015). Improved overall survival in melanoma with combined dabrafenib and trametinib. The New England journal of medicine *372*, 30-39.
Robinson, M.D., and Oshlack, A. (2010). A scaling normalization method for differential expression analysis of RNA-seq data. Genome biology *11*, R25.
Roden, D.M., and George, A.L., Jr. (2002). The genetic basis of variability in drug responses. Nature reviews Drug discovery *1*, 37-44.
Root, D.E., Hacohen, N., Hahn, W.C., Lander, E.S., and Sabatini, D.M. (2006). Genome-scale loss-of-function screening with a lentiviral RNAi library. Nature methods *3*, 715-719.
Rosenberg, N., and Witte, O.N. (1988). The viral and cellular forms of the Abelson (abl) oncogene. Advances in virus research *35*, 39-81.
Ross, D.M., Branford, S., Seymour, J.F., Schwarer, A.P., Arthur, C., Yeung, D.T., Dang, P., Goyne, J.M., Slader, C., Filshie, R.J.*, et al.* (2013). Safety and efficacy of imatinib cessation for CML patients with stable undetectable minimal residual disease: results from the TWISTER study. Blood *122*, 515-522.

Rothkamm, K., Kruger, I., Thompson, L.H., and Lobrich, M. (2003). Pathways of DNA double-strand break repair during the mammalian cell cycle. Molecular and cellular biology *23*, 5706-5715.
Rowley, J.D. (1973). Letter: A new consistent chromosomal abnormality in chronic myelogenous leukaemia identified by quinacrine fluorescence and Giemsa staining. Nature *243*, 290-293.
Sadowski, I., Stone, J.C., and Pawson, T. (1986). A noncatalytic domain conserved among cytoplasmic protein-tyrosine kinases modifies the kinase function and transforming activity of Fujinami sarcoma virus P130gag-fps. Molecular and cellular biology *6*, 4396-4408.
Saito, Y., Kitamura, H., Hijikata, A., Tomizawa-Murasawa, M., Tanaka, S., Takagi, S., Uchida, N., Suzuki, N., Sone, A., Najima, Y.*, et al.* (2010). Identification of therapeutic targets for quiescent, chemotherapy-resistant human leukemia stem cells. Science translational medicine *2*, 17ra19.
Saliba, A.E., Westermann, A.J., Gorski, S.A., and Vogel, J. (2014). Single-cell RNA-seq: advances and future challenges. Nucleic acids research *42*, 8845-8860.
Sander, J.D., and Joung, J.K. (2014). CRISPR-Cas systems for editing, regulating and targeting genomes. Nature biotechnology *32*, 347-355.
Sarasin, A. (2003). An overview of the mechanisms of mutagenesis and carcinogenesis. Mutation research *544*, 99-106.
Sarbassov, D.D., Guertin, D.A., Ali, S.M., and Sabatini, D.M. (2005). Phosphorylation and regulation of Akt/PKB by the rictor-mTOR complex. Science *307*, 1098-1101.
Sattler, M., Mohi, M.G., Pride, Y.B., Quinnan, L.R., Malouf, N.A., Podar, K., Gesbert, F., Iwasaki, H., Li, S., Van Etten, R.A.*, et al.* (2002). Critical role for Gab2 in transformation by BCR/ABL. Cancer cell *1*, 479-492.
Savona, M., and Talpaz, M. (2008). Getting to the stem of chronic myeloid leukaemia. Nature reviews Cancer *8*, 341-350.
Sawyers, C.L. (1999). Chronic myeloid leukemia. The New England journal of medicine *340*, 1330-1340.
Sawyers, C.L., Hochhaus, A., Feldman, E., Goldman, J.M., Miller, C.B., Ottmann, O.G., Schiffer, C.A., Talpaz, M., Guilhot, F., Deininger, M.W.*, et al.* (2002). Imatinib induces hematologic and cytogenetic responses in patients with chronic myelogenous leukemia in myeloid blast crisis: results of a phase II study. Blood *99*, 3530-3539.
Schena, M., Shalon, D., Davis, R.W., and Brown, P.O. (1995). Quantitative monitoring of gene expression patterns with a complementary DNA microarray. Science *270*, 467-470.
Schiffer, C.A., Hehlmann, R., and Larson, R. (2003). Perspectives on the treatment of chronic phase and advanced phase CML and Philadelphia chromosome positive ALL(1). Leukemia *17*, 691-699.

Schindler, T., Bornmann, W., Pellicena, P., Miller, W.T., Clarkson, B., and Kuriyan, J. (2000). Structural mechanism for STI-571 inhibition of abelson tyrosine kinase. Science *289*, 1938-1942.
Schittenhelm, M.M., Shiraga, S., Schroeder, A., Corbin, A.S., Griffith, D., Lee, F.Y., Bokemeyer, C., Deininger, M.W., Druker, B.J., and Heinrich, M.C. (2006). Dasatinib (BMS-354825), a dual SRC/ABL kinase inhibitor, inhibits the kinase activity of wild-type, juxtamembrane, and activation loop mutant KIT isoforms associated with human malignancies. Cancer research *66*, 473-481.
Schmidt, W.M., and Mueller, M.W. (1999). CapSelect: a highly sensitive method for 5' CAP-dependent enrichment of full-length cDNA in PCR-mediated analysis of mRNAs. Nucleic acids research *27*, e31.
Schonwasser, D.C., Marais, R.M., Marshall, C.J., and Parker, P.J. (1998). Activation of the mitogen-activated protein kinase/extracellular signal-regulated kinase pathway by conventional, novel, and atypical protein kinase C isotypes. Molecular and cellular biology *18*, 790-798.
Shah, N.P. (2005). Loss of response to imatinib: mechanisms and management. Hematology / the Education Program of the American Society of Hematology American Society of Hematology Education Program, 183-187.
Shah, N.P., Nicoll, J.M., Nagar, B., Gorre, M.E., Paquette, R.L., Kuriyan, J., and Sawyers, C.L. (2002). Multiple BCR-ABL kinase domain mutations confer polyclonal resistance to the tyrosine kinase inhibitor imatinib (STI571) in chronic phase and blast crisis chronic myeloid leukemia. Cancer cell *2*, 117-125.
Shah, N.P., and Sawyers, C.L. (2003). Mechanisms of resistance to STI571 in Philadelphia chromosome-associated leukemias. Oncogene *22*, 7389-7395.
Shah, N.P., Skaggs, B.J., Branford, S., Hughes, T.P., Nicoll, J.M., Paquette, R.L., and Sawyers, C.L. (2007). Sequential ABL kinase inhibitor therapy selects for compound drug-resistant BCR-ABL mutations with altered oncogenic potency. The Journal of clinical investigation *117*, 2562-2569.
Shah, N.P., Tran, C., Lee, F.Y., Chen, P., Norris, D., and Sawyers, C.L. (2004). Overriding imatinib resistance with a novel ABL kinase inhibitor. Science *305*, 399-401.
Shalek, A.K., Satija, R., Adiconis, X., Gertner, R.S., Gaublomme, J.T., Raychowdhury, R., Schwartz, S., Yosef, N., Malboeuf, C., Lu, D.*, et al.* (2013). Single-cell transcriptomics reveals bimodality in expression and splicing in immune cells. Nature *498*, 236-240.
Shalek, A.K., Satija, R., Shuga, J., Trombetta, J.J., Gennert, D., Lu, D., Chen, P., Gertner, R.S., Gaublomme, J.T., Yosef, N.*, et al.* (2014). Single-cell RNA-seq reveals dynamic paracrine control of cellular variation. Nature *510*, 363-369.
Sharma, S.V., Gajowniczek, P., Way, I.P., Lee, D.Y., Jiang, J., Yuza, Y., Classon, M., Haber, D.A., and Settleman, J. (2006). A common signaling cascade may underlie "addiction" to the Src, BCR-ABL, and EGF receptor oncogenes. Cancer cell *10*, 425-435.
Shtivelman, E., Lifshitz, B., Gale, R.P., and Canaani, E. (1985). Fused transcript of abl and bcr genes in chronic myelogenous leukaemia. Nature *315*, 550-554.

Shukla, D., Meng, Y., Roux, B., and Pande, V.S. (2014). Activation pathway of Src kinase reveals intermediate states as targets for drug design. Nature communications *5*, 3397.
Shultz, L.D., Lyons, B.L., Burzenski, L.M., Gott, B., Chen, X., Chaleff, S., Kotb, M., Gillies, S.D., King, M., Mangada, J.*, et al.* (2005). Human lymphoid and myeloid cell development in NOD/LtSz-scid IL2R gamma null mice engrafted with mobilized human hemopoietic stem cells. Journal of immunology *174*, 6477-6489.
Sillaber, C., Gesbert, F., Frank, D.A., Sattler, M., and Griffin, J.D. (2000). STAT5 activation contributes to growth and viability in Bcr/Abl-transformed cells. Blood *95*, 2118-2125.
Silva, C.M. (2004). Role of STATs as downstream signal transducers in Src family kinase-mediated tumorigenesis. Oncogene *23*, 8017-8023.
Silva, J.M., Li, M.Z., Chang, K., Ge, W., Golding, M.C., Rickles, R.J., Siolas, D., Hu, G., Paddison, P.J., Schlabach, M.R.*, et al.* (2005). Second-generation shRNA libraries covering the mouse and human genomes. Nat Genet *37*, 1281-1288.
Silverstein, A.M., Barrow, C.A., Davis, A.J., and Mumby, M.C. (2002). Actions of PP2A on the MAP kinase pathway and apoptosis are mediated by distinct regulatory subunits. Proceedings of the National Academy of Sciences of the United States of America *99*, 4221-4226.
Singh, S.K., Clarke, I.D., Terasaki, M., Bonn, V.E., Hawkins, C., Squire, J., and Dirks, P.B. (2003). Identification of a cancer stem cell in human brain tumors. Cancer research *63*, 5821-5828.
Singh, S.K., Hawkins, C., Clarke, I.D., Squire, J.A., Bayani, J., Hide, T., Henkelman, R.M., Cusimano, M.D., and Dirks, P.B. (2004). Identification of human brain tumour initiating cells. Nature *432*, 396-401.
Sirard, C., Lapidot, T., Vormoor, J., Cashman, J.D., Doedens, M., Murdoch, B., Jamal, N., Messner, H., Addey, L., Minden, M.*, et al.* (1996). Normal and leukemic SCID-repopulating cells (SRC) coexist in the bone marrow and peripheral blood from CML patients in chronic phase, whereas leukemic SRC are detected in blast crisis. Blood *87*, 1539-1548.
Skorski, T., Nieborowska-Skorska, M., Szczylik, C., Kanakaraj, P., Perrotti, D., Zon, G., Gewirtz, A., Perussia, B., and Calabretta, B. (1995). C-RAF-1 serine/threonine kinase is required in BCR/ABL-dependent and normal hematopoiesis. Cancer research *55*, 2275-2278.
Skorski, T., Nieborowska-Skorska, M., Wlodarski, P., Perrotti, D., Martinez, R., Wasik, M.A., and Calabretta, B. (1996). Blastic transformation of p53-deficient bone marrow cells by p210bcr/abl tyrosine kinase. Proceedings of the National Academy of Sciences of the United States of America *93*, 13137-13142.
Slinker, B.K. (1998). The statistics of synergism. J Mol Cell Cardiol *30*, 723-731.
Sloma, I., Jiang, X., Eaves, A.C., and Eaves, C.J. (2010). Insights into the stem cells of chronic myeloid leukemia. Leukemia *24*, 1823-1833.

Sontakke, P., Jaques, J., Vellenga, E., and Schuringa, J.J. (2016). Modeling of Chronic Myeloid Leukemia: An Overview of In Vivo Murine and Human Xenograft Models. Stem cells international *2016*, 1625015.
Sotillo, E., Barrett, D.M., Black, K.L., Bagashev, A., Oldridge, D., Wu, G., Sussman, R., Lanauze, C., Ruella, M., Gazzara, M.R.*, et al.* (2015). Convergence of Acquired Mutations and Alternative Splicing of CD19 Enables Resistance to CART-19 Immunotherapy. Cancer discovery *5*, 1282-1295.
Soverini, S., Hochhaus, A., Nicolini, F.E., Gruber, F., Lange, T., Saglio, G., Pane, F., Muller, M.C., Ernst, T., Rosti, G.*, et al.* (2011). BCR-ABL kinase domain mutation analysis in chronic myeloid leukemia patients treated with tyrosine kinase inhibitors: recommendations from an expert panel on behalf of European LeukemiaNet. Blood *118*, 1208-1215.
Sozeri, O., Vollmer, K., Liyanage, M., Frith, D., Kour, G., Mark, G.E., 3rd, and Stabel, S. (1992). Activation of the c-Raf protein kinase by protein kinase C phosphorylation. Oncogene *7*, 2259-2262.
Stam, K., Heisterkamp, N., Reynolds, F.H., Jr., and Groffen, J. (1987). Evidence that the phl gene encodes a 160,000-dalton phosphoprotein with associated kinase activity. Molecular and cellular biology *7*, 1955-1960.
Steelman, L.S., Pohnert, S.C., Shelton, J.G., Franklin, R.A., Bertrand, F.E., and McCubrey, J.A. (2004). JAK/STAT, Raf/MEK/ERK, PI3K/Akt and BCR-ABL in cell cycle progression and leukemogenesis. Leukemia *18*, 189-218.
Subramanian, A., Tamayo, P., Mootha, V.K., Mukherjee, S., Ebert, B.L., Gillette, M.A., Paulovich, A., Pomeroy, S.L., Golub, T.R., Lander, E.S.*, et al.* (2005). Gene set enrichment analysis: a knowledge-based approach for interpreting genome-wide expression profiles. Proceedings of the National Academy of Sciences of the United States of America *102*, 15545-15550.
Suzuki, T., Elias, B.C., Seth, A., Shen, L., Turner, J.R., Giorgianni, F., Desiderio, D., Guntaka, R., and Rao, R. (2009). PKC eta regulates occludin phosphorylation and epithelial tight junction integrity. Proceedings of the National Academy of Sciences of the United States of America *106*, 61-66.
Takahashi, T., Ueno, H., and Shibuya, M. (1999). VEGF activates protein kinase C-dependent, but Ras-independent Raf-MEK-MAP kinase pathway for DNA synthesis in primary endothelial cells. Oncogene *18*, 2221-2230.
Talpaz, M., Kantarjian, H.M., McCredie, K., Trujillo, J.M., Keating, M.J., and Gutterman, J.U. (1986). Hematologic remission and cytogenetic improvement induced by recombinant human interferon alpha A in chronic myelogenous leukemia. The New England journal of medicine *314*, 1065-1069.
Tam, W.L., Lu, H., Buikhuisen, J., Soh, B.S., Lim, E., Reinhardt, F., Wu, Z.J., Krall, J.A., Bierie, B., Guo, W.*, et al.* (2013). Protein kinase C alpha is a central signaling node and therapeutic target for breast cancer stem cells. Cancer cell *24*, 347-364.
Tang, D.G. (2012). Understanding cancer stem cell heterogeneity and plasticity. Cell research *22*, 457-472.

Tang, F., Barbacioru, C., Bao, S., Lee, C., Nordman, E., Wang, X., Lao, K., and Surani, M.A. (2010). Tracing the derivation of embryonic stem cells from the inner cell mass by single-cell RNA-Seq analysis. Cell stem cell *6*, 468-478.

Tang, F., Barbacioru, C., Wang, Y., Nordman, E., Lee, C., Xu, N., Wang, X., Bodeau, J., Tuch, B.B., Siddiqui, A.*, et al.* (2009). mRNA-Seq whole-transcriptome analysis of a single cell. Nature methods *6*, 377-382.

ten Hoeve, J., Arlinghaus, R.B., Guo, J.Q., Heisterkamp, N., and Groffen, J. (1994). Tyrosine phosphorylation of CRKL in Philadelphia+ leukemia. Blood *84*, 1731-1736.

Topalian, S.L., Sznol, M., McDermott, D.F., Kluger, H.M., Carvajal, R.D., Sharfman, W.H., Brahmer, J.R., Lawrence, D.P., Atkins, M.B., Powderly, J.D.*, et al.* (2014). Survival, durable tumor remission, and long-term safety in patients with advanced melanoma receiving nivolumab. Journal of clinical oncology : official journal of the American Society of Clinical Oncology *32*, 1020-1030.

Trapnell, C., Roberts, A., Goff, L., Pertea, G., Kim, D., Kelley, D.R., Pimentel, H., Salzberg, S.L., Rinn, J.L., and Pachter, L. (2012). Differential gene and transcript expression analysis of RNA-seq experiments with TopHat and Cufflinks. Nature protocols *7*, 562-578.

Trapnell, C., Williams, B.A., Pertea, G., Mortazavi, A., Kwan, G., van Baren, M.J., Salzberg, S.L., Wold, B.J., and Pachter, L. (2010). Transcript assembly and quantification by RNA-Seq reveals unannotated transcripts and isoform switching during cell differentiation. Nature biotechnology *28*, 511-515.

Trombetta, J.J., Gennert, D., Lu, D., Satija, R., Shalek, A.K., and Regev, A. (2014). Preparation of Single-Cell RNA-Seq Libraries for Next Generation Sequencing. Current protocols in molecular biology / edited by Frederick M Ausubel [et al] *107*, 4 22 21-17.

Tsai, S.Q., Zheng, Z., Nguyen, N.T., Liebers, M., Topkar, V.V., Thapar, V., Wyvekens, N., Khayter, C., Iafrate, A.J., Le, L.P.*, et al.* (2015). GUIDE-seq enables genome-wide profiling of off-target cleavage by CRISPR-Cas nucleases. Nature biotechnology *33*, 187-197.

Ueda, Y., Hirai, S., Osada, S., Suzuki, A., Mizuno, K., and Ohno, S. (1996). Protein kinase C activates the MEK-ERK pathway in a manner independent of Ras and dependent on Raf. The Journal of biological chemistry *271*, 23512-23519.

Uht, R.M., Amos, S., Martin, P.M., Riggan, A.E., and Hussaini, I.M. (2007). The protein kinase C-eta isoform induces proliferation in glioblastoma cell lines through an ERK/Elk-1 pathway. Oncogene *26*, 2885-2893.

Van Etten, R.A. (1999). Cycling, stressed-out and nervous: cellular functions of c-Abl. Trends in cell biology *9*, 179-186.

Vanhaesebroeck, B., Stephens, L., and Hawkins, P. (2012). PI3K signalling: the path to discovery and understanding. Nature reviews Molecular cell biology *13*, 195-203.

Visvader, J.E., and Lindeman, G.J. (2008). Cancer stem cells in solid tumours: accumulating evidence and unresolved questions. Nature reviews Cancer *8*, 755-768.
Vogelstein, B., Papadopoulos, N., Velculescu, V.E., Zhou, S., Diaz, L.A., Jr., and Kinzler, K.W. (2013). Cancer genome landscapes. Science *339*, 1546-1558.
von Bubnoff, N., Peschel, C., and Duyster, J. (2003). Resistance of Philadelphia-chromosome positive leukemia towards the kinase inhibitor imatinib (STI571, Glivec): a targeted oncoprotein strikes back. Leukemia *17*, 829-838.
Wagenaar, T.R., Ma, L., Roscoe, B., Park, S.M., Bolon, D.N., and Green, M.R. (2014). Resistance to vemurafenib resulting from a novel mutation in the BRAFV600E kinase domain. Pigment cell & melanoma research *27*, 124-133.
Wang, J.Y. (1998). Cellular responses to DNA damage. Current opinion in cell biology *10*, 240-247.
Wang, T., Wei, J.J., Sabatini, D.M., and Lander, E.S. (2014). Genetic screens in human cells using the CRISPR-Cas9 system. Science *343*, 80-84.
Wang, Y., Liu, Y., Malek, S.N., Zheng, P., and Liu, Y. (2011). Targeting HIF1alpha eliminates cancer stem cells in hematological malignancies. Cell stem cell *8*, 399-411.
Wang, Z., Gerstein, M., and Snyder, M. (2009). RNA-Seq: a revolutionary tool for transcriptomics. Nature reviews Genetics *10*, 57-63.
Warsch, W., Kollmann, K., Eckelhart, E., Fajmann, S., Cerny-Reiterer, S., Holbl, A., Gleixner, K.V., Dworzak, M., Mayerhofer, M., Hoermann, G*., et al.* (2011). High STAT5 levels mediate imatinib resistance and indicate disease progression in chronic myeloid leukemia. Blood *117*, 3409-3420.
Weinstein, I.B., and Joe, A.K. (2006). Mechanisms of disease: Oncogene addiction--a rationale for molecular targeting in cancer therapy. Nature clinical practice Oncology *3*, 448-457.
Weisberg, E., Manley, P.W., Cowan-Jacob, S.W., Hochhaus, A., and Griffin, J.D. (2007). Second generation inhibitors of BCR-ABL for the treatment of imatinib-resistant chronic myeloid leukaemia. Nature reviews Cancer *7*, 345-356.
Wellbrock, C., Karasarides, M., and Marais, R. (2004). The RAF proteins take centre stage. Nature reviews Molecular cell biology *5*, 875-885.
Wetzler, M., Talpaz, M., Van Etten, R.A., Hirsh-Ginsberg, C., Beran, M., and Kurzrock, R. (1993). Subcellular localization of Bcr, Abl, and Bcr-Abl proteins in normal and leukemic cells and correlation of expression with myeloid differentiation. The Journal of clinical investigation *92*, 1925-1939.
White, D.L., Saunders, V.A., Dang, P., Engler, J., Zannettino, A.C., Cambareri, A.C., Quinn, S.R., Manley, P.W., and Hughes, T.P. (2006). OCT-1-mediated influx is a key determinant of the intracellular uptake of imatinib but not nilotinib (AMN107): reduced OCT-1 activity is the cause of low in vitro sensitivity to imatinib. Blood *108*, 697-704.
Whitney, A.R., Diehn, M., Popper, S.J., Alizadeh, A.A., Boldrick, J.C., Relman, D.A., and Brown, P.O. (2003). Individuality and variation in gene expression

patterns in human blood. Proceedings of the National Academy of Sciences of the United States of America *100*, 1896-1901.
Witkin, E.M. (1976). Ultraviolet mutagenesis and inducible DNA repair in Escherichia coli. Bacteriological reviews *40*, 869-907.
Woll, P.S., Kjallquist, U., Chowdhury, O., Doolittle, H., Wedge, D.C., Thongjuea, S., Erlandsson, R., Ngara, M., Anderson, K., Deng, Q.*, et al.* (2014). Myelodysplastic syndromes are propagated by rare and distinct human cancer stem cells in vivo. Cancer cell *25*, 794-808.
Wu, J., Meng, F., Kong, L.Y., Peng, Z., Ying, Y., Bornmann, W.G., Darnay, B.G., Lamothe, B., Sun, H., Talpaz, M.*, et al.* (2008). Association between imatinib-resistant BCR-ABL mutation-negative leukemia and persistent activation of LYN kinase. Journal of the National Cancer Institute *100*, 926-939.
Yan, B., Zemskova, M., Holder, S., Chin, V., Kraft, A., Koskinen, P.J., and Lilly, M. (2003). The PIM-2 kinase phosphorylates BAD on serine 112 and reverses BAD-induced cell death. The Journal of biological chemistry *278*, 45358-45367.
Yan, J., Roy, S., Apolloni, A., Lane, A., and Hancock, J.F. (1998). Ras isoforms vary in their ability to activate Raf-1 and phosphoinositide 3-kinase. The Journal of biological chemistry *273*, 24052-24056.
Yang, E., Zha, J., Jockel, J., Boise, L.H., Thompson, C.B., and Korsmeyer, S.J. (1995). Bad, a heterodimeric partner for Bcl-XL and Bcl-2, displaces Bax and promotes cell death. Cell *80*, 285-291.
Yasuda, T., Shirakata, M., Iwama, A., Ishii, A., Ebihara, Y., Osawa, M., Honda, K., Shinohara, H., Sudo, K., Tsuji, K.*, et al.* (2004). Role of Dok-1 and Dok-2 in myeloid homeostasis and suppression of leukemia. The Journal of experimental medicine *200*, 1681-1687.
Yhim, H.Y., Lee, N.R., Song, E.K., Yim, C.Y., Jeon, S.Y., Shin, S., Kim, J.A., Kim, H.S., Cho, E.H., and Kwak, J.Y. (2012). Imatinib mesylate discontinuation in patients with chronic myeloid leukemia who have received front-line imatinib mesylate therapy and achieved complete molecular response. Leukemia research *36*, 689-693.
Zabriskie, M.S., Eide, C.A., Tantravahi, S.K., Vellore, N.A., Estrada, J., Nicolini, F.E., Khoury, H.J., Larson, R.A., Konopleva, M., Cortes, J.E.*, et al.* (2014). BCR-ABL1 compound mutations combining key kinase domain positions confer clinical resistance to ponatinib in Ph chromosome-positive leukemia. Cancer cell *26*, 428-442.
Zeisel, A., Munoz-Manchado, A.B., Codeluppi, S., Lonnerberg, P., La Manno, G., Jureus, A., Marques, S., Munguba, H., He, L., Betsholtz, C.*, et al.* (2015). Brain structure. Cell types in the mouse cortex and hippocampus revealed by single-cell RNA-seq. Science *347*, 1138-1142.
Zender, L., Xue, W., Zuber, J., Semighini, C.P., Krasnitz, A., Ma, B., Zender, P., Kubicka, S., Luk, J.M., Schirmacher, P.*, et al.* (2008). An oncogenomics-based in vivo RNAi screen identifies tumor suppressors in liver cancer. Cell *135*, 852-864.

Zhang, B., Li, L., Ho, Y., Li, M., Marcucci, G., Tong, W., and Bhatia, R. (2016). Heterogeneity of leukemia-initiating capacity of chronic myelogenous leukemia stem cells. The Journal of clinical investigation *126*, 975-991.
Zhang, B., Li, M., McDonald, T., Holyoake, T.L., Moon, R.T., Campana, D., Shultz, L., and Bhatia, R. (2013). Microenvironmental protection of CML stem and progenitor cells from tyrosine kinase inhibitors through N-cadherin and Wnt-beta-catenin signaling. Blood *121*, 1824-1838.
Zhang, B., Strauss, A.C., Chu, S., Li, M., Ho, Y., Shiang, K.D., Snyder, D.S., Huettner, C.S., Shultz, L., Holyoake, T.*, et al.* (2010). Effective targeting of quiescent chronic myelogenous leukemia stem cells by histone deacetylase inhibitors in combination with imatinib mesylate. Cancer cell *17*, 427-442.
Zhang, H., Peng, C., Hu, Y., Li, H., Sheng, Z., Chen, Y., Sullivan, C., Cerny, J., Hutchinson, L., Higgins, A.*, et al.* (2012). The Blk pathway functions as a tumor suppressor in chronic myeloid leukemia stem cells. Nat Genet *44*, 861-871.
Zhang, J., Yang, P.L., and Gray, N.S. (2009). Targeting cancer with small molecule kinase inhibitors. Nature reviews Cancer *9*, 28-39.
Zhao, C., Blum, J., Chen, A., Kwon, H.Y., Jung, S.H., Cook, J.M., Lagoo, A., and Reya, T. (2007). Loss of beta-catenin impairs the renewal of normal and CML stem cells in vivo. Cancer cell *12*, 528-541.
Zhao, C., Chen, A., Jamieson, C.H., Fereshteh, M., Abrahamsson, A., Blum, J., Kwon, H.Y., Kim, J., Chute, J.P., Rizzieri, D.*, et al.* (2009). Hedgehog signalling is essential for maintenance of cancer stem cells in myeloid leukaemia. Nature *458*, 776-779.
Zhao, J., Kardashliev, T., Joelle Ruff, A., Bocola, M., and Schwaneberg, U. (2014). Lessons from diversity of directed evolution experiments by an analysis of 3,000 mutations. Biotechnology and bioengineering *111*, 2380-2389.
Zuber, J., Shi, J., Wang, E., Rappaport, A.R., Herrmann, H., Sison, E.A., Magoon, D., Qi, J., Blatt, K., Wunderlich, M.*, et al.* (2011). RNAi screen identifies Brd4 as a therapeutic target in acute myeloid leukaemia. Nature *478*, 524-528.